Universidade de Aveiro
Departamento de Geociências

2016

U.PORTO Universidade do Porto
Faculdade de Ciências

Instituto de Ciências Biomédicas Abel Salazar

DANIELA MARIA SILVA GONÇALVES

Impactos de obras da engenharia costeira na morfodinâmica sedimentar nas zonas de Vale do Lobo e Barra de Aveiro

Impacts of coastal engineering works in the morpho-sedimentary dynamics in the areas of Vale do Lobo and Barra de Aveiro

Universidade de Aveiro
Departamento de Geociências

2016

U.PORTO Universidade do Porto
Faculdade de Ciências
Instituto de Ciências Biomédicas Abel Salazar

DANIELA MARIA SILVA GONÇALVES

Impactos de obras da engenharia costeira na morfodinâmica sedimentar nas zonas de Vale do Lobo e Barra de Aveiro

Impacts of coastal engineering works in the morpho-sedimentary dynamics in the areas of Vale do Lobo and Barra de Aveiro

Tese apresentada à Universidade de Aveiro para cumprimento dos requisitos necessários à obtenção do grau de Doutor em Ciências do Mar e do Ambiente, realizada sob a orientação científica do Professor Luis Menezes Pinheiro, Professor Associado do Departamento de Geociências da Universidade de Aveiro, e com co-orientação científica do Professor Doutor Paulo Alves da Silva, Professor Associado do Departamento de Física da Universidade de Aveiro.

O trabalho desenvolvido no decorrer desta tese foi financiado por uma bolsa individual de doutoramento (SFRH/BD /65770/2009) da Fundação para a Ciência e a Tecnologia (FCT) e pelo Programa Operacional Potencial Humano POPH – QREN – Tipologia 4.1 – Formação Avançada, comparticipado pelo Fundo Social Europeu e por fundos nacionais do MEC.

This work was supported by a PhD grant (SFRH/BD/63349/2009) funded by Portuguese Foundation for Science and Technology (FCT) and by the Human Potential Operational Program POPH – QREN – Type 4.1 – Advanced Training, subsidized by the European Social Fund and by MEC National Funds.

FCT Fundação para a Ciência e a Tecnologia
MINISTÉRIO DA EDUCAÇÃO E CIÊNCIA

GOVERNO DE PORTUGAL
POPH PROGRAMA OPERACIONAL POTENCIAL HUMANO
QREN QUADRO DE REFERÊNCIA ESTRATÉGICO NACIONAL PORTUGAL 2007.2013

Dedico este trabalho aos meus pais.

o júri / the board

presidente

Professor Doutor Valeri Skliarov
Professor Catedrático da Universidade de Aveiro

Professor Doutor Fernando Joaquim Tavares Rocha
Professor Catedrático da Universidade de Aveiro

Professor Doutor Óscar Manuel Fernandes Cerveira Ferreira
Professor Associado da Universidade do Algarve

Professor Doutor Luis Menezes Pinheiro
Professor Associado da Universidade de Aveiro (Orientador)

Professor Doutor Rui Miguel Marques Moura
Professor Auxiliar da Faculdade de Ciências da Universidade do Porto

Professor Doutor Paulo Manuel Cruz Alves da Silva
Professor Associado da Universidade de Aveiro (Co-orientador)

Doutora Paula Maria dos Santos Freire
Professora Auxiliar do LNEC - Laboratório Nacional de Engenharia Civil

Doutor Vitor Hugo da Silva Magalhães
Investigador Auxiliar do Instituto Português do Mar e da Atmosfera

agradecimentos

Ao longo deste trabalho várias foram as pessoas e as entidades que tornaram possível a sua realização, sem as quais dificilmente teria sido realizado.

Gostaria de começar por agradecer aos meus orientadores Luís Menezes Pinheiro e Paulo Silva sem os quais o presente trabalho não teria sido possível. Todos os agradecimentos que lhes possa fazer serão ainda assim insuficientes e incapazes de fazer justiça ao seu real apoio. Ao Luis agradeço todas as oportunidades que me proporcionou a nível académico e científico, os seus ensinamentos, a correcção exaustiva da tese, mas acima de tudo a sua amizade. Ao Paulo Silva agradeço a sua disponibilidade, os seus conselhos e sugestões científicas tão valiosas para a melhoria da tese.

À Administração da Região Hidrográfica do Algarve - ARH Algarve - e, em particular, ao Eng. Sebastião Braz Teixeira, agradeço a cedência de parte dos dados batimétricos de Vale do Lobo utilizados no âmbito deste trabalho (Março 2006, Maio 2006 e Maio 2010).

Ao Dr. Xavier Bertin um muito obrigada pelo apoio ao longo de todo o trabalho relativo ao caso de estudo de Vale do Lobo. Agradeço ao Dr. André Fortunato e à Dra. Anabela Oliveira do Laboratório Nacional de Engenharia Civil por gentilmente cederem o código do modelo numérico MOSYS2D.

Agradeço também à entidade de coordenação central dos portos espanhóis - Puertos del Estado – por gentilmente cederem dados de ondulação medidos e modelados (WAM) relativos à bóia do Golfo de Cádis.

Ao Instituto Hidrográfico e em especial ao Comandante Santos Martinho agradeço a cedência dos dados de ondulação relativos à bóia de Faro.

Um muito obrigada ao Prof. Pedro Terrinha, Dr. Rui Quartau e Dr. João Noiva pela excelente campanha de mar ERSTA-SANDEX realizada em Novembro de 2008 na qual tive oportunidade de participar e aprender.

Agradeço à Administração do Porto de Aveiro – APA por todo o apoio nas campanhas na Barra de Aveiro e pela cedência de dados. Um especial agradecimento vai para os Engs. Luis Cacho, Rui Paiva, Jorge Rua e Carla Garrido, assim como para toda a equipa de pilotos.

Um especial obrigada a todos os que participaram nas campanhas realizadas no âmbito deste trabalho na Barra de Aveiro, tornando possível a aquisição de dados fundamentais para o seu desenvolvimento: Vitor Magalhães, Clara Sena, Omar Benazzouz, João Quintas, Francisco Curado, Keynesménio Neto, Paulo Miranda, Gabriela Flemming e Paulo Silva. Agradeço também a preciosa ajuda no trabalho laboratorial da Carina Mousaco e da Mariana Benites.

agradecimentos

Ao Paulo Miranda agradeço acima de tudo a amizade. Sei que és daqueles amigos que ficam para vida e que estaremos sempre unidos pelo laço da amizade e companheirismo. A ti agradeço também todo o apoio laboratorial na análise e tratamento das amostras de sedimentos, assim como a partilha de material bibliográfico e de conhecimentos.

À Clara Sena agradeço do fundo do coração toda a tranquilidade que trouxe aos meus dias com os seus conselhos tão sábios e ponderados. Ao Omar um muito obrigada por todo o apoio e pelas discussões científicas e até pelas menos científicas. À Catarina Lemos pela pessoa especial e sempre pronta para ajudar que é. À Joana Pinheiro que apesar da sua passagem pelo LGGM ter sido breve nem por isso deixou de ser intensa. À Caroline por toda a sua ajuda no processamento de dados de sonar de varrimento lateral, mas também pela sua incansável tentativa de me disciplinar. À Carla Candeias, que partilhou comigo o mesmo espaço físico na altura da escrita da tese, pelas conversas, mas acima de tudo pelos conselhos valiosos e ajuda preciosa ao longo do processo de escrita da tese.

Um agradecimento muito especial a todos os meus outros colegas e amigos do LGGM e do departamento, nomeadamente ao Francisco Teixeira, ao Vitor Magalhães, ao João Quintas, à Putri Supriandini, à Mafalda Costa e ao Nuno Durães.

À GeoSurveys agradeço a compreensão e flexibilidade em facultar dias essenciais para a escrita da tese, sem os quais o seu *terminus* não teria sido possível.

Devo também um agradecimento especial a todos os meus colegas e amigos da GeoSurveys, em especial ao Miguel Oliveira e à Joana Santos, minha companheira das noitadas de escrita da tese, mas também amiga do coração.

Aos meus pais agradeço o apoio incondicional. À minha irmã e ao Francisco agradeço o carinho, a compreensão e o todo o apoio emocional.

palavras-chave

Morfodinâmica, obras de engenharia portuária, dragagem, impactos, exploração de areias *offshore*, banco de areia, Aveiro, Vale do Lobo.

resumo

Esta tese investiga a evolução morfodinâmica de duas áreas de estudo em contextos geográficos e hidrodinâmicos distintos, ambas sujeitas a atividades de dragagens e obras de engenharia: uma área *offshore* Vale do Lobo, Algarve, cujo litoral, seriamente afetado pela erosão costeira, foi sujeito nos últimos anos a alimentações artificiais de praia com recurso a manchas de empréstimo situadas ao largo; e a Barra de Aveiro e sua área adjacente, submetida a várias reconfigurações nas últimas décadas, e onde as atividades de dragagem para manutenção dos canais de navegação são recorrentes. Pretende-se com este trabalho uma melhor compreensão dos impactos das actividades de dragagem e obras de engenharia costeira na morfodinâmica local e estimar o tempo de recuperação de escavações no mar, o que é fundamental para a avaliação dos impactos associados.

A investigação da evolução da escavação localizada ao largo de Vale do Lobo, Algarve, foi baseada em 4 levantamentos batimétricos, antes e depois das operações de dragagem (num intervalo de tempo de quatro anos 2006-2010), complementada com a análise da ondulação e simulações com recurso a modelos numéricos. Os resultados mostram um enchimento da escavação de aproximadamente 17% nos primeiros 4 anos, com uma suavização geral da topografia inicial da escavação. Observações combinadas com os resultados da modelação demonstram que a evolução da escavação está maioritariamente dependente dos eventos de tempestade, uma vez que é essencialmente durante esses períodos em que há movimento significativo de sedimento à profundidade de estudo. Com base no número de dias de tempestade previstos para os próximos anos, o período de recuperação da escavação é de ca. 38 anos para o seu total preenchimento.

O estudo da evolução sedimentar e morfológica da Barra de Aveiro e da sua área adjacente foi baseado em dados batimétricos históricos (1936-1978) e recentes (2010-2013), complementados com a aquisição de dados de sonar de varrimento lateral e a colheita e análise de sedimentos de fundo. Os resultados indicam que a permanência e evolução do banco de areia são resultado de uma complexa interação de vários fatores: a deriva litoral, que parece representar a principal fonte sedimentar do banco; as correntes de jato, resultantes da interação entre a deriva litoral e o molhe norte, dirigidas para SW; as correntes de maré, cuja direção está relacionada com o orientação e comprimento do molhe norte; a diminuição de energia das correntes de vazante com a distância à entrada da barra, revelada pela variação granulométrica dos sedimentos de fundo, o que permitiu a acumulação de areia na zona do banco e/ou a remoção do sedimento mais fino nas partes mais energéticas; e as obras de engenharia, tais como a extensão do molhe norte, que redirecionam as correntes de maré e as correntes de jato, e as operações de dragagem de manutenção do canal de navegação.

keywords

Morphodynamics, port engineering works, dredging, impacts, offshore sand exploitation, sandbank, Aveiro, Vale do Lobo.

abstract

This thesis investigates the morphodynamic evolution of two study areas in distinct geographically and hydrodynamically contexts affected by anthropogenic activities related to port engineering works and dredging activities: an area offshore Vale do Lobo, Algarve, where the coastline is seriously affected by coastal erosion and where offshore sand exploitation took place for artificial beach nourishment; and an area adjacent to the entrance of the Port of Aveiro, which has been subjected to the influence of several jetty reconfigurations in the past decades, and where recurrent dredging activities are carried out for maintenance of the navigation channels. It aims at better understanding some of the impacts of jetty reconfiguration and dredging on the local morphodynamics in port areas, and also how offshore excavations are able to recover through time, which is fundamental for impact assessment.

The investigation of the evolution of the offshore sandpit located off Vale do Lobo, Algarve, was based on 4 bathymetric surveys, prior to and after the dredging operations (within a time span of four years 2006-2010), complemented with the analysis of wave data and numerical modelling simulations. The results show an infill of approximately 17% of the initial exploration pit in the first 4 years, with an overall smoothing of the initial excavation bottom topography. Observations combined with modelling results demonstrate that the pit evolution depends mainly on storm events, since it is essentially during these periods that there is significant sediment movement at the site depth, and, based on the predicted number of stormy days for the forecoming years, the sandpit recovery period is of ca. 38 years for its full, or near full, replenishment.

The study of the sedimentary and morphological evolution of the “Barra de Aveiro” and the adjacent near-shore shelf area was based on both old (1936-1978) and recent (2010-2013) bathymetric datasets, complemented with newly acquired sidescan sonar data and bottom sediment sampling and analysis. The results indicate that the sandbank permanency and evolution are related to a complex interaction of factors: the littoral drift, which seems to represent the main sedimentary source of the sandbank; the southwest-directed jet stream related to the littoral drift interaction with the north jetty; the ebb currents, whose direction is related to the north jetty length and orientation; the energy decrease of the ebb currents with the distance to the inlet, revealed by the granulometric variation of the surface bank sediments, which allowed the sand accumulation in the bank area and/or the removal of the finer sediment in the most energetic parts of the bank; and the engineering works such as the extension of the north jetty, that re-direct the ebb currents and the jet stream, and the dredging operations for navigation channel maintenance.

Table of contents

List of Figures

List of Tables

Chapter I. Introduction

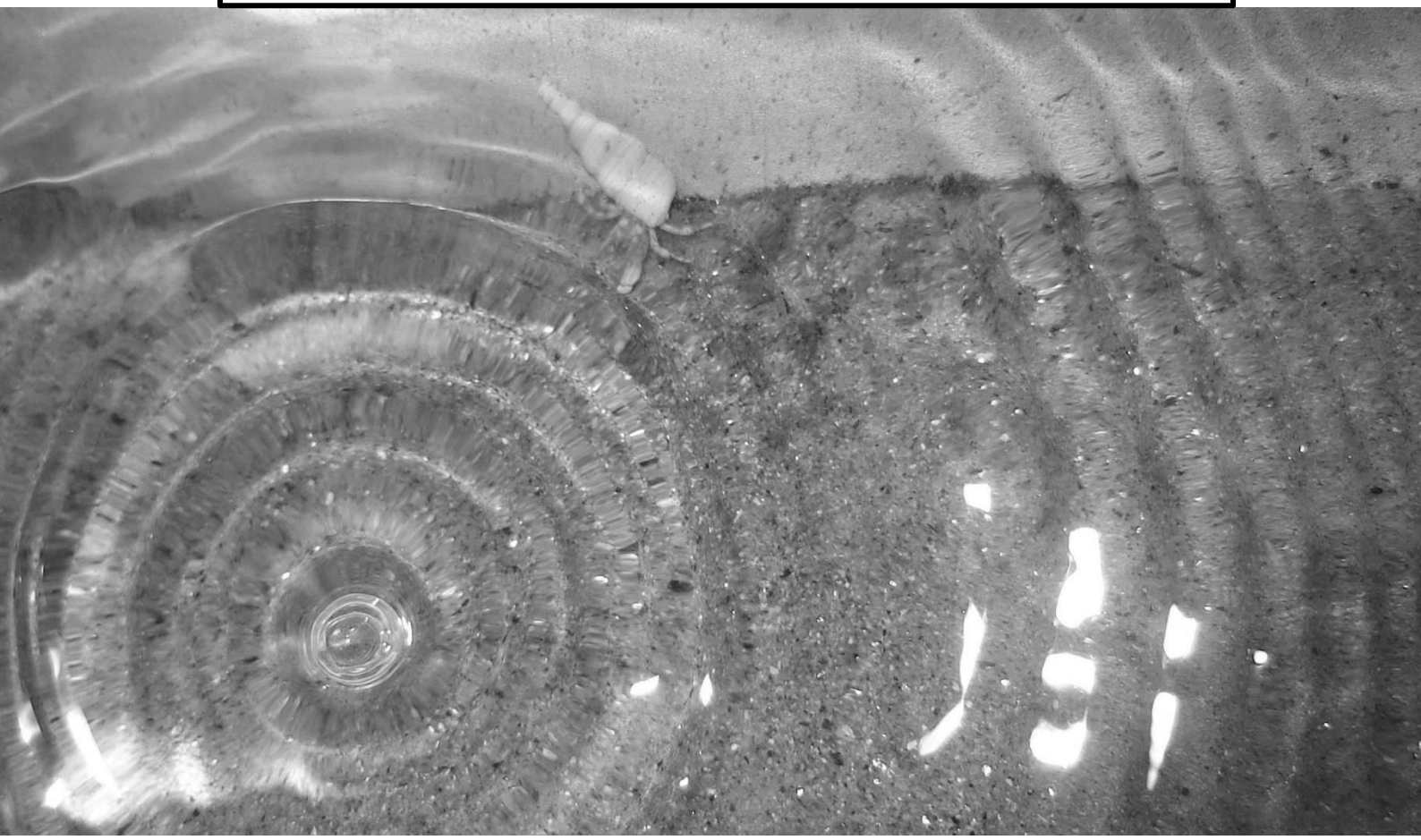

I.1. Nature and scope of this work

The coastal zone, broadly defined as the interface between land and ocean, represents a naturally dynamic area of high ecological diversity and critical economic significance. Coastal zones include beaches, estuaries, the adjacent land draining directly into the coastal waters, and the offshore, usually out to the edge of the (geomorphological) continental shelf (Stewart, 2009). According to Creel (2003), about half of the world's population lives within 200 kilometers of a coastline and, by 2025, that figure is likely to double. The population density in coastal zones is estimated to be about three times greater than the global average, which makes these areas increasingly subjected to human activities and interests. For these reasons, anthropogenic impacts in coastal areas are highly significant because of the extensive construction and polluting activities that cause important modifications on the coastal zones morphology, dynamics and ecosystems. Therefore, a detailed knowledge of coastal dynamics and of the geological and morphodynamic processes operating in these zones is crucial for an appropriate management of the natural resources, for risk assessment of the potential natural hazards and to mitigate environmental impacts. Furthermore, a deep understanding of the impacts caused by coastal activities, such as the opening and maintenance of navigation channels in port areas, coastal engineering defense works, and marine aggregate extraction, are crucial in the decision-making processes (Pacheco *et al.*, 2007).

This thesis investigates the morphodynamic evolution in two coastal zone areas with different local hydrodynamic conditions, affected by anthropogenic activities related to port engineering works and dredging activities. It focuses on two main aspects related to such activities: the evolution and recovery times of an offshore excavation for sand exploitation; and the dynamics of sandbank formation and evolution in an area affected by recurrent dredging operations and port inlet reconfiguration. For this purpose, two geographically and hydrodynamically distinct areas of the Portuguese coast were selected (Figure 1): an area offshore Vale do Lobo, Algarve, where the coastline is seriously affected by coastal erosion and where offshore sand exploitation took place for artificial beach nourishment; and an offshore area adjacent to the entrance of the Port of Aveiro, which has been subjected to several jetty reconfigurations in the past decades, and where recurrent dredging activities takes place for maintenance of the navigation channels.

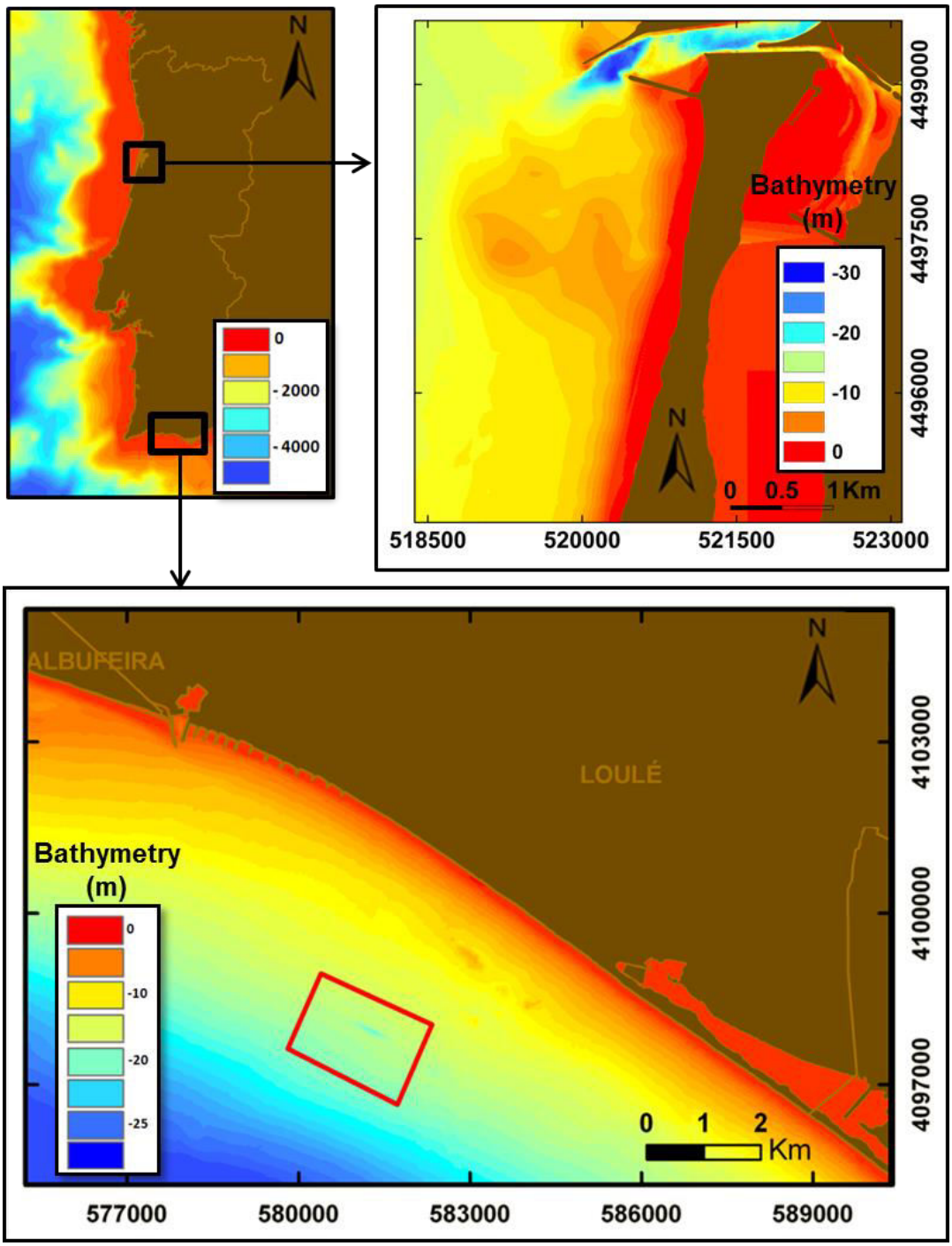

Figure 1. Geographic location of the two study areas: the area adjacent to the Barra of Aveiro, West Portugal, and the area offshore Vale do Lobo, Loulé, in the Algarve. Coordinate system in UTM Zone 29N, datum WGS84. Bathymetry referred to the Hydrographic Zero datum (ZH).

The Vale do Lobo area is situated in Loulé, in the South Portuguese coast (Figure 1) and has suffered serious erosion problems in the recent past (e.g. Magalhães et al., 2004; Teixeira, 2011). The intense anthropogenic changes due to tourism and urban development close to the sea, in particular, have had a strong negative impact on the shoreline, with a significant increase in coastal erosion (Magalhães et al., 2004).

In order to mitigate this intense coastal erosion, artificial beach nourishments have been carried out. The Vale do Lobo beach nourishment undertaken between October 1998 and January 1999 was the first case of an offshore sand exploitation in the Algarve, and approximately 700 000 m^3 of sand were extracted (Teixeira, 2011). In 2006, between March and May, a second artificial beach nourishment was performed, from a localized offshore sandpit excavation in the same area. In this second artificial nourishment, approximately 370 000 m^3 of sediments were dredged from the internal continental shelf off Vale do Lobo (Teixeira, 2011). In this thesis we focus our study on the evolution of the second offshore excavation, for which an adequate dataset of several bathymetric surveys covering the dredging area, prior to and after the excavation, was acquired and made available for this study (most of the bathymetric data was courtesy of the Administration of the Hydrographic Region of the Algarve - ARH Algarve). This bathymetric dataset allows a detailed monitoring and analysis of the sandpit evolution through time, making this an excellent opportunity for a case study.

The Aveiro area is located on the northwest Portuguese coast (Figure 1) and encompasses the Aveiro lagoon entrance, usually called “Barra de Aveiro”, and its near-shore shelf. The “Barra de Aveiro” represents the connection between the Aveiro lagoon, commonly known as the “Ria de Aveiro”, and the Atlantic Ocean. The present artificial connection was made possible by two jetties created in 1808, to prevent the inlet migration. Regular engineering works, including dredging activities for maintenance of the navigation channels and jetty’s structural maintenance, have maintained the lagoon entrance. The “Barra de Aveiro” and its adjacent continental shelf are subjected to a highly energetic wave climate, mainly from Northwest, which results in a strong southward littoral drift (Andrade *et al.*, 2002). The north jetty, in particular, due to its location and orientation, protects the Ria de Aveiro inlet from the waves, but becomes highly exposed and vulnerable to the wave action. The high-energy wave regime in this area and the intense sedimentary dynamics creates the need for frequent remedial and preventive engineering interventions, such as dredging operations and structural jetty maintenance or reconfiguration works. However, these interventions change not only the inlet dynamics, but also the dynamics of the entire lagoon (e.g. Silva and Duck, 2001; Araújo et al., 2008; Dias and Mariano, 2011; Dias and Picado, 2011) and of the adjacent coastal areas (e.g. Coelho et al., 2009). In this thesis we investigate the influence of recent engineering works on the formation and evolution of the external sandbank and on the sediment dynamics and the sedimentary and morphological evolution of the “Barra de Aveiro” and the adjacent near-shore shelf area. This study is based on a bathymetric, geophysical and sedimentological dataset, a significant part of which was acquired in the scope of this investigation.

I.2. Objectives

Morphodynamic, hydrodynamic and sedimentological studies are essential for understanding coastal systems and for properly managing coastal and marine natural resources. As stated above, the main objective of this thesis is to investigate the local morphodynamic evolution of two areas affected by anthropogenic activities related to port engineering works and dredging activities, located in two geographically and hydrodynamic distinct areas along the Portuguese coast: an area offshore Vale do Lobo, Algarve, and an area near the entrance of the Port of Aveiro. In particular, it is aimed to better understand the evolution and recovery times of offshore excavations for sand exploitation, a topic of growing importance for Portugal, and the dynamics and sandbanks formation and evolution associated with port inlets reconfiguration and dredging activities, also of significant interest for port authorities and administrations.

The specific objectives for each of these two study areas are listed below.

I.2.1. Vale do Lobo - Algarve

The main objectives of the study of the excavation site located offshore Vale do Lobo, Algarve, are to understand the evolution of the offshore sandpit through time and its impacts on the local sediment and hydrodynamics, and in particular to assess how the excavation is being filled by sediments, and to estimate the time needed for its recovery. Besides contributing to a better knowledge of the sedimentary dynamics of the study area, this work has implications for the assessment of impacts of future offshore dredging and aggregate exploitation in this area and elsewhere. The study of the evolution of offshore excavation recovery times is also important for future offshore mining impact assessment studies. Specific objectives are:

a) To follow and understand the sandpit evolution, based on bathymetric datasets acquired prior to and after the sand extraction (2006-2010).
b) To characterize the regional wave climate, namely the significant wave height, mean period, and mean wave direction in the study area during the period in analysis.
c) To estimate the sandpit recovery time from the observed and predicted filling rate.
d) To correlate the wave climate conditions, namely the storm events, with the sandpit dynamic evolution.

I.2.2. The "Barra de Aveiro" and the adjacent near-shore shelf

The main objective of the sedimentary and geophysical study of the "Barra de Aveiro" and near-shore shelf offshore Aveiro is to understand the sedimentary dynamics of a very dynamic area often subjected to a several engineering works. This work will hopefully contribute to a better understanding of the sedimentary dynamics of the study area, in particular as concerns the sandbank formation and evolution, and its results have implications for the impact assessment of future jetty reconfigurations and dredging operations in this area. Specific objectives are:

a) To understand the sedimentary and morphological evolution of this area based on bathymetric datasets acquired over time, based on both historical and recent bathymetric and geophysical data (1936 – 2013).
b) To investigate the sedimentary dynamics of the "Barra de Aveiro" and the near-shore shelf, in particular of the external sandbank, based on grain-size distribution of the sediments, and on the acquired geophysical data.
c) To assess the lagoon influence on the near-shore shelf.
d) To create a conceptual model of the present-day sedimentary dynamics of the "Barra de Aveiro" and near-shore shelf.

I.3. Data and methods

The study of the morpho-sedimentary evolution of the excavation area offshore Vale do Lobo in the Algarve, south of Portugal, was carried out based on 4 bathymetric surveys acquired prior to (March 2006) and after (May 2006, November 2008 and May 2010) the dredging operation carried out in May 2006. The methodology used was the following:

- The various bathymetric datasets were first inserted into a georeferenced GIS database (ArcGIS, ESRI), which allowed to estimate the sediment budget in the excavation pit and surrounding area, and to understand the sandpit morphology evolution through time, in particular its migration and replenishment.
- The estimation of the recovery time for the excavation area was calculated assuming a variable refilling rate, exponentially decreasing in time.
- The significant wave height (Hs), mean period (T), and mean wave direction (θ) datasets from the Faro directional wave buoy (operated by the Portuguese Hydrographic Institute), for the period 2006-2010, were used to characterize the wave climate in the study area during the period in analysis.

- The gaps identified in the wave dataset were filled in by direct interpolation of buoy data (weighted mean) for a time span of 6 hours or less; for longer gaps (more than 6 hours) the data were filled in using data from the numerical model WaveWatchIII (Tolman, 2009).
- The classification, quantification and characterization of the storm events were carried out for the periods of time between bathymetric surveys (from May 2006 to November 2008 and from December 2008 to May 2010) in order to assess the influence of such events on the mobilization of the sediments.
- The numerical simulations of the sediment dynamics and morphological evolution of the sandpit were performed with the morphodynamic modeling system MORSYS2D (Fortunato and Oliveira, 2004, 2007; Bertin et al., 2009), to better understand the morphodynamic evolution of the study area and to assess the conditions that generate significant sediment movement.

The datasets and methodology used for study of the morpho-sedimentary dynamics offshore Aveiro, were the following:

- 8 historical bathymetric maps from 1936 to 1985, were digitalized, georeferenced, vectorized and inserted into a georeferenced GIS database (ArcGIS, ESRI) in order to understand the long term evolution of the "Barra de Aveiro" and the adjacent near-shore shelf morphological evolution, mainly the sandbank sedimentary structure.

- 5 recent bathymetric datasets acquired from November 2010 to November 2013 were inserted into the same georeferenced GIS database (ArcGIS, ESRI) and were used for spatial computations to determine the recent evolution of the "Barra de Aveiro" and the adjacent near-shore shelf morphological evolution through time, specially the sandbank structure evolution, migration and volume.

- The sedimentary and geophysical superficial characterization of the "Barra de Aveiro" and the near-shore shelf area was performed using a set of 49 surface sediment grab samples and almost 40 sidescan sonar lines acquired in the study area in the scope of this work. The sedimentary data were analysed for grain size (based on the European Standard EN 933-1:2000) with the fine fraction <63 μm being separated by wet sieving and the sedimentary fraction >63 μm being dry sieved through a battery of sieves spaced ½ phi. The sidescan sonar data was processed using the SonarWeb software, from *Chesapeake Technology*, and the final mosaic obtained was inserted into a georeferenced GIS database (*ArcGIS*).

The integrated interpretation of all the available data allowed assessing the most important sedimentary, hydrodynamic and anthropogenic processes involved in the evolution of the "Barra de Aveiro" and its adjacent near-shore shelf.

More detailed information about the fundamentals of the methods applied and the methodology used can be found in Chapter III and in Sections IV.4 and V.4.

I.4. Structure of the thesis

This thesis is structured around 2 major questions:

1. What is the morphodynamic evolution through time of an offshore sandpit site after a localized dredging operation in an area with low hydrodynamism such as offshore Vale do Lobo?
2. How did the "Barra de Aveiro" and its adjacent near-shore shelf evolve through time in the past decades and how did the port engineering works affect its sedimentary dynamics and morphological evolution?

The thesis starts with this brief introduction (Chapter I) in which the nature and scope and the main objectives of the present work, as well as the most relevant data and methodology used in this investigation, are presented. Chapter II provides the geological, oceanographic and climatic setting of the two study areas. Chapter III describes the fundamentals of the methods used.

Chapters IV and V are structured in the format of research papers and address the two main topics of this thesis. Chapter IV describes the morphodynamic evolution of a sandpit site offshore Vale do Lobo, Algarve, resulting from the sand exploitation for the nourishment of the Vale do Lobo beach. In this chapter the sandpit evolution is analyzed and it is explained how it is being filled over time, in particular during storm events – the essentials of this Chapter have been published in the peer reviewed SCI journal *Coastal Engineering* (Gonçalves et al., 2014). Chapter V discusses the results of the investigation carried out at the Aveiro Harbor entrance and the adjacent near-shore shelf. This chapter includes a bathymetric, sedimentary and geophysical characterization of the study area, in particular of the external sandbank, and proposes a conceptual model of the most important sedimentary and hydrodynamic processes that act on the area. Chapter VI discusses, in general terms, the implications of these studies and addresses future research directions.

Chapter II. Geological, oceanographic and climatic settings of the study areas

II.1. Vale do Lobo - Algarve

Vale do Lobo is located in Loulé, central-eastern Algarve, on the southern Portuguese coast (Figure 2). The Algarve region has a typical Mediterranean climate, with dry summers and rainy winters. Its coast, surrounded by the Atlantic Ocean, is characterized by a mesotidal regime, with a tidal amplitude that can reach 3.5 m at spring tides, and a wave regime less than 1 m wave heights, mainly from southwest (inducing a longshore drift predominantly eastwards), with occasional periods with waves from the southeast (IH, 1994; ARH, 2012a). The western and central parts of the Algarve are dominated by cliff coasts under erosion rates that can reach a few meters per year in some places, being the main source of sediment for the longshore drift that feeds the Ria Formosa barrier island system (Figure 2; Correia et al., 1996).

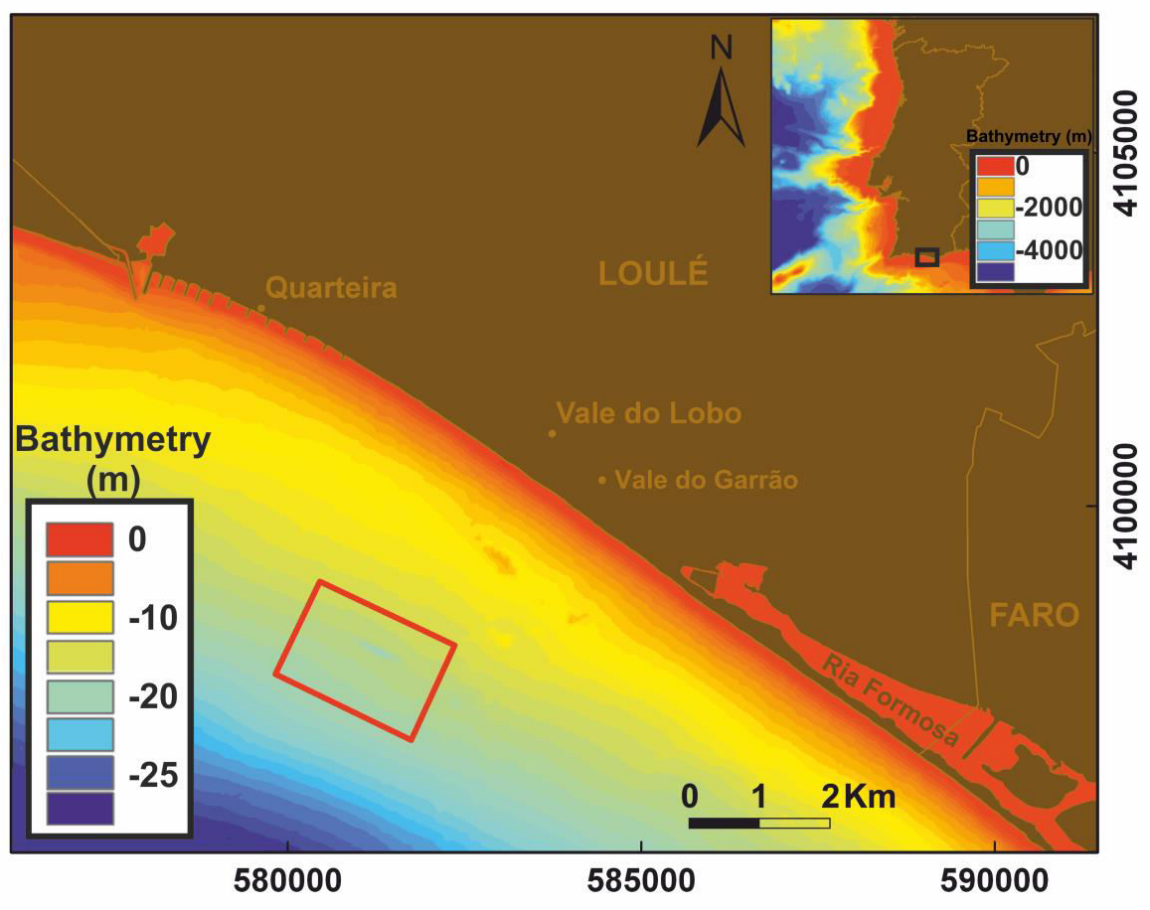

Figure 2. Study area offshore Vale do Lobo, Algarve, showing the location of the main excavation areas studied in this thesis (red rectangle). The bathymetry shown is from the Portuguese Hydrographic Institute (2001 survey), courtesy of the Administration of the Hydrographic Region of the Algarve - ARH Algarve. The inset in the upper right corner shows the location of the study area in mainland Portugal. Bathymetry from the GEBCO 2008 (2 miles spacing) digital bathymetric grid and referred to the Hydrographic Zero datum (ZH). Coordinate system in UTM Zone 29N, datum WGS84.

Vale do Lobo coast is characterized by the existence of a medium height (10 to 15m) active cliff and a narrow beach. The almost vertical cliff that extends from Quarteira, in the west, to the Vale do Garrão area, in the east, is shaped in poorly consolidated red sandstones from the Plio-Pleistocene (Manuppella, 1992). The cliffs in the Quarteira - Vale do Garrão coast are intercalated by sandy barriers that enclose the stream mouths of the area (Teixeira, 2011). This coastal area has been affected by serious problems of coastal erosion which have become evident from the extreme decrease of the beach width and the observed cliffs retreat (estimated by Correia et al. (1996) between 0.6 and 2 m/year in the Vale do Lobo area). The construction of the Vilamoura jetties (west of Quarteira; Figure 2) and the Quarteira groins in the 70's appears to have led to an interruption of the eastwards littoral drift, inducing serious erosional problems for that coastal sector and increasing the natural trend of coastline and cliffs retreat.

II.1.1. Geological setting

The Algarve geological province stands out as unique from both stratigraphic and morpho-tectonic points of view, due to its geographical location and lithological diversity. The Algarve lithological record spans from the Paleozoic to the Holocene (Figure 3). The Paleozoic rocks outcrop only in the northern area (Figure 3), consisting of flysch sequences of late Carboniferous age that were intensely folded and faulted during the Variscan orogeny (Hercynian orogeny; Oliveira, 1990; Manuppella, 1992). On top of this unit rests the Algarve Sedimentary Basin consisting of two superposed Mesozoic and Cenozoic basins (Terrinha, 1998). The two basinal cycles are separated by the Upper Cretaceous - Miocene unconformity (Figure 4), which corresponds to an important phase of the tectonic inversion and uplift of the Mesozoic rift basin (Kullberg et al., 1992; Terrinha, 1998).

The Mesozoic Algarve basin was formed by extensional tectonics from the Lower Triassic until the Upper Cretaceous, during the opening of the Tethys Sea and the Central Atlantic Ocean (Palain, 1976; Rey, 1983; Terrinha, 1998). Siliciclastic sediments are abundant in the Triassic, and limestones and marls are predominant from the Upper Triassic to the Cretaceous (Terrinha, 1998; Figure 4). The sedimentary depositional environments evolved from continental siliciclastics (fluvial red sandstones) in the Triassic, through littoral red shales, dolomites and evaporites in the early Lower Jurassic, to marine carbonates and marls with ammonoids during the Lower Jurassic (Terrinha et al., 1990; Ribeiro and Terrinha, 2007).

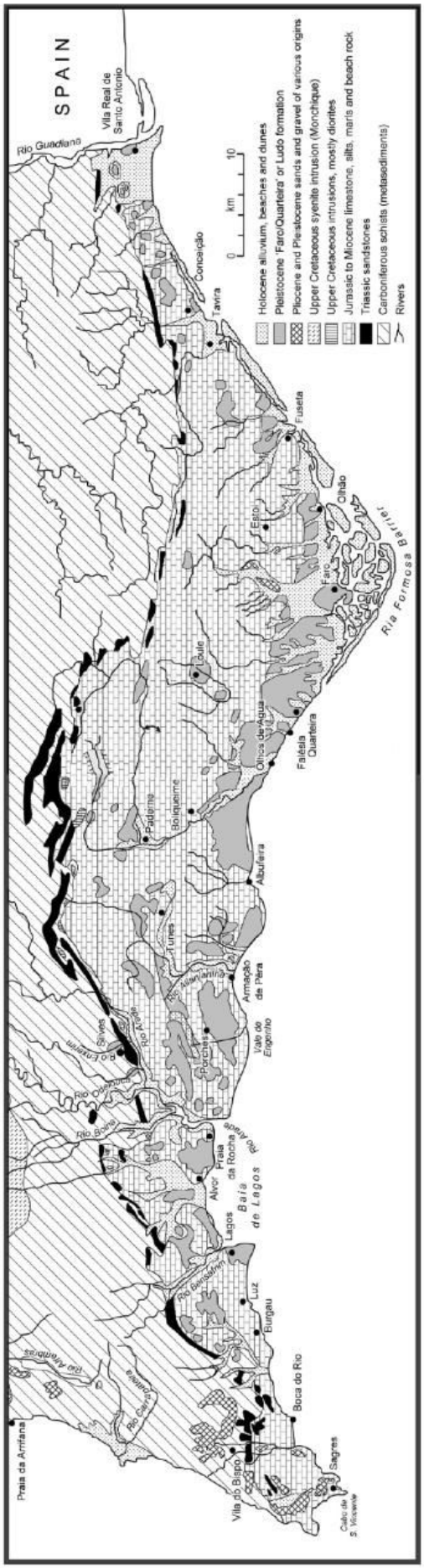

Figure 3. Simplified geological map of the Algarve Basin. For further details on one geological units see Figure 4 (modified from Chester, 2012).

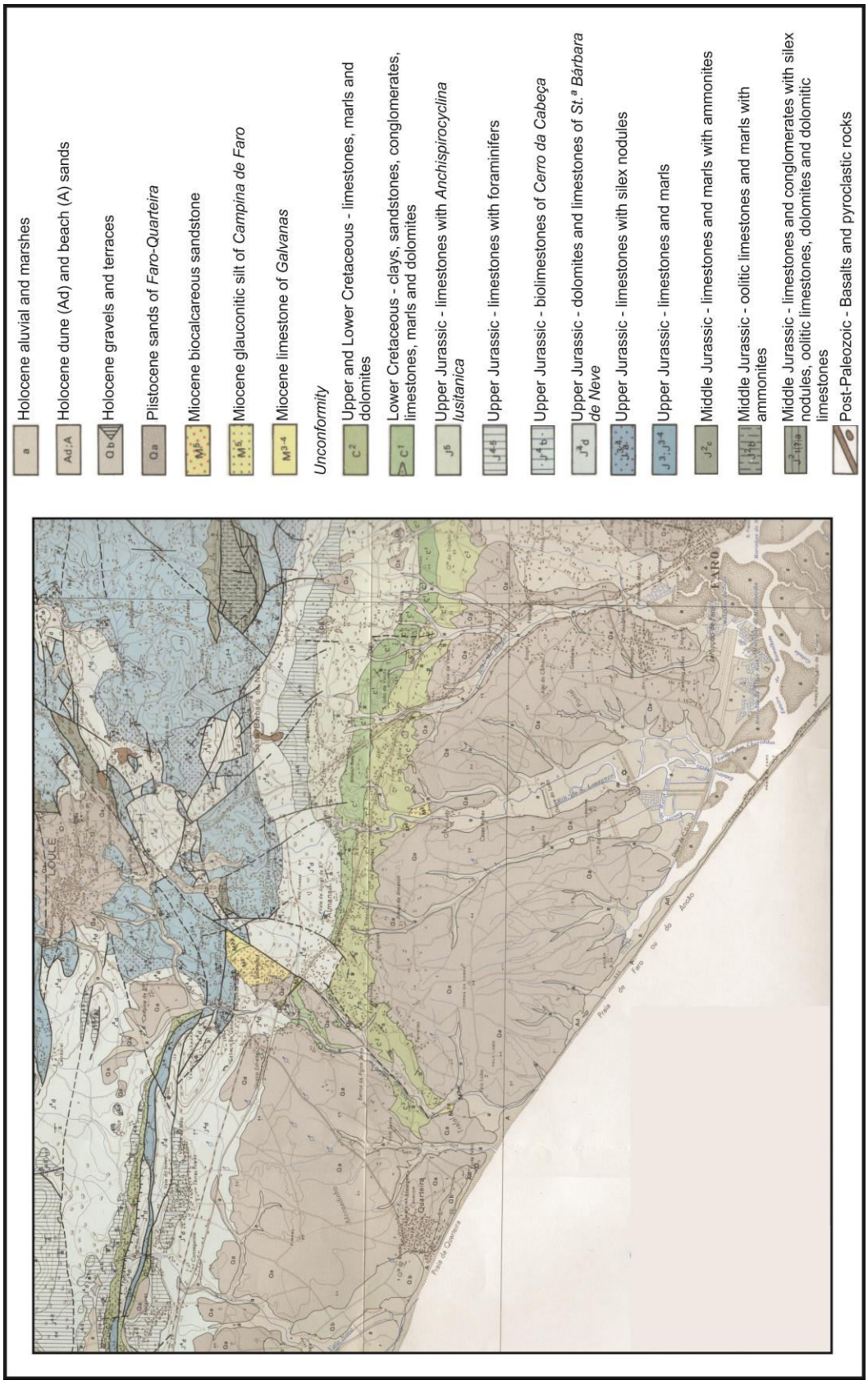

Figure 4. Geological map of the Vale do Lobo region (from the Geological Map of Portugal 53 A Faro 1:50000; Manuppella et al. 1985).

The Cenozoic basin is characterized by sandy limestones from the Lower and Middle Miocene, silts and sands from the Upper Miocene (Cachão, 1995; Cachão et al., 1998; Pais et al., 2000) and the Pliocene-Pleistocene Faro-Quarteira Formation, later renamed as Ludo Formation (Moura and Boski, 1999; Figure 3 and Figure 4). This sedimentary formation, dominant in the Vale do Lobo area, is mainly composed of red and feldspathic sand and gravel, with very variable amount of clays and a few rounded pebbles of quartz and iron nodules (Devereux, 1983; Manuppella et al., 1987). Mineralogical, sedimentological and paleontological studies (Moura and Boski, 1999; Pais et al., 2012) divided this formation into four units that were deposited under differing paleoenvironmental conditions (from the oldest to the youngest): the Monte Negro sands, the Quarteira sands, the Ludo sands and the Gambelas sands and gravels (Figure 5). The Monte Negro sands were deposited during the Pliocene marine transgression, that occurred across the Algarve Basin; later, in the Lower Pleistocene, the Quarteira sands were deposited under shallow continental shelf conditions. The Ludo sands mark the beginning of the fluvial deposition during a regressive phase. During the Middle and Upper Pleistocene, under semi-arid conditions, the Gambelas sands and gravels were deposited, with episodes of river incision (Moura and Boski, 1999; Pais et al., 2012).

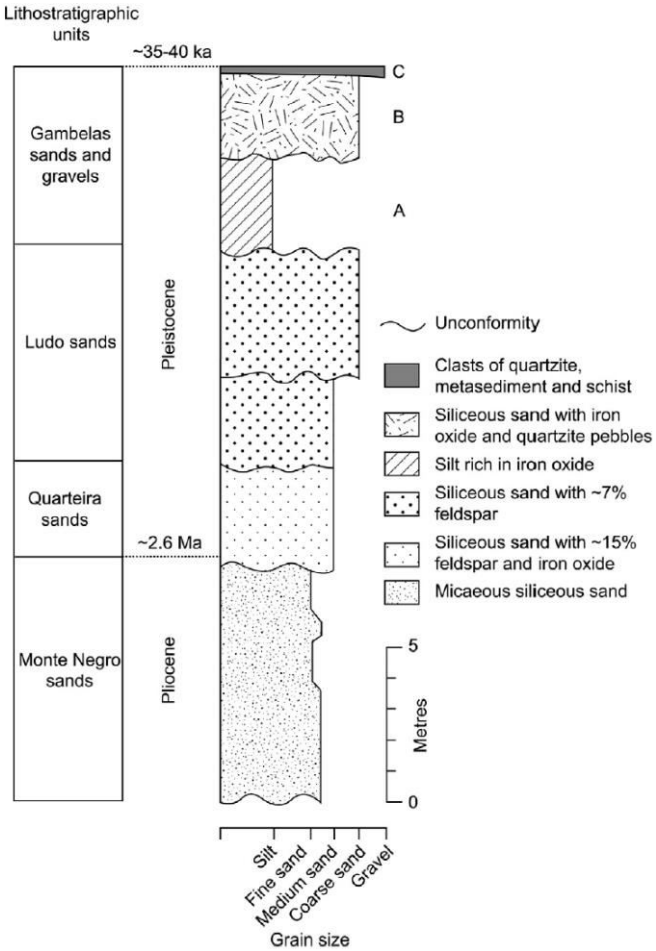

Figure 5. Ludo Formation stratigraphic profile showing its four main units (modified and simplified from Moura and Boski (1999) *in* Chester, 2012).

Offshore Algarve, the Meso-Cenozoic stratigraphic record spans from the Triassic to the Quaternary, with an important unconformity (correlated with the hiatus recognized onshore Algarve Basin) between the Upper Cretaceous and the Tertiary (see Figure 4; Pais et al., 2000). According to Roque (2010), the Neogene deposits offshore the Algarve basin consist of Lower Miocene limestones followed by calciclastic and siliciclastic sequences from the Middle/Lower Miocene, composed of sand, silt and mud. The Pliocene-Quaternary sequences are well developed on the continental shelf and consist of interchanging sand and mud layers; the most recent deposits (Holocene) are composed of sand and mud (Moita, 1986).

The Algarve coast presents a great variety of geomorphological forms and lithological types that become successively younger eastwards: north of Cabo de São Vicente the littoral is composed of Paleozoic formations; east of this cape the formations are gradually younger, of Jurassic, Cretaceous, Miocene and Plio-Quaternary ages (Figure 3). From Quarteira to Garrão (Vale do Lobo included) the coast is characterized by the existence of poorly consolidated red sandstones cliffs from the Plio-Pleistocene (Figure 3 and Figure 5; Manupella, 1992) intercalated by Holocene sandy barriers that, as mentioned before, enclose the stream mouths of that area (Figure 4). These soft cliffs are easily eroded by oceanic and subaerial processes. According to Correia et al. (1996) and based on a cliff retreat dataset from 1958 to 1991, between Quarteira and Vale do Lobo the mean retreat rates were estimated between 0.7 to 3.5 m/year for the Eastern Quarteira area, and 0.6 to 2 m/year in the Vale do Lobo area. Part of this eroded sediment remains in this sector as less mature sand deposits; however, a significant amount is incorporated in the littoral drift and redistributed eastward along the coast and adjacent inner shelf (Alveirinho Dias, 1988; Rosa et al., 2013). According to Correia et al. (1997), the amount of sediment supplied from cliff erosion along this coastal stretch to the littoral drift between 1983 and 1991 was ca. 36 400 m^3/year. The cliffs are, therefore, the main source of sand that feeds the longshore sediment transport (Alveirinho Dias and Neal, 1992; Correia et al., 1996) with a small fluvial direct contribution into this area of the Algarve coast (Rosa et al., 2013). Nevertheless, the discharges of the Quarteira stream might have had an important contribution in the past (Rosa et al., 2013). In fact, due to the construction of the Marina of Vilamoura and the regular dredging works, the Quarteira stream nowadays does not connect directly to the sea (Rosa et al., 2013).

Based on the rate of sediment loss in the Vale do Lobo beach nourishment between 1999 and 2006, Teixeira and Rosa (2009) estimated an annual eastwards net transport rate of 110 000 m^3/year. The depth of closure that controls the sediment exchange between the coastal system and the inner shelf area has been estimated at about 6 m to 10 m for this area (Andrade, 1990; Dolbeth et al., 2007), although it may vary locally.

The distribution of the superficial sediments in the Algarve continental shelf shows the presence of a great variety of sediment types and size classes, with the predominance of bioclastic sands and gravels, showing the deficiency of fluvial input into the shelf, and high silty-mud content, suggesting low energetic conditions (Moita, 1986). Alveirinho Dias et al. (1980) characterized the superficial sedimentary deposits on the Portuguese continental shelf based on the Nickless classification (Nickless, 1973; Figure 6). According to these authors, the Algarve continental shelf is a lot muddier than the western Portuguese coast, being essentially covered by sandy-silty-muddy sediments (Figure 6). The major deposits fall within the muddy class (blue color in Figure 6) and an important part corresponds to silty-muddy sand and gravel with more than 10% of silt and clay (white color in Figure 6). Two main gravelly deposits were identified (dark orange color in Figure 6): offshore São Vicente, at about 125 m water depth, and offshore Albufeira, at about 37 m water depth; both deposits have a significant bioclastic contribution. Gravelly sand sediments are found in the inner shelf of the central and eastern parts of the Algarve (light orange color in Figure 6). Between Albufeira and Faro, at depths that span from 13 to 26 m, the sand presents a mean gravel percentage of 20% and a mean silty-muddy fraction percentage of less than 3% (Alveirinho Dias et al., 1980). The biogenic contribution is dominated by mollusk shell fragments and spans from 20% (in average) in the sandy fraction to 32% (in average) in the gravelly fraction. The terrigenous component of these sandy sediments is poorly sorted and is mainly siliciclastic, with hyaline as the dominant quartz type (Alveirinho Dias et al., 1980).

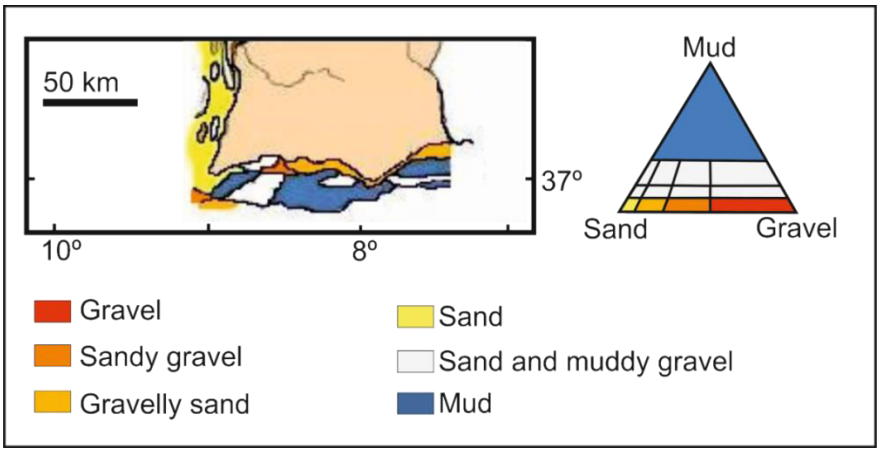

Figure 6. Distribution of the sedimentary deposits in the Algarve continental shelf based on the Nickless classification (Alveirinho Dias et al., 1980).

A similar characterization of the aggregate deposits in the Portuguese shelf was more recently performed by Magalhães (1999, 2003), also using the Nickless classification, but, according to this author, with an appropriate sampling grid for a more detailed study (Figure 7). Based on the textural characteristics, composition and

physiographic distribution of the sediments, Magalhães (1999) identified six main types of superficial deposits in the Algarve continental shelf:

(a) Littoral sands that cover the littoral domain parallel to the shoreline and reach about 20 m water depths. These consist of modern deposits that correspond to quartz medium to fine sands with variable sorting and predominant terrigenous composition (generally more than 70%). The gravelly fraction, with a minor extent, is mainly biogenic.

(b) Middle-shelf gravelly sands that form coarse to medium grained bioclastic sandy deposits, which occur at several meters water depth. The gravelly fraction is significant and mainly of terrigenous origin, and the fine fraction is almost absent. The characteristics of these deposits cannot be explained by the present-day supply and distribution conditions, and so they are classified as relict[1]-palimpsest[2] deposits.

(c) Middle-shelf sands, which only occur at the western and central part of the Algarve shelf and form medium to fine grained, poorly sorted, bioclastic sandy deposits with an insignificant gravelly fraction (predominantly bioclastic).

(d) Middle-shelf muddy sands and mud, that form modern poorly to moderately sorted deposits which occur in the eastern and central part of the Algarve shelf (east of Potimão canyon). These consist of fine to very fine grained bioclastic sandy deposits, with an important muddy fraction. The gravelly fraction, if present, has a predominant biogenic composition.

(e) Outer-shelf and shelf edge sands, that are bioclastic coarse grained sands, classified as relict deposits with a small modern component of foraminifera and muddy sediments.

The area offshore Vale do Lobo is mainly constituted by lithoclastic coarse sand (CS-1 in Figure 8). Nearer shore, the sediments consist in general of lithoclastic medium sand (grain size between 0.25 and 0.5 mm and identified as MS-1 in Figure 8); further offshore, lithoclastic gravelly sand (grain size higher than 2 mm; gS-1 in Figure 8) predominates (IH, 1985).

[1] Relict sediment is a deposit that consists solely of particles supplied to the shelf before the present.
[2] Palimpsest sediment is a deposit that mainly contains particles supplied to the shelf before the present, but also includes some particles now being supplied to the shelf.

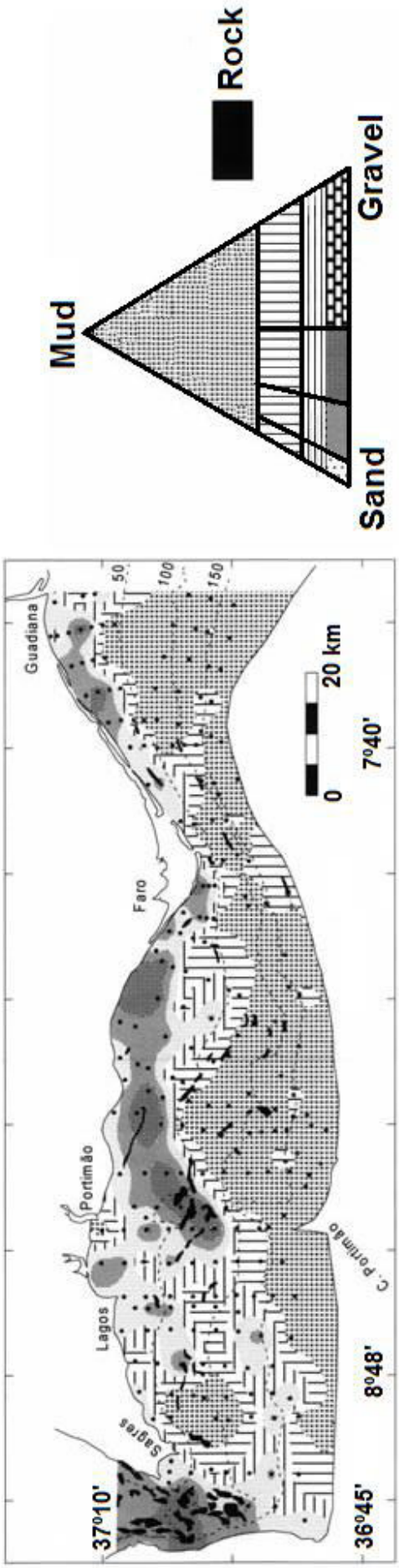

Figure 7. Distribution of the sedimentary deposits in the Algarve continental shelf based on the Nickless classification (Magalhães, 1999).

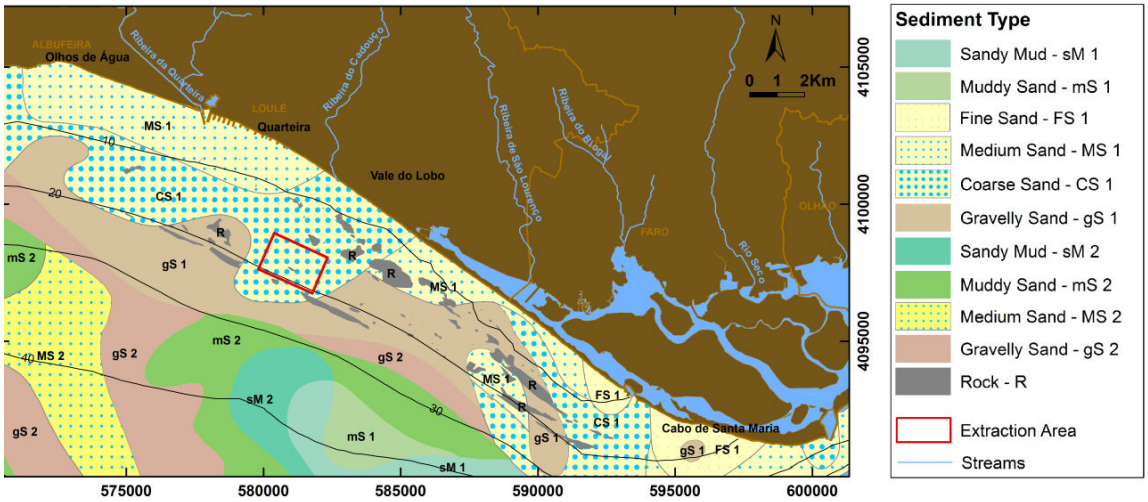

Figure 8. Superficial sediments in the study area, based on the Hydrographic Institute Map of Superficial Sediments (modified from IH, 1985), sidescan sonar data, *in situ* observations and manual sampling (60 cm deep) through scuba diving (Teixeira, 2011). The numbers 1 and 2 after the sediment type indicate if it corresponds to a lithoclastic or lithobioclastic sediment, respectively. Coordinate system in UTM Zone 29N, datum WGS84 and bathymetric contours are referred to the Hydrographic Zero datum (ZH).

The lithoclastic coarse sand identified in the excavation area (red box in Figure 8) presents a dominant grain size between 0.5 and 2 mm, with a fraction of sediments with a grain size higher than 2 mm that is lower than 15%, and is essentially quartzitic with a low percentage (<10%) of carbonates (Teixeira, 2011). Based on sidescan sonar data and *in situ* observations through scuba diving, Teixeira (2011) mapped the rocky outcrops offshore Vale do Lobo shown in Figure 8 (R - grey polygons).

II.1.2. Oceanographic and climatological setting

The Algarve coast is protected from the most dominant and important swell source, the North Atlantic. The storms generated in the North Atlantic have to travel long distances and circumvent the southern Portuguese continental shelf to reach the Algarve coast, which contributes to an important dissipation of storm energy and wave height. Therefore, the wave climate is characterized by prevailing moderate sea states, with less than 1 m significant wave heights (Hs) and less than 5 seconds mean period (IH, 1994). Incident waves from the W-SW are dominant, representing 71% of the occurrences, and incident waves from the SE, called "Levante[3]", represent 23% of the total occurrences (Costa et al., 2001). Based on 14 years of measurements of Faro

[3] Short period waves generated by SE Mediterranean wind.

buoy (1995 to 2009), Almeida et al. (2011) characterized the wave climate regime as smooth to moderate, with approximately 90% of the significant wave heights (Hs) lower than 2 m, and 5 to 10% of the wave heights reaching a 2.5 m to 3.5 m range (Figure 9).

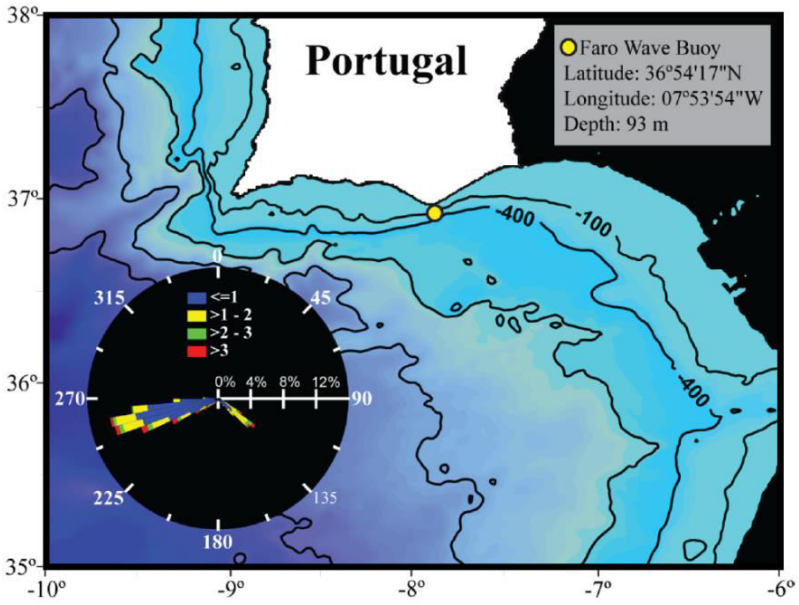

Figure 9. Wave rose diagram for the mean wave direction and the significant wave height in the Faro buoy based on 14 years of measurements (1995 to 2009) and map showing the location of the Faro buoy (yellow dot; Almeida et al., 2011).

Storm events in the area have been defined by Pessanha and Pires (1981) as events with offshore significant wave heights greater than 3m. The establishment of return periods for the main incident wave directions indicates that SW storms are more energetic than SE storms for the same return period (Pires, 1998). Furthermore, the shape of the central-eastern Algarve coast generates two different areas in terms of wave action exposure (Figure 9): the central Algarve coast (Faro buoy, western area) is more energetic because it is directly exposed to the dominant wave conditions (W-SW); and the eastern area (Faro buoy eastern area) is relatively protected from the more energetic waves, however it is exposed to the “Levante” waves. According to Almeida et al. (2011), the storm occurrences from the southwest quadrant in Faro area are dominant (70% of storm events), take place mainly during the winter and are responsible for the highest waves (the typical significant wave heights during storms is about 4 m, but it can reach 7 m). Southeastern storms occur when the Mediterranean easterly winds are strong (30% of storm events), mainly between October and May, with typical significant wave heights lower than 4 m and maximum values under 6 m (Almeida et al., 2011).

Almeida et al. (2011) investigated the historical variations and trends in storminess for the coast in South Portugal for the period 1952 to 2009 using both measured and modeled data (Figure 10). According to that study, the year with the maximum number of storms was 1963 and the minimum was 1954 (Figure 10a). The period from 1952 to 1965 was very stable with a yearly average of 5 storms and the period between 1973 and 1988 presented the lowest annual average number of storms, with many years having less than 3 storms (Figure 10a). From 1989 until 2005, the storm occurrence presents a sinusoidal trend, with peaks around 1989, 1996, and 2001 (Figure 10a). The years with a higher number of storms generally have higher number of stormy days, higher wave heights and higher maximum individual storm durations (Figure 10b and Figure 10c). No statistically significant linear trend was found by the authors for any of the storm characteristics (wave height, storm duration, and number of storms). The main pattern of historical storminess variability is an oscillatory variability in storm parameters, with peaks every 7 to 8 years on average (Almeida et al., 2011).

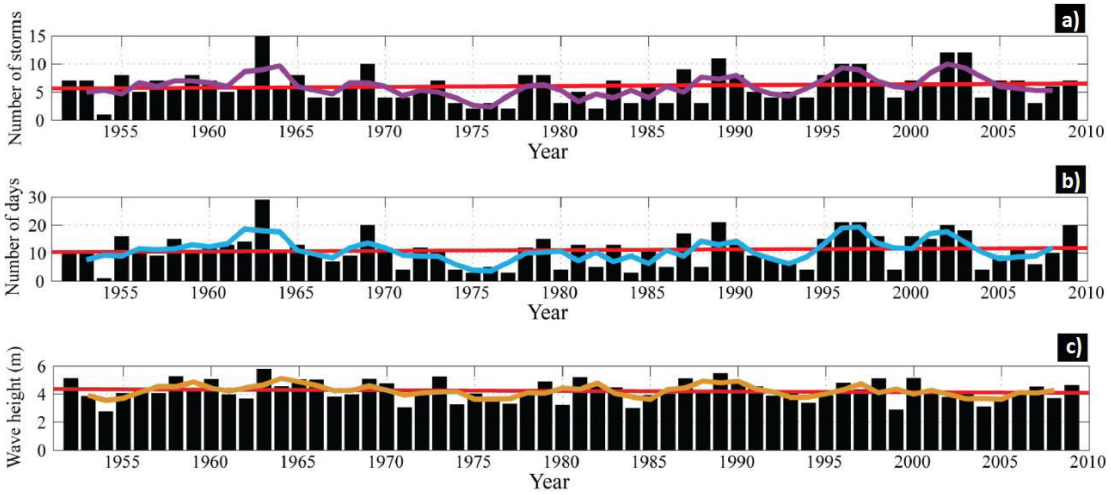

Figure 10. Variations in annual storm parameters and extreme wave height percentile: **(a)** histogram of annual number of storms with the moving average data (purple curve) and linear regression line (red line) on top; **(b)** histogram of the annual number of days with storms with the moving average data (blue curve) and linear regression line (red line) on top; **(c)** histogram of the annual $Hs_{99.8}$ with the moving average data (brown curve) and the linear regression line (red line) on top (Almeida et al., 2011).

The hydrodynamic regime in the Algarve coast is mesotidal and characterized by semi-diurnal tides with average ranges of 1.3 m and 2.8 m for neap and spring tides, respectively, although maximum ranges of 3.5 m can be reached (Rosa et al., 2013). According to Lopes et al. (2009), in the inner continental shelf off Vale do Lobo the tide is well polarized, mainly aligned along the N-S direction, and the maximum tidal currents can reach 0.15 m/s in Vale do Lobo area. The mean currents are strongly

correlated with the wind field: for calm wind conditions, the velocity intensity is insignificant; however, during the storms from the SW quadrant, the wind induces strong currents (~0.2 m/s) southeastwards (Rosa et al., 2011a, b).

The Algarve coast has a typical temperate climate – mesothermal - with hot and dry summers and rainy winters. During the year, the weighted mean air temperature spans from 10.7 ºC in January and 23.4 ºC in August (ARH, 2012a). The mean insolation is highest in July, varies from 340 hours in Sagres and 395 hours in Tavira, and has minimum values in January, spanning from 127 hours in Alvalade (Santiago do Cacém) and 162 hours of sun exposure in Faro (ARH, 2012a). The mean annual precipitation is between 600 and 700 mm, and 80% of that precipitation occurs in the wet season, from October to March (Figure 11; Teixeira, 2006). The dry season (April to September) contributes with about 131 mm of precipitation in average, value just slightly higher than the mean precipitation registered in December, the rainiest month (Figure 11; ARH, 2012a).

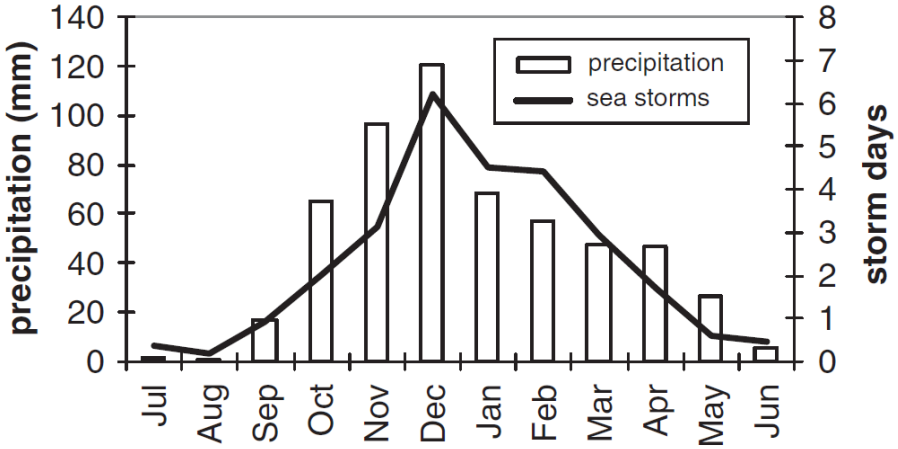

Figure 11. Mean precipitation between 1976 and 2004 monthly distributed at the Lagos meteorological station (Teixeira, 2006).

The wind is differentially felt according to the coast vicinity (mainly in the western coast), topography and altitude. In the western coast, more exposed to the Atlantic circulation regimes, the winds are mainly from N-NW, followed by winds blowing from north, called “Nortada”. The influence from the northern winds is reduced eastwards, particularly if there are morphological and topographic structures. In the southern coastal areas, the mean wind velocity (monthly distributed) spans from 4.9 km/h in Quarteira meteorological station and 20 km/h in Sagres. The mean wind velocity is higher during the spring and summer months, due to the significant role of the temperature on the sea winds and “Nortada” winds, conditioning the atmospheric

circulation regime. In Faro (Figure 12), the mean wind velocity (monthly distributed) varies from 12.7 km/h in November and almost 16 km/h in May (ARH, 2012a).

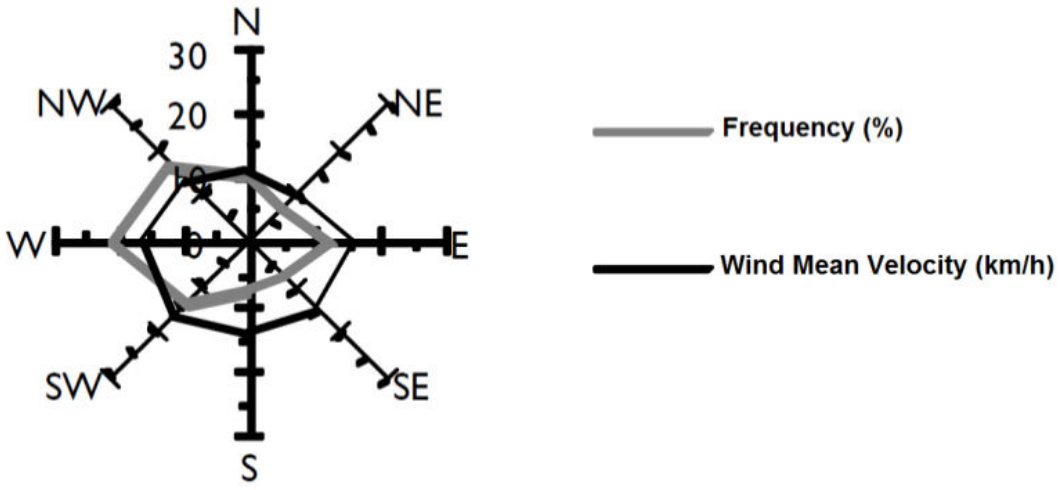

Figure 12. Wind rose diagram for the annual mean wind direction and velocity for the Faro meteorological station (ARH, 2012a).

II.2. The "Barra de Aveiro" and the adjacent near-shore shelf

The "Barra de Aveiro" represents the communication of the "Ria de Aveiro" barrier-lagoon system with the Atlantic Ocean by an artificial inlet (two offshore-directed jetties) built in 1808 (Figure 13). Located in the northwest Portuguese coast, the "Ria de Aveiro" is geologically very recent; its formation started about a thousand years ago when a sand spit started to proceed southwards due to the alongshore sediments transport, isolating the estuary of the Vouga river from the coastal ocean (Martins, 1946; Girão, 1951; Abecasis, 1955; further historical information on the formation of the Aveiro lagoon and the evolution of the "Barra de Aveiro" is included in section V.3).

The "Ria de Aveiro" is composed of long and narrow tidal channels, tidal flats, salt marshes and supra-tidal sand isles, and presents a maximum width of 10 km and a length of 45 km along its longitudinal axis, covering a variable area of 83 km^2 at high tide, that decreases to 66 km^2 at low tide, both during the spring tides (Dias and Lopes, 2006). The lagoon has four main branches connected to its entrance: the Mira channel, 20 km long, south directed, parallel to the coastline; the S. Jacinto channel, 29 km long, north directed, parallel to the coastline; the Ílhavo channel, 15 km long, southeast directed; and the Espinheiro channel, 17 km long, northeast directed (Dias, 2001). The

hydrodynamic and morphodynamic pattern of the lagoon is mainly imposed by tides, whose influence can be felt even upstream into the lagoon (Dias et al., 1999). According to Lopes and Dias (2007), the estimated tidal prism in the lagoon is 136.7×10^6 m^3 for the maximum spring tide and 34.9×10^6 m^3 for the minimum neap tide. Comparatively, the rivers have a smaller contribution in terms of water inputs (about 1.8×10^6 m^3 during a tidal cycle); however they have a long-term influence in the residual transport (Lopes and Dias, 2007). The lagoon is supplied in freshwater by the Vouga hydrographic basin that corresponds to a drainage network of 3 680km^2 that flows annually in average 2 609 hm^3 (~82m^3/s) of freshwater (ARH, 2012b).

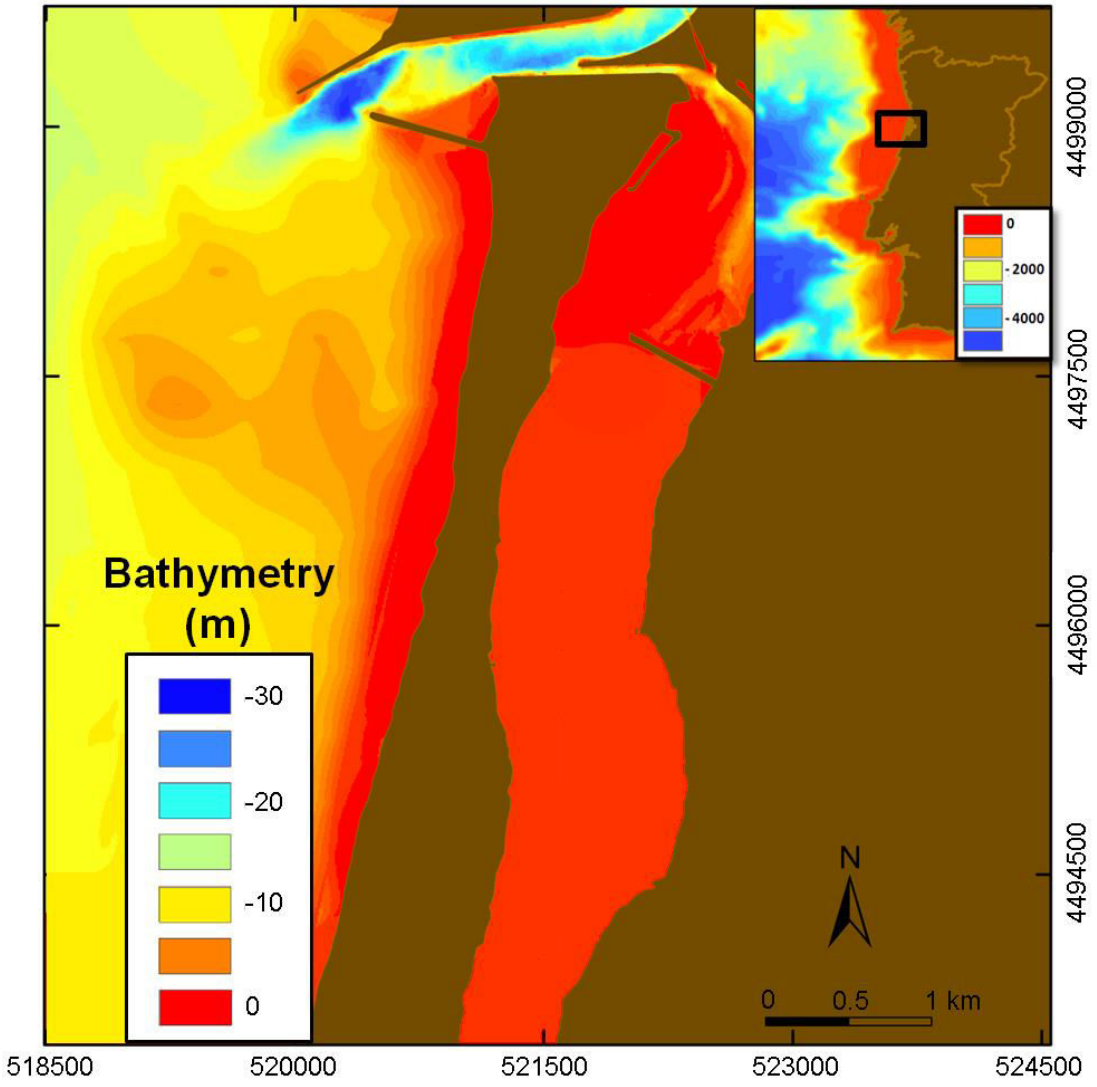

Figure 13. Study area offshore Aveiro, which includes the "Barra de Aveiro" and the adjacent near-shore shelf. The bathymetry is from the Aveiro Port Authority (June 2011 survey). The inset in upper right corner shows the location of the study area in mainland Portugal. Bathymetry is from the GEBCO 2008 (2 miles spacing) digital bathymetric grid and referred to the Hydrographic Zero datum (ZH). UTM coordinates - Zone 29N/WGS84.

In general, the depths in the lagoon are smaller than 3 m and most frequently close to 1 m, mainly at the upper reaches. The deepest areas can be found in the inlet navigation channel, essentially in some areas close to the lagoon entrance (see Figure 13), where the water depth can reach values of the order of 30 m, dug by the strong tidal currents of over 3 m/s (Dias et al., 2000, 2003; Lopes and Dias, 2007). According to Plecha et al. (2010), the average depth of the lagoon entrance area, including the inlet navigation channel and the ebb-delta is between 5 and 10 m. The strong tidal forcing is responsible for a high mixture of the fresh and salty water masses, making this lagoon, in general, a well-mixed system, although areas close to the lagoon inlet present some vertical stratification patterns in salinity and water temperature. The longitudinal salinity and temperature gradients are significant: close to the inlet the water mass presents high salinity levels and low temperature, due to the seawater input; upstream into the lagoon the salinity decreases and the temperature rises (Dias et al., 1999).

The inlet of the "Ria de Aveiro" lagoon lies in a sandy coast subjected to a highly energetic wave climate, typical of the western Portuguese coast, which leads to a strong littoral drift, both with south and north directions. In average conditions, there is a net rate of over 1×10^6 m^3 per year southwards (Castanho et al., 1974; Vicente and Clímaco, 1986).

II.2.1. Geological setting

The "Ria de Aveiro" lagoon is a Holocene sedimentary basin located in the northern section of the Mesozoic Lusitanian basin, which overlies the Hercynian Massif mainly composed of folded, thrust and metamorphosed igneous and sedimentary rocks of Precambrian and Paleozoic age. The Lusitanian basin, located on the central part of the Iberian Occidental Margin, is approximately 200 km long in the NNW-SSE direction and 100 km wide, occupying an area greater than 20 000 km^2, of which 2/3 outcrops onshore and the remaining is immersed in the continental shelf (Kullberg et al., 2013). The formation and geometry of this basin was controlled by the extensional events related to the opening of the North Atlantic Ocean during the Mesozoic, when sediments supplied by the surrounding continental areas, both from the high continental area to the east and from an elevated area to the west (of which the granitic Berlengas and Farilhões Islands represent nowadays the only testimony) filled the basin (Wilson, 1988; Kullberg et al., 2013).

Wilson (1988, 1989) identified four unconformities in the Mesozoic sedimentary sequences that may be related to different rifting stages. The first rifting stage occurred during the Late Triassic to the Middle Jurassic, when the deposition of

fluviatile siliciclastics and evaporites in fault bounded basins occurred. The regional hiatus that followed the Middle Jurassic is related to the opening of the central Atlantic Ocean. The second extensional phase occurred during the Late Jurassic and Early Cretaceous when lacustrine carbonates were succeeded by marine carbonates, within which facies distributions indicate contemporaneous movement of salt structures and faults. An influx of siliciclastic sands dominates the succession in the north and east part of the basin, replaced southwestwards by carbonate deposits. The third and fourth sequences, respectively, from the Lower Cretaceous and from the Lower to the Upper Cretaceous, show a similar facies distribution to the end of the previous sequence, with fluviatile sands in the north being replaced southwards by marine marls and limestones. According to Wilson (1988), relative sea-level changes rather than relative tectonic movements were probably the major controlling factor on the facies distribution of these two sequences.

In contrast to the Mesozoic, the Cenozoic in the Iberian Peninsula is dominated by compressional deformation related to the Pyrenean and Betic orogenies (Garcia Mondejar, 1988 *in* Andeweg, 2002; Wilson et al., 1989). The start of closure of the Bay of Biscay and the migration of the Pyrenean zone to the west caused the inversion of the Mesozoic extensional basins (Garcia Mondejar, 1988 *in* Andeweg, 2002). During the Pyrenean compression, the sedimentation in the Lusitanian basin was controlled by pre-existing late Hercynian basement faults, often amplified by halokinesis, sometimes leading to the formation of diapirs that pierced the entire sedimentary cover (Alves et al., 2003). Sedimentation during the Paleogene consisted mostly of sands and conglomerates, while in the Neogene, sedimentation evolved to shallow marine clastic and carbonate deposits due to subsidence and marine transgression. In the North Lusitanian basin, Pliocene sedimentation recorded multiple transgression and regression cycles. Several erosional surfaces developed during the Quaternary, and deposition consisted mainly of coarse sand and gravel, often affected by mild neotectonic movements (Rocha, 1993; Granja et al., 1999; Dinis, 2004).

In the Aveiro region the Hercynian basement consists of micaschists and schists from the Proterozoic (Precambrian), with occasional gneisses and migmatites of the same age, and granitoids from the Paleozoic in the northern part of the Aveiro region (Figure 14). These units are exposed along a NNW-SSE trend and close to the Porto-Tomar fault, east of the Ria de Aveiro. The bedrock dips westward and it is affected by several N-S and NNE-SSW faults that form a system of horsts and grabens (Figueiredo, 2002; Duarte et al., 2007).

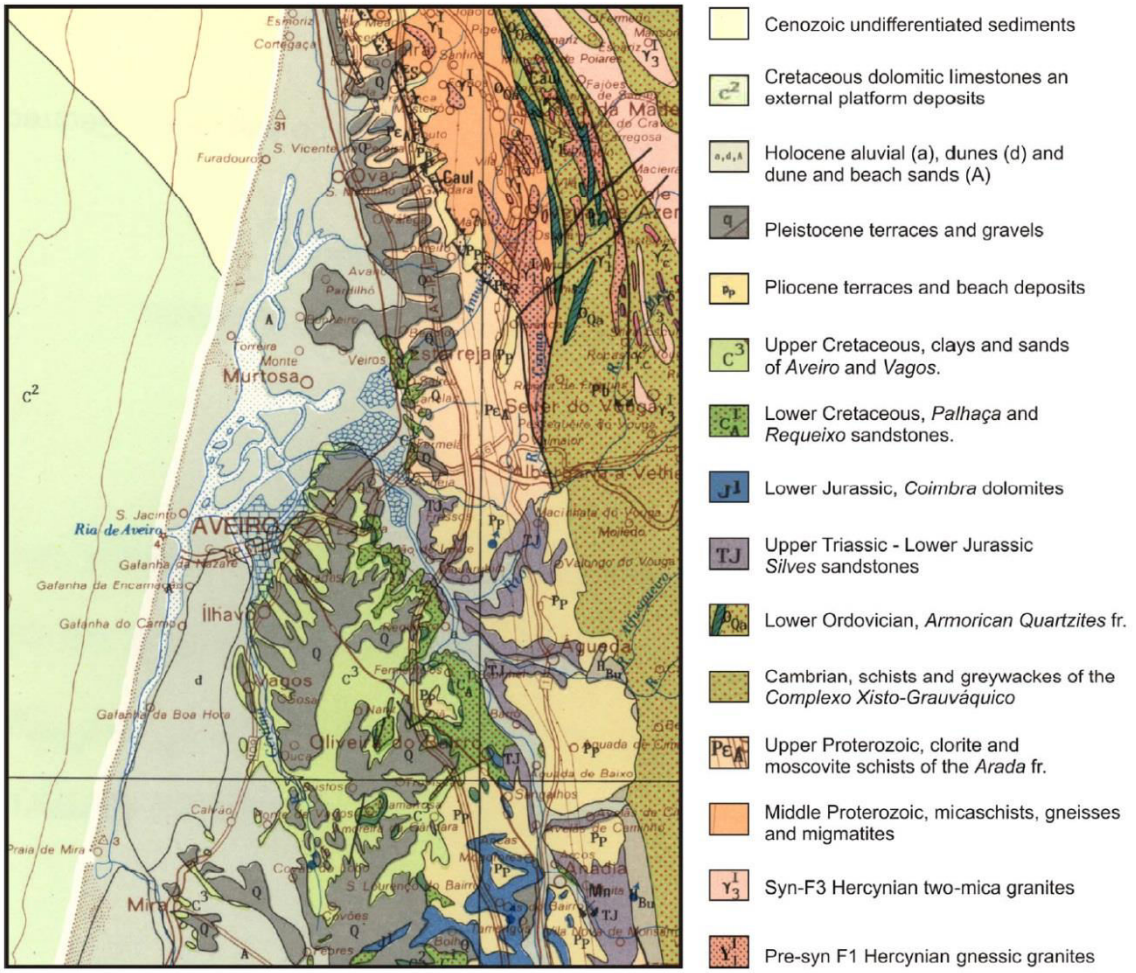

Figure 14. Geological map of the Aveiro region (from the Geological Map of Portugal 1:500.000; Oliveira et al., 1992).

In most of the Aveiro region, the Hercynian basement is overlain by a discontinuous sequence of Mesozoic sedimentary formations, with ages ranging from the late Upper Triassic to the Upper Cretaceous (Figure 14; Teixeira and Zbyszewski, 1976; Rocha, 1993; Rocha and Gomes, 1995). These include the following formations:

- The Triassic sandstone formation ("Arenitos de Eirol"): red sandstones of late Upper Triassic age that outcrop along the eastern part of Aveiro region between the villages of Angeja and Requeixo, and whose origin is related to the weathering of rocks of the Hesperic Massif (mainly biotite and chlorite schists and granitoids) and the deposition of the sediments in a littoral platform;
- The Early Lower Jurassic sandy marls ("Margas da Dagorda"): brown-reddish sandy marls formed in a littoral marine environment with lagoon characteristics that occur in the east and southeast part of the Aveiro region;

- The Lower Jurassic marly dolomitic limestones ("Camadas de Coimbra"): greyish marly sandstones, sandy marls or marly dolomites, whose origin is related to the deposition of terrigenous sediments eroded from a nearby continental margin;
- The Mid Lower Jurassic marly limestones ("Camadas de S. Miguel"): greyish marly sandstones or sandy marls, deposited in a low hydrodinamic marine environment under transgression conditions;
- The Late Lower Jurassic sandy marls and marly sands ("Margas de Eiras"): marl formation deposited in a very low hydrodynamic and shallow marine environment, with mostly anoxic conditions, typical of a closed lagoon;
- The Lower Cretaceous sandstone ("Areias da Palhaça"): brown-yellowish medium to coarse sands, usually interlayered with clay levels or coarse sandy levels with pebbles, increasing clay and carbonate contents towards the top of the unit. It was probably deposited in a flooding deltaic plain with a complex network of fluvial channels;
- The Early Upper Cretaceous carbonate formation ("Calcários de Mamarrosa"): marly limestones, marls and fine marly sandstone deposited during the Cenomanian transgression, with the marine influence more evident in the coastal and central parts of the basin, where the dominant clay minerals indicate shallow marine waters with low hydrodynamism.
- The Early Upper Cretaceous micaceous sandstone ("Areias do Furadouro"): Coarse to medium micaceous sandstones with some marly-clayey levels deposited during the Turonian in a predominantly littoral environment;
- The Mid Upper Cretaceous sandstone formation ("Areias de Oiã"): clayey sandstones and sandy clays formed under a fluvial continental environment, due to a regressive movement of the sea during the Upper Turonian until the Lower Coniacian;
- The Mid Upper Cretaceous sandstone formation ("Areias de Verba") – grey-brownish fine to medium clayey-marly sand interlayered with marls and marly clays deposited under a transgression period;
- The Late Upper Cretaceous marly clay formation ("Argilas de Aveiro") - greyish marly clays, occasionally with an important content of sand and layers of marly limestone, deposited during a long regression period under temperate climate. This unit is roughly uniform in the Aveiro region, with thicknesses over 150 m near the coast; however it is not present in the east where the uplift led to its erosion.

The Mesozoic sediments are overlain by Plio-Pleistocene and Holocene deposits. The deposits of Plio-Pleistocene age are old beach deposits and fluvial

terraces composed mainly of medium to coarse sands with rolled pebbles, overlain by a clay and clayey sand cover (Teixeira and Zbyszewski, 1976; Rocha, 1993). The Holocene deposits are mostly fine to medium sands divided into three different litho-stratigraphic units (see Figure 14; Teixeira and Zbyszewski, 1976; Rocha, 1993):

- Recent alluvial deposits – composed of sediments that range from clay and fine sand to coarse sand and gravel; their fluvial-marine origin is related to sediments transported downstream and by tidal currents;
- Beach sands – medium sand deposits, 15 m height in maximum, that form the littoral sand spit and separate the ocean from the lagoon;
- Sand dunes – Aeolian sands that form the active dunes parallel to the coast.

According to Duarte (2009), there are accumulations of gas (biogenic methane) both in the Holocene sediments and in the Mesozoic bedrock of marls and clays, with most of the gas probably generated in Holocene lagoon sediments. Nevertheless, the location and geometry of fluid escape features in some channels follows the fracture pattern that affects the Mesozoic bedrock, indicating a possible deeper source of gas and that these fractures function as preferential pathways for fluid migration and exert a structural control on the gas occurrences in the “Ria de Aveiro” (Duarte et al., 2007).

The nature and the distribution of the bottom sediments in the Aveiro lagoon channels are a combination of medium to fine sands with a variable content of finer particles (silt and clay), which increase upstream with the distance from the lagoon mouth. There are also some differences between the north and the south parts of the lagoon with the fine cohesive particles and sands, mainly, composing the northern channels, whereas the southern channels are composed mostly by coarse sediments and sands. In general, the grain size composition of the lagoon bottom sediments is distributed between 2 to 90% of sands, 10 to 80% of silts and 0 to 30% of clays, with the presence of shells in the main channels of the “Ria de Aveiro”, which indicates the ocean influence inside the lagoon. The inner zone of intertidal flats integrates, from top to bottom, medium to fine sand, mixed clay silty sediments, and pelitic flats composed mainly by clay sandy sediments (Rocha et al., 2000).

According to previous studies, the bottom sediment in the inlet area is mostly composed of medium sand (85%), followed by 9% of coarse sand, 5% of fine sand, and 1% and lower of very coarse and very fine sand, respectively (Freitas et al., 2005; Plecha, 2011). Spatially, the sediment distribution is characterized by coarser sediment next to the north jetty, which corresponds to deeper and eroded zone, decreasing in size southeastwards, with the finer sediment being located close to the south jetty and the beach located between the central dike and the south jetty, which correspond to shallow and accretion zones, characterized by reduced flow velocities (see Figure 15; Martins et al., 2007; Plecha et al., 2010; Martins et al., 2011).

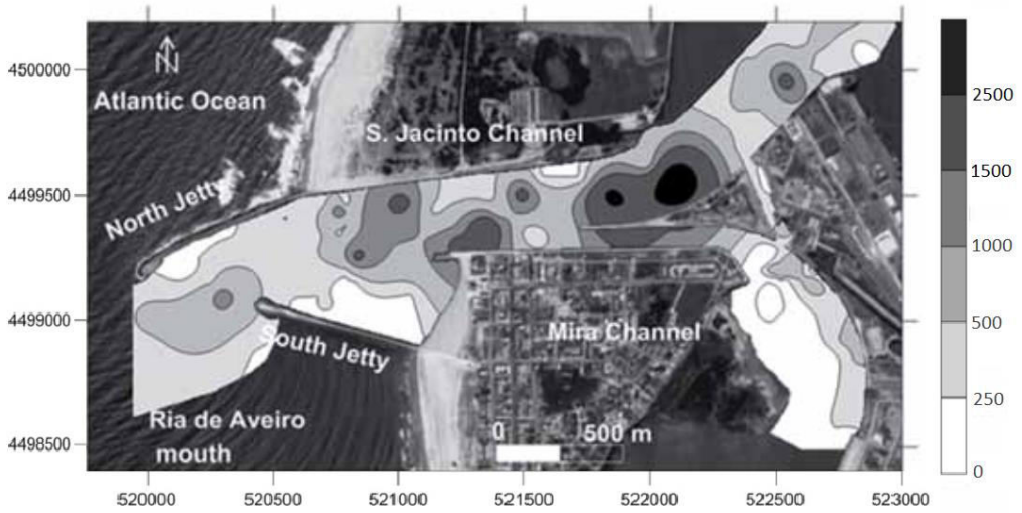

Figure 15. Sediment median grain size (in µm) distribution map (Martins et al., 2011). Coordinate system in UTM Zone 29N, datum WGS84.

The sediment transport in the lagoon is essentially dominated by the tidal currents, fluctuating with the tidal amplitude and phase (Abrantes et al., 2005; Lopes et al., 2006), and showing a temporal and spatial variability. The mineral composition is a function of the fluvial contribution, the bottom composition, and the oceanic input (Abrantes et al., 2005; Lopes and Dias, 2007; Martins et al., 2011). According to Plecha et al. (2010), in the inlet and adjacent areas the sediment balance is also determined by the wave regime. The transport of sediments in suspension is in general greater during the winter, due mainly to severe climatic conditions, higher wind and wave induced current velocities, greater wind stress and larger availability of sediments, essentially supplied by fluvial inputs (Martins et al., 2011). Other variability in the sediment transport is related to tides; in fact, during the ebb and low tide the suspended sediment concentrations are predominantly higher when compared to flood and high tide periods, leading to a greater flux of sediments transported seawards rather than landwards (Martins et al, 2011). According to Martins et al. (2011), the Aveiro lagoon exports to the continental shelf mostly muddy sediments, composed essentially of quartz and phyllosilicates. Strong tidal currents, mostly during spring tides and under strong wind stress, increase the suspended sediment concentrations along the main channels, due to the increase of the bottom erosion and the advective transport of sediments (Lopes et al., 2006). Thus, the higher budget of sediments delivered from the lagoon to the shelf can be supplied by the rivers contribution during flood events or by remobilization of the bottom sediments by tidal re-suspension. According to Martins et al. (2011), the Aveiro lagoon acts simultaneously as a system that supplies fine particles to the shelf, transported mainly

in suspension, and as a receptor of coarser particles supplied by the fluvial and littoral systems.

The Aveiro continental shelf is narrow, approximately 40 km wide, and is characterized by a gentle sloping surface and bathymetric lines roughly parallel to the coast line (Figure 16). This moderate slope is interrupted by rocky outcrops, such as "Pontal da Cartola" and "Pontal da Galega" (see rocky outcrops in Figure 16), which represent Cretaceous carbonate complexes, and by some geomorphological features, such as the Aveiro Canyon (Figure 16), and is delimited westwards by the shelf-break at depths of around 160 m (Vanney and Mougenot, 1981). There are several mechanisms that play an important role in the continental shelf offshore Aveiro, such as nearshore processes, waves, density gradients due to the lagoon discharges, oceanic fronts, shelf/slope exchanges, wind stress and topographical effects; however, the relative significance of some of these agents may vary over a short time scale (Peliz et al., 2002). The distribution of the sediments on the continental shelf is mainly controlled by the characteristics of the sediment supply and the oceanographic conditions (waves, storms and ocean currents). According to Abrantes and Rocha (2007), terrigenous inputs are the major influence on the clay mineralogy of the surface sediments of the Aveiro shelf region, whose composition can be explained by detrital derivation from adjacent continental formations, dominated by granites and schist-greywakes. The direct input of clay minerals from land on the shelf is led by rivers discharge, the Douro River being the main source of sediments, with approximately 8 500x10^3 m^3 of transported sediments per year, and the Ria de Aveiro lagoon contribution much less significant, with approximately 200x10^3 m^3 of transported sediments per year (Alveirinho Dias, 1987; Abrantes and Rocha, 2007; Martins et al., 2012). The small contribution of the Vouga River leads to the conclusion that the majority of the Aveiro shelf sediments are supplied by the rivers located to the North, mainly the Douro River. However, the fluvial contribution has been decreasing since the last century due mainly to anthropogenic actions (e.g. dam construction, sand and gravel exploitation, dredging operations), leading to the increase of the coastal erosion, essentially beaches and dunes, in order to compensate for the sedimentary deficit (Ferreira and Alveirinho Dias, 1992).

The superficial sediments of the Aveiro shelf area are dominated by sand particles (average 78%), with a fine fraction (<63 μm) content generally low (3% silt and 2% clay in average), increasing from the coast westwards (Figure 16a). A gravelly fraction occurs mainly in the middle and outer shelf (Figure 16b), consisting of relict sediments deposited during the last glaciation (Alveirinho Dias, 1987; Alveirinho Dias et al., 1980; Abrantes, 1994; Alveirinho Dias et al., 2000).

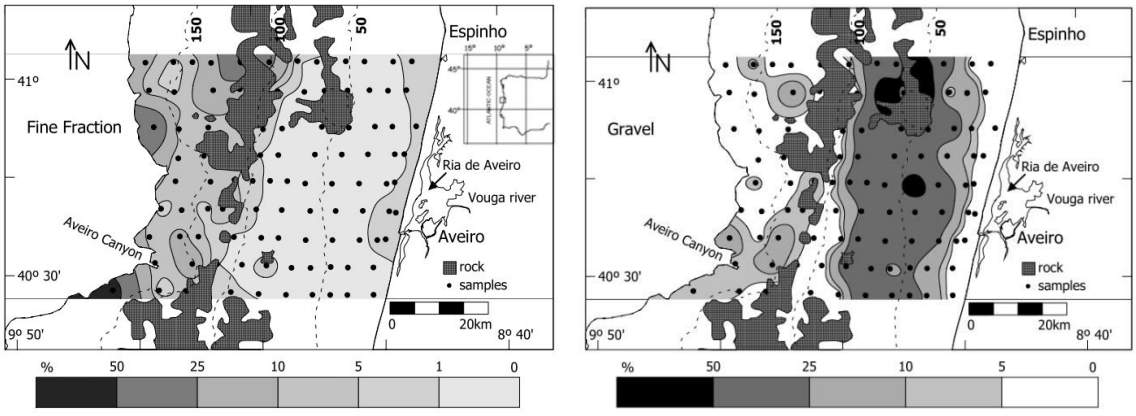

Figure 16. (a) Fine fraction (<63µm) and **(b)** gravel distribution maps offshore Aveiro. The dots show the sample sites used by the authors to obtain the maps (Abrantes and Rocha, 2007).

The nearshore sedimentary cover (depth <30 m) is composed mostly of moderately to well calibrated fine to very fine siliciclastic sand (63 – 250 µm). The fine fraction (silt and clay - <63 µm) is lower than 5% and primarily includes quartz, feldspars and phyllosilicates. The distribution of superficial sediments is linked to the hydrodynamic conditions that determine sediment transport (see conceptual model in Figure 17) and the geological evolution of the continental shelf associated with mean sea-level changes. According to Alveirinho Dias (1987), Taborda (1999), and Magalhães (1999), waves are the main mechanism (if not the unique) controlling the sediment remobilization in the continental shelf, the currents being responsible for the transport of the particles already in suspension. The wave action on the shelf is capable to put in suspension fine sediments (silt and very fine to fine sand), but its action decreases with depth. Close to the shore, strong wave induced currents and wave breaking are also important mechanisms for sediment remobilization and sediment transport. Moderated waves (2.5 to 3.5 m) are energetic enough to remobilize and transport sediment, whereas more energetic events (4.5 m) are responsible for 20% of the transport. In contrast to the fine sediments that are transported in suspension westwards, the coarser sediments are bedload transported under the action of waves (Figure 17; Taborda, 1999).

The inner shelf very fine and fine sands (63 – 250 µm) are transported mainly by the longshore currents, usually southwards and mainly provided by the Douro River (Martins et al., 2012), and occasionally deposited in the inner and middle shelf. However, due to the high energetic characteristics of these sectors, the fine fraction (<63 µm), often (40% of the time) are remobilized by waves and bottom currents, and tend to be transported westwards, where the hydrodynamic conditions are favorable to a more stable deposition of clay particles, normally in the outer shelf and upper slope (Taborda, 1999; Abrantes and Rocha, 2007). Therefore, the coarse sand and gravelly deposits are identified mostly on the inner and middle shelf, transported and

accumulated under high-energy environments, probably during lower sea level stands and related to the ancient location of the Vouga river estuary and the paleo-littoral surfaces. For the present day distribution of sediments (Figure 16) the hydrodynamic conditions are not strong enough to erode these coarser sediments but they have enough energy to avoid the deposition of fine-grained particles keeping coarser deposits on the surface (Martins et al. 2012).

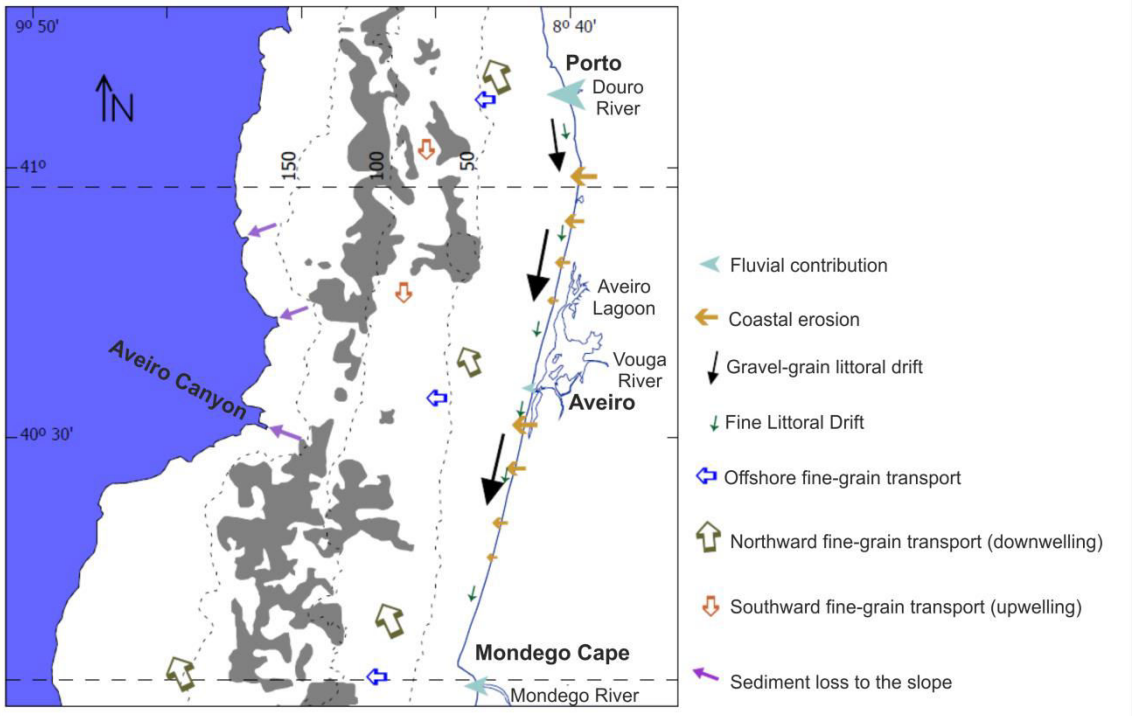

Figure 17. Conceptual model of the modern sediment dispersion in the Aveiro continental shelf (between Porto and Mondego Cape). The arrows length denote different relative significance of a specific process. The grey areas represent the rocky substrate (Abrantes, 2005).

II.2.2. Hydrodynamic and climatic setting

The hydrodynamics of the "Ria de Aveiro" lagoon are mainly driven by the wind effect, the freshwater input by rivers, and the tidal energy (Teixeira, 1994; Dias et al. 2000; Vaz and Dias, 2008). However, the contribution of the wind and the river runoff is lower than the tidal influence; therefore, the hydrodynamic pattern of the lagoon is primarily determined by tides, and this influence is detected even at the far end of each channel (Dias, 2001; Lopes and Dias, 2007). Tides are semidiurnal and mesotidal, with an average range of about 2 m at the lagoon inlet, fluctuating from 2.57 m during the spring tides to a minimum of 1.22 m at neap tides (Teixeira, 1994). More recent

studies by Dias (2001) and Dias and Lopes (2006), by applying a two-dimensional hydrodynamic depth integrated model, indicate maximum and minimum ranges of 3.2 m (spring tides) and 0.6 m (neap tides), respectively. Based on the same numerical model, Dias (2001) estimated the tidal prism in the lagoon inlet as 136.7×10^6 m^3 for maximum spring tide and 34.9×10^6 m^3 for a minimum neap tide, with the tidal prisms at S. Jacinto, Espinheiro, Mira and Ílhavo channels, respectively, being approximately 35%, 26%, 14% and 10% relative to the tidal prism at the mouth. Directly connected to the lagoon inlet, the S. Jacinto and Espinheiro channels are the most important channels from the dynamical point of view, reaching, during spring tides and flood periods, values of about 2 m s^{-1} in the sections closer to the mouth. On the contrary, shallow channels and tidal flat areas are characterized by very irregular geometry, which contributes to a strong reduction of the currents and an increase of the phase delay of the tidal wave (Dias at al., 1999; Lopes and Dias, 2007). In fact, tidal currents are strongly dependent on the local geometry and bathymetry, which leads to a tidal distortion inside the lagoon, with a decrease of the amplitude and an increase of the phase lag upstream (Dias et al., 1999).

The flood duration is higher than the ebb duration, with differences of approximately 2 hours in neap tides and 1.2 hours in spring tide conditions, inducing greater velocities in ebb than in flood periods (Dias et al., 2000). The “Ria de Aveiro” is therefore characterized as an ebb-dominant lagoon and the residual circulation in the lagoon is mainly determined by the flood and ebb regime asymmetries, which results in a tendency to export sediments to the ocean (Lopes and Dias, 2007). Numerical simulations performed by Silva et al. (2006) have shown that the ebb jet extends into the shelf.

The tidal regime in the lagoon is characterized by two main periodic time-scales, the semi-diurnal, which is the dominant tidal period, and the fortnight cycle, which corresponds to one-half the lunar month and is associated to the spring–neap cycle. The semi-diurnal tidal period is the main period characterizing the sediment transport in the lagoon; however, the lunar month determines the net erosion and deposition regimes, due to fortnight variability of the currents intensity, which reaches extreme low and high values during neap and spring tides, respectively (Lopes and Dias, 2007). In fact, the tidal currents are capable to mobilize and distribute the sediments, being responsible for the tidal flats formation and to feed the sediments to the marsh. The tidal flooding is also responsible for carving the internal channel network and carrying marine salt into the lagoon (Teixeira, 1994). As such, the present geomorphology of the lagoon is the result of a complex combination of several processes, where the most significant is the tide. In fact, the “Ria de Aveiro” had, in a recent past, the common attributes to an estuarine environment; however, and according to Teixeira (1994), the hydrodynamic regime of the “Ria de Aveiro” was significantly altered after the 1930s, mainly due to the engineering works developed

on the Aveiro inlet (see section V.3) that led gradually to an increase of the tidal amplitude as well as the daily water outflow at the entrance. The tidal flooding allowed the appearance and development of the sedimentary environments of the lagoon evolving to a genuine coastal lagoon (Teixeira, 1994).

Nowadays, the tidal prism is significantly larger than the fluvial input to the lagoon. The annual surface runoff to the "Ria de Aveiro" lagoon is approximately 2.0 km^3, corresponding to an average output of approximately $2.7x10^6$ m^3 for each tidal cycle (Teixeira, 1994), while the mean tidal prism at the mouth is about $70×10^6$ m^3 (Lopes and Dias, 2007). The Aveiro lagoon is supplied with freshwater by a drainage network of about 3 685 km^2, known as the Vouga hydrographic basin (Figure 18; ARH, 2012b), which includes nine drainage sub-basins: Ovar creek, Antuã river, Vouga river, Angeja creeks, Aveiro creeks, Águeda river, Boco river, Cértima river, and Mira river (Teixeira, 1994). The main contributions from the Vouga hydrographic basin are made by the Vouga river, with an average flow of 50 m^3 s^{-1} (which represents 2/3 of the total fresh water in the lagoon) and the Antuã river, with an average flow of 5 m^3 s^{-1} (Moreira et al., 1993; Teixeira, 1994; Dias et al., 1999; Dias, 2001; ARH, 2012b). Therefore, the rivers in this area have a small contribution in terms of freshwater inputs when compared with the tidal prism influence; however, they may have a long-term influence in the residual transport (Lopes and Dias, 2007).

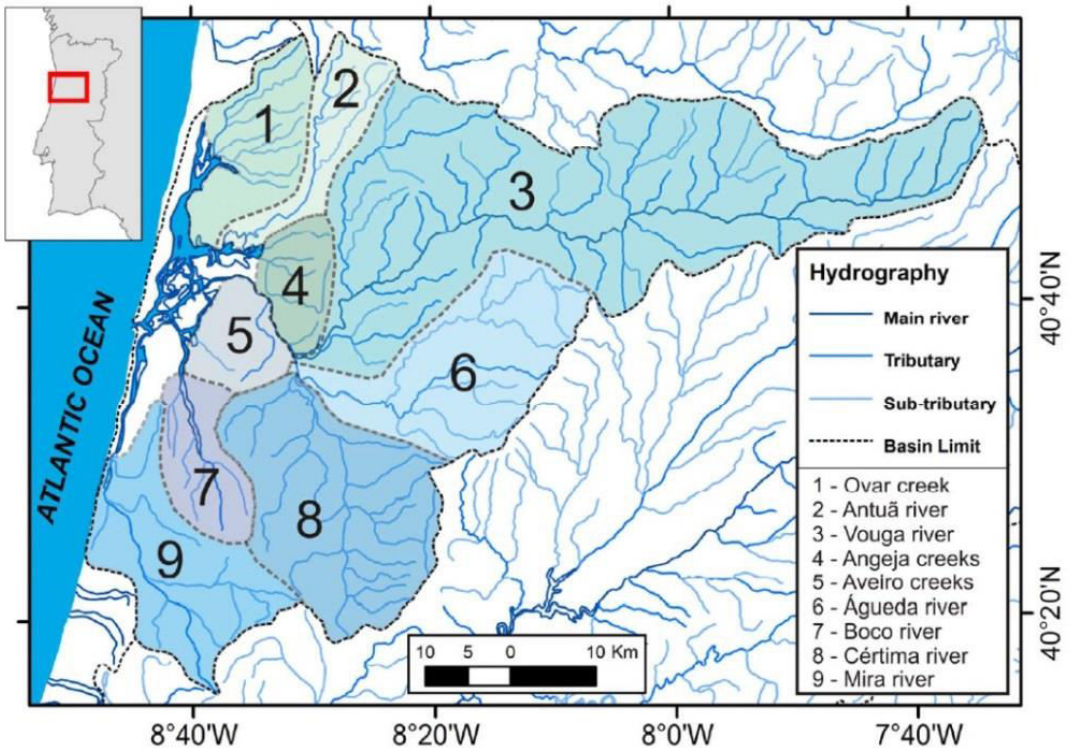

Figure 18. Vouga hydrographic basin and sub-basins (adapted from Teixeira, 1994, *in* Duarte, 2009).

Additionally to the tidal forcing and the freshwater discharge, also the wind affects the “Ria de Aveiro” hydrodynamics and the mixing processes in the lagoon by generating surface shear stress and waves. Extreme conditions of strong wind may induce particular circulation patterns, mainly in shallow areas and wide channels (Dias, 2001). The wind regime is characterized by north-western winds during the summer that change to more variable conditions during the winter, with strong variations in direction and intensity (Fiúza et al., 1982).

Dias et al. (2011) characterized the wind field using a meteorological station located 50 km south of Aveiro (Figueira da Foz: 40°09'12.5'' N, 8°50'36.1'' W). According to these authors (Figure 19), the most representative values of wind speed are between 0 and 8 m s^{-1}, with maximum values around 18 m s^{-1}, blowing mainly from the northwest (37%) and the southeast (27%). During spring, about 60% of the wind records are from north, with considerable intensity, mainly the winds coming from NW, usually referred as 'Nortada'. This phenomenon is even more evident in the summer with about 70% of wind records coming from the north and the wind that comes from south is typically weaker. The patterns observed during the autumn and the winter months show higher frequency of wind records from the NW (35% in the autumn and 25% during the winter) and SE (30% in the autumn and 35% during the winter) quadrants, with the winds from the north being commonly stronger (almost always greater than 4 m s^{-1}) than the south winds (frequently with intensities of 2 to 4 m s^{-1}; Dias et al., 2011).

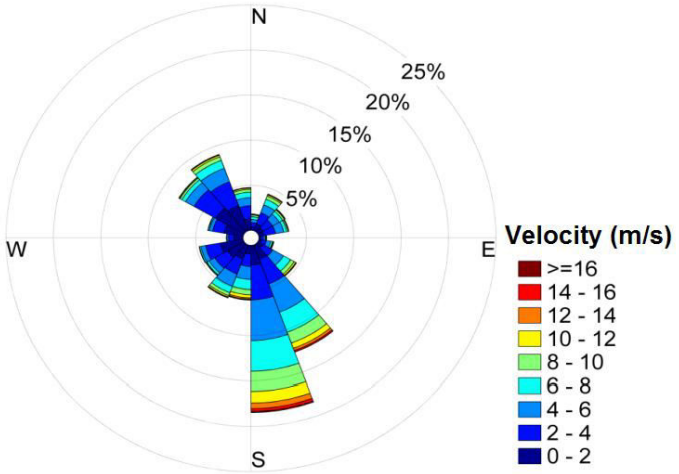

Figure 19. Wind rose diagram for the wind direction (wind blowing to) and the corresponding velocity based on 9 years of data, from 2001 to 2009, from a meteorological station located 50km South of Aveiro at 40°09'12.52'' N and 8°50'36.07'' W (Dias et al., 2011 *in* Vaz, 2012).

The complex interaction between the processes described above determines the hydrological regime of the lagoon as a well-mixed system, due to its vertical

homogeneity mainly during the dry seasons, which progressively behaves as a more stratified estuary upstream. After a significant rainfall and consequent increase in freshwater, however, the stratification becomes important near the mouth (Dias et al., 1999). The salinity in the Aveiro lagoon is typically high, around 35, presenting its maximum value during high tide that falls during ebb until it reaches the minimum value at low tide, with a resultant residual salt transport into the lagoon (Matos, 1990; Teixeira, 1994).

The adjacent coastal zone offshore Aveiro presents a highly energetic wave climate regime, related with the North Atlantic wind regime, with a yearly mean significant wave height (Hs) of 2 to 2.5 m, coming mainly from WNW to NNW (see Figure 20), and the wave period that ranges from 6 to 18 s, with a modal value around 9-11 s, for every wave direction (Andrade et al., 2002). The highest waves mainly come from WNW and decrease as the wave origin direction rotates to the NW. The significant wave heights lower than 2.5 m are dominant and have a frequency of occurrence close to 75%, whereas significant wave heights higher than 5 m have a frequency of occurrence generally smaller than 5%, which roughly corresponds to the storm events occurrence. According to Pires (1985), there are two types of storm events: (1) the most common storm events are characterized by strong NW or SW waves that affect the coast for one to two days; and (2) the “westerly storms”, that typically occur once per year during one or two weeks when the Azores anticyclone is located at its most extreme southerly position, and which are responsible for the most extreme wave conditions observed on the northern Portuguese shelf associated mainly with a southerly wind regime.

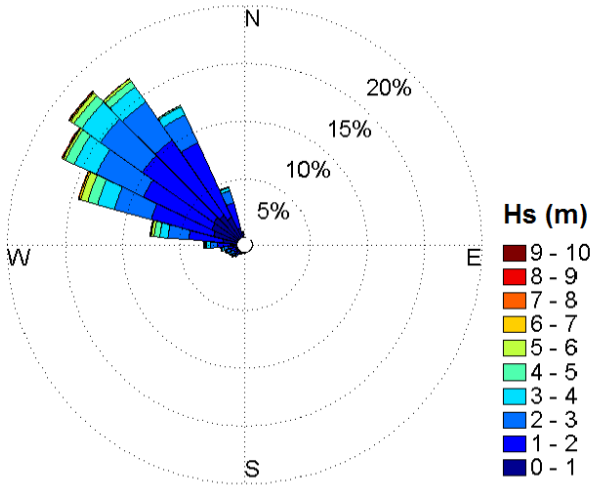

Figure 20. Offshore Aveiro wave regime illustrated by a rose diagram for the wave direction (waves coming from) and the corresponding significant wave height in meters and based on data collected from 1984 to 1996 from Figueira da Foz (40°11'08'' N and 9°08'44'' W at 92 m deep ZH) and Leixões (41°19'00'' N and 8°59'00'' W at 83 m deep ZH) wave directional buoys (Capitão et al., 1997; Costa et al., 2003 *in* Plecha, 2011).

The wave influence in Ria de Aveiro is generally restricted to the outer part of the inlet due to the protective effect of the two jetties that lead to a significant decrease of the wave amplitude inside the lagoon. Offshore the inlet and in the adjacent areas, the highly energetic wave climate leads to a strong littoral drift to both south and north directions, although on average and due to the wave predominance from WNW to NNW, there is a net sediment transport rate of over $1x10^6$ m^3year^{-1} in the south direction (Castanho, 1971). More recent studies indicate a littoral drift ranging from 1 to $3.5x10^6$ m^3year^{-1} southwards (Teixeira, 1994; Taborda, 1999, Andrade, 2002; Coelho, 2005). According to Teixeira (1994), waves higher than 6 m are responsible for 20% of the sediment transport.

The climate of the Aveiro region is classified as subtropical, with an average temperature higher than 10°C in more than 8 months per year, although the average temperature fluctuates between 6°C during the winter and 20°C during the summer (Faria and Machado, 1979; Fonseca et al., 1988; Rebelo, 1992). The average annual precipitation in the lagoon is about 1000 mm and approximately 75% of this precipitation occurs from October to March, due to the frequent presence of cold and maritime polar air masses which originate low pressures over the Atlantic coast, whereas in the summer trimester only occurs 5% of the whole precipitation, prevailing the arid conditions due to the northwards movement of the Azores anti-cyclone, which carries with it the precipitation front (Manso et al., 1996).

Chapter III. Fundamentals of the applied methodology

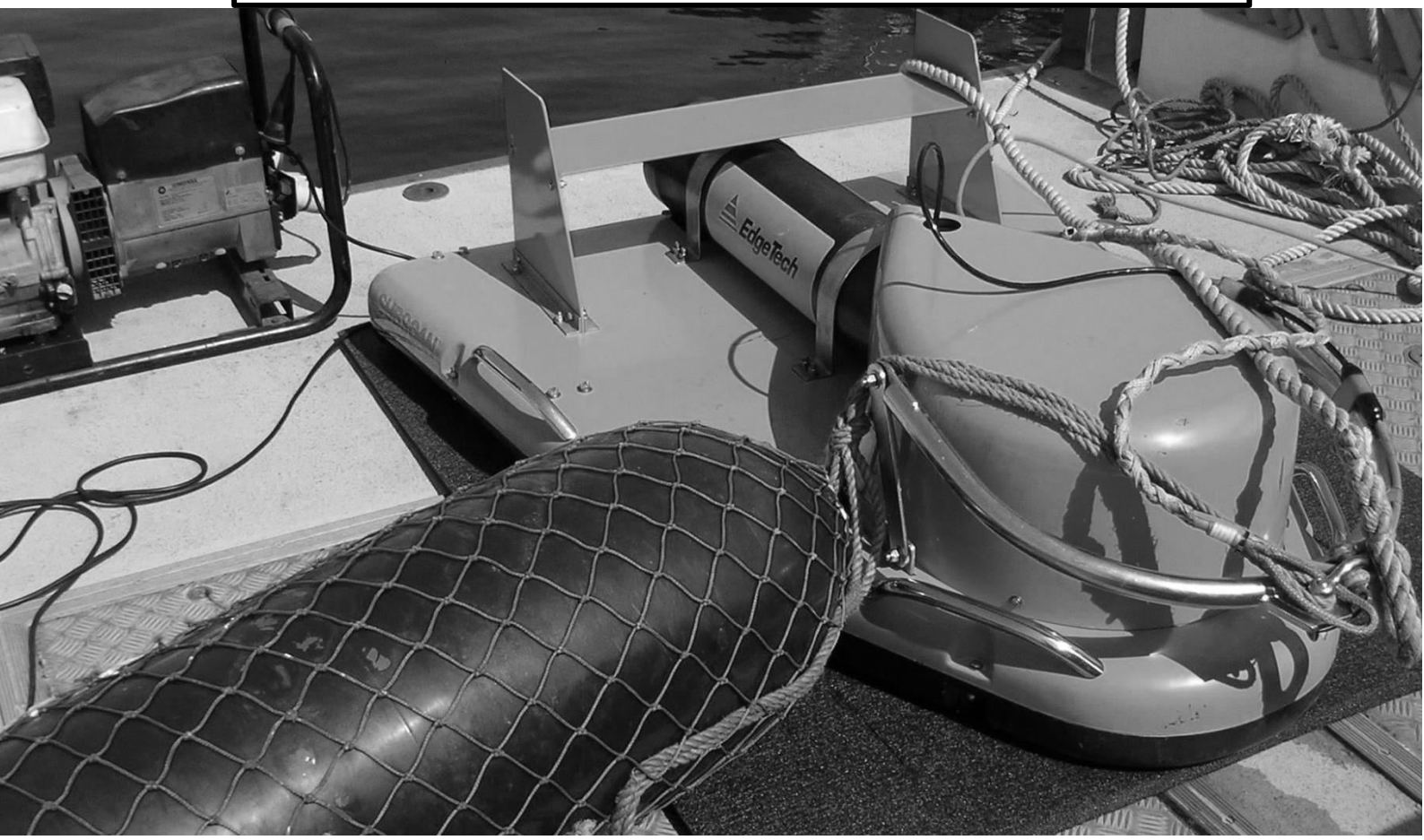

This Chapter introduces the fundamentals of the geological and geophysical methods and the physical oceanographic modelling procedures applied in this thesis. It includes a review of the basic principles of echo-sounding techniques, in particular single and multibeam systems, sidescan sonar (including both data processing and interpretation), grain size analysis, and MORSYS 2D the morphodynamical model used for non-cohesive sediment dynamic simulations in coastal areas driven by tides, wind, river flows and waves.

III.1. Echo-sounding systems

Echo-sounders, derived from military sonars, are the most widespread acoustic systems used for hydrography and seafloor mapping, since the 1920s. These systems measure the depth by generating a short pulse of sound, or ping, emitted from the sea-surface or from a towed instrument, and then registering the echo of the pulse from the seafloor (Jones, 1999). The time (t) between the transmission of the pulse and the return of its echo (TWT – two way time) can be converted into distance, in this case depth (d), knowing the speed of sound in water (V_w) and using the Equation (1):

$$d = \frac{t}{2} v_w \quad \textbf{(1)}$$

Sonars use piezo-electric ceramic transducers that can repeatedly produce acoustic pulses with precise, controllable, and repeatable characteristics. In fact, an echo-sounder uses specific voltages to cause the piezo-electric projector to oscillate, transmitting a pressure wave with specific frequency characteristics that expands spherically into the water (for constant sound speed). The return of the sound pulse is detected by a hydrophone that converts the physical oscillations made by the sound waves (pressure) into voltages (Seippel, 1983; Seabem Instruments, 2000).

The received signal (RS), which represents the strength of the measured echo that returns from the amount of acoustic energy put into the water by the acoustic source (source level – SL), can be represented by the Sonar Equation (2).

$$RS = SL - 2TL + BS - NL - DT + DI \quad \textbf{(2)}$$

The sound pulse expands spherically from the source, being spread over a wider area with depth causing a drop in energy per unit area, called *spreading loss*, that together with the *attenuation loss* (derived by the *absorption*), are known as

transmission loss (TL). When the sound wave strikes the ocean bottom the energy is transmitted into the seafloor, reflected by the ocean bottom, or scattered back into the water. The fraction of incident energy per unit area that is directed back in the direction of the transducer is called the backscattering strength (BS) of the bottom (see section III.2.2). During the ping generation, propagation, echoing, and reception, other sources of sound add to the final received signal forming the so-called *noise level* (NL), which includes ocean sounds (waves, for example), marine creatures, shipboard sounds, and also noise from the sonar electronics. The *detection threshold* (DT) is a system-dependent parameter which establishes the lowest level above which the echo-sounder can detect the returning echoes; the *directivity index* (DI) is a measure of the focusing of the acoustic energy into a narrower beam in order to improve sonar efficiency (Urick, 1983 *in* Jones, 1999; Nishimura, 1997; Seabem Instruments, 2000).

Echo-sounders can be divided into *single-beam* (SBES), limited to the basic geometry of one single vertical beam, and *multibeam* (MBES), using multiple beams; the later are able to cover a large swath width simultaneously (Figure 21). SBES requires only a single transducer, for both transmission and reception, but a transducer array is normally used when stabilization is required; MBES use transducer arrays built up from several elements to produce a wide beam. The MBES is a result of the need for beam forming in multiple directions and also beam steering to compensate for platform attitude (IHO, 2005).

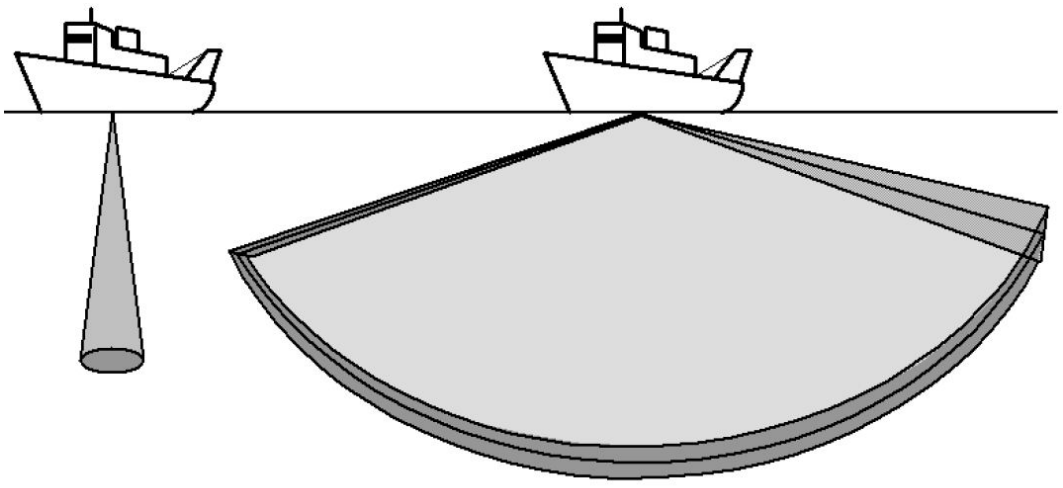

(a) **(b)**

Figure 21. Sketch of water column ensonification by: **(a)** a SBES (a vertical conical lobe); and **(b)** a MBES, presented here with two adjacent fan-shaped sectors (Lurton and DeRuiter, 2011).

III.1.1. Single-beam echo-sounder (SBES)

The single-beam echo-sounder (SBES) systems were the earliest and are still nowadays the most widely used echo-sounding devices. They can be used to measure the ocean depth at many locations, which are then combined to build bathymetric maps of the ocean floor (Seabem Instruments, 2000). SBES operate at various frequencies, that typically range from 12 to 200 kHz, although some systems dedicated to very shallow waters may work with frequencies as high as 700 kHz (Lurton and DeRuiter, 2011).

SBES systems consist of four basic components: a transmitter, a transducer, a receiver, and a control and display system. The control and display system triggers the transmitter system to produce a sound pulse, which generates an oscillating electric signal with unique frequency characteristics. The transducer converts this electrical energy into sound waves that are then transmitted into the water as an oscillating pressure. The return echo from the seafloor is received and converted back into an electrical signal by the transducer and passed to the receiver system, where it is amplified; the time between transmission and reception is used to compute the depth, see Equation (1), which is recorded by the control and display system that then triggers the next ping (Seabeam Instruments, 2000). The sound pulse produced by the transducer is not transmitted in all directions; instead, the acoustic energy is projected into the water in the form of a vertically oriented beam (IHO, 2005). The most common geometry is a conical vertical beam (Figure 21a), with a fixed *aperture* of a few degrees (most commonly between 5° and 15°), which is usually not steerable (Lurton and DeRuiter, 2011). The *beam width* is a function of the transducer dimensions and the acoustic wave length: the higher the frequency and the larger the transducer is, the narrower the beam will be; therefore, to have a narrow beam in low frequencies, a large transducer is required (IHO, 2005). The transducer selected for a SBES may have a narrow beam when high directivity is required, although when directivity is not the main concern but the detection of minimum depths or obstacles on the seafloor is the priority, a wide beam is more adequate (IHO, 2005).

The size of the solid angle beam determines how accurately a beam sonar can determine the location of the measured depth at the seafloor and therefore the resolution of the sonar. The resolution, related to the area ensonified by the beam, is not fixed, being larger as the ping goes deeper (wave spherical divergence). In general, the bottom ensonified area is proportional to the beam solid angle and to the square of the depth (Seabeam Instruments, 2000).

III.1.2. Multibeam echo-sounder (MBES)

Originally, multibeam echo-sounder (MBES) systems consisted of an extension of single-beam echo-sounders with arrays of sonar projectors producing acoustic

pulses not only along the track, but also for a significant distance across to the ship track. Nowadays, instead of lines of single soundings, the MBES systems produce a swath of soundings (Figure 21b) that can be, in modern deep-water systems, up to 7 times the water depth. Therefore, these systems are the most valuable tool for depth determination when full seafloor coverage is required, since they allow complete seafloor ensonification with the consequent increase in resolution and detection capability. In addition, MBES systems, besides acquiring bathymetry data, also very efficiently provide an acoustic backscatter image of the seafloor (similar to those provided by sidescan sonar systems – see section III.2; IHO, 2005; Lurton and DeRuiter, 2011).

In these systems, the *transmitter* (projector) creates a transverse narrow ensonified beam that is wide across-track and narrow along-track. The *receiver* (*hydrophone*) is set up perpendicular to the transmitter, so that the reading areas are narrow across-track and wide along-track. The intersections of these beams/areas with the seafloor plan are the ensonified areas, named *footprints*, for which the depths are measured. The position of each footprint is then accurately deduced from the travel time and the angle of reception (IHO, 2005; White et al., 2007).

The operational principle of a MBES system is therefore based on the transmission of a short pulse, fan shaped and perpendicular to the vessel track, composed by several beams that are electronically formed with known angles by using signal processing and beam forming techniques. In the most recent models, several adjacent sectors can be transmitted simultaneously (Figure 21b), hence widening the along-track angular aperture and requiring transmission at several different neighboring frequencies (IHO, 2005; Lurton and DeRuiter, 2011). Multibeam systems are able to determine the depth by accurately measuring the two-way travel time and the angles of reception, and tracing the ray path for each beam (IHO, 2005; White et al., 2007). For an accurate computation of depth and its associated positioning, because multibeam transducers are fixed to a vessel's hull and, therefore subjected to a six possible degrees of freedom (three translations and three rotations), accurate measurements of latitude, longitude, heave, roll, pitch and heading are required (IHO, 2005).

III.2. Sidescan sonar systems

The present day sidescan sonars are based on systems built during World War II, which emitted sound pulses from sideways-looking transducers to detect underwater objects, such as submarines, from their echo returns (Jones, 1999). During the 1950s a group of British scientists realized that bottom irregularities produced

clear echoes, thereby discovering the potential of this technique to study the continental shelves and seafloor (Jones, 1999); in the late 1950s the first commercial sidescan sonar was built (Xu, 1998).

Sidescan sonars, along with single and multibeam echo-sounders, are acoustic remote sensing methods to image the seabottom (Henriques et al., 2012). Sidescan sonars are primarily designed to provide "acoustic images" of the seafloor with high resolution. In marine geoscience, they are used to obtain a near-visual representation of the geological facies of the seafloor. Additionally, sidescan sonars are useful tools for target detection, such as for example ship wrecks, pipelines and cables.

Typically, a sidescan sonar system consists of a displaying and recording unit, connected to an underwater sensor, called sonar or "*towfish*", by an electro-mechanical cable. The sonar has two transducers (linear array of piezo-electric elements), one per side (port and starboard), that emit pulses in a fan-shape beam (Figure 22), designed to be narrow along-track ($\theta \approx 0.2 - 2^{o}$), to allow a high resolution, and wide across-track, ensuring coverage ($\varphi \approx 40 - 70^{o}$; Xu, 1998; Jones, 1999). Furthermore, the main axis of the beam is typically angled 10-20^{o} down from the horizontal, to cover as much seabed as possible. The sound directionally and intensity is expressed by the beam pattern shape, known as *directivity*, which is dependent of the shape and dimension of the transducer arrays and the frequency used. Each emitted pulse will ensonify a thin bottom strip, called *footprint*, perpendicular to the movement direction of the sonar. The magnitudes of the bottom echoes for the ensonified strip originate a scan line of the seafloor. With the moving of the sonar, the scan lines are accumulated ping by ping, forming an acoustic image of the seafloor (Xu, 1998).

In order to ensure a full coverage, no gaps between ensonified areas from two successive pings should exist (Lurton, 2002). This complete coverage condition depends on the transducer length, the vessel speed, and the ping rate. The ping rate, f_p, can be estimated by dividing the water sound velocity *c*, by the double of the selected range R, Equation (3).

$$f_p = \frac{c}{2R} \quad \textbf{(3)}$$

For a constant transducer length L, a *ping rate* (determined by the selected range) allows a complete coverage when a maximum vessel speed, v_{max}, Equation (4), is not exceeded.

$$v_{\max} = L.f_p = \frac{L.c}{2R} \quad \textbf{(4)}$$

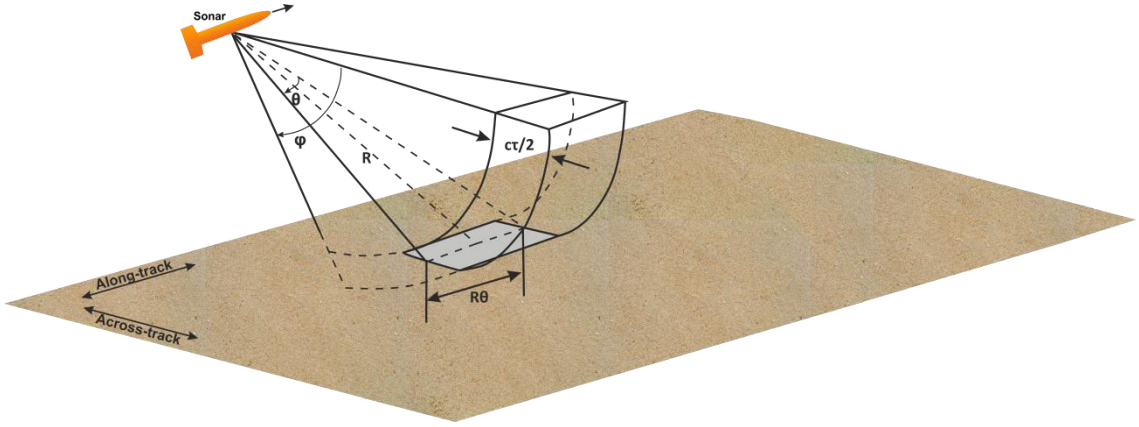

Figure 22. Pulse geometry in perspective view for a conventional sidescan sonar system. In the illustration θ and ϕ represent, respectively, the horizontal and vertical beam angles, R the range, τ the pulse length, and c the sound speed (modified from Xu, 1998).

For greater seabed depths the ping rate must decrease to cope with the longer range involved. In such cases, the vessel speed may be slowed down in order to maintain the total coverage along the study area.

The frequency (*f*) and the wavelength (λ) of the signal are the main operational parameters used to characterize the acoustic systems. These parameters are related by Equation (5), where *c* corresponds to the sound velocity in water.

$$\lambda = \frac{c}{f} \quad \textbf{(5)}$$

As the attenuation increases with the frequency, lower frequencies allow energy to travel larger distances, but provide lower resolution than higher frequencies (Table 1). Consequently, low frequencies (e.g. 1-25 kHz) may be used to survey large and deep areas with lower resolution, whereas high frequency systems (e.g. 500-1000 kHz) are more appropriate for detailed (high resolution) studies, surveying shallow and smaller areas.

Table 1. Sidescan sonar system characterization according to the operating frequency, *f*, and wavelength, λ (USGS, 2014).

Frequency	Resolution	Wavelength	Range
1 kHz	Low	1.5 m	>100 km
10 kHz	Low	15 cm	10 km
25 kHz	Low	6 cm	3 km
50 kHz	Medium	3 cm	1 km
100 kHz	Medium	1.5 mm	600 m
500 kHz	High	3 mm	150 m
1000 kHz	High	1.5 cm	50 m

III.2.1. Resolution

The acoustic pulses in a sidescan sonar system are emitted at specific ping rates (f_p, in Hz) and pulse lengths (τ, in milliseconds). The width of the pulse (see Figure 22) is half of the product of the pulse length and the sound speed ($c\tau/2$); therefore, a short pulse will produce a narrower pulse resulting in a higher resolution acoustic image (Blondel, 2009). When the pulse interacts with the seafloor, the size and shape of the ensonified area – *footprint* – will depend on the range, which determines the resolution.

The spatial resolution of a sidescan sonar system corresponds to its capability to distinguish two or more close objects and can be split into two perpendicular components: (1) the *along-track resolution*, defined as the minimum distance between two objects located parallel to the direction of the sonar movement that can be distinguished as separated entities in the sonar image; and (2) the *across-track resolution*, that corresponds to the minimum distance between two objects located perpendicularly to the line of travel that can be distinguished as separated entities in the acoustic image (Blondel, 2009).

The resolution in the along-track direction, Δx (Equation (6) and Figure 23), it is strongly dependent on the horizontal beam angle θ (in radians) and the range R (Nishimura, 1997; Jones, 1999).

$$\Delta x = R.\theta \quad \textbf{(6)}$$

According to Equation (6), Δx increases with the distance to the transducer (*R*), which means that the along-track resolution of a sidescan sonar, working under the same operational conditions, degrades with the range (Figure 23). Therefore, two objects will be detected as individual entities if they are separated by a distance which is less than the spread of the sonar beam (Δx) at a specific range.

The across-track resolution Δy (Equation (7) and Figure 24), depends on the pulse length τ, the sound speed in the water column c, and the incidence angle β (Nishimura, 1997; Quinn *et al.*, 2005; Blondel, 2009).

$$\Delta y = \frac{\tau.c}{2.\cos\beta} \quad \textbf{(7)}$$

According to Equation (7), Δy decreases with the decreasing of the incidence angle β, what means that the across-track resolution of a sidescan sonar, working under the same operational conditions, is better further away from the sonar (Figure 24).

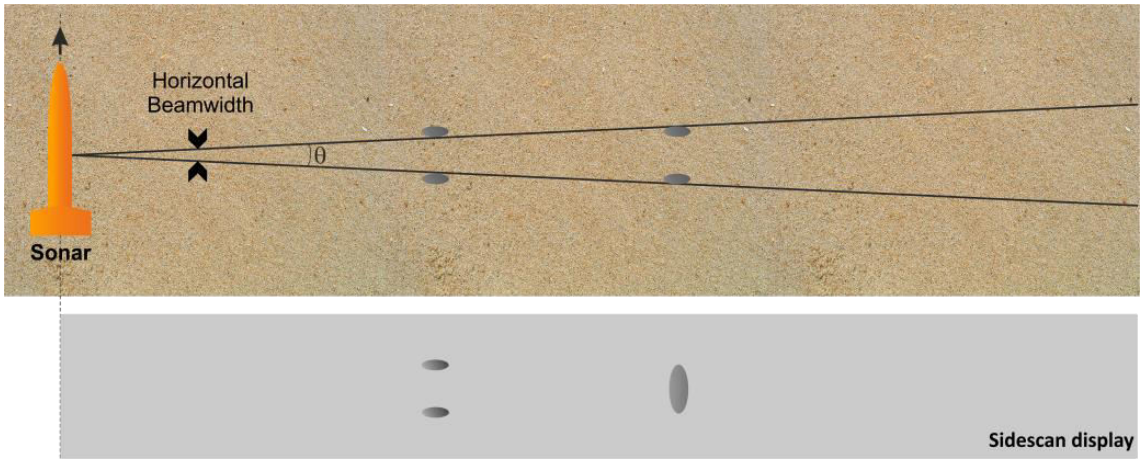

Figure 23. Illustration (plan view) showing that the along-track resolution depends on beam spreading and, therefore, it is better near the nadir (modified from Mazel, 1985).

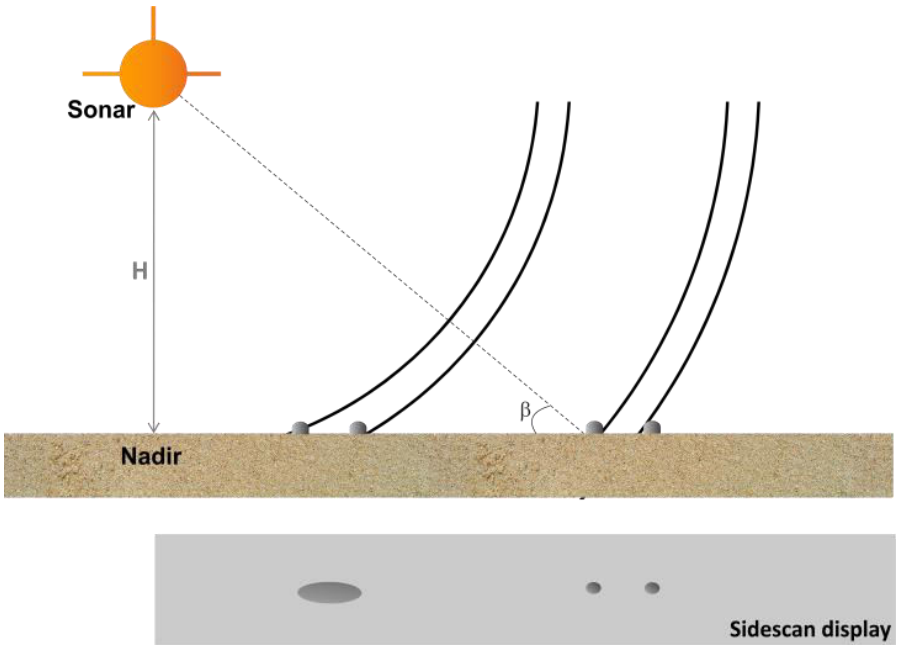

Figure 24. Illustration (vertical section view) showing that the across-track resolution increases with range (modified from Mazel, 1985).

III.2.2. Acoustic scattering

Most of the incident energy that reaches the seafloor is reflected in the specular direction (reflection), some is lost in the seabed (absorption), some is scattered, and only a very small portion is scattered back toward the sonar as *backscatter* (Figure 25; Nishimura, 1997; Blondel, 2009).

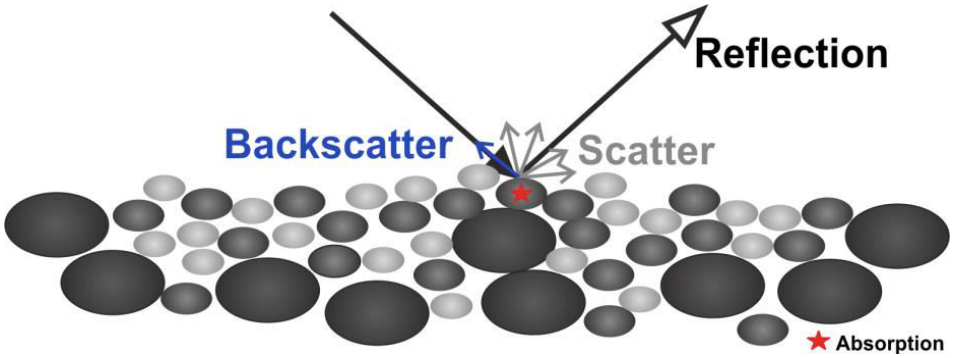

Figure 25. Schematic diagram indicating what happens to the incident energy when it reaches the seabed (modified from Mazel, 1985).

The intensity of backscattering from the seafloor is governed by the *backscattering coefficient*, S_b, Equation (8), which is the ratio of the intensity of sound scattered, P_b, and the intensity of the incident wave, I_i, in the ensonified area of the seabottom, A (Urick, 1983 *in* Jones, 1999).

$$S_b = \frac{\mathrm{P_b}}{I_i.A} \quad \textbf{(8)}$$

The backscattering coefficient is closely related to the properties of the seabed materials, such as *roughness*, *sound velocity* and *density*. *Roughness* can be simply described by the *Rayleigh parameter*, r, which depends on the wavenumber, $k=2\pi/\lambda$, the root mean square of the bedforms' height, H, and the incidence angle, β, Equation (9). If the *Rayleigh parameter* is significantly smaller than 1, the surface is smooth and acts as a specular reflector, all the incident energy is reflected. For values significantly higher than 1, the surface is rough and acts as a scatterer, producing omnidirectional energy, which includes the backscatter component (Jones, 1999).

$$r = kH.\sin\beta \quad \textbf{(9)}$$

The backscattering is affected, in decreasing order of significance, by the geometry of the sonar-target system (angle of incidence, seabed slope and angle of returning of the acoustic wave); the physical characteristics of the seabottom, such as the micro-scale roughness; and the intrinsic nature of the seabed, such as its composition and density (Blondel and Murton, 1997; Nishimura, 1997; Blondel *et al.*, 1998). According to Urick (1983, *in* Davis *et al.*, 1996), the backscatter strength is a function of the bottom roughness, grain size, and volume scattering. In fact, as noted by Blondel (2009), the *volume scattering* should not be neglected. In case of sediments there may be penetration of sound through the seabed causing reverberation which can also be a significant contribution to the total energy returned – *volume scattering* (Jones, 1999). The volume scattering depends not only on the type of seabed, but also

on the possibility of penetration at the frequencies used. In fact, a seafloor can appear smooth at a certain wavelength and rough at another wavelength, because of buried objects or bioturbation, for example (Blondel, 2009).

Slopes facing toward the sonar produce stronger backscatter images than slopes facing away from the sonar. Similarly, a smooth surface scatters mostly along the specular direction, presenting a very low backscatter, and a rougher surface, because it has micro-surfaces facing toward the sonar, presents a higher backscatter. Therefore, gravelly bottoms appear acoustically brighter than muddy seafloors (Blondel, 2009).

In the absence of significant bathymetric variations and in case of unconsolidated sediments, it is commonly assumed that the grain size is the dominant factor affecting the backscatter strength. According to Davis *et al.* (1996), variations in relative backscatter strength correspond directly to changes in the grain size and composition of the superficial sediments. Coarse sediments cause higher backscatter strength than fine sediments and sediments that are coarse-grained sands with high carbonate contents have higher relative backscatter intensities (Davis *et al.*, 1996; Goff *et al.*, 2000; Collier and Brown, 2005). Goff *et al.* (2000) also establish a very strong degree of correlation between backscatter strength and the mean grain size, but they conclude that such correlation is strongly dependent also on the shape of the grain-size frequency distribution; therefore such a clear correlation is only possible for a unimodal distribution with a good sediment sorting. Also topography effects need to be taken into account as they affect the backscatter intensity, as already referred above.

III.2.3. Data processing

The digital processing of sidescan sonar data consists of several steps, which may be grouped in 3 main categories: *pre-processing*, *processing* and *post-processing* (Blondel and Murton, 1997; Blondel, 2009). The *pre-processing* corresponds to the preparation of raw data for processing and consists of smoothing of the navigation data and corrections for horizontal offsets of the towfish relative to the GPS-antenna. The *processing* step comprehends the radiometric and geometric corrections, discussed below, and the mosaicking, which transform the raw data into images that correspond to correct representations of the seafloor. Additionally, *post-processing* procedures correspond to advanced image analysis techniques, such as computation of image statistics, contrast enhancement, multiple reflections removal and automatic classification (Blondel and Murton, 1997; Blondel, 2009).

The *geometric corrections* rectify the discrepancies between the relative position of features on the sonar image and their real position at the seabed (Cobra *et*

al., 1992; Chavez *et al.*, 2002). Some of the geometric distortions that need to be corrected are (1) the water column offset, (2) the *slant-range* effect; (3) variations of the sound speed in water; (4) the *anamorphic ratio*; and (5) variations in the trajectory, speed, or orientation of the towfish (Cobra *et al.*, 1992; Chavez *et al.*, 2002; Capus *et al.*, 2007; Blondel, 2009):

(1) Sidescan sonar systems start recording data as they transmit the acoustical wave; therefore, there are a set of pixels on the center of the swath that do not have information about the seafloor, but correspond to the water column below the transducers (Figure 26). The removal of this blind zone is done by detecting the first return from the seafloor, through bottom-tracking, and represents one of the first steps in the sidescan sonar processing flow (Chaves et al., 2002).

(2) Another geometric effect in the sidescan sonar data is manifested in the across-track direction and is called *slant-range distortion*. This effect occurs because the sonar system measures the time for a transmitted pulse (T_i) to travel, at a certain speed (c), from the transducer to the seafloor and the same way back – Equation (10). Therefore, the features in a raw sidescan sonar image are positioned according to the slant range (R_i) and not to the ground range (D_i), which results in a more compressed image in near-range areas than in far-range areas (Blondel, 2009). For example (Figure 27), two targets close to the nadir (D_1 and D_2) are going to be associated with nearly identical slant ranges (R_1 and R_2). However, two targets at far range (D_3 and D_4), at the same distance from one to another, are going to be associated to with slightly different slant-ranges (R_3 and R_4) and therefore placed further apart in the sidescan sonar image (R_2-R_1< R_4-R_3).

$$R_i = \frac{cT_i}{2} \tag{10}$$

The *slant range correction* consists in a repositioning of the pixels from their apparent position, based on the slant range distances, R_i, to their real position, based on the ground range, D_i, Equation (11). This correction assumes a flat seafloor in the across-track direction, which may introduce errors mainly in areas of high relief (Blondel, 2009). Therefore, if bathymetric data is available, it should be included in the later stages of processing.

$$D_i = \sqrt{\left(\frac{cT_i}{2}\right)^2 - H^2} = \sqrt{R_i^2 - H^2} \tag{11}$$

(3) Variations of the speed of sound in the water column are caused by differences in water temperature, pressure and/or salinity and generate the refraction of the sound waves. These type of distortions are mainly observed at longer ranges and are less frequent in high frequency and high resolution systems (Cobra *et al.*, 1992).

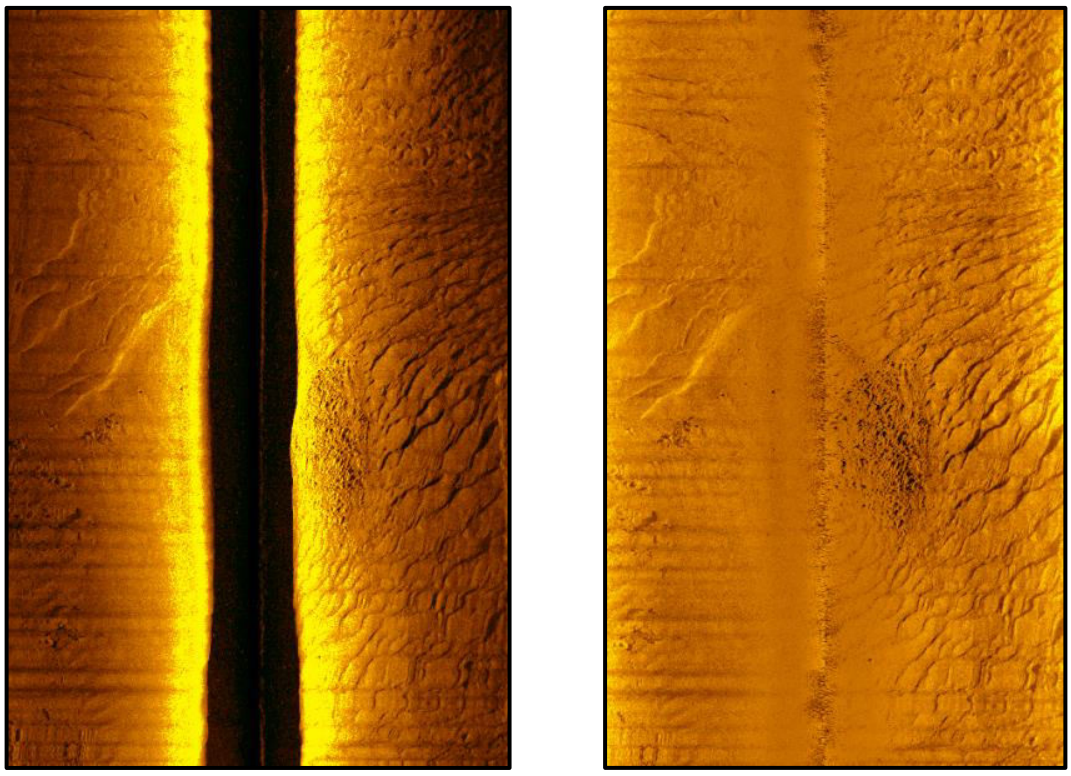

(a) **(b)**

Figure 26. Sidescan sonar line acquired in Aveiro lagoon **(a)** Raw data; **(b)** After water column offset removal, slant-range effect correction and beam angle compensation (Pinheiro *et al.*, 2011).

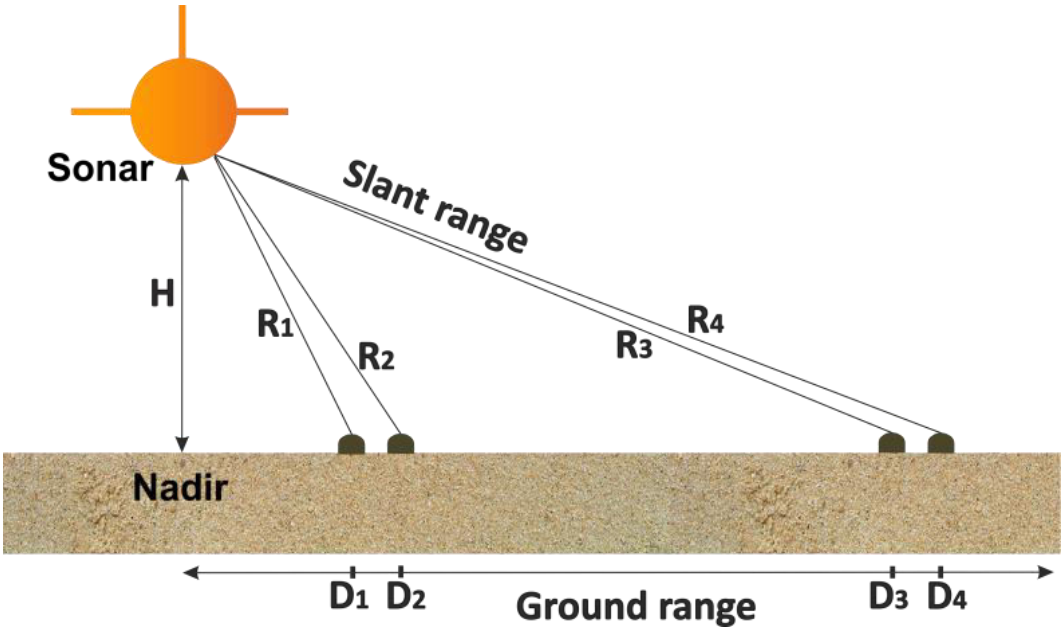

Figure 27. Slant range effect illustration in a vertical section view: two pairs of targets at the same distance from each other (D_2-D_1=D_4-D_3) are going to appear in the sidescan sonar register closer at near ranges and farther at far ranges (modified from Blondel, 2009).

(4) The *anamorphic ratio effect* results from a different pixel spatial resolution between the along and the across-track directions. The along-track spacing is defined by the width of the horizontal beam on the ground or the distance travelled by the transducer during the reception interval, whichever is smallest; therefore the variation in the towfish speed is one of the parameters that can affect the spatial resolution in the along-track direction. The correction of the anamorphic ratio between the along and the across-track directions – called *anamorphosis* produces an image in which the inter-pixel spacing is the same across and along-track. The result is an image in which features are correctly represented with a 1/1 aspect ratio (Chavez *et al.*, 2002; Blondel, 2009).

(5) Ideally, the sonar would be towed above the bottom at a constant speed, in a straight trajectory, and free of motion instabilities (either rotational - pitch, roll and yaw - or translational - surge, sway and heave). However, in practice, the towfish is often subject to variations in the trajectory, speed, and/or orientation, as a result of, for example, the effect of wind and sea currents, causing important geometric distortions in the sidescan sonar data (Cobra *et al.*, 1992). The correction of these distortions, related with towfish motion instabilities, usually requires knowledge of the towfish attitude parameters (needs sonars equipped with attitude sensors) or assumes that the towfish follows the variation in course of the towing vessel, which are determined from navigation data (Cobra *et al.*, 1992).

While *geometric corrections* change the spatial position of a pixel, *radiometric corrections* change the return signal amplitude assigned to a certain pixel (Chavez *et al.*, 2002). *Radiometric corrections* include (1) *beam pattern compensation* and (2) *noise removal* (Fonseca, 1996; Chavez *et al.*, 2002; Blondel, 2009; Chang *et al.*, 2010):

(1) Across the swath, the amount of sonar energy hitting the seabed and the angle at which the sonar wave hits the seafloor vary with the distance from the towfish. Therefore, because raw sidescan sonar data corresponds to the scattered energy returned from the seabed, both the amount of incident energy and incidence angle will affect the data. The result is generally a strong response near the towfish nadir and a weak response at the outer edge of the swath (Chang et al., 2010). To compensate for this uneven illumination, it is important to know the energy distribution as a function of the incidence angle, which can be assessed by estimating the average of the energy levels for each angle over the whole data series. The inverse of this average can be applied as a correcting factor for this beam pattern distortion (Chang et al., 2010).

(2) Other radiometric distortions that can affect the sidescan sonar data are the *speckle and striping noises*. The *speckle noise* corresponds to high amplitude single echoes (Blondel, 2009) and the *stripping noise* is related to very low amplitude echoes strips in the across-track direction, as a result of pitch movements of the towfish. The correction of these artifacts can be done by applying a spatial filtering procedure.

After the geometric and radiometric corrections are applied to the individual track-lines, the data is prepared for the creation of geo-referenced sidescan sonar images representative of the seafloor – this processing step is called *mosaicking* (Chavez *et al.*, 2002). After processing and mosaicking, the sidescan sonar data are ready for interpretation.

III.2.4. Sidescan sonar data interpretation

Sidescan sonar techniques have been used in the last years by several authors for seabed mapping, bedforms identification, dredging operations and object detection: Boos et al. (1999), Brissette and Clarke (1999), Dartnell and Gardner (2004), García-Gil et al. (2000), Quaresma et al. (2000), Huvenne et al. (2002), Quinn et al. (2005), Lankneus and Jonghe (2006), Lafferty et al. (2006), McMullen et al. (2008). Backscatter techniques have been also widely used for habitat mapping by Blondel (2008), Brown and Blondel (2009), Le Bas and Huvenne (2009), among several others. In fact, sidescan sonar data interpretation can give important indications about the morphological and sedimentological character of the seafloor, in particular relating to the bottom relief, bedforms and the superficial sediment distribution (type, composition, texture and structures orientation), as well as about the presence of any anthropogenic objects on the seabed, and allows carrying out, among others, the following tasks (Riddy and Masson, 1996; Neto, 2001; Blondel, 2009):

- Superficial sediment mapping;
- Outcrop mapping;
- Identification of faults and other morphological lineations or features with superficial expression;
- Anthropogenic object detection (e.g. shipwreck and pipelines);
- Ripples, megaripples, sand waves and prevailing currents identification;
- Benthic habitat mapping.

The sidescan sonar mosaic images represent the backscatter intensity, which depends on the reflective nature of the seafloor and the orientation of the bottom features or topography (see section III.2.2). The result is a representative image of the seafloor, which makes the sidescan sonar images suitable for identification and interpretation of seabed features, according to the study aims (Riddy and Masson, 1996). It is however important to keep in mind that the mosaic images are artificial seabed views, reconstructed from the backscatter. For example, the material reflectors and the topographical reflectors may often produce a similar result on the sonograph and it is up to the operator to interpret the image carefully in order to determine the actual composition of the seabed (Kenny et al., 2001). Therefore, sidescan sonar

mosaic interpretation requires experience, and preferably some knowledge about the study area, in order to better classify the seabottom features and identify possible artifacts (Riddy and Masson, 1996). Of course, groundtruthing through sediment sampling is absolutely required to calibrate the sidescan sonar interpretation based on the backscatter intensity.

Usually, more reflective bottoms (high backscatter), like harder features or gravelly bottoms, are represented as lighter tones, while less reflective bottoms (low backscatter) are shown as darker tones. The causes for darker tones on a sonar record may be grouped in 3 main categories:

- Sediment type that provides less backscattering of the sonar beam, such as soft or smooth bottom sediments;
- Seafloor orientation that provides less backscatter, such as an area inclined away from the towfish;
- Shadow zones generally mean absence of energy return, associated to topographic features on the terrain (both positive and negative) or objects at the bottom (Figure 28).

Shadows are often one of the most important interpretation tools, providing a three dimensional assessment of features on a two dimensional sonar record. Shadows are therefore of extreme importance and the interpreter can use their position, shape and intensity to interpret the sonar records and determine object height and vertical geometry (Kenny *et al.*, 2001). The shadows intensity also may give some important information about the character of the objects: some bottom features, such as a gentle upward localized slope or an acoustically translucent object, cause only a slight shadow in the sonar record; however, other objects, such as rocks, berforms or shipwrecks, can cause a strong shadow.

As mentioned above, besides features identification, the shadows also allow to estimate the object height. The acoustic energy path from the sonar until reaches the seafloor is relatively straight, and therefore a right triangle with the angles at the sonar, the nadir (right angle) and the tip of the feature shadow is formed (Figure 29). The feature of interest intersects the base and the hypotenuse of this triangle, forming a smaller right triangle, which is geometrically similar to the other one. According to the Thales Theorem, the target's height may be estimated by the product of the acoustic shadow length (S) and the height of the towfish (H) above the seabed, divided by the slant range (S_r) from the sonar to the end of the feature shadow (Figure 29 and Equation (12); Kenny *et al.*, 2001). This estimation is generally accurate in normal sonar operations; however, when operating in unusual conditions, such as severe water stratification that induces the ray path refraction or the presence of other targets that affect the primary target's shadow, the interpretation should be done more carefully.

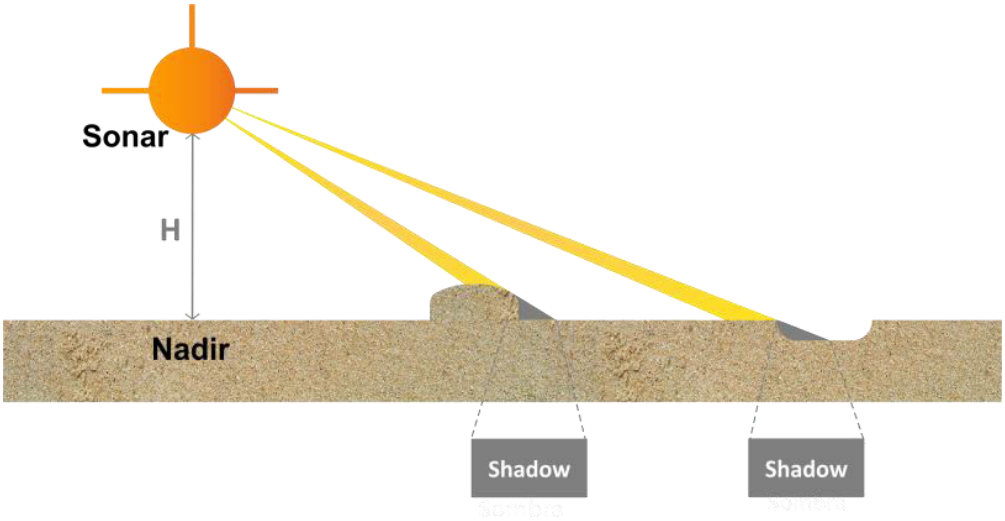

Figure 28. Illustration (vertical section view) showing the shadow formation.

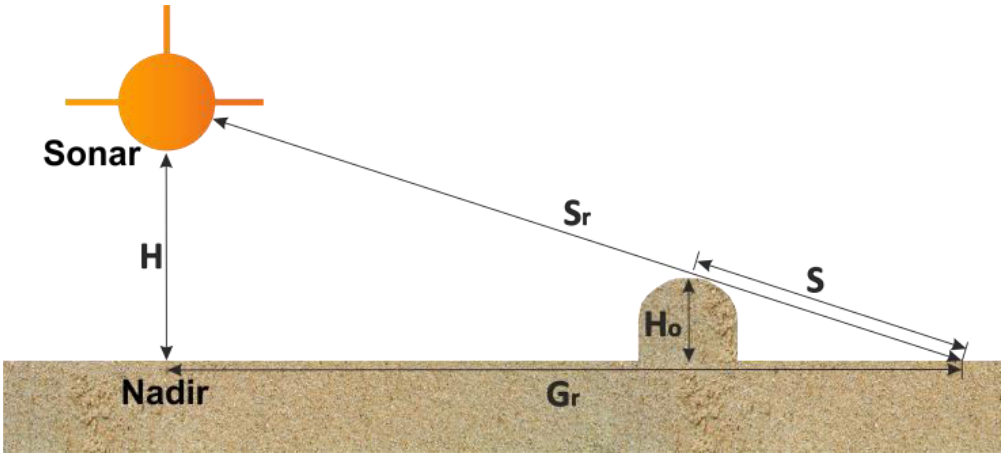

Figure 29. Illustration (vertical section view) showing object height estimation from the shadow size recorded in a sonograph, according to Thales Theorem.

$$H_0 = \frac{S.H}{S_r} \quad \textbf{(12)}$$

Several works have demonstrated the dependence of the acoustic backscatter variations on the sediment grain-size distribution. Davis et al. (1996) investigate the relationship between spatial variations of the properties of seafloor sediments and acoustic backscatter, concluding that acoustic backscatter strength also correlates directly with the carbonate content of the sediments, because large, irregularly shaped, carbonate particles affect both the mean grain size of the sediments and the roughness of the surface of the seafloor. Blondel et al. (1998) presented a method of textural analysis (TexAn technique) that enables quantitative assessments of sidescan sonar imagery, at all stages of processing and in all conditions. Goff et al. (1999) showed that, under well-controlled circumstances, a degree of correlation can be obtained; however, since backscatter intensity is influenced by several factors

including slope, surface roughness and volumetric heterogeneity, its interpretation is often difficult. Preston et al. (2004) described techniques, based on amplitudes and texture, for automated classifications of sidescan sonar images. Collier and Brown (2005) studied the dependence of acoustic backscatter on sediment grain size distribution, finding a positive correlation between mean backscatter intensity and mean grain size and also between the standard deviations of the backscatter and grain size distributions, meaning that poorly sorted sediments present the most variable backscatter.

Sidescan sonar is also an important tool for the study of sedimentary bedforms (see for example Chapter V). Ocean currents interact with bottom sediments of various grain sizes and compositions to produce a variety of bedform types and dimensions. In fact, the transport of sediment in bedload or close to the bed by waves and by combined wave and current flow leads to the development of characteristic forms on the bottom surface, such as ripples, megaripples or dunes, sand waves, sand ridges, shorelines, and subsurface channels (Davidson-Arnott, 2010).

The creation and morphology of the bedforms have been studied in wave tanks and oscillatory tubes by Mogridge and Kamphuis (1972), O'Donoghue and Clubb (2001) and van derWerf et al. (2006), as well as in the field, by Inman (1957), Clifton et al., (1971), Miller and Komar (1980), Sherman and Greenwood (1984), Osborne and Vincent (1993), and Swales et al. (2006). The bedforms' morphology seems to be mainly controlled by the diameter of the sediment, the shear stress exerted on the bed, the flow depth, and the velocity asymmetry in the waves or combined wave and current flow (Davidson-Arnott, 2010). Several experiments have demonstrated the sequences of bedforms produced as these parameters are varied. Harms et al. (1975), for example, showed the stability fields of bedforms for flow depths of about 20 cm (see Figure 30, Miall, 1990).

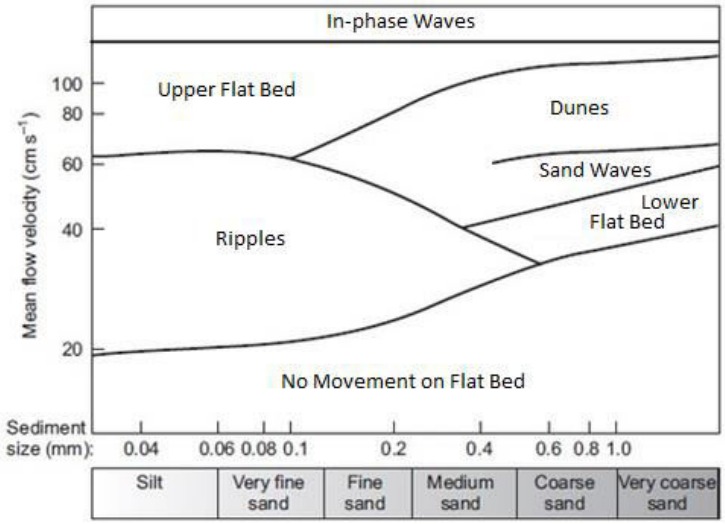

Figure 30. Bedforms stability fields in sand and silt in a flow depth of 20 cm (adapted fron Harms et al., 1975 *in* Miall, 1990).

Ripples, megaripples, and sand waves are bedforms associated with sediment redistribution that occur on non-cohesive surfaces as undulations oriented transverse to the main direction of water flow (Blondel, 2009). The classification of these bedforms regarding the size is not completely uniform, although dunes are larger scale bedforms than ripples (Table 2; Turcker, 1982).

Table 2. Bedform classification based on size (wavelength, L, and height, H) and according to different authors (Turker, 1982; Elliot, 1978; Bird, 2008).

	Wavelength (L)	Height (H)	According to
Wave ripples	9 mm – 2 m	3 mm – 25 cm	Turcker (1982)
Current ripples	< 60 cm	< 6 cm	Turcker (1982)
Dunes or megaripples	1 – 10 m (or more) Several meters	> 50 cm < 1 m (or more)	Turcker (1982) Bird (2008)
Sand waves or bars	Hundreds of meters 30 – 500 m	Several meters 1.5 - 15 m	Turcker (1982) Elliot (1978)

Ripples may be formed either by wave action, or by currents, or by a combination of both processes (Bird, 2008). Wave-formed ripples are usually symmetrical and parallel, shaped by eddies that form as a wave passes, separating, steepening and sharpening the ripple crests (Bird, 2008); asymmetrical varieties do occur and may be difficult to distinguish from straight-crested current ripples (Turker, 1982). The crests of wave-formed ripples are generally straight and crest bifurcation is common. Wave length is affected by sediment grain size and water depth; larger ripples occur in coarser sediment and deeper water (Turker, 1982). Ripples produced by pure oscillatory flow are well studied and understood; however it is still very difficult to predict bedform type and dimensions in the highly variable flows in the breaker and surf zones where wave motion is highly asymmetric and where the contribution of unidirectional flows varies rapidly both temporally and spatially (Davidson-Arnott, 2010).

Current ripples are produced by unidirectional currents so they are asymmetric with a steep lee side and gentle stoss side (Dunbar and Rodgers, 1957; Turker, 1982). Their axes are approximately at right angles to the current with a steeper face away from the current (Dunbar and Rodgers, 1957; Bird, 2008). According to Turker (1982), current ripples do not form in sediment coarser than 0.6 mm diameter (coarse sand). On the basis of shape, four types of current ripples are common: straight crested, sinuous or undulatory, catenary and linguoid ripples (Figure 31). Lunate ripples do occur but are rare. With the increasing flow velocity of the current and the decreasing of flow depth, straight ripples pass into linguoid ripples via the transitional sinuous and catenary ripples (Turker, 1982; Miall, 1990).

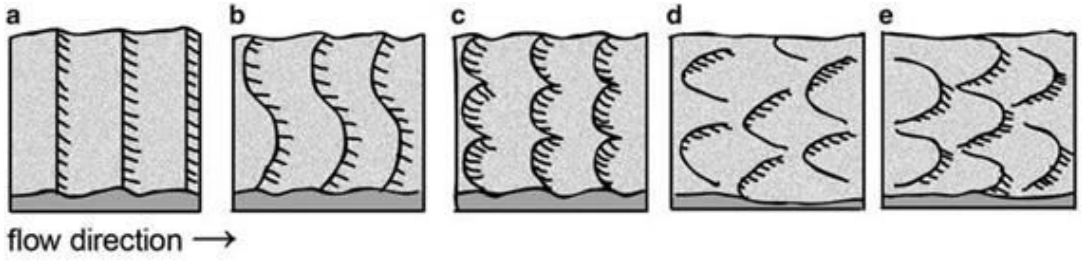

Figure 31. Crest plans of current ripples and megaripples: **(a)** straight-crested; **(b)** undulatory or sinuous; **(c)** catenary; **(d)** lunate; and **(e)** linguoid (adapted from Turcker, 1982).

Associations of cross-currents generated by waves and tides can produce decussate or rhomboidal networks of transverse current ripples. In addition, there are longitudinal ripples that form parallel to a strong unidirectional current, and these can be complicated by interfering wave motion and cross-current patterns (Bird, 2008).

Underwater ripples increase in length up to a critical flow velocity at which they disappear (Figure 30). In fact, the length of ripples formed under water varies greatly and is controlled by definite factors among which current velocity and coarseness of the sand are absolutely important (Gilbert, 1914 *in* Dunbar and Rodgers, 1957; Figure 30).

Dunes or megaripples are particularly common on the floor and flanks of channels and correspond to larger-scale structures of similar shape to ripples (Table 2). Dune shape varies from straight-crested to sinuous to lunate with increasing flow velocity and decreasing flow depth (Figure 31); linguoid dunes are very rare (Turker, 1982; Miall, 1990). They are formed by strong currents, and are usually aligned at right angles to the tidal flow, migrating in the direction of the current, but sometimes they run diagonally or parallel to the current flow (Bird, 2008). Magerippples frequently present ripples on the banks and in the troughs (Turker, 1982).

Sand waves (bars) are larger scale than dunes (Table 2) straight crested asymmetrical bedforms, although some authors apply this term to straight crested dunes. They occur where current velocities are greater than 65 cm/s (Elliot, 1978). Sand waves are present in rivers and similar structures occur on shallow marine shelves. In rivers, sand waves form at lower velocities and at shallower depths than dunes (Turker, 1982).

Bedforms may reverse or retain their orientation during the ebb-flood cycle which depends on the size of the bedform and the degree of time-velocity asymmetry. Current ripples always reverse, however megaripples reverse in some cases. For example, in estuaries with pronounced time-velocity asymmetry, megaripples retain their orientation and form semi-permanent fields of ebb or flood-oriented dunes (Elliot, 1978).

Finnally, sidescan sonar data interpretation can be significantly facilitated when draped on top of bathymetric data, in particular on top of high resolution bathymetry such as standard multibeam. The same type of sediment, for example, will appear with much stronger backscatter if it is lying on a slope facing the sidescan sonar beam, than when it is lying on a horizontal seafloor or on a slope with the opposite dip - this can be easily mistaken by a change in type or grain size of sediment. The inclusion of the bathymetric information therefore allows distinguishing topographic effects from variations in geological character on the backscatter intensity (Figure 32; Pinheiro *et al.*, 2011).

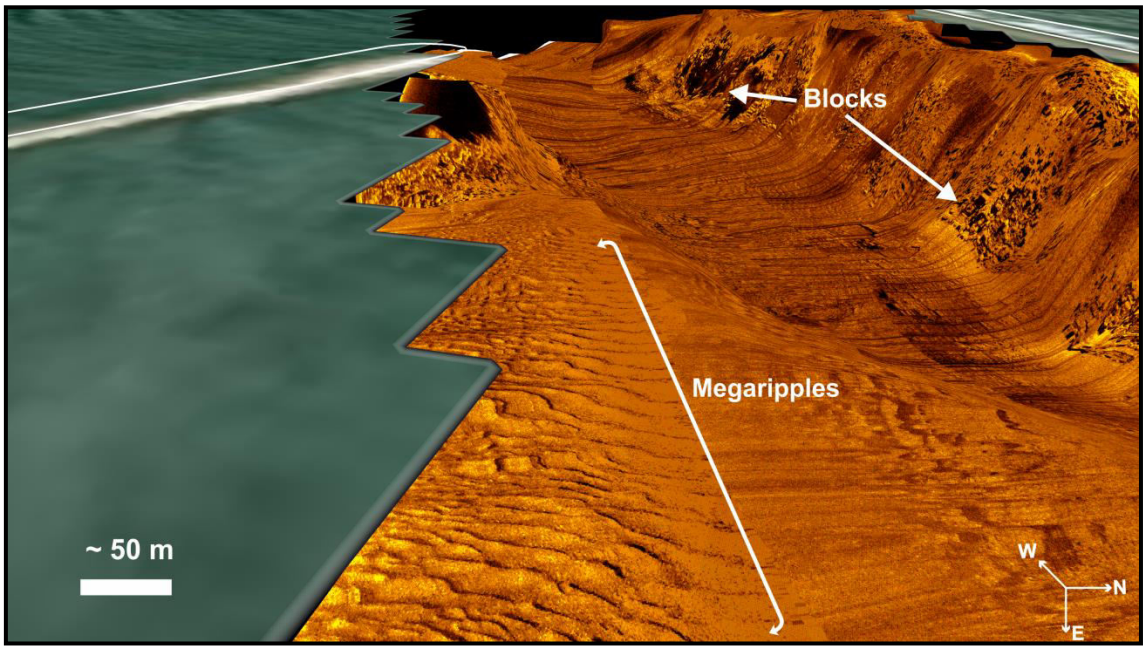

Figure 32. Sidescan sonar mosaic image from Aveiro entrance to the Port area projected on top of the bathymetry (Pinheiro et al., 2011). Note the very interesting bedforms (dunes) observed in the first plan.

III.3. Grain size analysis

Sediment grain size (granulometry) affects the particles entrainment, transport and deposition, thereby providing important clues about the sediment provenance, transport history, and depositional conditions (e.g. Folk and Ward, 1957; Friedman, 1979). The size of the sedimentary particles reflects: the availability of different kinds and sizes of grain from different kinds of bedrock or even preexisting sediment; the resistance of particles to weathering, erosion, and abrasion; and the processes of transportation by air or water and deposition (Friedman and Sanders, 1978; Friedman, 1979).

Sediment particles range, as a continuous spectrum, from a fraction of a micron, to boulders measuring meters in diameter. Geologists have developed standard size classes of sediment based on a logarithmic grade scale, where the boundaries between successive size classes differ by a factor of two (see Table 3; Udden, 1914; Wentworth, 1922).

Table 3. Classification of sediment grain sizes by their diameters (in both metric -mm/μm- and logarithmic -ϕ- units) based on different authors: Udden (1914) and Wentworth (1922); Friedman and Sanders (1978); and Blott and Pye (2001) adopted in "GRADISTAT" version 8.0.

Grain Size			Descriptive terminology		
phi	mm/μm		Udden (1914) and Wentworth (1922)	Friedman and Sanders (1978)	Blott and Pye (2001)
-11	2048	mm	Cobbles	Very large boulders	
-10	1024			Large boulders	Very large boulders
-9	512			Medium boulders	Large boulders
-8	256			Small boulders	Medium boulders
-7	128			Large cobbles	Small boulders
-6	64			Small cobbles	Very small boulders
-5	32		Pebbles	Very coarse pebbles	Very coarse gravel
-4	16			Coarse pebbles	Coarse gravel
-3	8			Medium pebbles	Medium gravel
-2	4			Fine pebbles	Fine gravel
-1	2		Granules	Very fine pebbles	Very fine gravel
0	1		Very coarse sand	Very coarse sand	Very coarse sand
1	500	μm	Coarse sand	Coarse sand	Coarse sand
2	250		Medium sand	Medium sand	Medium sand
3	125		Fine sand	Fine sand	Fine sand
4	63		Very fine sand	Very fine sand	Very fine sand
5	31		Silt	Very coarse silt	Very coarse silt
6	16			Coarse silt	Coarse silt
7	8			Medium silt	Medium silt
8	4			Fine silt	Fine silt
9	2		Clay	Very fine silt	Very fine silt
				Clay	Clay

In order to facilitate graphical presentation and statistical manipulation of grain size distribution, Krumbein (1934) proposed that the grade scale should be transformed into a phi (ϕ) scale, by using the expression described on Equation (13), where *d* corresponds to the grain diameter in millimeters. Distributions using these scales are named log-normal and are conventionally used in sedimentology (e.g. Visher, 1969; Middleton, 1976). The nomenclature used to classify sediment particles based on their grain diameters and according to different authors is shown in Table 3.

$$\phi = -\log_2 d \quad \textbf{(13)}$$

Any individual particle can be referred to one of the individual size classes and many sedimentary deposits consist in pure sand, silt, or clay (Table 3), although natural populations of sediments commonly include particles from several size classes, making the granulometry analysis a study of mixture of sizes. There are several techniques employed to determinate the proportions of each size class, including direct measurement, dry and wet sieving, sedimentation rates determination, laser granulometry, and using equipments such as the X-ray sedigraph or the Coulter counter. All these techniques involve the division of the sediment sample into a number of size fractions, allowing the creation of a grain size distribution from the weight or volume percentage of sediment in each size fraction (Blott and Pye, 2001).

In order to compare different sedimentary deposits, grain size distributions have most frequently been described by their deviation from a prescribed ideal distribution – normal distribution, also known as Gaussian, mainly based on five principal parameters: (a) the median, (b) the mean size, (c) the standard deviation or sorting, (d) the symmetry or skewness, and (e) the kurtosis. These parameters, mainly the mean, sorting, and skewness of grain size frequency distributions, follow trends that may indicate the direction of transport and the sedimentary processes of winnowing, selective deposition, and total deposition (McLaren and Bowles, 1985). The median diameter, also known as particle size distribution D_{50}, corresponds to the value of the particle diameter at 50% in the cumulative distribution, i.e., to the grain size value at which 50% of the grains are coarser. The mean ($\overline{x}$), also referred as average, identifies the central location of the data and the standard deviation (σ) measures the spreading of the sizes around the mean, which defines the concept of sorting. A frequency curve of a well-sorted sediment is sharp peaked and narrow, meaning that only a few size classes are present, and a poorly sorted sediment presents a low and wide distribution curve, indicating the presence of many size classes (see Figure 33; Friedman and Sanders, 1978).

The skewness is a statistical parameter that measures the deviation from the symmetry of the distribution, indicating the preferential spread to one side of the average (see Figure 34), and therefore if the fraction in excess of the normal

distribution corresponds to the coarser or finer fraction. This parameter has been used in interpreting how particles were deposited (Freidman and Sanders, 1978) and may also give clues about the erosion process.

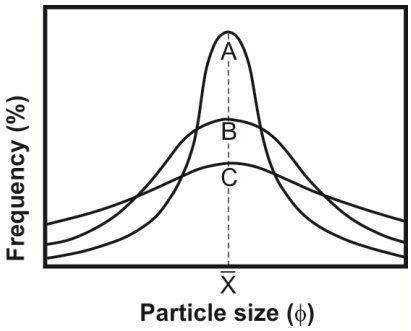

Figure 33. Normal size frequency distribution curves of different shapes, showing that steep curves (curve A) encompass a small number of phi classes between the two inflection points and flat and wide curves (curve C) comprehend a large number of phi classes (Friedman and Sanders, 1978).

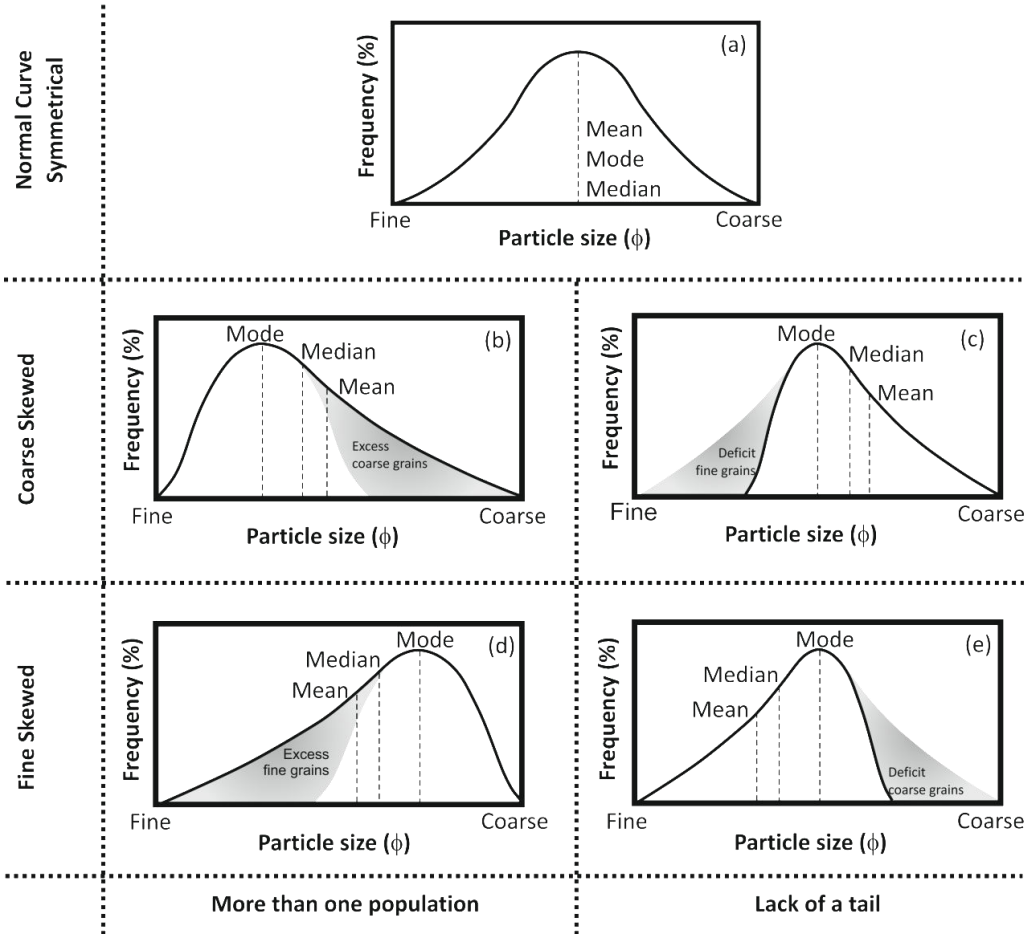

Figure 34. Frequency distribution curves with different skewness: **(a)** symmetrical; **(b)** coarse skewed by introduction of coarse particles; **(c)** coarse skewed by removal of fine particles; **(d)** fine skewed by introduction of fine particles; and **(e)** fine skewed by removal of coarse particles (adapted from Friedman and Sanders, 1978).

The kurtosis measures the degree of concentration of the grains relative to the average (Freidman and Sanders, 1978). Sharper peaks than the normal curves (*mesokurtic*) are described as *leptokurtic*, indicating a high concentration of grains close to the mean size, and distributions with flatter peaks are termed *platykurtic*, indicating a more equitable distribution of sediments throughout the classes (see Figure 35).

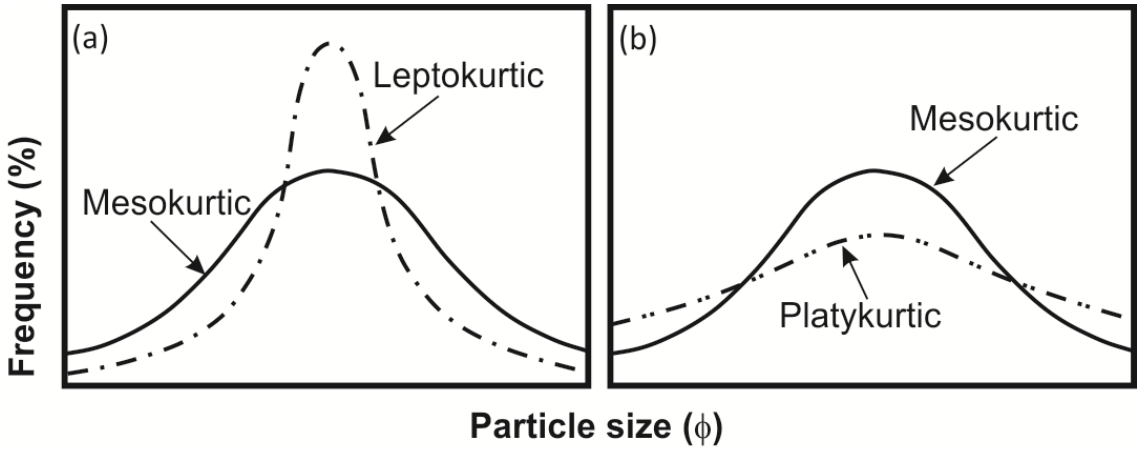

Figure 35. Frequency distribution curves with different kurtoses: **(a)** leptokurtic and **(b)** platykurtic (adapted from Friedman and Sanders, 1978).

According to Folk and Ward (1957), both skewness and kurtosis are vital clues to distinguish characteristics of polymodal sediments, even when the modes are not immediately apparent. The mode corresponds to the most frequently occurring particle size (graphically matches to the peak of a simple frequency curve as shown in Figure 34). Strictly unimodal sediments should give normal curves, non-normal values of skewness and kurtosis may indicate a mixing of two or more modal fractions (Folk and Ward, 1957), suggesting the presence of sub-populations. This fact may be due to one of the following situations: (1) the particles have been derived from several sources and the deposit corresponds to a mixture of different populations (Folk and Ward, 1957; Spencer, 1963, Komar, 1976), or (2) the removal of part of the sediment of a single population originally projected in one of the tails of the normal curve (Komar, 1976). Therefore, in the multipopulation or polymodal sedimentary deposits, the magnitude of the modes may give significant information on the mixing of sediments (Friedman and Sanders, 1978).

The above mentioned parameters can be obtained by mathematical or graphical methods. The mathematical “method of moments” (Krumbein and Pettijohn, 1938; Friedman and Johnson, 1982) uses the entire sample population and therefore is the most accurate method; however, the statistics are significantly affected by outliers in the extremes of the distribution (McManus, 1988). The graphical methods, based on

plotting the frequency data as a cumulative frequency curve, extracting prescribed values and introducing them into established formulations, are more suitable for the analysis of open-ended distributions, because the tails, and so the extreme outliers, are ignored. Many alternative formulations have been proposed (e.g. Trask, 1932; Krumbein, 1938; Otto, 1939; Inman, 1952; McCammon, 1962) but still the most widely used is the one proposed by Folk and Ward (1957) which will be the one used in the present work (see Table 4).

Table 4. Statistical formulations for grain size parameters estimation and respective descriptive terminology, both based on logarithmic Folk and Ward (1957) graphical measures. ϕ_x represents the grain diameters, in phi units, at the cumulative percentile value of x (Folk and Ward, 1957; Blott and Pye, 2001).

	Interval	***Descriptive terminology***
Mean size (ϕ)		
$M_Z = \frac{\phi_{16} + \phi_{50} + \phi_{84}}{3}$	See Table 3 (Grain size)	See Table 3 (Descriptive terminology – Blott and Pye, 2001)
Sorting (ϕ)		
$\sigma_I = \frac{\phi_{84} - \phi_{16}}{4} + \frac{\phi_{95} - \phi_5}{6.6}$	<0.35	*Very Well Sorted*
	0.35 – 0.50	*Well Sorted*
	0.50 – 0.70	*Moderately Well Sorted*
	0.70 – 1.00	*Moderately Sorted*
	1.00 – 2.00	*Poorly Sorted*
	2.00 – 4.00	*Very Poorly Sorted*
	>4.00	*Extremely Poorly Sorted*
Skewness		
$Sk_I = \frac{\phi_{16} + \phi_{84} - 2\phi_{50}}{2(\phi_{84} - \phi_{16})} + \frac{\phi_5 + \phi_{95} - 2\phi_{50}}{2(\phi_{95} - \phi_5)}$	$^{+}$0.3 - $^{+}$1.0	*Very Fine Skewed*
	$^{+}$0.1 - $^{+}$0.3	*Fine Skewed*
	$^{+}$0.1 - $^{-}$0.1	*Symmetrical*
	$^{-}$0.1 - $^{-}$0.3	*Coarse Skewed*
	$^{-}$0.3 - $^{-}$1.0	*Very Coarse Skewed*
Kurtosis		
$K_G = \frac{\phi_{95} - \phi_5}{2.44(\phi_{75} - \phi_{25})}$	<0.67	*Very Platykurtic*
	0.67 – 0.90	*Platykurtic*
	0.90 – 1.11	*Mesokurtic*
	1.11 – 1.50	*Leptokurtic*
	1.50 – 3.00	*Very Leptokurtic*
	>3.00	*Extremely Leptokurtic*

In order to estimate the parameters mentioned above and to analyze the grain size distributions, the GRADISTAT version 8.0 program (Blott and Pye, 2001) was used in this study. This program, written in Microsoft Visual Basic and integrated into a Microsoft Excel spreadsheet, allows the estimation of grain size statistics by both Folk and Ward (1957) and using the moments methods. Besides the statistical parameters already mentioned, the program also provides a physical description of the textural group and the sediment name based on Folk (1954). This author considers two main parameters for sediment classification: the percentage of gravel and the sand to mud ratio (see Figure 36). According to Folk (1954), this sediment classification system allows the distinction of different depositional regimes, since the gravel content gives indications about the maximum current velocities and the sand to mud ratio reflects

the characteristics of the flow (see an example printout from the program in Figure 37).

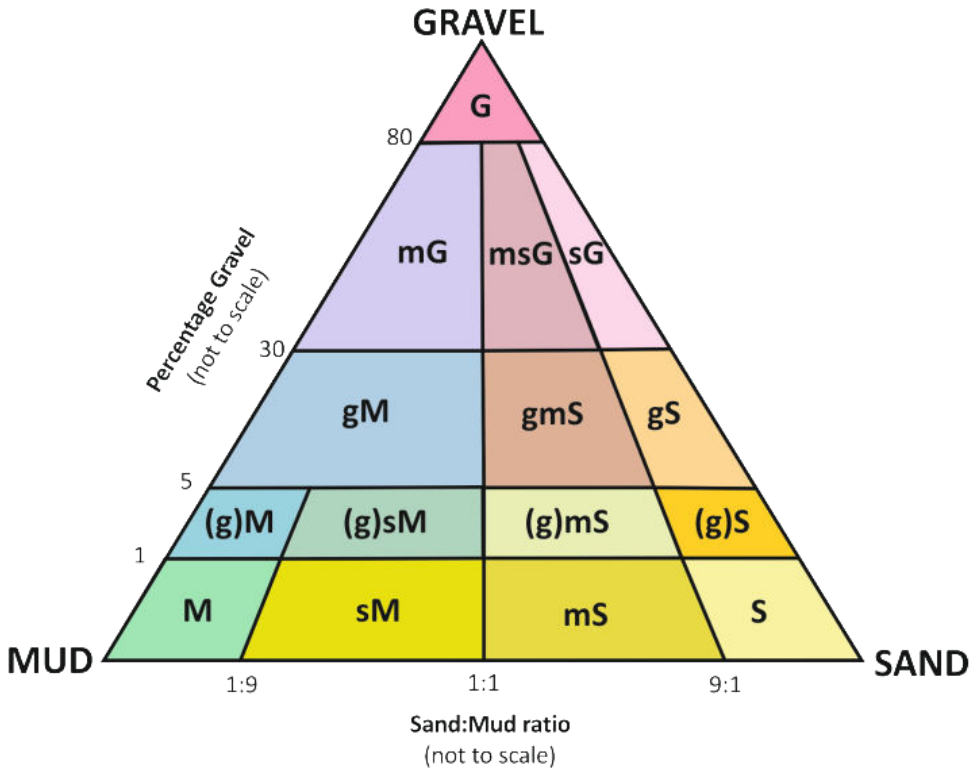

M	Mud		
sM	Sandy mud	**(g)mS**	Slightly gravelly muddy sand
(g)M	Slightly gravelly mud	**gmS**	Gravelly muddy sand
(g)sM	Slightly gravelly sandy mud	**gS**	Gravelly sand
gM	Gravelly mud	**G**	Gravel
S	Sand	**mG**	Muddy gravel
mS	Muddy sand	**msG**	Muddy sandy gravel
(g)S	Slightly gravelly sand	**sG**	Sandy gravel

Figure 36. Folk triangular diagram to coarse sediment classification (adapted from Folk, 1954).

SIEVING ERROR: 1,2%

SAMPLE STATISTICS

SAMPLE IDENTITY: **BARRA1** ANALYST & DATE: ,

SAMPLE TYPE: Unimodal, Moderately Well Sorted TEXTURAL GROUP: Slightly Gravelly Sand

SEDIMENT NAME: Slightly Very Fine Gravelly Medium Sand

	µm	ϕ
MODE 1:	427,5	1,247
MODE 2:		
MODE 3:		
D_{10}:	216,4	0,492
MEDIAN or D_{50}:	379,1	1,399
D_{90}:	711,2	2,208
(D_{90} / D_{10}):	3,286	4,491
(D_{90} - D_{10}):	494,8	1,716
(D_{75} / D_{25}):	1,802	1,865
(D_{75} - D_{25}):	225,4	0,850

GRAIN SIZE DISTRIBUTION

GRAVEL:	1,4%	COARSE SAND:	20,5%
SAND:	98,4%	MEDIUM SAND:	59,0%
MUD:	0,2%	FINE SAND:	14,9%
		V FINE SAND:	0,3%
V COARSE GRAVEL:	0,0%	V COARSE SILT:	0,0%
COARSE GRAVEL:	0,0%	COARSE SILT:	0,0%
MEDIUM GRAVEL:	0,0%	MEDIUM SILT:	0,0%
FINE GRAVEL:	0,6%	FINE SILT:	0,0%
V FINE GRAVEL:	0,8%	V FINE SILT:	0,0%
V COARSE SAND:	3,6%	CLAY:	0,0%

	METHOD OF MOMENTS			FOLK & WARD METHOD		
	Arithmetic	Geometric	Logarithmic	Geometric	Logarithmic	Description
	µm	µm	ϕ	µm	ϕ	
MEAN ($\bar{x}$):	485,9	395,3	1,339	389,7	1,360	Medium Sand
SORTING (σ):	474,5	1,749	0,806	1,614	0,691	Moderately Well Sorted
SKEWNESS (Sk):	6,065	0,344	-0,344	0,131	-0,131	Coarse Skewed
KURTOSIS (K):	49,64	10,46	10,46	1,162	1,162	Leptokurtic

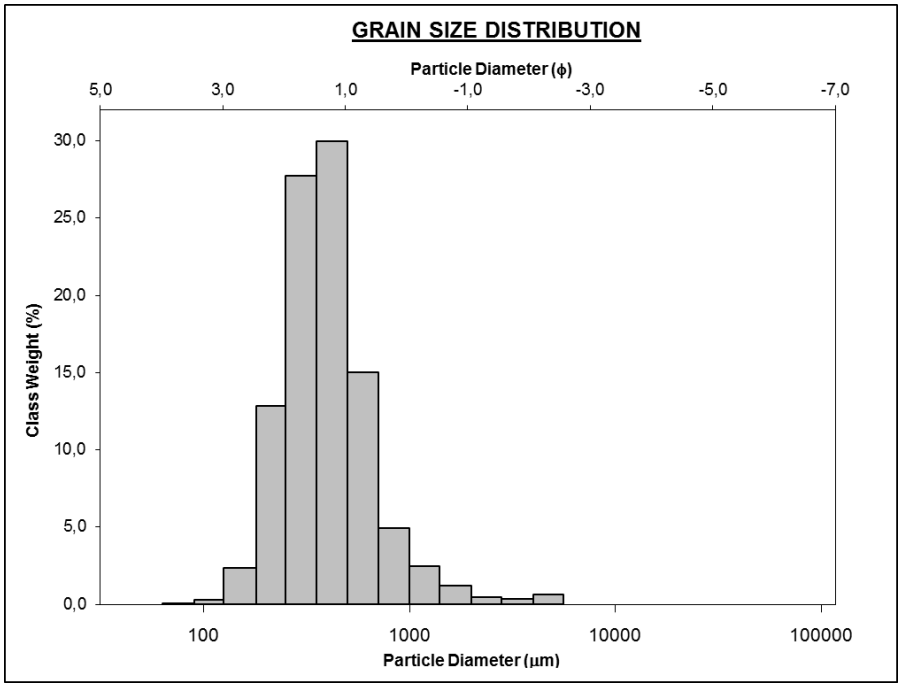

Figure 37. Example of a GRADISTAT v8.0 printout for the sediment sample "BARRA1". The black box highlights the parameters values obtained by the chosen statistical method.

III.4. Morphodynamical Model – MORSYS 2D

The morphodynamic modeling system MORSYS2D (Figure 38; Fortunato and Oliveira, 2004, 2007; Bertin et al., 2009) integrates the circulation model ELCIRC (Zhang et al., 2004), the wave propagation model SWAN (Booij et al., 1999) and the sediment transport and bottom evolution model SAND2D (Fortunato and Oliveira, 2004, 2007;

Bertin et al., 2009), in order to simulate the non-cohesive sediment dynamics in estuaries, tidal inlets and coastal areas, driven by tides, wind, river flows and waves.

SWAN or *Simulating Waves Nearshore* is a numerical wave model that, based on an Eulerian formulation, computes random and short-crested waves in coastal regions, by describing the evolution of the two-dimensional wave energy spectrum in arbitrary conditions of wind, currents, and bathymetry (Booij et al., 1999; Ris et al., 1999). In MORSYS2D, SWAN is used in a stationary mode to simulate wave propagation and deformation from the open sea up to coastal zones (Bertin et al., 2009).

The hydrodynamic model ELCIRC is an open-source three-dimensional baroclinic model that calculates tidal elevations and currents and wind-induced mean currents by solving the shallow water equations using a semi-implicit Eulerian–Lagrangian finite volume and finite differences method (Zhang et al., 2004). Within MORSYS2D a single vertical layer is used.

SAND2D (Fortunato and Oliveira, 2004, 2007; Bertin et al., 2009) computes the sand fluxes in combined current and wave flows, from three well known semi-empirical formulations (Bijker, 1971; Ackers and White, see van de Graaff and van Overeem, 1979; Soulsby van Rijn, see Soulsby, 1997), and computes the seabottom changes through the numerical resolution of the Exner equation that describes the conservation of mass of the sediment.

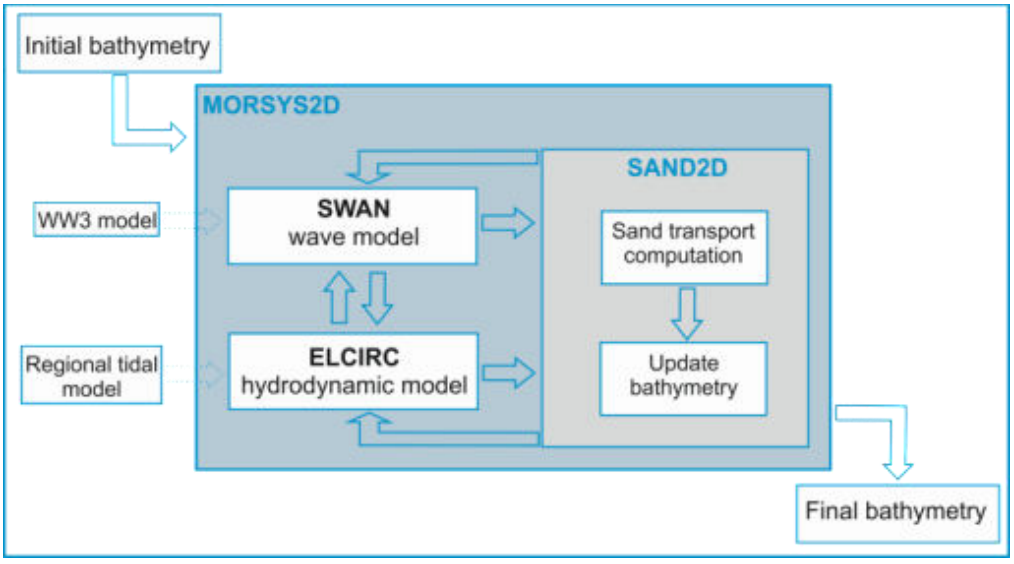

Figure 38. Flowchart of MORSYS2D numerical model procedure used in this work.

Chapter IV. Evolution of a sand extraction excavation offshore Vale do Lobo, Algarve

IV.1. Introduction

This chapter investigates the morpho-sedimentary evolution of an excavation area located offshore Vale do Lobo in the Algarve, south of Portugal, resulting from the sand exploitation for the nourishment of the Vale do Lobo beach (see section II.1). The study is based on 4 bathymetric surveys, prior to and after the dredging operations and within a time span of four years (2006-2010), complemented with the analysis of wave data and numerical morphodynamic modelling simulations. The main aims are to understand the evolution of the offshore sandpit through time and the physical mechanisms responsible for this evolution and to estimate the sandpit recovery time from the observed and predicted filling rate. Specific objectives are:

- To follow and understand the sandpit evolution based on bathymetric datasets acquired prior to and after the sand extraction (2006-2010);
- To characterize the regional wave climate, namely the significant wave height, mean period, and mean wave direction, in the study area during the period in analysis;
- To estimate the sandpit recovery time from the observed and predicted filling rate;
- To correlate the wave climate conditions, namely the storm events, with the sandpit dynamic evolution.

The main results of this part of the thesis were published in Gonçalves et al. (2014), *Coastal Engineering*, 88, 75-87 (Appendix I).

IV.2. Brief overview of some case studies of offshore sand extraction

The offshore extraction of sediments from coastal areas, namely in the continental shelf and shoreface, has been a common practice in many countries for many years, and it has become, in some places, such as United Kingdom and Japan, the main source of aggregates for beach nourishment and for construction (Demir et al., 2004, Cooper et al., 2007; Kubicki et al., 2007). It has been shown to have several advantages compared with onshore exploitation, since extraction from rivers, estuaries and nearshore sand bars has proven in the past few years to have significant negative environmental and social impacts. Nevertheless, offshore sand extraction can also have negative impacts in the marine environment, not only in the morphodynamics of the region, but also in the local ecosystems, and this is often not restricted to the excavation area (van Rijn and Walstra, 2002; van Rijn et al., 2005; Kubicki et al., 2007).

The morphology and morphodynamics of the seabed are strongly affected by the creation of the local depression due to the excavation. The induced bottom morphology changes will in general influence the local flow, the wave field and consequently the sand transport rates (van Rijn and Walstra, 2002). Locally, the sediments from the surrounding areas tend to move inside the depression. Changes in the wave field, through refraction and, less significantly, also through diffraction, can modify the longshore sediment transport patterns and affect the shoreline morphology (Demir et al., 2004). Over longer time scales, the sandpit area can migrate towards the shore and may act as a sink for the sediments from the nearshore system (van Rijn and Walstra, 2002). The severity and persistence of such impacts depend, among other factors, on the hydrodynamic conditions, the nature of the substrate, the sandpit geometry and its distance to the shore, and the time-scale of the seabed perturbation (Cooper et al., 2007; Roos et al., 2008). In order to minimize these effects and the nearshore coastal erosion, the extraction areas need to be located offshore of the closure depth.

The temporal evolution of sandpits and the associated coastline impacts have been studied and are well documented (e.g. Bender and Dean, 2003; Hitchcock and Bell, 2004; Roos, 2004; Diesing et al., 2006; Kubicki et al., 2007; and Teixeira, 2011). Roos (2004) summarizes several pits monitored through time and located both in the Dutch part of the North Sea and elsewhere around the world (Table 5). Most of the pits referred in Table 5 are relatively small (with sizes smaller than 1 Mm^3 and excavation depths that vary from 7 to 15 m), located in nearshore waters (with 2 to 10 m water depths) and almost all tend to fill in with sand from the surrounding areas, in the course of several years. Exceptions are the excavations performed in Hook of Holland and Terschelling, both in Holland, with high volume and located at higher depths (Roos, 2004).

Table 5 shows recovery times of around 1 year or less, in general, for pits located nearshore ($h_0 < 10$ m) and higher recovery times for pits located at depths greater than 10 m. The Hook of Holland sandpit (Table 5), a large and deep pit (500 m × 1300 m × 10 m), was extensively monitored during half a year, showing a small morphological evolution, weak migration and sedimentation at the pit slopes (Roos, 2004).

Kubicki et al. (2007) studied the morphological evolution of two extraction sites (gravel and sand pits) located at Tromper Wiek in the Baltic Sea (Figure 39), for a six years period (1999-2005). Based on sidescan sonar data acquired between 1999 and 2004, multibeam bathymetric data from 2003 to 2005, and grab samples collected in 2004, these authors determined the natural refiling speed of the pits, which slowed during the monitoring period. The mean refilling rates of the sand pits, which are located at almost twice the water depth as the gravel pit, were higher over the same monitoring period. Since the finer sediment is mobilized in lower energy events, the

changes observed in the sand pit area were more dynamic than at the gravel pit site (Kubicki et al., 2007).

Table 5. Overview of the field experience regarding marine sand extraction (Roos, 2004), with the sandpit location, year of the extraction, pit size in Mm^3, pit depth (h_{pit}), water depth (h_0), and refill time. Sources: [1]Svašek (1965), [2]Kojima et al. (1987), [3]Hoogewoning and Boers (2001), [4]Combe and Soileau (1987), [5]Uda et al. (1995), [6]Van Dalfsen and Essink (1997) and Van Dalfsen (1998), [7]MAGIS (n.d.), [8]Hesp and Hilton (1996), [9]Hoogewoning (2000) and Svašek (2001abc).

	Year	Size (Mm^3)	h_{pit} (m)	h_0 (m)	Refill time(yr), observations
Scheveningen[1]	1964	0.02	2	7-10	0.5, flattening slopes
Tosa Bay (Jap)[2]	1978	0.4	5–7	5–7	severe wave-induced erosion
Loswal/Stevin pit[3]	1981–83	0.06	6	15.5	0.6, both sand and silt
Louisiana (US)[4]	1983	2.5	3-6	10	wavy pattern on the beach
Kyushu (Jap)[5]	1983	1-2	2-6	15-40	shallow pits affect shoreline
Ameland[3]	1990	0.14	7	9	1.0, migration 20 m yr^{-1}
Ameland (ctd.)[3]	1992–93	0.25	4	10	0.5, migration
Terschelling[3,6]	1993	2.5	2	>20	no activity in 4 years
Bloemend./Zandv.[3]	1993–94	-	-	7	already closed after 8 days (artificially refilled)
Heemskerk[3]	1996–97	0.15	8	7-8	0.6, cross-shore refilling (artificially refilled)
Sylt (Ger)[7]	-	-	6	14	more stable than expected
Wadden Sea (Ger)[7]	1994–98	-	-	-	stable over 4 years
Pakiri beach (N-Zl)[8]	1993-	0.1	-	<8	weaker recovery from storms
Hook of H/PUTMOR[9]	1999-2000	6.5	10	24	flow contr., no morph. evolution (monitoring period -5 months- too short to detect significant morphological changes)

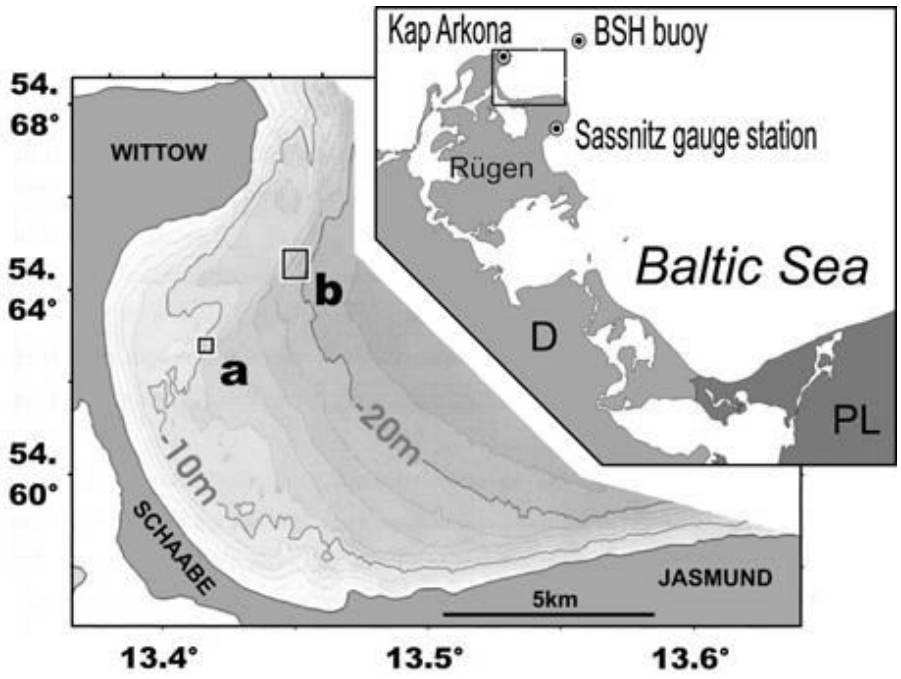

Figure 39. Location of the Tromper Wiek in Baltic Sea and indication of the gravel **(a)** and the sand **(b)** pit sites (Kubicki et al., 2007).

Diesing et al. (2006) compared time scales of regeneration of different extraction sites located at different water depths, with most of the sites located near the seaward limit of the shoreface (GM1, WU, and WL in Figure 40), one located on the upper shoreface (PAK in Figure 40), and two deeper pits (TW0 and TW1 in Figure 40) situated in the continental shelf (Figure 40). These authors concluded that the time scales of regeneration are profoundly determined by the position of the extraction site relative to the seaward limit of the shoreface: extraction sites located well beyond this limit generally present a slow regeneration; in contrast, sand extractions located on the upper shoreface may exhibit a fast regeneration, although negative impacts on the coastal sediment budget cannot be excluded. According to the same authors, other factors may control the velocity of a pit regeneration such as the depth of the extraction and the character and availability of the potential material for the pit regeneration (Diesing et al., 2006).

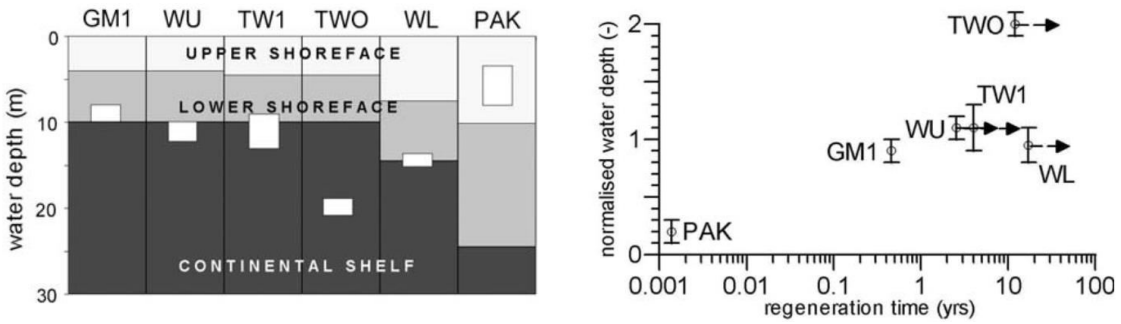

(a) **(b)**

Figure 40. Comparison of extraction sites: **(a)** Extension of upper shoreface, lower shoreface and continental shelf in terms of water depth. Wave energy input is increasing from left to right. White boxes indicate position of extraction sites. **(b)** Normalized water depth (calculated by dividing the water depth (h) of the extraction site by the depth of the seaward limit of the lower shoreface (h_i) - h/h_i) plotted against assessed regeneration times. Hatched arrows indicate possibly longer regeneration times, as regeneration was not completed until the end of observation. Pit location: GM1 - Graal-Muritz in Baltic Sea, WU – Wustrow in Baltic Sea, TW1 and TW0 – gravel and sand pits, respectively, in Tromper Wiek Ost, Baltic Sea, WL - Sylt Island in North Sea, PAK – Pakiri in New Zeland (Diesing et al., 2006).

Bender and Dean (2003), based on three case studies of beach nourishment (Grand Isle, Louisiana; Anna Maria Key, Florida; and Martin County, Florida), provide a review of available studies on wave transformation by bathymetric changes and the resulting shoreline impacts. These authors concluded that the effect of wave transformation by an offshore pit is complex and can result in substantial shoreward salient formation (Bender and Dean, 2003). The beach nourishment project at Grand Isle, Louisiana, represents one of the most interesting examples. There, in 1984,

around 4 Mm^3 of sediment were dredged from a borrow area lying 800 m from shore in 4.6 m of water depth (Bender and Dean, 2003). The dredging resulted in a "dumbbell" shaped sandpit with two outer lobes dredged to a depth of 6.1 m below the seabed connected by a channel of approximately 1370 m in length dredged to 3.1 m below the bottom (Combe and Soileau, 1987). One year after the excavation and probably associated with storm events occurred during the winter and spring of 1984–1985, two large salients, flanked by areas of increased erosion, developed immediately shoreward of the offshore borrow area (Figure 41, Bender and Dean, 2003). Bathymetric surveys revealed that, 2 years later, the outer lobes had filled to about half their original depth and the channel connecting the lobes were completely recovered (Combe and Soileau, 1987). In 2002, the borrow area is reported to be completely filled by very fine (silt and clay) material (Combe, 2002), finer than the sediment dredged for the nourishment project. The size and the location of the borrow area affected the local wave climate and even after the pit recovery, continue to modify the wave field (Combe, 2002), probably due to wave damping and energy dissipation caused by fluid–mud interaction with the extremely fine material that has filled the pit (Bender and Dean, 2003).

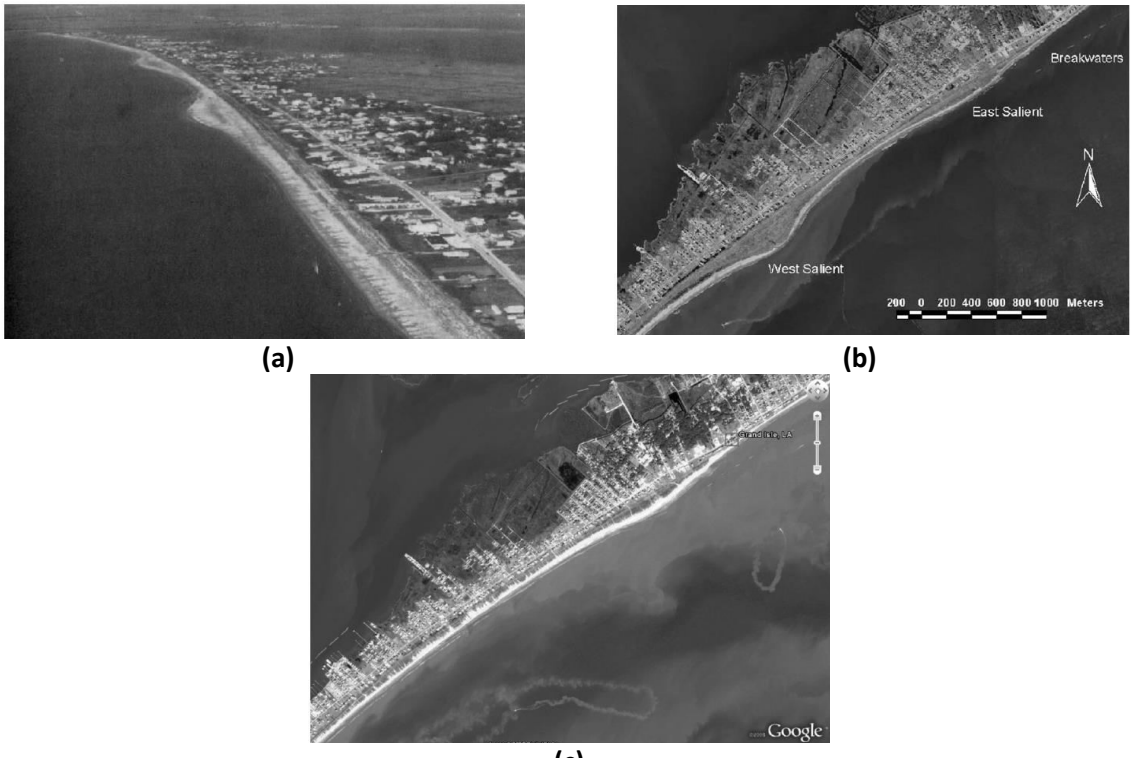

(a) **(b)**

(c)

Figure 41. Aerial photograph showing coastal salients shoreward of borrow area looking East to West along Grand Isle, Louisiana: **(a)** in August, 1985 (Combe and Soileau, 1987 *in* Bender and Dean, 2003); **(b)** in 1998 (LOSCO, 1999 *in* Bender and Dean, 2003); **(c)** in 2004 (Google Earth, 2009 *in* Silva, 2011).

IV.3. The Vale do Lobo study area

Vale do Lobo area is located in Loulé on the Southern Portuguese coast (Figure 42). As mentioned in section II.1, this coastal area has suffered serious erosion problems in the recent past, evident from the extreme decrease of the beach width and the observed bordering cliffs retreat (see Figure 43a and Gomes and Pinto, 2007). The construction of several groins in the Vilamoura area in the 70's (west of Quarteira; Figure 42), to attenuate the coastal erosion, has interrupted the downdrift littoral transport and induced significant erosional problems eastwards, increasing the natural coastline retreat trend for that costal sector (Correia et al. 1996; Marques, 1997).

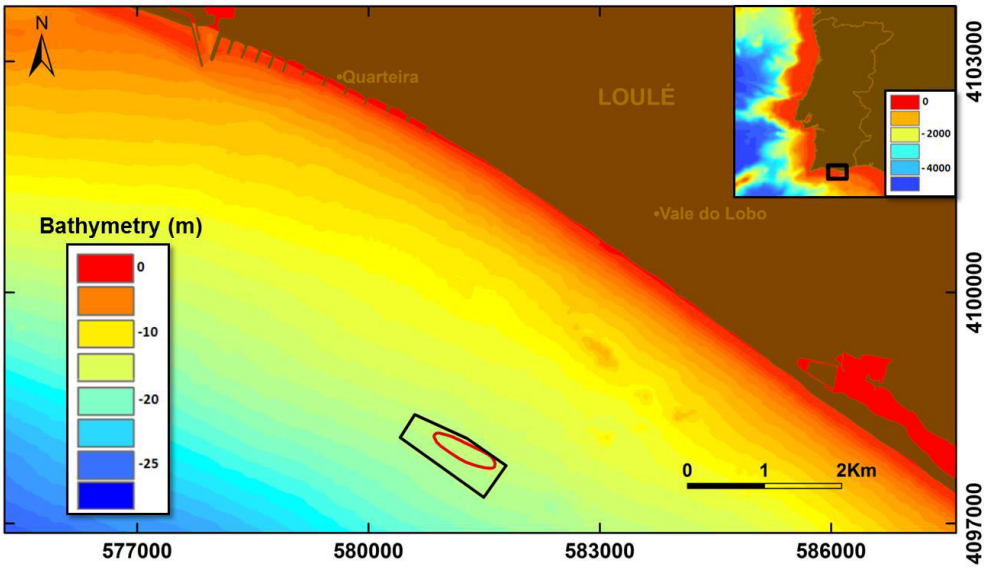

Figure 42. Study area offshore Vale do Lobo, Algarve, showing the location of the main excavation area (red ellipse) and the area common to all available bathymetric surveys (black polygon). The bathymetry shown is from the Portuguese Hydrographic Institute (2001 survey, courtesy of the Administration of the Hydrographic Region of the Algarve - ARH Algarve). The inset in upper right corner shows the location of the study area in mainland Portugal; bathymetry from the GEBCO 2008 (2 miles spacing) digital bathymetric grid. Coordinate system in UTM Zone 29N, datum WGS84 and bathymetry referred to the Hydrographic Zero datum (ZH).

In order to mitigate the intense coastal erosion felt in this zone, an artificial beach nourishment was carried out in 1998. The Vale do Lobo beach nourishment undertaken between October 1998 and January 1999 was the first case of an offshore sand extraction in the Algarve, and a total of approximately 700 000 m^3 of sand were extracted (Teixeira, 2011). The dredging area was located approximately 3.5 km offshore Vale do Lobo, between the 15 and 20 m isobaths (referred to the Hydrographic Zero datum - ZH[4]) and, according to the information provided by

[4] The Hydrographic Zero (ZH) is the vertical reference for water level measurements which corresponds to the level of the lowest astronomical tide recorded for a nodal period (18.6 years) plus the under-keel clearance value (30 cm). In 1938 was stablished as 2.00 m bellow the MSL (Mean Sea Level) for the Portuguese coast (mainland, except Tagus estuary).

Regional Hydrographic Administration for the Algarve Region - ARH Algarve, the dredging method employed in this extraction caused shallow dredging depressions across a wide area. In 2006, between March and May, a second artificial beach nourishment was performed (Figure 43a shows the Vale do Lobo beach in 1996 and Figure 43b illustrates the situation in 2006, after the second beach nourishment), this time from a more localized offshore sandpit excavation (Figure 44).

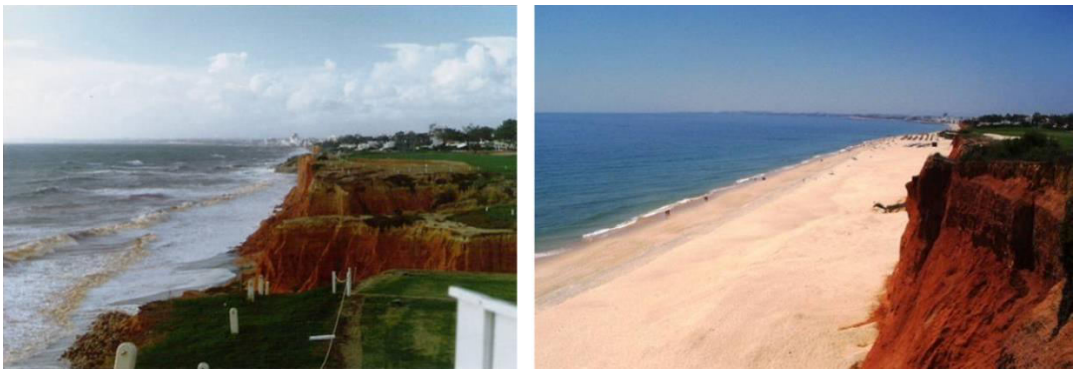

(a) **(b)**

Figure 43. (a) Vale do Lobo beach in November 1996 under storm conditions; **(b)** the same area in July 2006, just after the second beach nourishment (reproduced from Teixeira, 2011).

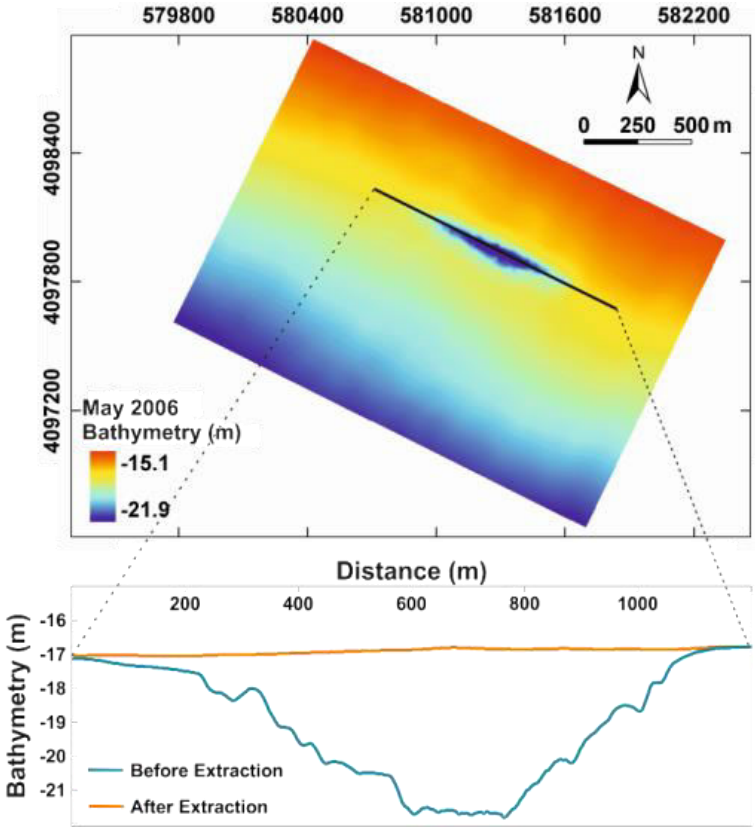

Figure 44. Sandpit bathymetry just after the second sand extraction in May 2006 and sandpit longitudinal profile before (orange line) and after (blue line) the sand extraction. Coordinate system in UTM Zone 29N, datum WGS84 and bathymetry referred to the Hydrographic Zero datum (ZH).

Approximately 370 000 m^3 of sediments were dredged from the internal continental shelf off Vale do Lobo (Teixeira, 2011), creating a local depression on the seabed. The borrow pit was located about 3.5 km offshore Vale do Lobo, between the 16 and 18 m isobaths (referred to ZH), and therefore offshore of the closure depth, located at about 6 to 10 m for the study area in section II.2.1. The resultant sandpit presented an elongated shape with the main axis oriented NW-SE, approximately parallel to the shoreline with the longest side aligned by the bathymetric contours (see Figure 44).

IV.4. Data and methods

The datasets used for this work consisted of: (1) 4 bathymetric datasets surveys acquired prior to and after excavation performed in 2006; and (2) wave data from the Faro Directional Wave Buoy, for the period 2006-2010. The data processing methodology used for each dataset is described in detail below.

IV.4.1. Bathymetric data and estimation of recovery time

The sandpit area of the sand extraction (see the location in Figure 44 and the sandpit bathymetric surface and longitudinal profile in Figure 44), carried out in May 2006, was monitored with bathymetric surveys prior to (March 2006) and after the excavation (May 2006, November 2008 and May 2010). The author participated on the bathymetric survey that took place in November 2008. The bathymetric data used for this work were acquired with single beam echosounders, with the exception of the data from May 2010, which was acquired with a multibeam system.

The 4 bathymetric datasets were inserted into a georeferenced GIS database (ArcGIS) and converted to UTM coordinates, datum WSG84. The data were filtered with a low-pass Gaussian filter to reduce the noise, and interpolated with the Natural Neighbors (NaN) method (cell size 5 x 5 m^2). The bathymetric surfaces obtained (Figure 45) were used to calculate the sediment budget in the excavation pit and surrounding area (the accumulated and eroded sediments, either due to the extraction or to natural readjustments of the bottom surface between successive surveys). For that purpose, the ArcGIS tools *minus* and *cut/fill* were used. These tools allow the subtraction of successive bathymetric surfaces, which is essential to understand the sandpit morphology evolution through time, in particular its migration and replenishment.

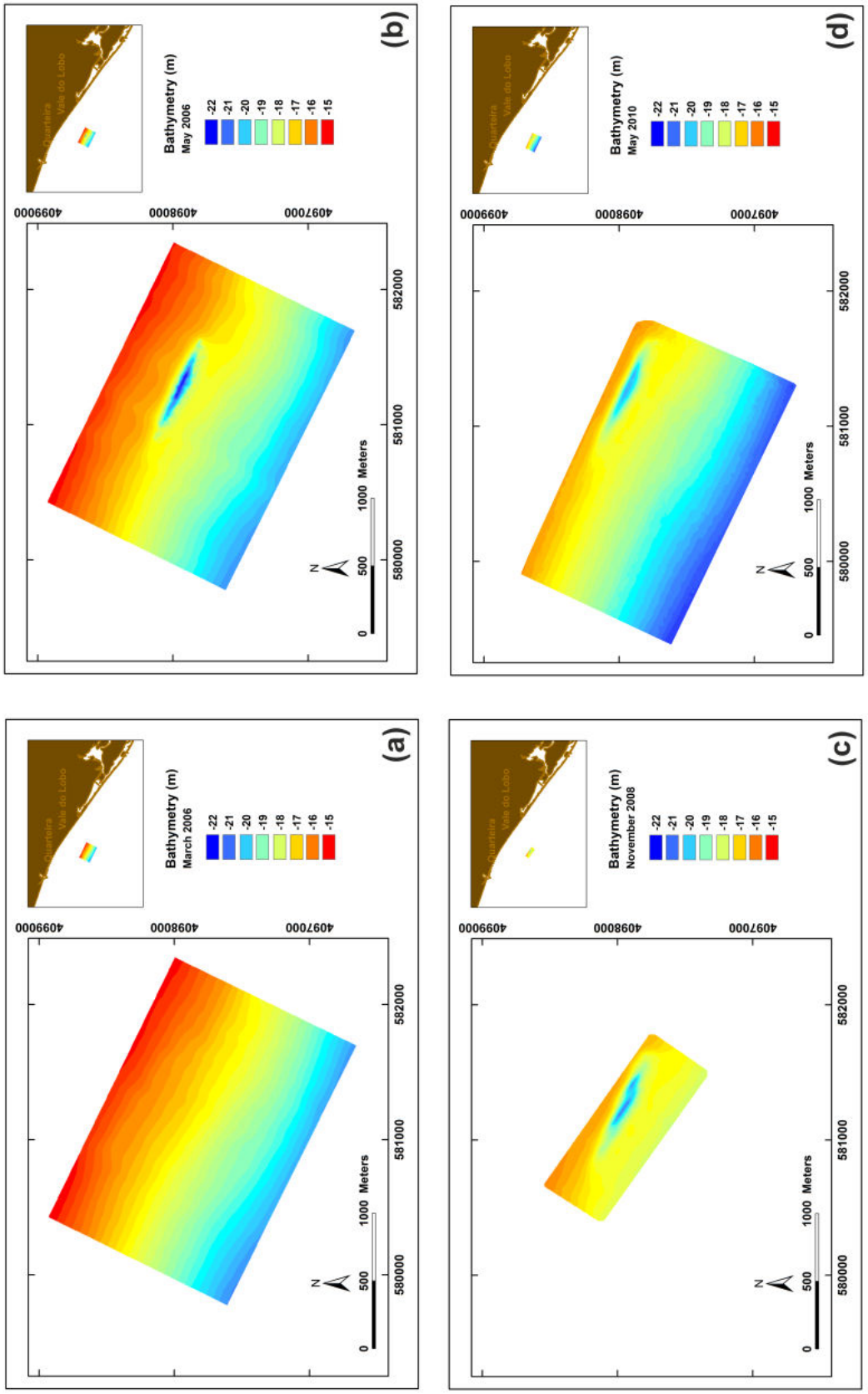

Figure 45. Bathymetric bottom surfaces used for this study: **(a)** March 2006; **(b)** May 2006;**(c)** November 2008; **(d)** May 2010. Coordinate system in UTM Zone 29N, datum WGS84 and bathymetry referred to the Hydrographic Zero datum (ZH).

In order to obtain a first estimate of the recovery time for the excavation area and to test if a variable refilling rate, exponentially decreasing in time, is applicable to the study area, Equation (14), which assumes a continuous sediment mobilization in time, was used. In this equation, the remaining excavation volume, V, after a period of time, t, is determined based on the initial excavation volume, V_0, and the recovery characteristic time-scale, τ (time after which the excavation volume is 37% of the initial volume; Vicente and Uva, 1984; Ramos et al., 2005).

$$V = V_0 e^{-t/\tau} \Leftrightarrow \tau = \frac{t}{\ln\left(\frac{V_0}{V}\right)} \quad \textbf{(14)}$$

IV.4.2. Wave data

With the intend to characterize the wave climate in the study area during the period analyzed, the measured three-hourly values of significant wave height (Hs), mean period (T), and mean wave direction (θ) from the Faro directional wave buoy (operated by the Portuguese Hydrographic Institute – IH) were used, from 2006 to 2010. This is a Datawell-Waverider buoy located offshore Faro (36°54'17"N, 7°53'54"W), at approximately 93 m water depth (ZH). However, a set of gaps was identified in the data. The missing data for a time span of 6 hours or less were filled in by direct interpolation (weighted mean); for longer gaps (more than 6 hours) the data were filled in using data from the numerical model WaveWatchIII (Tolman, 2009) forced by wind fields originating from the Climate Forecast System Reanalysis (CFSR, Saha et al., 2010), with spatial and temporal resolutions of 0.3° and 3h, respectively.

The numerical modeling of waves in the Southern Coast of Portugal is very challenging due to the superimposition of the two wave regimes. As previously described in section II.2.2, one corresponds to a long-period swell generated in the North Atlantic Ocean and coming from the WSW to WNW while the other corresponds to wind seas coming from the SE and locally called “Levante” wind. This bi-modal wave regime causes the wave direction and peak period to jump regularly from one mode to another and this phenomenon is difficult to reproduce with a numerical model. For modelling purposes, a first grid of the numerical model WaveWatchIII (Tolman, 2009) was implemented for the North Atlantic Ocean with a 0.5° resolution, following the configuration described in Dodet et al. (2010), with a second grid nested in the Gulf of Cadiz and the SW Portuguese Coast (6-10°W; 31-39°N) with a 0.05° resolution.

WaveWatchIII results were evaluated against wave measurements from the Faro wave buoy (Figure 46). This comparison shows firstly that significant wave heights Hs are well reproduced, with a root mean square discrepancy (RMSD) of 0.26 m, which results in a 25 % discrepancy once normalized by the data. The bias in Hs is -0.1 m, which is in accordance with the results of Dodet et al. (2010), who found a negative bias between 0.10 and 0.30 m considering 6 buoys located in the west and north coast of the Iberian Peninsula. However, there is a discrepancy observed for significant wave heights lower than 1 m. Since this problem essentially concerns small waves (Figure 46c and d), the bias and the RMSD normalized by the observed data (NRMS) were recalculated for Hs larger than 1 m. This new comparison yields a bias of 0.02 m and a NRMSD of 20%. Wave direction (Figure 46a and b) and peak periods have a RMSD of 48° and 2.3 s, respectively. These weaker scores result mainly from the regular jumps between the two modes described above, which are not all captured by the model. As described above, this problem essentially concerns small waves (Figure 46c and d) and the recalculated RMSD for Hs larger than 1 m yields a RMSD of 30° and 1.3 s for wave direction and peak period, respectively. According to these errors, it can be argued that the model accuracy is sufficient to produce a continuous time series of wave parameters for the period 2006-2010 in order to fill the gaps of the Faro buoy measurements for storm events identification proposes. The result was a complete and unique three-hourly interval dataset covering the whole period from January 2006 to December 2010.

The 2006-2010 wave dataset was analyzed for two periods of time: May 2006 to November 2008, and December 2008 to May 2010. For both these periods, the duration and frequency of storms were calculated. In order to classify a data sequence as a storm, the following criteria need to be satisfied (Zhang et al., 2000; Li et al., 2009):

1) The event should consist of at least one sample above the peak threshold value (Hpeak = mean+2 standard deviations);

2) The storm continues while the significant wave height remains above the duration threshold value (Hdur = mean + standard deviation);

3) Two consecutive storms are distinguished if the storm interval is not shorter than three hours and if the interval between storm peaks is not less than 30 hours.

According to Pessanha and Pires (1981), in the portuguese south coast, a storm is defined as an event with a Hs offshore higher than 3 m. According to Almeida et al. (2011), this corresponds to the mean Hs plus two times the standard deviation (Hpeak). Therefore, since the average of the significant wave height is close to 1 m (Costa et al., 2001), the Hpeak used in this work is 3 m and the Hdur considered is equal to 2 m.

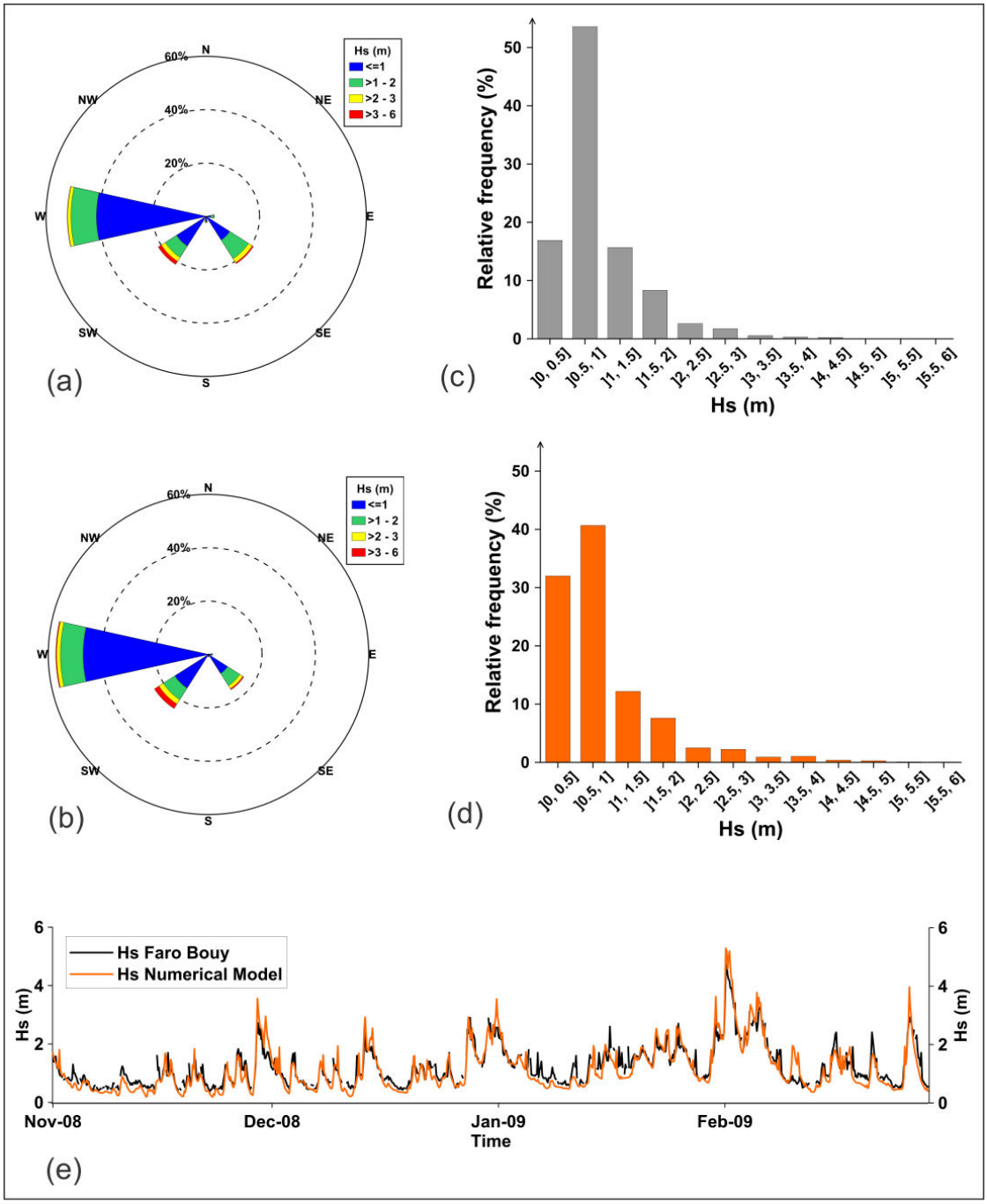

Figure 46. Comparison between wave measurements at the Faro wave buoy and WaveWatchIII modeling results: wave rose diagram for the wave direction and the significant wave height considering the whole dataset (2006-2010) based on **(a)** Faro buoy measurements and **(b)** WaveWatchIII modeling results; Hs relative histogram based on **(c)** Faro buoy measurements and **(d)** WaveWatchIII modeling results; and **(e)** measured Hs (black line) plotted over numerical modeling results (orange line) for a period of 4 months (November 2008 – March 2009).

After the classification of a data sequence as a storm, individual storm characteristics were assessed through the calculation of the Hs minimum, maximum, median and mean, storm duration and wave mean direction of the individual storm

event. The number of stormy days and the number of storms for the two periods were identified. According to Almeida et al. (2011), to properly characterize the variability of storm occurrence in the study area, a high percentile of Hs 99.8 is required to assess extreme wave height variability of occurrence of storms. Therefore, the Hs 99.8 was also estimated for the two intervals of time.

IV.4.3. Morphodynamic modeling system

The understanding of the morphodynamic evolution of the study area in the periods between the 4 bathymetric surveys, and the determination of which periods there was a more significant sediment movement, was performed using a numerical modeling system. The numerical simulations of the sediment dynamics and morphological evolution of the sandpit were performed with the morphodynamic modeling system MORSYS2D (Fortunato and Oliveira, 2004, 2007; Bertin et al., 2009), previously described in section III.4.

In the present work, the numerical model configuration includes the most representative forcing, such as tides, wind, and waves, provided by regional models. The ELCIRC model was forced by a regional model of tides (Fortunato et al., 2002) and the SWAN spectral wave model was forced offshore by a regional application of the WAVEWATCH III (WW3) model (Dodet et al., 2010). As concerns wind, WW3 was fed by data obtained from the National Centers for Environmental Prediction (NCEP) and a uniform computational domain was assumed. The wave model WW3 was validated through the comparison of the model data with the Faro buoy data (see section IV.4.3). For the ELCIRC model, an unstructured triangular grid with 6710 nodes was used, where the element size ranges from 1500 m offshore to 5m at the sandpit area. SWAN was run with 3 nested grids: a larger grid with a spacing of 1000 m and an area of 65x110 km; an intermediate grid with a spacing of 100 m and an area of 20x42 km; and a high resolution grid centered in the sandpit with a spacing of 20 m and an area of 6x10 km. The net sediment transport rates were computed considering a constant median sediment size (D_{50}) of 0.77 mm, based on granulometry analysis conducted by Teixeira (2011). Previous applications of the MORSYS2D have shown a dependence of the morphodynamic numerical solutions on the sediment transport formulation considered. The results of Bertin et al. (2009) to a dissipative beach and of Plecha (2011) to a tidal dominated inlet have shown a better performance of Ackers and White formulation than the Bijker and Soulsby-van Rijn formulations, which estimated larger transport rates. However, in the present work, the sediment fluxes are computed in non-breaking wave conditions with rather small mean currents and Ackers and White formulation did not provide an accurate morphodynamic evolution of the sandpit. Instead, as shown in Rosa et al. (2011a), the Bijker formula provided the

best results when compared with the bathymetric observations for a constant bottom roughness, Ks equal to 0.1 m.

The MORSYS2D numerical model simulations were used in this work to assess the morphological changes in the sandpit during two different time intervals with very contrasting weather and wave conditions:

- From March 28th to April 29th 2008 (henceforth referred to as April 2008), when two important storm events took place;
- From April 30th to May 31st 2008 (henceforth referred to as May 2008), a period without storm events.

In order to estimate the sandpit morphological variations during these two time intervals, the bathymetric datasets generated by the numerical model, concerning the dates previously described (March 28th, April 29th, and May 31st, 2008), were inserted into a georeferenced GIS database (ArcGIS), converted to UTM coordinates, datum WSG84, and interpolated using the Natural Neighbors (NaN) method (cell size 5x5 m). The obtained bathymetric surfaces were used to assess the sandpit evolution between March 28th and May 31st 2008, using the ArcGIS tools m*inus* and c*ut/fill*.

IV.5. Results and discussion

IV.5.1. Sediment balance, sandpit evolution and recovery time

Between March and May 2006 approximately 370 000 m^3 of sediments were dredged from the internal continental shelf off Vale do Lobo (Teixeira, 2011), creating a local depression on the seabed located about 3.5 km offshore Vale do Lobo, between the 16 and 18 m isobaths (referred to ZH), with the main axis oriented NW-SE (Figure 44). After the dredging operation, the borrow pit was small and deep, approximately 90 m long, 150 m wide and 5 m deep, as shown in Figure 44.

This excavation has been monitored with an adequate dataset of repetitive bathymetric surveys covering the study area, prior to, and after the dredging. In order to assess the sandpit evolution through time, these data sets were interpolated and are shown in Figure 45.

The volumes of sediment accumulation and removal for the area common to all the available bathymetric surveys (ca. 615 000 m^2; black polygon in Figure 42), which covers essentially only the main pit area and its immediate vicinity, were computed (Figure 47 and Table 6). This was carried out through the subtraction of the successive bathymetric surfaces described in section IV.4.1.

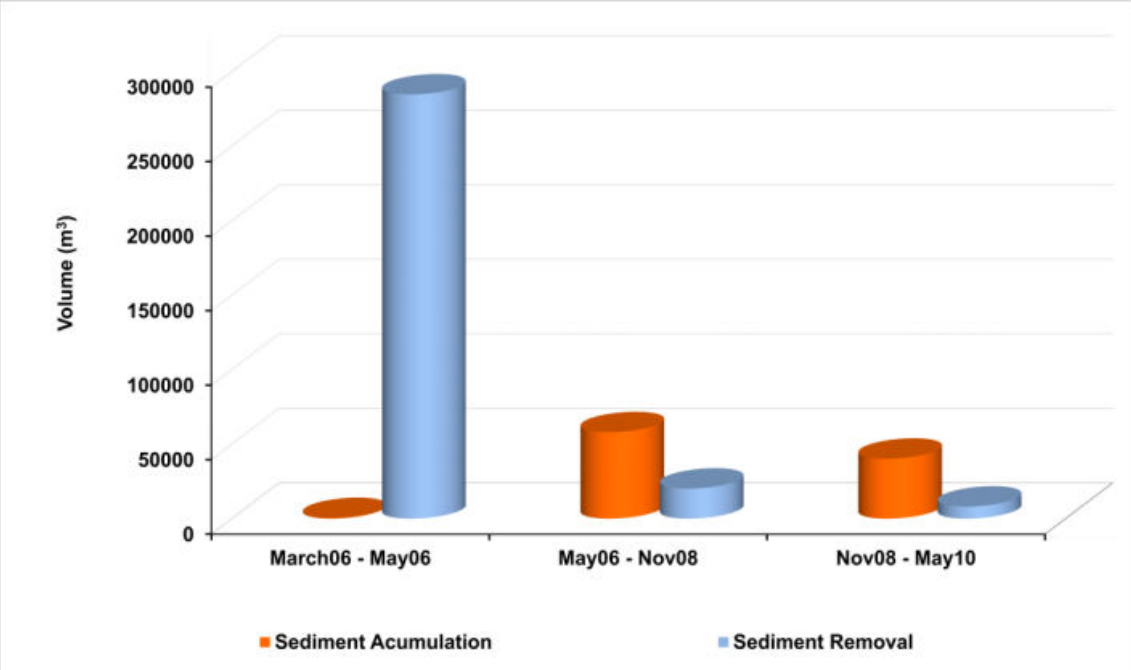

Figure 47. Volumes of sediment accumulation (orange) and removal (light blue) between successive bathymetric surveys in the main pit area, calculated in ArcGIS. The first dataset corresponds to a time span of about 2 months, whereas the others correspond to periods of about 2.5 and 1.5 years, respectively.

Table 6. Volumes (m^3) of sediment accumulation and removal between successive bathymetric surveys in the main pit area, calculated using ArcGIS. The first dataset corresponds to a time span of about 2 months, whereas the others correspond to periods of about 2.5 and 1.5 years, respectively.

Period in consideration	*March to May 2006*	*May 2006 to November 2008*	*November 2009 to May 2010*
Sediment Accumulation	0	58000	40000
Sediment Removal	285000	20000	8000
Balance	-285000	+38000	+32000

Considering the common area to the various bathymetric surveys, the extracted sand volume for the 2006 surveys gave a net value of 285 000 m^3, which corresponds to ca. 77% of the value reported by the contractor of 370 000 m^3 (Teixeira, 2011). However, for this comparison, the full excavation area should be used. As can be observed in Figure 45, the 2006 surveys, just prior to and just after the excavation, cover a much larger area, which corresponds to the full area of excavation; the subsequent bathymetric surveys cover only smaller areas in the vicinity of the main pit area. Calculating the extracted sand volume for the 2006 surveys for the full excavation area, a net value of 340 000 m^3 was obtained, which corresponds to ca. 91% of the value reported by the contractor of 370 000 m^3 (Teixeira, 2011).

Between May 2006 and November 2008 there were no sand extractions. The observations show for this period an accumulation of about 58 000 m^3 and a sediment removal of approximately 20 000 m^3, resulting in a net positive sedimentary balance of about 38 000 m^3. A similar trend was observed for the period between November 2008 and May 2010, with an accumulation of about 40 000 m^3 and a sediment removal of about 8 000 m^3, resulting in a positive sedimentary balance near to 32 000 m^3 (Figure 47 and Table 6). Therefore, assuming that there are no significant errors in the bathymetric datasets, it is possible to estimate a net accumulation rate of about 2.85 cm/year for the study area, during the 4 year period between May 2006 and May 2010. The sand removed during the dredging process in March 2006 left an oval shape depression on the seabed, referred to above as the main pit area, elongated in the NW-SE direction (Figure 45 and Figure 49).

The analysis of the bathymetric profiles of the sandpit (Figure 48) shows a smoothing of the topography roughness with time; in general, the sandpit topography in 2010 became smoother and less deep (about 2 m) than the original topography of May 2006.

The bathymetric profiles along the pit axis (Figure 48) demonstrate that 2.5 years after the excavation (in November 2008) the pit was filled in its deepest and central parts and that its slopes were accumulating sediment mainly on the upper part of the NE flank (red and yellow curves in Figure 48). 4 years after the extraction (May 2010 – green curve in Figure 48), an infill of the deepest area of the pit is clearly visible, with the flanks are still accumulating sediment, once again, mainly the NE flank (the onshore flank).

Figure 49 shows the pit edge evolution in time; in this work, a slope value of 0.5º, higher than the maximum natural slope in the study area, was used to delimit the pit edge. During the four years after the dredging, the NE flank showed a displacement of about 15 m in average towards SW, with a maximum displacement of about 20 m. However, there was an increase in the pit's maximum length along the main axis, due to sediment loss (see also Figure 48a), and the excavation became more elongated in the NW-SE direction (Figure 49). The shrinking observed mainly in the NE flank, due to sediment accumulation, is causing the migration of this flank southwestwards (see also the transverse profiles in Figure 48). This migration is also evident from the analysis of the sandpit centroid, shown in Figure 49, which moved about 7.8 m to the SW. The same trend is shown by the longitudinal axis of the sandpit, which moved southwestwards about 8.7 m (Figure 49). The perimeter of the excavation rim grew around 25%, from about 2 000 m in May 2006 to more than 2 500 m four years later (Table 7 and Figure 49). The same trend was observed for the area of the pit at the surface, which increased about 10% during the same four years, from around 162 500 m^2 in 2006 to 178 000 m^2 in 2010. These results suggest that the sandpit is becoming shallower and smoother but also slightly wider.

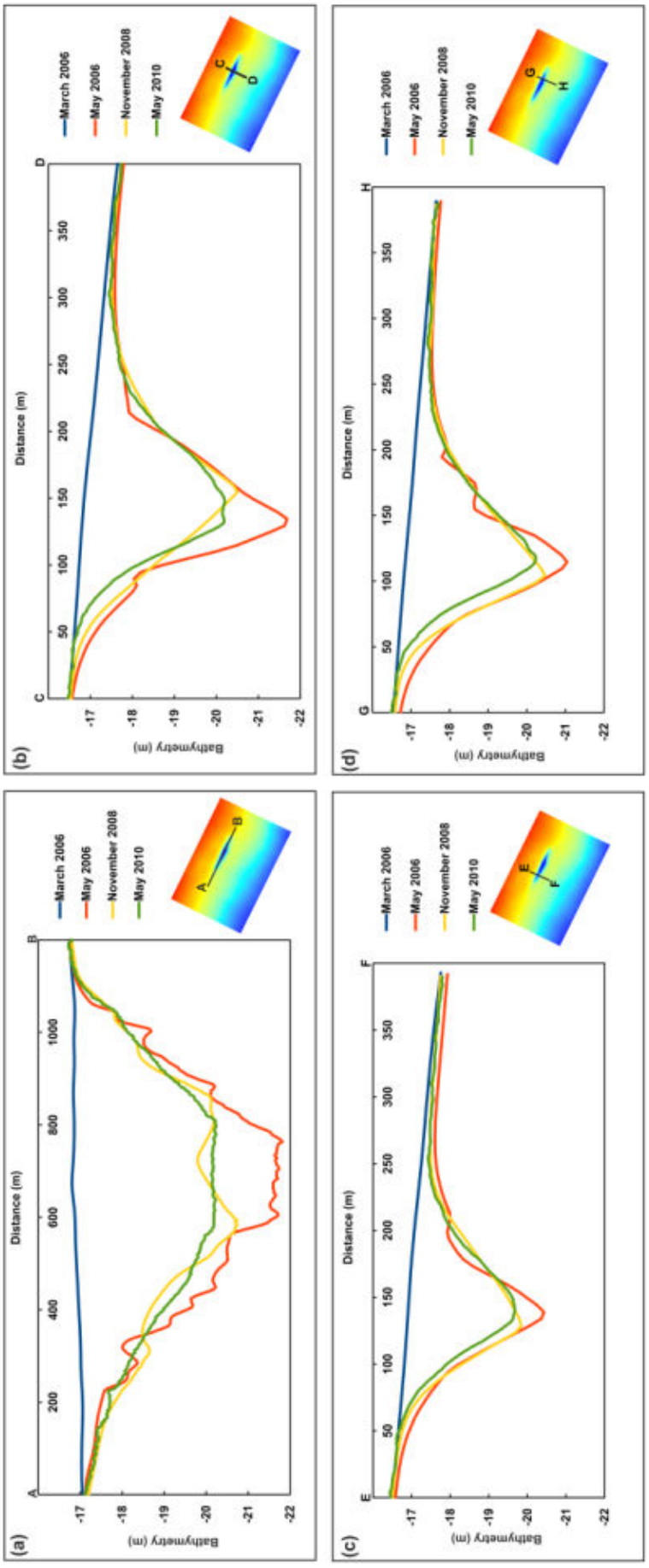

Figure 48. Bathymetric profiles in the pit-area. **(a)** Longitudinal profile along the main pit axis; **(b)** Transversal profile to the main pit axis in the central part of the pit; **(c)** Transversal profile to the main pit axis in the NW part of the pit; **(d)** Transversal profile to the main pit axis in the SE part of the pit. Bathymetry referred to the Hydrographic Zero datum (ZH).

Table 7. Quantitative estimates of the pit extent and maximum slope of the flanks.

Date	*Pit perimeter (m)*	*Pit area (m^2)*	*Maximum slope (°)*	*Mean slope (°)*	*Standard deviation (°)*
May 2006	2 000	162 500	7.6	1.7	1.4
November 2008	2 350	165 500	4.2	1.4	0.9
May 2010	2 530	178 000	3.7	1.2	0.8

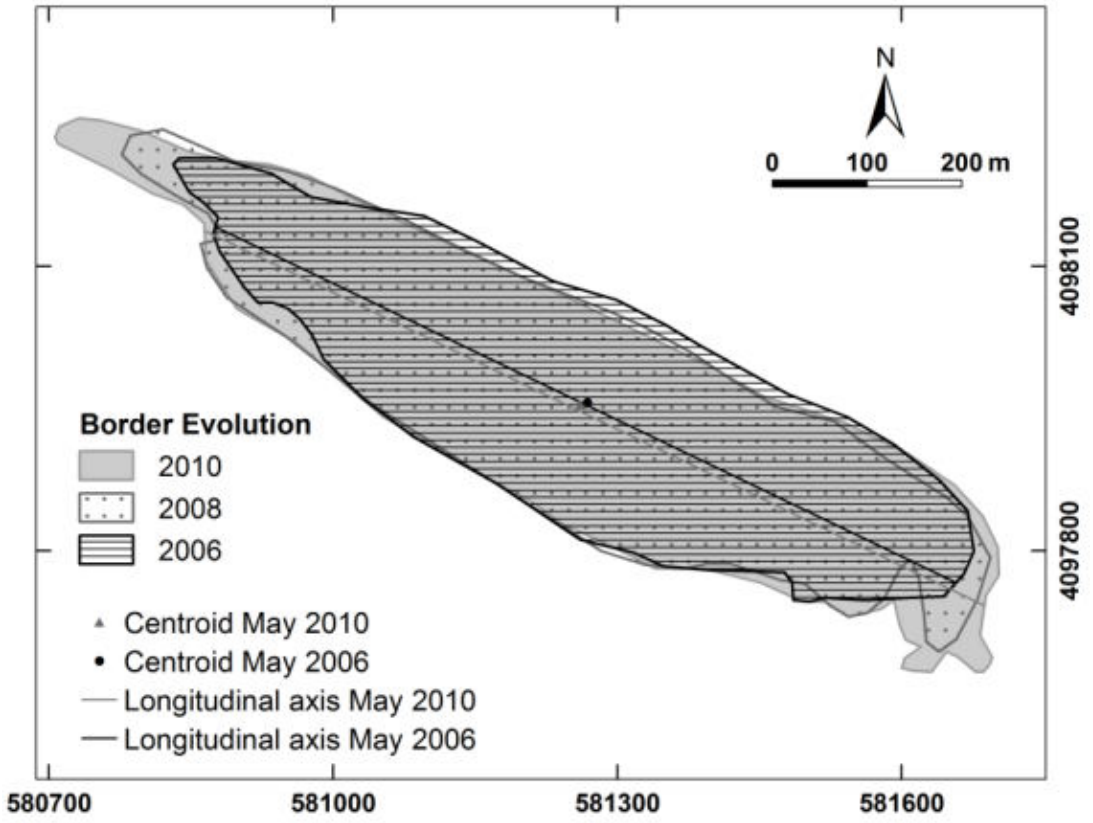

Figure 49. Pit-area rim evolution through time: May 2006, November 2008 and May 2010. Coordinate system in UTM Zone 29N, datum WGS84.

An estimation of the recovery time for the sandpit between 2006 and 2010 was obtained from Equation (14) based on the bathymetric data that encompasses just the main excavation area (red ellipse in Figure 42); this gave an estimated value of 22 years. Since this corresponds only to a 63% infill, the full recovery time will necessarily be longer.

The sandpit refilling rate for the periods between May 2006 and November 2008, and from November 2008 to May 2010 were also estimated based on the observed bathymetric data. In November 2008, 2.5 years after the extraction, about 22 000 m^3 of sediment was accumulated in the sandpit, resulting in a refilling rate of

about 6.5 cm/yr for this period. However, between November 2008 and May 2010, almost 17 000 m^3 of sediment were accumulated in the excavation area, corresponding to a recovery rate of about 7.2 cm/yr. According to these results, the refilling rate in our case study, contrary to what is expected from Equation (14) and other authors (Kubicki et al., 2007), is increasing in time. An explanation for this fact is proposed in the following sections IV.5.3 and IV.5.4.

IV.5.2. Ocean wave climate between 2006 and 2010

From 2006 to 2010 the Faro buoy wave data show that the wave climate of the study area was mainly dominated by smooth to moderate sea states. The significant wave height average for this 5-year period was almost 1 m and the corresponding mean period (T) was 4.8 s. The wave histogram for these 5 years (Figure 50b) further shows that almost 70% of the significant wave height was lower than 1 m and more than 95.5% was smaller than 2.5 m. The wave rose diagram (Figure 50a) for the 5-year measurements shows that about 73% of the incident waves were from W-WSW and about 20% from the SE quadrant. These results are in agreement with the hydrodynamic and climatic description of the area performed on section II.1.2.

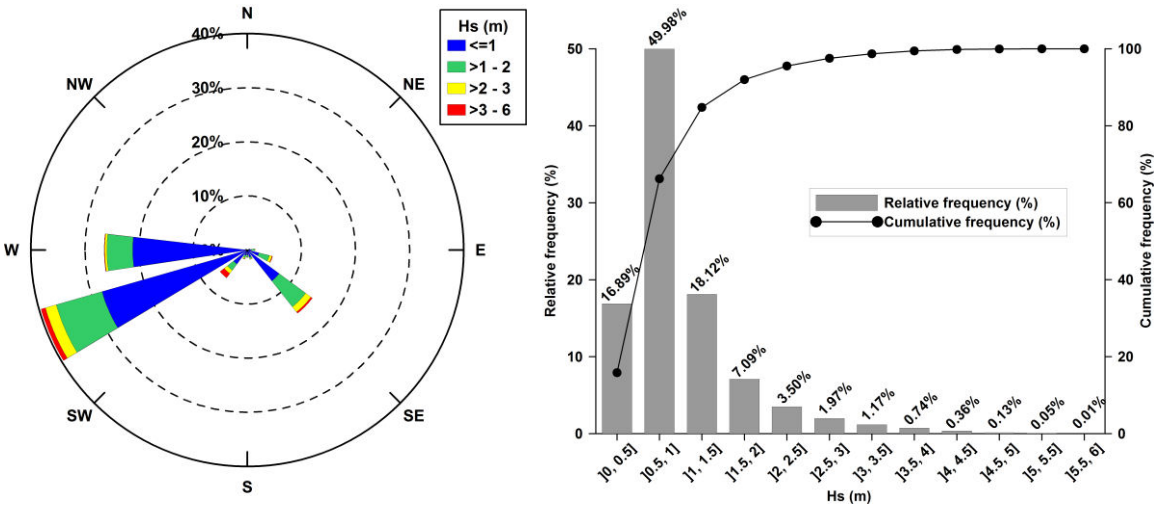

(a) **(b)**

Figure 50. Significant wave height and wave direction from 2006 until 2010: **(a)** wave rose diagram for the wave direction and the significant wave height and **(b)** Hs relative and cumulative frequency histogram.

Based on the criteria previously presented for storm classification (see section IV.4.2), the storm events that occurred in the study area from May 2006 to May 2010 were identified and are described in Table 8 (May 2006 - November 2008) and in Table

9 (December 2008 - May 2010). For each individual storm event, the average, minimum, and maximum significant heights (Hs) were estimated, as well as the mean period, the mean direction and the storm duration. According to Table 8 and Table 9, the storm events only occurred from October to April. Furthermore, during these 4 years in study (May 2006 to May 2010), the winter stormy days (from December 21st to March 21st) represent more than 70% of the total stormy days, and February was the month with the higher number of stormy days, almost 35% of the total.

Table 8. Identified storm events from May 2006 to November 2008.

Storm Event	*Date (at Hs Max)*	*Mean Hs (m)*	*Hs Min (m)*	*Hs Max (m)*	*Mean T (s)*	*Mean Direction*	*Duration (d hh)*
S1	18 Oct 2006	2.49	2.02	3.30	6.16	WSW	1 03
S2	26 Oct 2006	2.93	2.01	4.03	6.66	WSW	1 03
S3	24 Nov 2006	3.27	2.25	4.19	6.77	WSW	2 12
S4	16 Feb 2007	2.36	2.04	3.12	5.91	SW	1 15
S5	20 Nov 2007	2.54	2.05	3.22	6.16	SW	1 09
S6	19 Dec 2007	3.45	2.20	5.26	6.05	SSE	3 09
S7	03 Jan 2008	2.67	2.02	4.41	7.12	WSW	2 06
S8	13 Feb 2008	2.87	2.02	3.71	5.77	SE	5 15
S9	17 Feb 2008	2.95	2.04	4.31	5.76	SE	2 06
S10	23 Feb 2008	3.04	2.19	4.13	5.76	SE	2 00
S11	05 Mar 2008	2.52	2.01	3.05	5.91	E	0 12
S12	10 April 2008	3.84	2.20	5.35	8.67	SW	3 18
S13	19 April 2008	2.58	2.01	3.15	5.62	WSW	2 21

Table 9. Identified storm events from December 2008 to May 2010.

Storm Event	*Date (at Hs Max)*	*Mean Hs (m)*	*Hs Min (m)*	*Hs Max (m)*	*Mean T (s)*	*Mean Direction*	*Duration (d hh)*
S14	01 Feb 2009	2.91	2.02	4.70	6.69	SW	3 15
S15	05 Feb 2009	2.63	2.02	3.20	6.40	WSW	3 00
S16	17 Mar 2009	3.01	2.16	3.82	5.94	SE	2 12
S17	19 Dec 2009	3.17	2.21	4.06	6.86	SW	1 06
S18	23 Dec 2009	3.56	2.12	4.98	7.65	SW	6 06
S19	31 Dec 2009	3.47	2.06	5.00	7.40	WSW	4 12
S20	04 Jan 2010	3.24	2.10	5.15	8.86	WSW	2 12
S21	11 Jan 2010	2.97	2.16	3.82	7.90	WSW	1 03
S22	12 Jan 2010	2.65	2.08	3.24	5.74	SW	0 12
S23	14 Jan 2010	2.70	2.12	3.70	8.07	WSW	1 06
S24	28 Jan 2010	2.77	2.03	3.19	5.32	ESE	0 06
S25	16 Feb 2010	3.22	2.10	4.26	6.74	SW	3 03
S26	21 Feb 2010	3.01	2.05	3.97	6.58	SW	3 21
S27	27 Feb 2010	3.04	2.10	4.63	8.84	WSW	2 03
S28	03 Mar 2010	3.29	2.05	4.80	8.47	SW	2 09
S29	09 Mar 2010	2.64	2.10	3.12	7.69	WSW	0 12
S30	16 April 2010	2.67	2.24	3.75	6.00	S	2 15

In order to better visualize the information presented in Table 8 and Table 9, for each study period (May 2006 to November 2008 and December 2008 to May 2010) the significant wave height frequency histograms (Figure 51c and d) and a wave rose diagram for the mean wave direction and the significant wave height (Figure 51a and b) were calculated. From May 2006 to November 2008, during the identified storm events more than 71% of the significant wave heights were higher than 2.5 m and about 40% were higher than 3 m. For the storm events identified from December 2008 to May 2010, more than 71% of the significant waves were higher than 2.5 m and 40.5% higher than 3 m. For the first period and according to Table 8, the storm events occurred mainly during the winter, and February was the month with more stormy days (almost 37% of the total stormy days). The longest storm that occurred during this period took place in February 2008 with 5.6 stormy days; however, the highest Hs maximum (5.35 m) and Hs mean (3.84 m) were observed in the storm that took place in April 2008. For the second study period (December 2008 to May 2010; see Table 9), the storm events occurred almost all during the winter and February was again the month with more storms and more stormy days, corresponding to more than 47% of the total stormy days in this period. December had also a significant number of stormy days (almost 30%). Within this period, the storm with the highest significant wave height occurred in January 2010, with 5.15 m of Hs maximum and an Hs mean of 3.24 m. However, and once again, this storm was not the longest storm, which took place in December 2009, with almost 6.3 stormy days. From May 2006 to November 2008, the wave rose diagram (Figure 51a) shows that, during the storm events, the SE-ESE incident waves had a significant contribution (almost 40%), when compared with the period from December 2008 to May 2010 (Figure 51b), where the SE-ESE component was significantly smaller (about 10%). In both periods the incident waves from WSW-SW are the most representative during the storm occurrences, and correspond to almost 55% in the first study period and 85% in the second.

From May 2006 to November 2008 (Table 10) thirteen storms were identified, in a total of 30.6 stormy days. Concerning these storm events, the average significant wave height was 2.9 m and the Hs for 99.8 percentile was estimated at 5.2 m. The average of the wave period was 6.3 s. For the other study period between December 2008 and May 2010 (Table 10), seventeen identified storms had a total duration of 41.4 days, with an average significant wave height of 3.0 m, an Hs 99.8 of 5.3 m, and a mean wave period of 7.1 s. Therefore, the period from December 2008 to May 2010 (Table 10), although shorter, presented a larger number of storm events and stormy days than the precedent study period (2006-2008). Moreover, the Hs for the 99.8 percentile, which according to Almeida et al. (2011) properly characterizes the variability of storm occurrence in the study area, is higher in the second study period than in the first 2.5 years after the sand extraction.

Table 10. Comparison between the two intervals of time, from May 2006 to November 2008 and from December 2008 to May 2010, showing the number of storms, total duration of the storm event (days), Hs (mean, maximum, minimum and Hs 99.8), mean period, mean direction and the sedimentation rate previously estimated from the bathymetric data.

Interval of time	*Time (yr)*	*Number of storms*	*Stormy Days/year*	*Hs Mean (m)*	*Hs Max (m)*	*Hs Min (m)*	*Hs99.8*	*Mean T (s)*	*Sed. rate (cm/year)*
May 2006 to Nov. 2008	2.5	13	12.3	2.9	5.35	2.0	5.2	6.3	6.5
Dec. 2008 to May 2010	1.5	17	27.6	3.0	5.15	2.0	5.3	7.1	7.2

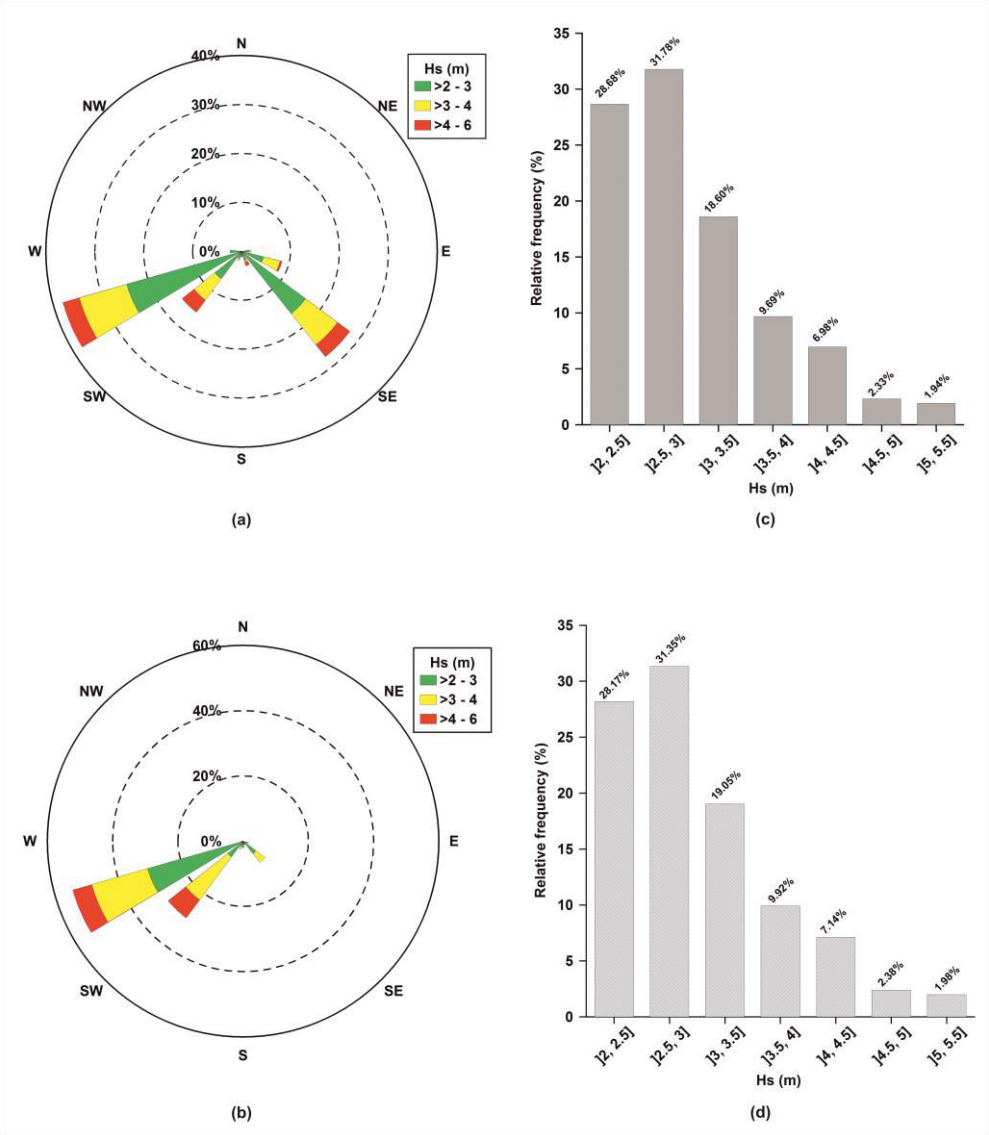

Figure 51. Significant wave height and wave direction: wave rose diagram for the wave direction and the significant wave height for the identified storm events **(a)** from May 2006 to November 2008 and **(b)** from December 2008 to May 2010; and Hs relative histogram for the identified storm events **(c)** from May 2006 to November 2008 and **(d)** from December 2008 to May 2010.

IV.5.3. Influence of storm events on sediment mobilization

Rosa et al. (2011a,b) computed the total (wave and mean current) sediment fluxes at the sandpit site for the month of April 2008 from two well-known formulations - Bijker (Bijker, 1971) and Soulsby-van Rijn (Soulsby, 1997), and showed that the sediment fluxes are different from zero only when the significant wave height exceeds 1.5 to 2 m (Figure 52). Only in this case, the near bed wave orbital velocity exceeds the critical value and is capable of mobilizing the bottom sediments promoting, in conjunction with the wind induced mean current, significant changes in the sandpit morphology.

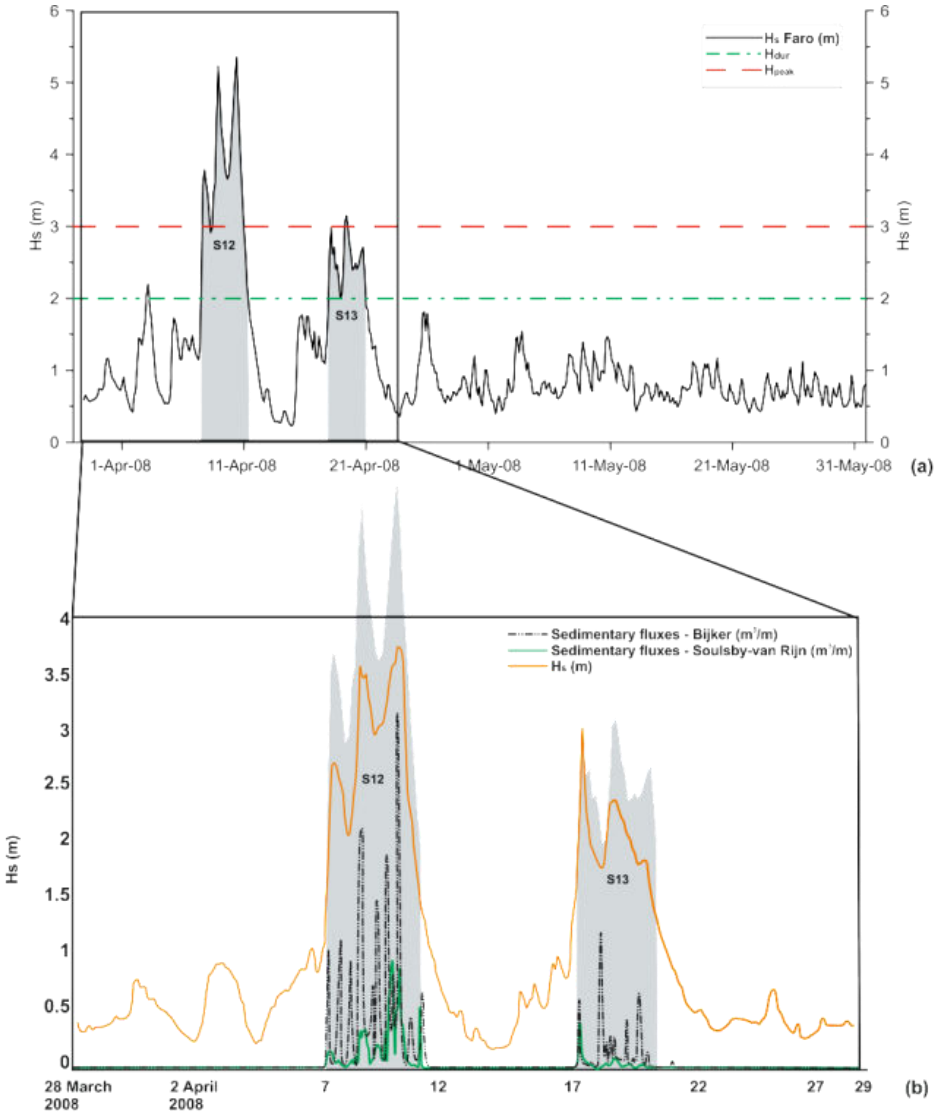

Figure 52. (a) Measured significant wave height (black line) between March 28th and May 31th 2008. The dashed red and green lines represent, respectively, the H peak and the H duration used to identify the storm events. **(b)** Computed significant wave height - m (orange line) and sedimentary fluxes for Bijker - m^3/m (black dot line) and Soulsby-van Rijn - m^3/m (green line) formulations for a point inside the sandpit, in the period between March 28th and April 29th 2008. The grey shadows in both graphics represent the storms S12 and S13 based on measured significant wave height (adapted from Rosa et al., 2011b).

In order to further verify the effect of the significant wave height in the sandpit morphological variations, two different time intervals with very different weather and wave conditions were selected: March 28th to April 29th and April 30th to May 31st, 2008. As shown in Figure 52a, on April 2008 two very important storm events occurred, identified as S12 and S13 in Table 8. The first storm (S12) was felt during almost 4 days (90 hours), with the predominant incident waves from SW-WSW, a significant wave height mean of 3.84 m, and a maximum significant wave height of 5.35 m felt on April 10th. The second storm (S13) had a maximum significant wave height of 3.15 m on April 19th, was felt during almost 3 days (69 hours), the incident waves come from WSW-SW, and had a mean significant wave height of 2.58 m. In contrast, throughout May 2008 the significant wave height was always lower than 1.54 m with an average value of 0.78 m for the whole period, which corresponds to a low energy sea state.

The comparison between two output models' interpolated bathymetries (Figure 53a), before (March 28th) and after (April 29th) the two important storm events, shows areas with a significant accretion, mainly in the deepest part and in the north flank of the sandpit, or erosion, in the south flank. A similar analysis carried out for May 2008 (Figure 53b), shows that almost no bathymetric changes occurred during this time period in the sandpit.

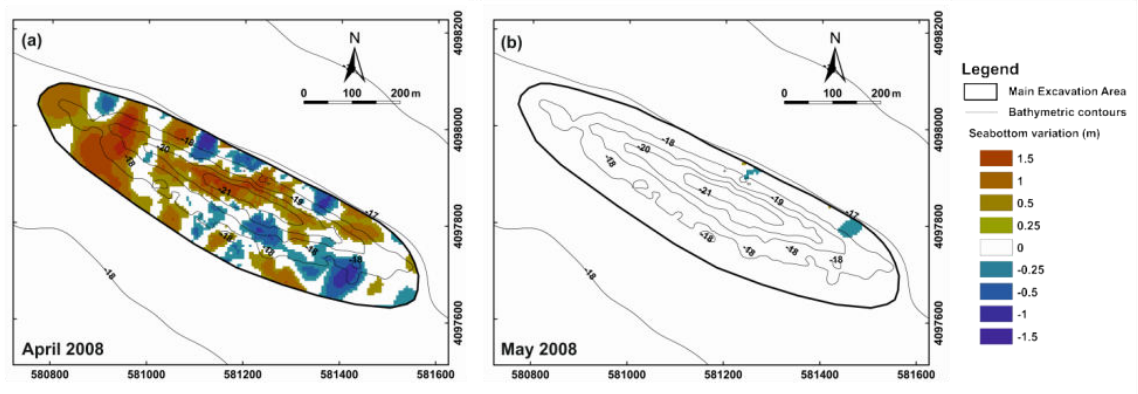

Figure 53. Computed sea bottom variation, in meters, between **(a)** March 28th and April 29th, and **(b)** April 29th and May 31st. The cold colors represent sediment removal and the warm colors indicate sediment accumulation. Bathymetric contours are referent to May 2006 survey. Coordinate system in UTM Zone 29N, datum WGS84.

The volume calculations confirm that an important quantity of sediment was mobilized during April 2008 within the excavation and surrounding areas, recovering the sandpit in about 14% of its initial excavation volume; in contrast, a similar estimation for May 2008, shows that the sandpit evolution in this month is almost null (about 0.3% of the initial excavation volume). These results therefore corroborate the

idea that high significant wave heights, such as those observed during a storm, play an important role in the sandpit morphological evolution and recovery. Furthermore, the numerical results suggest that sedimentation inside the sandpit is episodic rather than continuous in time. This fact, together with the increasing number of stormy days observed during the period between December 2008 and May 2010, can explain why, against theoretical expectations (e.g. Kubicki et al., 2007), the sandpit filling rate estimated from the bathymetric data increased from 6.4 cm/yr, in the first period between May 2006 and November 2008, to 7.2 cm/yr, in the second period between December 2008 and May 2010.

Based on these results, it was estimated that on average, the sandpit recovers 0.24% for every stormy day. Therefore, for a complete sandpit replenishment, about 350 stormy days are required. Almeida et al. (2011) combined measured and modeled wave data, creating a single dataset covering the period of January 1952 to December 2009. According to these data, an average of 11 stormy days per year was estimated. Considering this average number of stormy days per year representative of the future wave climate and the 350 stormy days required for a full sandpit recovery, then 32 years are needed for the complete sandpit replenishment. However, a decrease in the refilling rate in time, as stated in Equation (14), is probably a more suitable model, with "t" now representing the number of stormy days. According to this model, for a near-full (63%) sandpit recovery, about 412 stormy days are needed, which corresponds to 38 years, considering the same average of 11 stormy days/yr (Almeida et al., 2011) used before.

IV.5.4. Physical processes controlling the sandpit evolution

A study of the sediment dynamics was also made in the scope of this work based on the computed sediment fluxes with the Bijker formulation and encompassing the S12 storm. Figure 54 shows the magnitude and direction of the mean sediment fluxes between the 9th and the 14th of April, 2008 in the vicinity of the sandpit. The magnitude of the sediment fluxes is well related with the water depth showing higher values in the shallower zones. Inside the pit the magnitude of the flux has a minimum, explaining a decrease in the sediment transport capacity and pit infill over time. This arises from a decrease of the magnitude of the orbital velocity and mean current inside the sandpit. Lopes et al. (2009) have run SWAN for an extreme wave condition (Hs = 6 m; WSW and T = 16 s), which is similar to the maximum wave height registered during the period in analysis, and showed that the amplitude of the wave orbital velocity inside the sandpit decreases 15%. Moreover, a considerable attenuation of the orbital velocity was also observed on the lee side of the sandpit arising from energy dispersion, which can justify the lower values of sediment transport at the east-north end of the excavation.

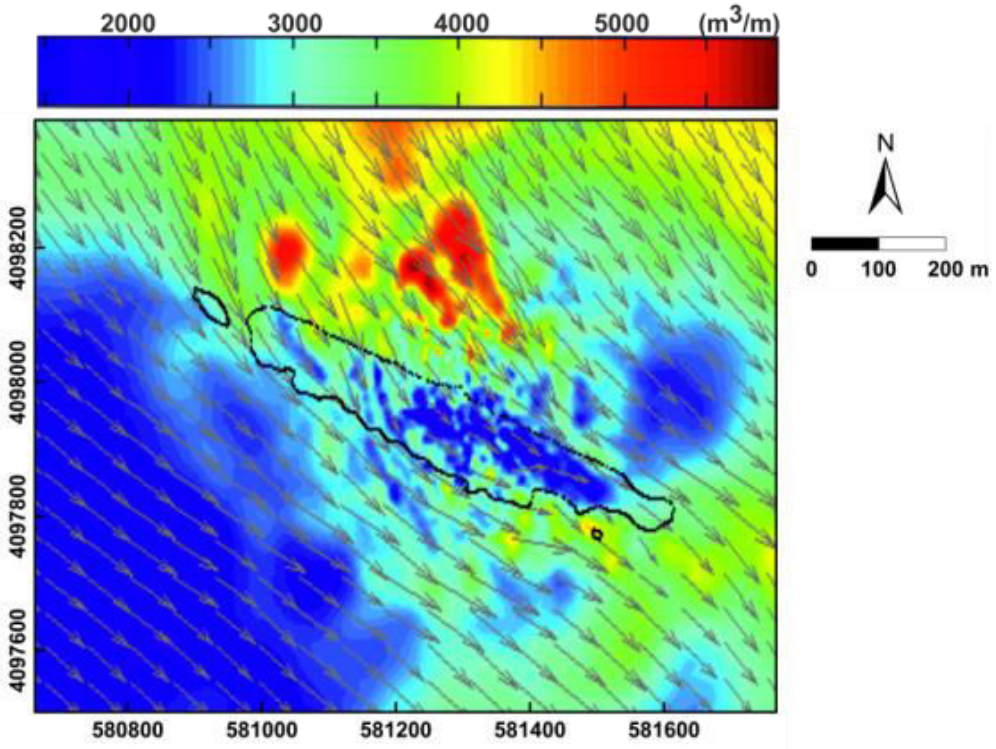

Figure 54. Magnitude and direction of the sedimentary fluxes (m^3/m) for Bijker formulations inside and in the vicinity of the sandpit. MORSYS2D results between 9th and 14th of April 2008. Coordinate system in UTM Zone 29N, datum WGS84.

Concerning the sediment flux directions, they follow the pattern of the mean wind induced currents (see Rosa et al., 2011a): the fluxes are mainly oriented from the NW to SE, along the sandpit longitudinal axis, responding to the southwesterly strong winds, and inflect at the NE sandpit flank to the south direction. The sediment fluxes field in Figure 54 is representative of the conditions that the sandpit is subject when it is morphodynamically active. Although a fully coupled 2DH modelling system was employed, the water depth where the sandpit lies implies that wave-induced currents are negligible and thereby, wave effects are mostly restricted to sediment stirring.

Figure 55 shows the conceptual map of the most important processes that act on the sandpit during the storm events with the predominant incident wind and waves coming from WSW-SW: the mean wind induced currents are SE directed and the sediment flux follows the same pattern, with the exception of the NE sandpit flank where the sediment fluxes slightly inflect to the south direction. Inside the pit and on the lee side of the sandpit the magnitude of the flux is lower allowing the accumulation of the sediment in these areas of the pit.

For significant wave heights higher than 2 m, the wave direction is mainly from WSW-SW (55-85%, as depicted in Figure 51) and in 65% of the cases the wind direction is from the SW (Rosa and Silva, personal communication, 2012). Therefore, the patterns of the evolution of the sandpit behavior suggested in Figure 54 and Figure 55,

namely the pit infill and its migration, can be extrapolated for the overall period in study.

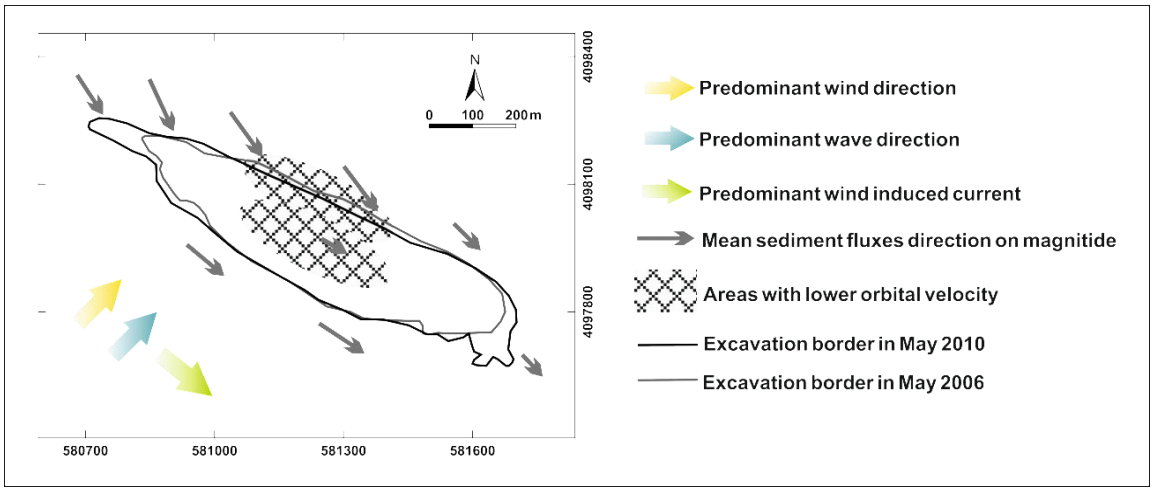

Figure 55. Conceptual map of the different processes that act on the excavation in a WSW-SW storm event. Coordinate system in UTM Zone 29N, datum WGS84.

IV.6. Conclusions

The evolution of a sandpit offshore Vale do Lobo, Portugal, resulting from the sand extraction performed in 2006 for beach nourishment purposes was investigated based on four bathymetric datasets (one before, March 2006, and three after the sand extraction, May 2006, November 2008, and May 2010), wave data from 2006 to 2010, and numerical modeling. The integration of the observations and modeling results led to the following conclusions:

(1) The sand extraction carried out between March and May 2006 of about 340 000 m^3 produced a small, deep, and oval shaped borrow pit, elongated in the NW-SE direction, about 900 m long, 150 m wide and 5 m deep (Figure 44).

(2) The sandpit represents a depression on the seafloor and therefore acts as a trap for the sediment, fostering sediment accumulation and the pit recovery. In fact, the mean flow velocity and the orbital velocity decrease inside the pit, resulting in a decrease of the sediment transport capacity inside the excavation area and, as a consequence, the pit tends to be filled through time.

(3) 2.5 years after dredging (in November 2008), an infill of the deepest area of the sandpit was observed, as well as some sediment accumulation mainly on the upper part of the NE flank, resulting on the migration to the SW of the excavation rim. A reduction in 45 % of the maximum slope of the flanks, as well as a reduction of almost

18% of the mean slope, was observed during this period (Figure 48, Figure 49, and Table 7).

(4) 4 years after the extraction (May 2010), the trend remains almost the same, with an infill of the deepest area of the pit, which is almost 2 m less deep, and some sediment accumulation in the upper part of the flanks (mainly in the NE flank). The topography of the excavation area became smoother, with the surface roughness decreasing through time. Overall, the sandpit bathymetry in May 2010 became smoother and less deep than the original pit shape four years earlier (Figure 48 and Table 7).

(5) Until the last survey used in this work (May 2010), the pit recovered almost 17% at a recovery rate estimated of 6.5 cm/yr until November 2008, and 7.2 cm/yr since then, until May 2010. The increasing refilling rate can be explained by the storm occurrences during these two periods. The period from December 2008 to May 2010, although shorter, presented a larger number of stormy days and a higher Hs 99.8 than in the first 2.5 years after the extraction (Table 10 and Figure 51).

(6) The numerical model results suggest that the sandpit refilling process is essentially storm-dependent and, therefore, episodic rather than continuous in time. In fact, significant wave height greater than 2 m, combined with strong winds, generate currents and wave orbital velocities capable of high sediment mobilization.

(7) The perimeter and the area of the pit are growing through time. However, this growth is mostly in the NW-SE direction, resulting in an elongation of the sandpit (Figure 49).

(8) The NE flank of the sandpit is migrating southwestwards, what results in a migration in the same direction of the sandpit centroid and the sandpit longitudinal axis (Figure 49).

(9) The seaward prograding pattern of the sand deposition on the onshore flank (NE), the S-SE directed wind induced mean currents (Rosa et al., 2011a), and the sediment fluxes pattern suggest that the main source of the sediment accumulated on the pit should be sand from the N-NW surrounding areas, meaning that the pit worked as a drain for these sediments.

(10) The estimates for the sandpit recovery time based on a mean refilling rate points toward a value of approximately 22 years for near-full pit refill. However, the calculated estimations proposed here use the number of stormy days, rather than the total time, and point to the need of 412 stormy days, which corresponds to 38 years for a near-complete sandpit recovery, considering the wave data set used by Almeida et al. (2011) as representative of the future wave climate.

Chapter V. Sedimentary dynamics of the “Barra de Aveiro” and the outer sandbank

V.1. Introduction

The “Barra de Aveiro” forms the communication between the “Ria de Aveiro” barrier-lagoon system and the Atlantic Ocean (Figure 56 and section II.2). Artificially opened in 1808, it is presently delimited by two jetties offshore-directed (Figure 56). Several engineering works have been performed (ahead described is section V.3), both for the harbor and inlet configuration and for the maintenance of the navigation channels, to guarantee the secure navigational access to the port. The present configuration of the “Barra de Aveiro” and the adjacent area is therefore the result of a long term evolution, as a consequence of both the frequent engineering construction works and its natural evolution. In fact, the construction of the jetties and the extensions of the north jetty through time, together with the frequent dredging operations, induced strong modifications in the littoral drift, the coastline evolution and the general geomorphology of the area, such as the sedimentary accumulation in S. Jacinto (north of the northern jetty), the development of an external sandbank, and the coastline retreat to the south (Abecassis, 1955; Castanho et al., 1974).

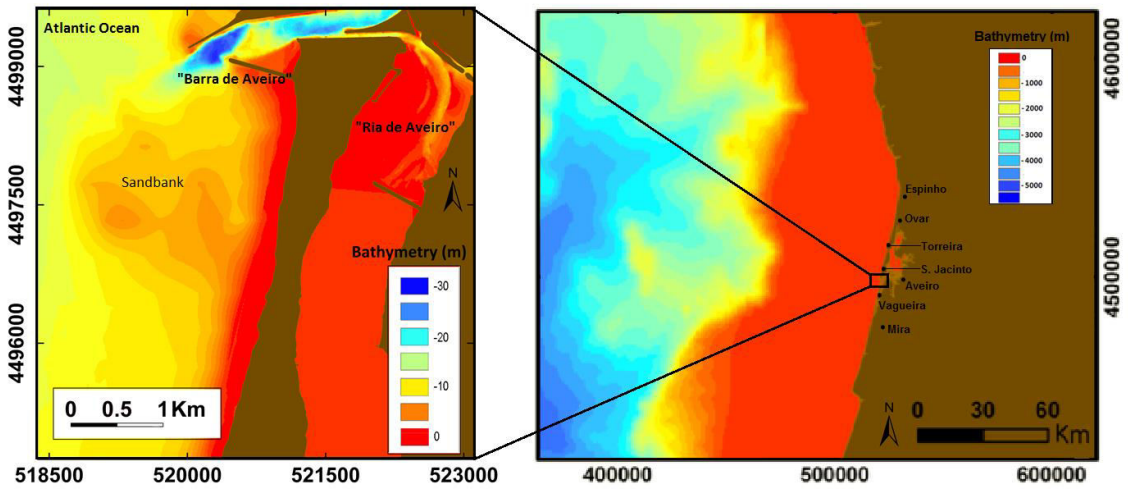

Figure 56. Study area offshore Aveiro, which includes the “Barra de Aveiro” and the adjacent near-shore shelf. The bathymetry is from the Aveiro Port Authority (June 2011 survey). The inset in right shows the location of the study area - bathymetry from the GEBCO 2008 (2 miles spacing) digital bathymetric grid. Coordinate system in UTM Zone 29N, datum WGS84 and bathymetry referred to the Hydrographic Zero datum (ZH).

The Aveiro lagoon external sandbank (Figure 56) is a sedimentary structure, adjacent to the Aveiro inlet, originated and maintained by two main factors: the sediments transported by the lagoon ebb currents and the littoral drift sediments deflected due to the effect of the north jetty (Alveirinho Dias et al., 1994). The evolution of this structure has been extremely dependent of the engineering works developed in the “Barra de Aveiro” and the adjacent area.

This chapter aims to characterize morphologically and study the evolution of the Aveiro inlet and its adjacent area, with a special emphasis on obtaining a better understanding of the sandbank formation and its evolution through time, based on bathymetric, geophysical and sedimentary data. Similar to the Vale do Lobo area investigated in the previous chapter, the morphodynamic evolution of this study area is also the result of the complex interaction of natural costal evolution processes and the impacts of offshore engineering works; however, and in contrast to the Vale do Lobo area, the coastal hydrodynamism is here much stronger (see section II.2.2). In order to integrate the case of Aveiro in the wider context of tidal sandbanks in general, an overview of the main types of the sandbanks and their classification is presented below, together with three relevant case studies.

V.2. Overview of sandbank formation processes and evolution – Case studies

Sandbanks are found widely on shallow, tidal and wave-dominated continental shelves and within coastal and estuarine environments (Bastos et al., 2004), where there is abundant sand and the currents are strong enough to induce the sediment movement (Dyer and Huntley, 1999). These features occur in the mouths of estuaries, harbor inlets, adjacent to headlands and beaches, on the exposed shelf, and close to the continental shelf edge. They may have a wide variety of forms and often store large amounts of sand, generally medium or coarse sand (Dyer and Huntley, 1999). The formation of these features is associated with the accumulation of sand as a response to regional sediment transport patterns and gradients in the transport rates (Bastos et al., 2004). In fact, sand accumulation occurs when there is a convergence of the sediment transport fluxes resulting from a reduction of the sediment transport capacity.

Different types of sandbanks have been described in the literature regarding their formation, morphology, regional setting and maintenance processes (e.g. Off, 1963; Swift, 1975; Pattiaratchi and Collins, 1987; Swift et al., 1991 and Dyer and Huntley, 1999). Off (1963), based up on twelve world-wide occurrences, described these bedforms as rhythmic linear sand bodies caused by currents. Based on this description, Swift (1975) distinguished two different types: class-1 tidal massifs, which are tidal ridge fields whose ridges were hydraulically packaged in an estuarine environment; and class-2 tidal massifs, which occur off promontories in tidal seas.

More recently, an extensive review of the different types of natural sandbanks was performed by Dyer and Huntley (1999), who proposed a generic classification into three main types, based upon their formation and development:

- Type 1: open shelf ridges;
- Type 2: estuary mouth
    - (A) ridges (wide mouth)
    - (B) tidal deltas (narrow mouth)
        - (i) without recession (ebb tidal deltas)
        - (ii) with recession (shoreface connected ridges);
- Type 3: headland associated banks
    - (A) banner banks (non-recessional headland)
    - (B) alternating ridges (recessional headland).

Open shelf linear ridges (Type 1) are oriented at an angle to the flow, are asymmetrical and appear to migrate in the direction of their steep face. These contrast with linear ridges formed in mouths of wide estuaries (Type2A), which are aligned with the flow and migrate away from their steeper face. In narrow-mouthed estuaries and inlets, tidal currents are strong only close to the mouth and waves are more dominant; therefore the banks (Type 2Bi) form close to the mouth as ebb and flood deltas. When the coast is retreating, the ebb delta forms a primary source of sand to the nearshore region, which can become modified by the action of storm events into shore attached banks at angles to the coastline (Type 2Bii). The presence of headland induces tidal eddies that can create banner sandbanks (Type 3A), but when the headland is retreating, alternating ridges (Type 3B) can be formed which can become isolated from the coast as it recedes (Dyer and Huntley, 1999).

Based on the Dyer and Huntley (1999) review and considering other more recent published and unpublished work, Kenyon and Cooper (2005) classified the sandbanks as follows (Figure 57):

- **Non-tidal banks** (Type 2Bii of Dyer and Huntley (1999) classification; Figure 57a) are develop as products of the ebb tidal deltas in areas where there is significant barrier beach recession, combined with migration of active inlets in a longshore direction (Dyer and Huntley 1999). When compared with the tidal features, non-tidal banks are smaller, showing heights of 3 to 12 m; with gentle slopes, usually less than 1^{o}; generally form closer together; and are usually rounded in profile (Kenyon and Cooper, 2005).

- **Headland banner banks** (Figure 57b and c) are located near headlands, islands or large rocks and separated from them by a channel that is shaped by strong currents. In areas of tidal currents where the sand supply and current speeds are similar on either side, the arrangement of the banks tends to be symmetrical; however, the banks located on one side of the obstacle will often be better developed than those on the other side. In non-tidal areas, with

unidirectional flow, the banks will be present on only one side of the headland and they will be attached to the obstacle rather than separated by a channel (Kenyon and Cooper, 2005). There are two main types of tidal banner banks: banks tied to rocky headlands or islets (Type 3A of Dyer and Huntley (1999) classification) and banks tied to moving sedimentary headlands (Type 3B of Dyer and Huntley (1999) classification).

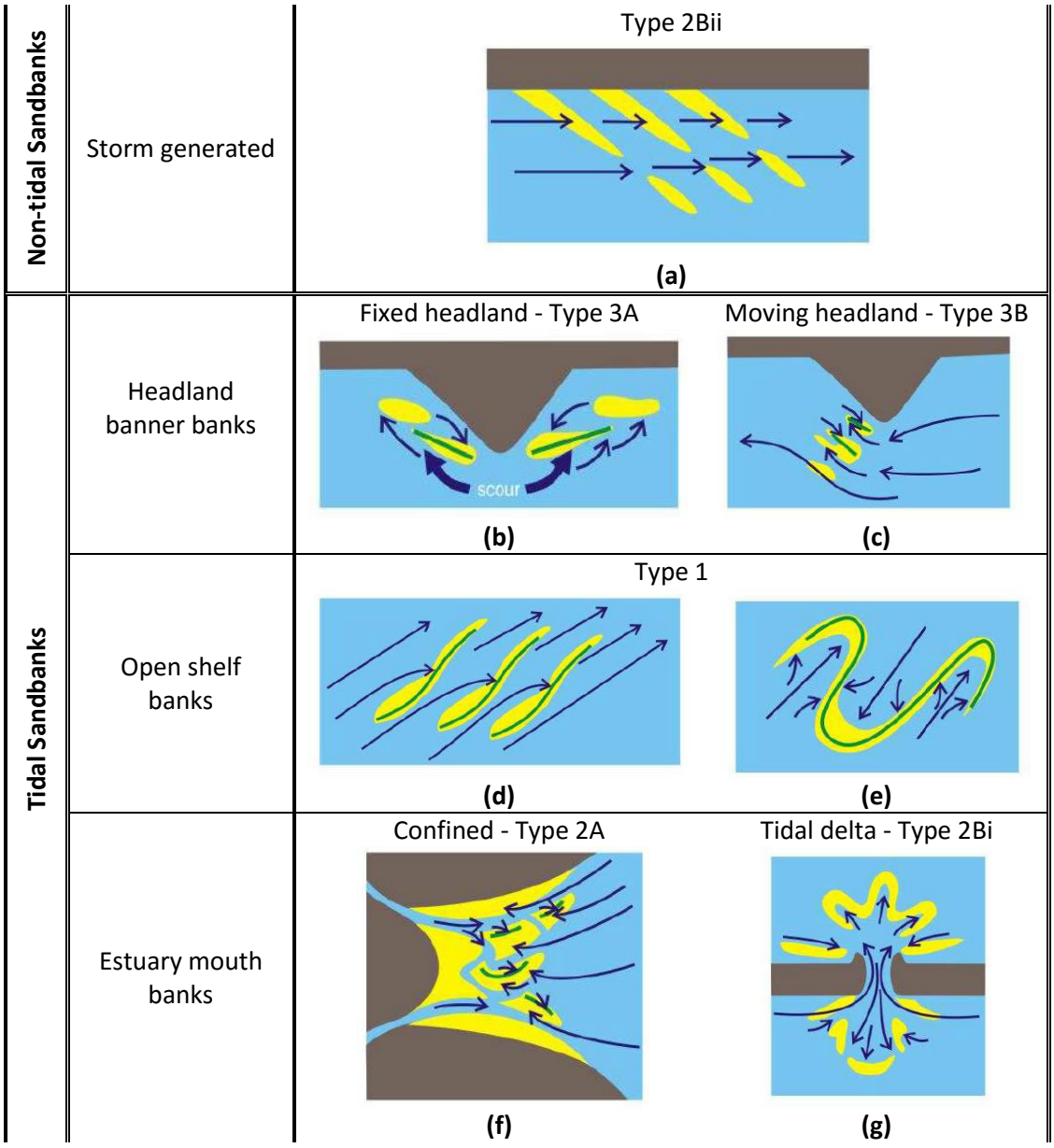

Figure 57. Sandbank classification according to their relation to the local and regional sand transport paths: **(a)** storm generated ridges (shoreface connected and offshore); **(b)** fixed headland banner banks; **(c)** moving headland banner banks; **(d)** open shelf linear banks; **(e)** open shelf sinuous banks; **(f)** confined (estuary) sandbanks; **(g)** ebb/flood tidal delta. Dark blue arrows correspond to bed load transport path and green lines indicate bedload convergence (adapted from Kenyon and Cooper, 2005).

- **Open shelf banks** (Figure 57d and e) generally occur on open tidal shelves, as group of parallel banks that are regularly sized and spaced, with a spacing that tends to be proportional to their widths (Type 1 of Dyer and Huntley (1999) classification). They are mostly asymmetrical (having slopes of about 6º on the steeper side, and less than 1º on the gentler side) and moving slowly towards the steeper side (Dyer and Huntley, 1999; Kenyon and Cooper, 2005). Open shelf banks can be up to 80 km long, typically average 13 km width and tens of meters in height (Dyer and Huntley, 1999). According to Caston (1981) open shelf sandbanks may be formed in one of three ways: (a) an excess of sand supply originates the ridges and their growth is dependent on a greater supply being added to the head than being lost from the tail; (b) ridges are a remnant of a larger deposit which is being shaped by selective transport; or (c) they are an expression of an equilibrium with the ridges maintained within an active sand transport path. Therefore, sandbanks on the open shelf are created by remodeling sand deposits (Dyer and Huntley, 1999). When the open shelf sandbanks present a sinuous crest (Figure 57d), instead of the linear (Figure 57c), they are called sinuous sandbanks, that commonly present a parabolic shape in plant view (Figure 57d) and are more often found in areas of greater bottom stress than the linear banks. Sinuous sandbanks may be an inherently unstable type, which might evolve into a series of linear banks (Caston, 1972; Kenyon and Cooper, 2005).

- **Estuary mouth banks** are divided into confined estuary sandbanks (Figure 57f) for macro-tidal estuaries that present wider mouths and ebb/flood tidal delta (Figure 57g) for meso-tidal or micro-tidal estuaries with mouths presenting small widths (Hayes, 1975; Harris, 1988; Dyer and Huntley, 1999; Kenyon and Cooper, 2005). Confined (estuary) sandbanks correspond to the Type 2A of Dyer and Huntley (1999) classification and are mainly linear sandbanks, which build up to sea level and increase in width, eventually forming extensive intertidal flats (Kenyon and Cooper, 2005). Due to the lateral constrains, the banks tend to be aligned with the water flow, rather than being at an angle (Dyer and Huntley, 1999). Ebb/flood tidal deltas (Type 2B of Dyer and Huntley (1999) classification) are formed at the narrow mouths of meso and microtidal estuaries, and the inlets through barrier islands, when there is an abundance of sand or gravel available. They may be formed in pairs with ebb tidal deltas formed seaward of the mouth, and flood deltas formed landward of the mouth (Figure 58; Dyer and Huntley, 1999). This is the case of the “Barra de Aveiro” exterior sandbank, which can be classified as an estuary mouth sanbank of ebb tidal delta type (Teixeira, 1994). Therefore, this type of sanbanks is described in more detail below.

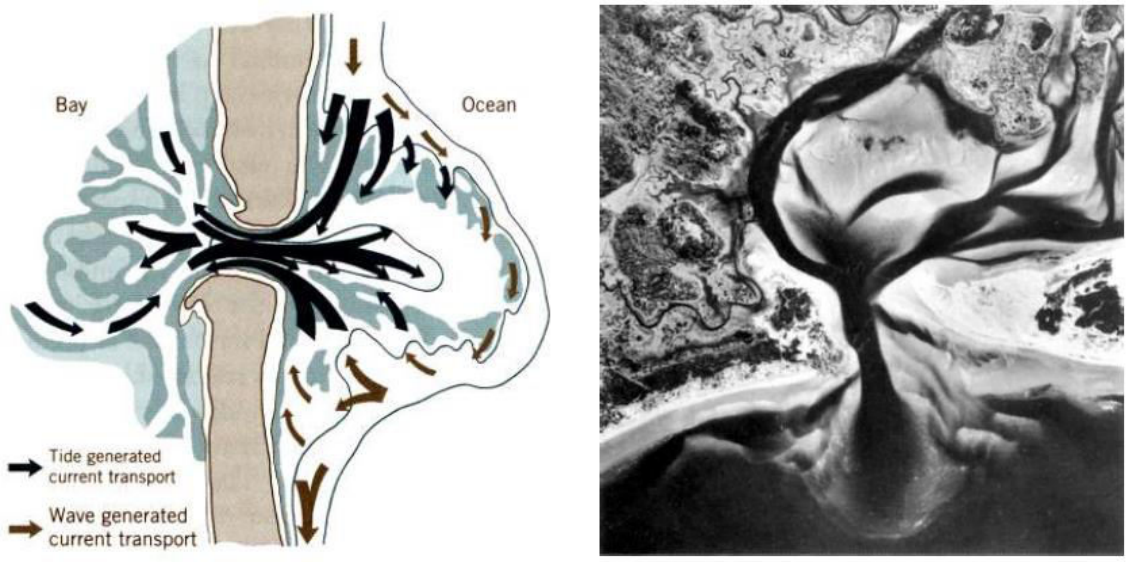

(a) **(b)**

Figure 58. Ebb-flood tidal delta: (a) diagram showing the typical bedload transport paths and (b) aerial photograph (Hayes, 1975 *in* Kenyon and Cooper, 2005). In the case of the Barra de Aveiro sandbank only the ebb-delta is well developed.

The ebb deltas are formed seaward of the mouth, shaped by the ebb currents issuing from the mouth and modified by wave action and shore parallel currents (Dyer and Huntley, 1999; Kenyon and Cooper, 2005). The main sedimentary source is the littoral transport that carries sand under wave action along the beach towards the spits that constrict the mouth (Dyer and Huntley, 1999) and it is deposited when the flow diverges. A terminal lobe takes place outside the mouth where the current flow causes deposition (Kenyon and Cooper, 2005). An important feature of the tidal delta is the deep trench formed in the mouth which can persist on the shelf after coastal retreat (Dyer and Huntley, 1999). Hayes (1975) proposed a model for ebb delta morphology: the sand transport in the main channel is dominated by ebb currents and a large terminal lobe at the outer end of the ebb channel occurs due to the expansion of the currents that create an area of deposition. The crest of the shoal thus becomes a bottom current convergence zone at times of maximum sand transport.

The morphologic asymmetries of ebb-tidal deltas, also called ebb-tidal shoals or entrance bar, and the orientation of the entrance channel are the result of the interaction of both dynamic and static factors. Dynamic factors are: (1) the magnitude and direction of net longshore sediment transport, (2) the tidal prism, (3) the relict ebb shoal, (4) the offshore extent of the ebb jet, (5) the riverine sediment supply, (6) the flood shoal evolution, (7) the dredging of the channel, and (8) the wave refraction and diffraction over the offshore and ebb shoal bathymetry are dynamic factors. Static factures include: (9) the location and configuration of jetties, (10) the offshore and nearshore bathymetry, (11) the size and shape of the back bay, and (12) the geological

constraints imposed by the local structures such as hard bottom (Carr and Kraus, 2001). The ebb delta (Figure 59) in a broad sense consists of the ebb shoal proper (formed in the stream of the ebb jet), the updrift and downdrift bypassing bars (formed as a result of the wave action and wave-induced currents), and the attachment bars also called the "tie-in" or "weldment" area (developed from material bypassed around the ebb shoal complex, either arriving to or leaving from the shore; Carr and Kraus, 2001).

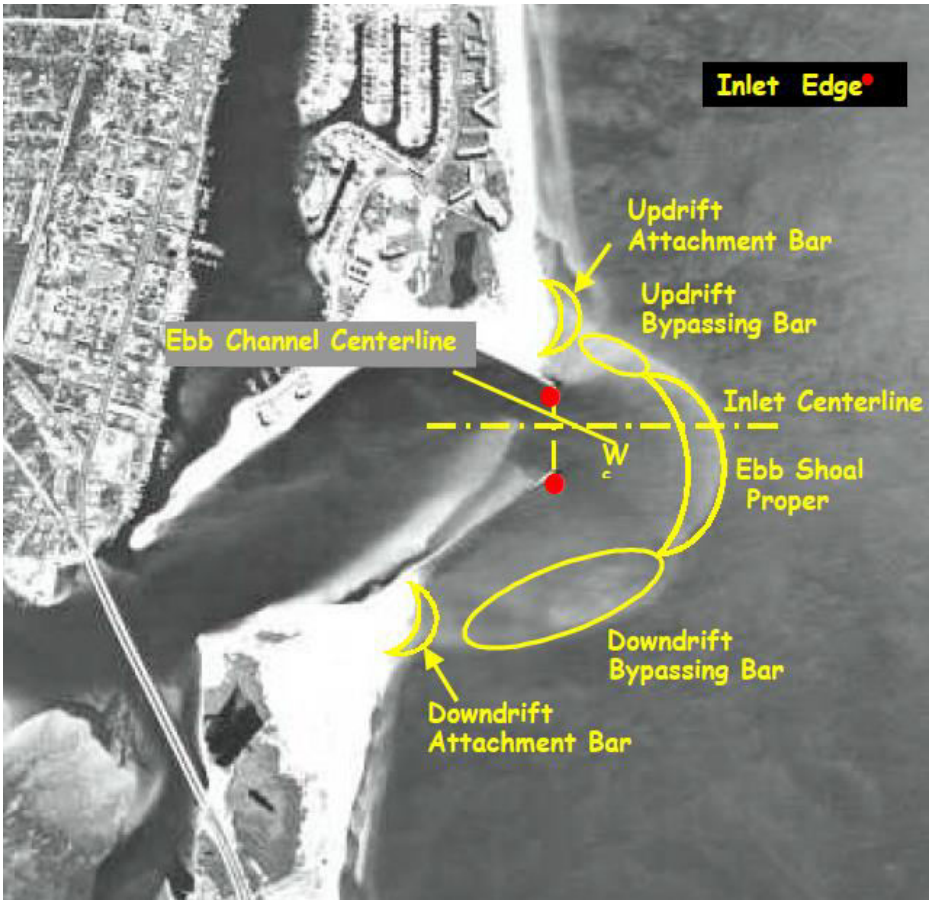

Figure 59. Ebb-tidal delta morphology (Carr and Kraus, 2001).

The geomorphology of ebb-tidal deltas is also controlled by the sand bypassing processes. Bruun and Gerritsen (1959) described sand bypassing at inlets using the parameter r is defined as:

$$r = P/M_{tot} \quad \textbf{(15)}$$

where P is the tidal prism and M_{tot} is the average annual longshore transport at the inlet. Inlets that tend to have stable and deep channels and a poor bypassing from updrift to downdrift present a value of r greater than 150, whereas inlets that tend toward closure and have a significant bypassing present r values smaller than 50 (Carr and Kraus, 2001). For the case of the Aveiro, assuming the mean tidal prism and the littoral drift values presented in section II.2, a value of r around 70 is obtained, which indicates a tendency for sand bypass.

A relationship between the volume of the sand in the ebb delta and the tidal prism of the estuary was stablished by Dean and Walton (1975), suggesting that there is a balance between the sediment released by coast erosion and the portions that are transported into the estuary and deposited, thus modifying the tidal prism. According to Powell et al (2006), the volume of a mature ebb delta is equal to one fifth of the prism at the spring range of tide.

Several authors have studied the formation, evolution and maintenance of estuary mouth sandbanks: Robinson (1975), Fitzgerald et al. (2004), Kruger and Healy (2006), Powell et al. (2006), Elias and Hansen (2013), Wang et al. (2014), Pianca et al. (2014), Ridderinkhof et al. (2016). Below three case studies are presented, considered relevant for the present study.

Elias et al (2006) and Elias and Spek (2006) conducted several studies to understand the sand exchange between the inlet, the ebb-tidal delta and the adjacent coastlines in the largest inlet in the Dutch Wadden Sea, Texel inlet (Figure 60). Analysis of the evolution of the ebb-tidal delta morphology spanning a period of over 400 years shows different stages, characterized by specific orientations of the main channels and shoals (Elias et al. (2006); Figure 61): (1) Prior 1750, the ebb-tidal delta showed a downdrift asymmetry, with periodic shoal breaching and downdrift channel relocation being the dominant mechanisms for sediment by-passing; (2) after the construction of the coastal defense works (in 1750), a stable ebb-tidal delta with a westward stretching main ebb-channel developed over a period of ca. 60 years; (3) the damming of the major part of the back-barrier basin in 1932, distorted this stable state and over a period of approximately 40 years the main channel switched to a southward course, remaining stable ever since (Figure 61). Elias et al. (2006) pointed out that a correct description of the ebb-tidal delta dynamics and processes of the Texel Inlet needs to incorporate the inlet modifications and back-barrier processes, and suggested a conceptual model to describe the process–response relation between the human intervention and ebb-tidal delta change. In fact, the substantial changes in ebb-tidal delta evolution are a response of the inlet system to the cumulative effects of human intervention (Figure 61).

The present-day ebb-tidal delta (Figure 60) developments correspond to a phase of redistribution and recirculation of sediments in order to achieve a natural

dynamic equilibrium state, adapted to the changed configuration of the main-ebb channels. According to Elias and Spek (2006), the sediment is transported from the abandoned ebb-delta front (western margin of Noorderhaaks, 11 in Figure 60) and along the adjacent coastlines into the basin where it is partly deposited as a result of a net flood dominated transport due to tidal asymmetry, landward directed wind and wave-driven flow, and larger flood transport capacities due to wave effects that exceed the net ebb-dominated tidal residual transports.

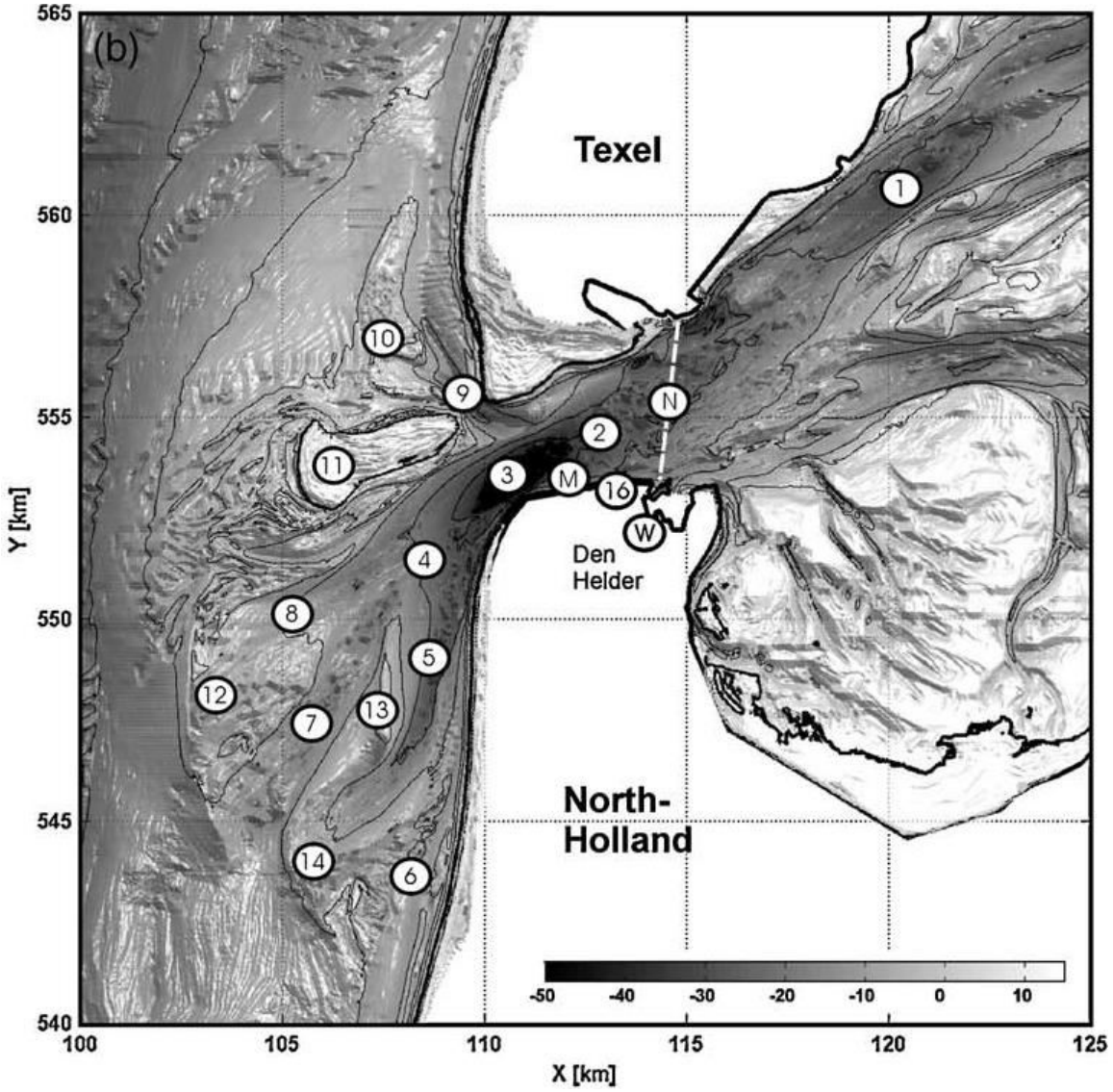

Figure 60. Present-day morphology of Texel Inlet located at the Western part of the Dutch Wadden Sea. Numbers from 1 to 9 identify channels and from 10 to 16 identify shoals (co-ordinates are based on the Paris co-ordinate system; Elias et al (2006); Elias and Spek (2006)).

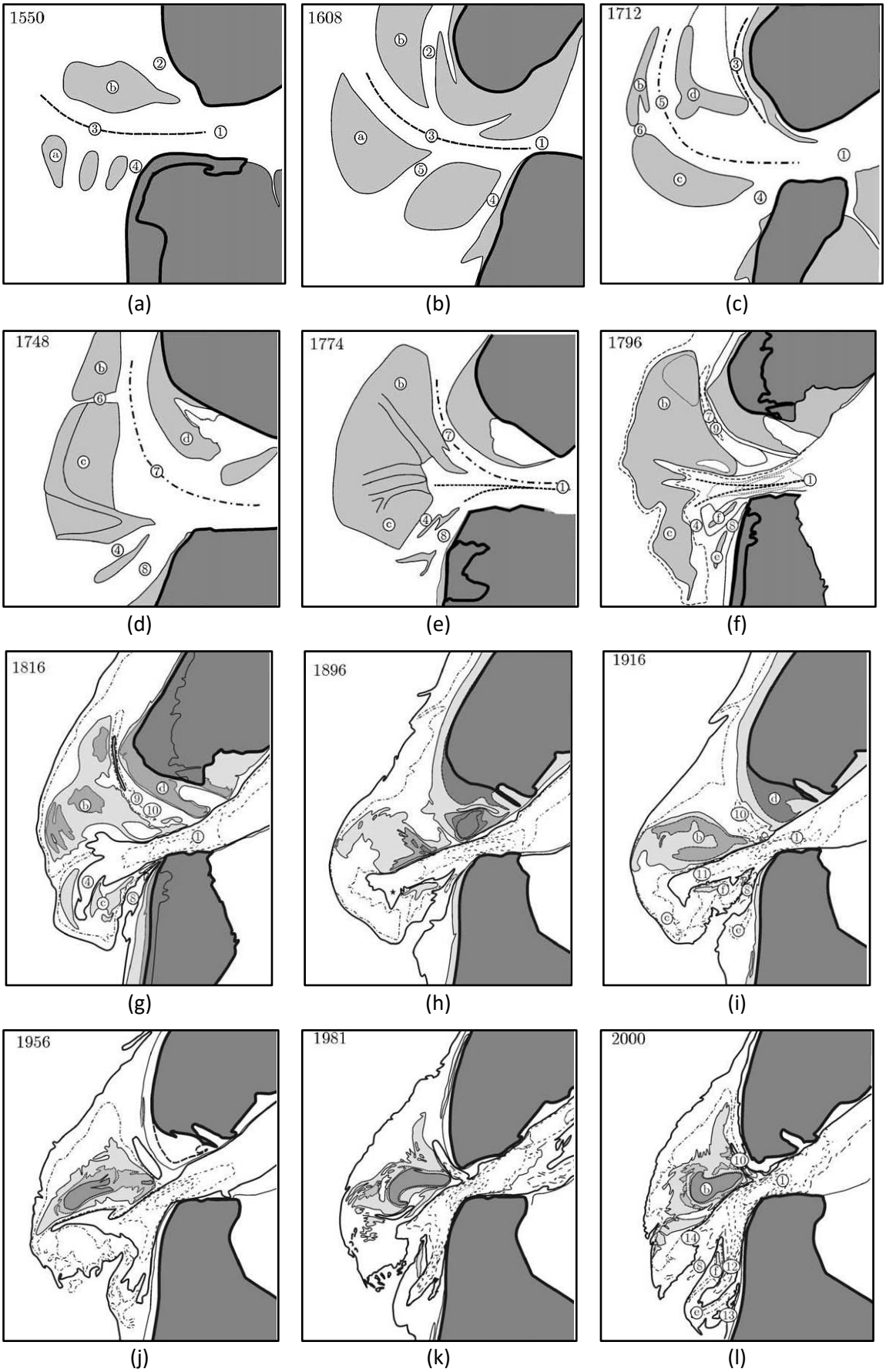

Figure 61. Ebb-tidal delta development Texel Inlet from 1550 to 2000. Numbers identify channels and letters identify shoals (modified from Elias and Spek, 2006).

Garel et al. (2014) investigated the morphodynamic response of a mixed-energy ebb-tidal delta (including its down-drift coast) located at the Guadiana estuary, southern Portugal, to channel relocation and stabilisation by jetties (constructed in 1972–1974). These authors found large modifications of the morphology and dynamics of the inlet, with drastic implications in terms of sediment bypassing and coastal evolution (Figure 62). However, the lack of fully developed morphological features that are typically found at jettied inlets (that typically responds with the formation and seaward migration of the ebb shoal proper and with the collapse and erosion of its downdrift domain) indicates that the delta has not yet achieved its equilibrium in volume. Therefore, bypassing is weak and the delta behaves as a sink for sediment.

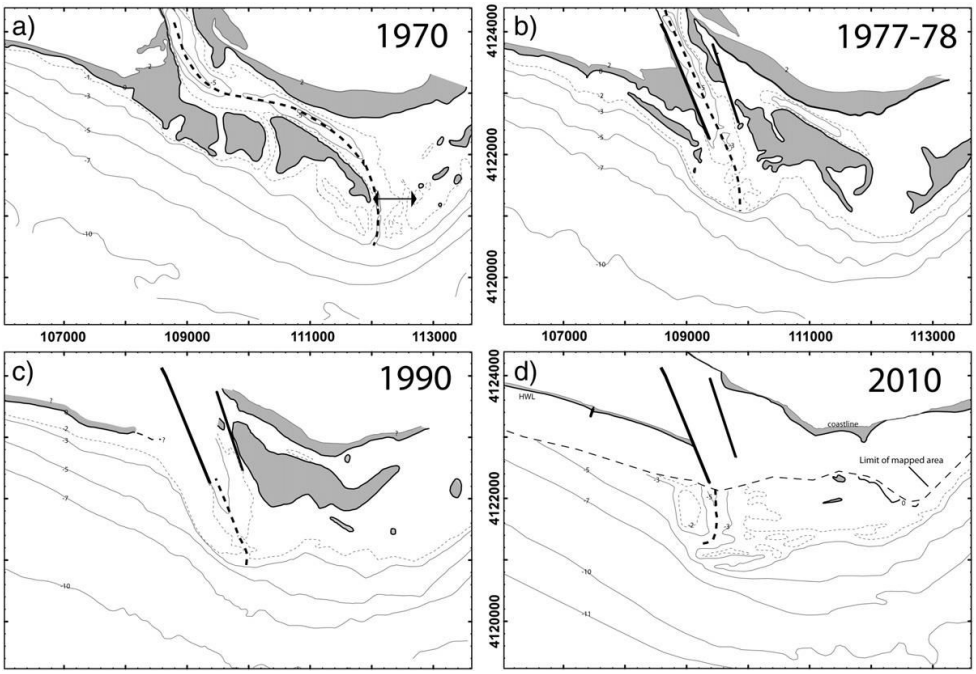

Figure 62. Bathymetric evolution of the Guadiana ebb-tidal delta from 1970 to 2011. Grey areas correspond to shoals (above MSL), the thick dashed line indicates the position of the inlet channel and the arrows in (a) indicate the location of the tip of the inlet (isobaths are in metres and referred to MSL; Garel et al., 2014).

The sediment pathways in the Guadiana ebb-tidal delta are characterised by two main processes (Figure 63): (1) a weak bypassing where sediment from the up-drift and downdrift coasts accumulates at the ebb shoal proper; and (2) a large-scale landward transport of sand inherited from the pre-jetty (bank breaching) bypassing process, with significant effects (accretion) on the down-drift coast (Garel et al., 2014). According to these authors, the main impact of the jetties is the creation of an erosion area in the central portion of the barrier island down-drift located, related with the development of a persistent divergent longshore transport that feeds the surrounding areas. Furthermore, the large-scale erosive effects of the jetties on the down-drift coast will be observed more than 50 years after their construction (Garel et al., 2014).

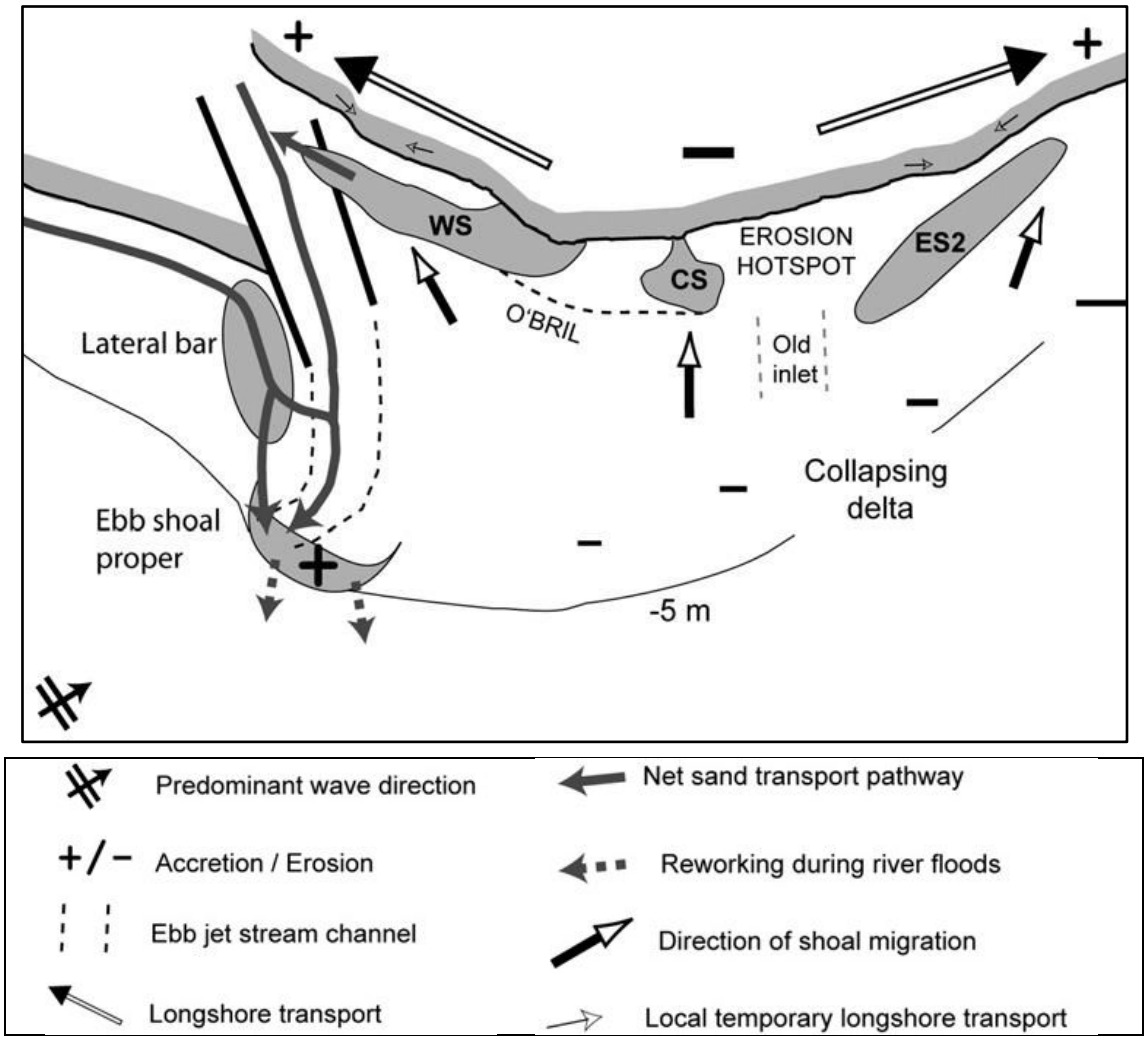

Figure 63. Conceptual model of the net sand pathways at the Guadiana ebb-tidal delta (Garel et al., 2014).

The same ebb-tidal delta was analyzed by Garel et al. (2015) based on 24 aerial photographs (1940-2012) and 13 bathymetric maps (1969-2014; Figure 64). The reworking of sand from the historical delta area is an important contribution for: (1) the post-jetty progradation of the updrift beach, which resulted from a large accretion event (1985-1994) due to beach attachment of a shoal produced by the erosion of a broad shallow area relict of the historical delta; (2) the individualisation of a lateral updrift bar simultaneously with the new ebb shoal proper formation (Figure 64). The authors show that the erosion of the historical delta may enhance significantly the updrift shoreline progradation and may promote the re-establishment of sand bypassing after jetty construction earlier than predicted with important implications with respect to the management of jettied inlets and their adjacent coasts.

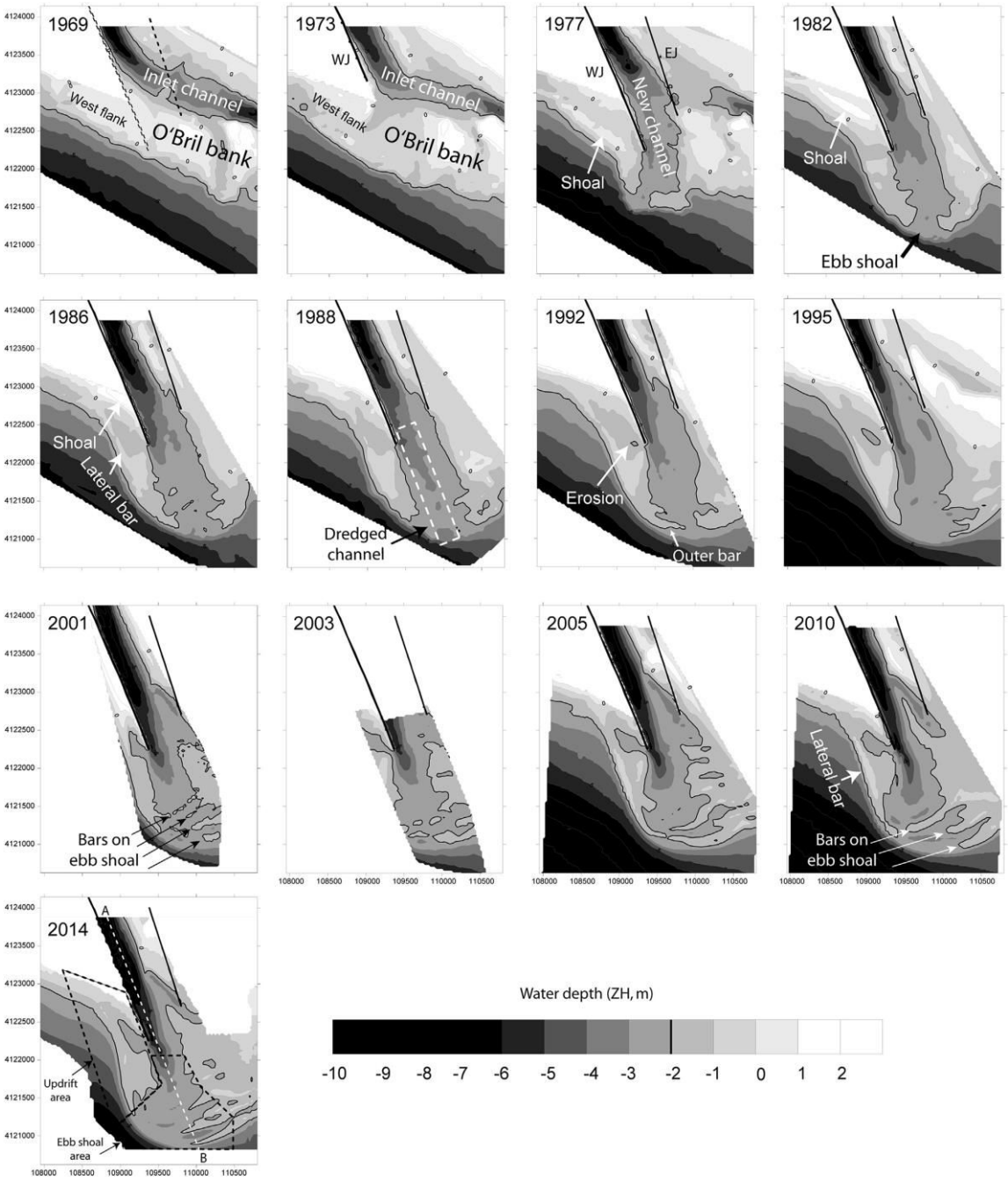

Figure 64. Bathymetric maps of the Guadiana ebb-tidal delta from 1969 to 2014. Gray scale: light is shallower and dark is deeper water depths. The thick contour line corresponds to the -2 m isobath (Garel et al., 2015).

Recently, Cáceres et al. (2016) studied the Mar del Plata Harbor, in Argentina, characterized by the development of a sandbank across the access channel, the shoreline advance in the south and shoreline retreat in the north of the harbor, associated to the partial blockage of the sediment transport caused by the harbor jetties. According to the morphological modeling and for the present hydrosedimentological conditions, the sandbank tends to move toward the access

channel (Figure 65) with high sedimentation rate, implying a regular maintenance of the navigation channel (Cáceres et al., 2016).

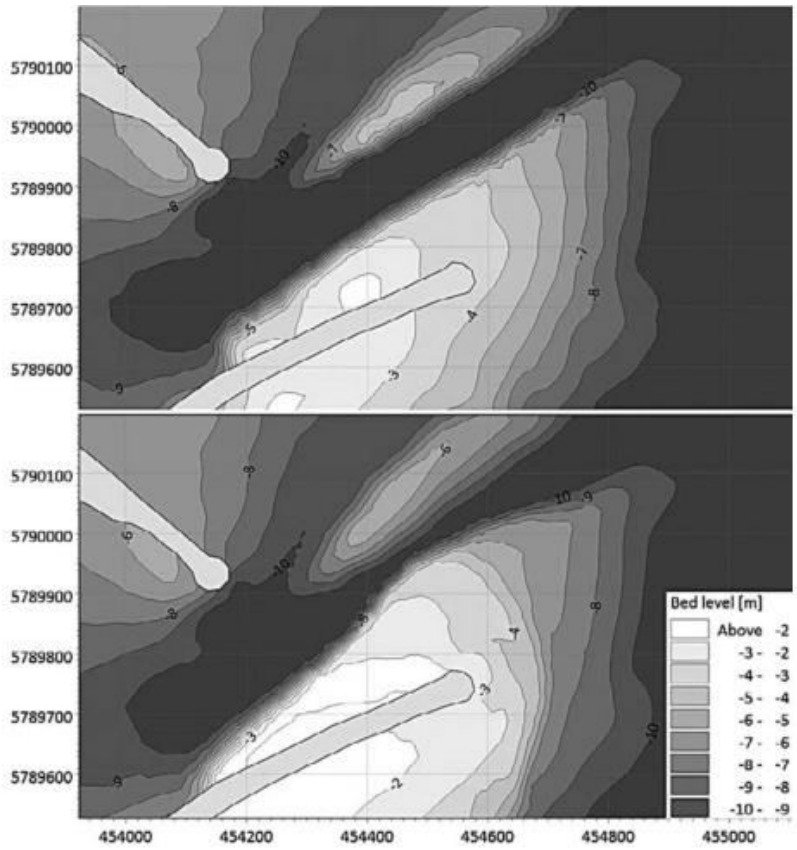

Figure 65. Bathymetric evolution at Mar del Plata Harbor entrance after 3 years of morphological simulation: (a) 2008 and (b) 2010 (Cáceres et al., 2016).

V.3. Historical evolution of the "Barra de Aveiro" and adjacent area

The "Ria de Aveiro" is geologically a very recent feature formed in the Xth century, when a sandy spit started to form and progressed southwards from Espinho (Figure 56), due to the southward alongshore sediment transport, progressively isolating the ancient gulf from the sea (Figure 66; MOP, 1951; Abecasis, 1955; Alveirinho Dias et al., 1994). According to Abecasis (1955), the documents prior to the Xth century do not refer the existence of a lagoon in Aveiro, and cities such as Ovar, Aveiro, and Vagos are mentioned as being on the sea coast (Figure 66; Cunha, 1930; Abecasis, 1955). From the Xth to the XVth centuries, a gulf approximately 70 km long and 20 km wide, at the latitude of the Vouga estuary with an incipient sand spit in the

North, is reported in the literature (Figure 66; Abecasis, 1955; Alveirinho Dias et al. 2000).

In the XIIth century, the sand spit reached the North of Torreira, three centuries later the sandbar extended to São Jacinto, and at the end of the XVth century it reached the location of the present artificial inlet, where it remained until the middle-end of the XVIth century. With the inlet in front of Aveiro, the number of ships coming to the harbor increased and the city was at the peak of its prosperity. In the end of the XVIth century the inlet was located about 3 km south of the actual position, but it was very unstable, changing its position three to four times a year. In the XVIIth century (1643) the inlet was located at Vagueira and in the middle of the XVIIIth century the sandy bar reached Mira (Abecasis, 1955; Figure 67).

The evolution and enclosing of Aveiro Lagoon was synchronous with the Little Ice Age (from the XIVth to the XIXth century), characterized by low temperatures, reduction of the mean sea level and intense sedimentation (Alveirinho Dias et al., 2000), which promoted the accretion trends at the sand spit and consequently the inlet instabilities. According to Alveirinho Dias et al. (2000), mainly since XVth century, the process of enclosing by the sand spit involved the accretion of more than $2x10^{10}$ m^3 of sediments.

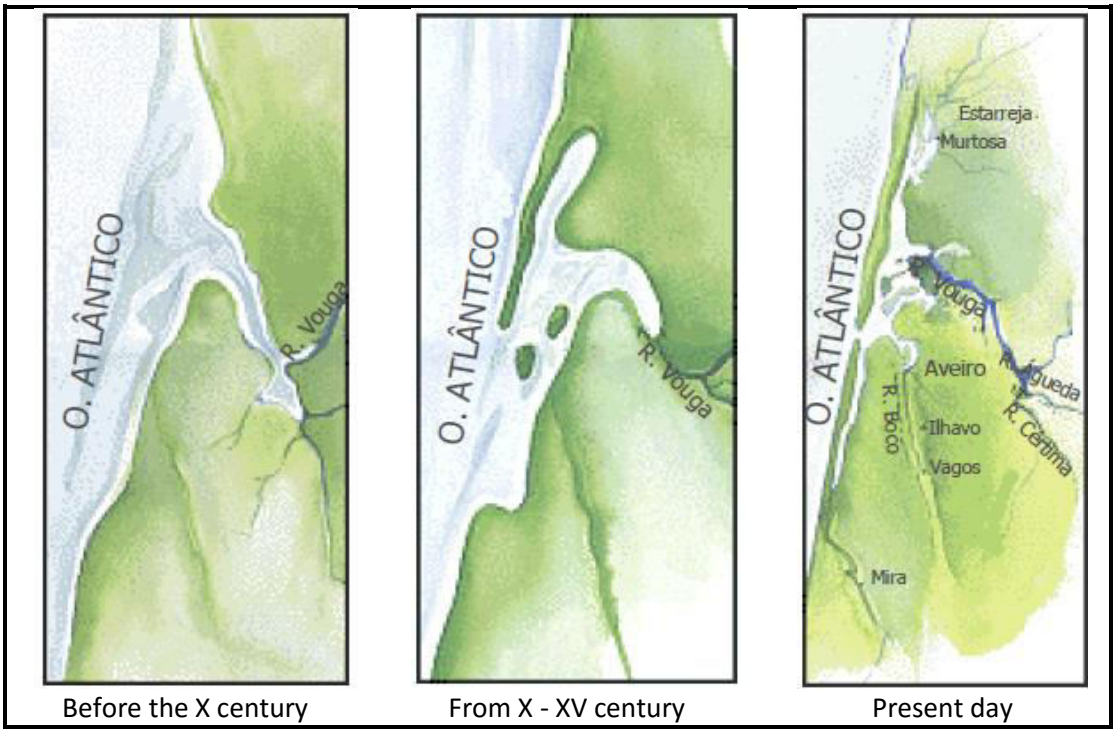

Figure 66. Evolution of the "Ria de Aveiro" in the last 1000 years: from the Xth to present day (*in* Abrantes, 2005).

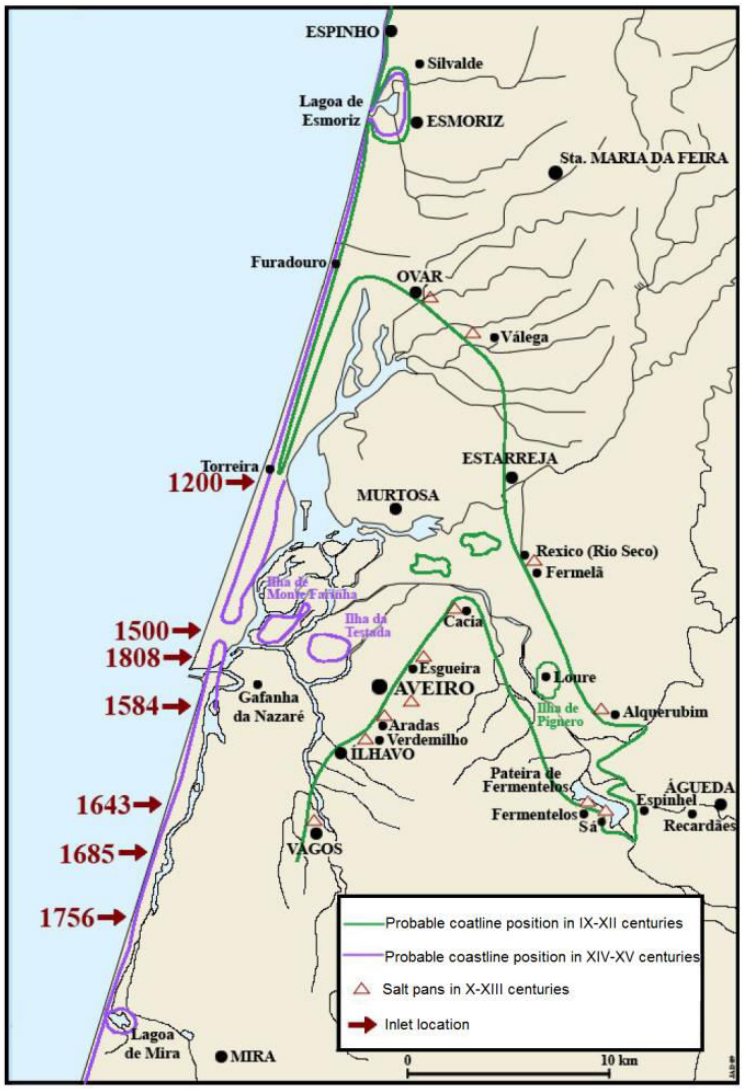

Figure 67. Coastline probable evolution between Espinho and Mira and inlet location from 1200 until the artificial opening in 1808 (modified from Bastos, 2009).

After the middle-end of the XVIth century, with the progressive sand spit migration to the south, the access to the harbor (located in the inner lagoon) became gradually longer and more difficult to navigate, leading to a significant reduction of the marine traffic, with direct consequences to the economy of the region (Abecasis, 1955; Alveirinho Dias et al., 1994; Teixeira, 1994). Furthermore, the total or partial obstruction of the inlet, which occurred several times after middle/end XVIth century, brought serious problems to the city and surrounding areas, not only because of its impacts on the maritime activities, but mainly due to the loss of the water drainage that prevented the cultivation and led to the degradation of the sanitary conditions, causing serious diseases and deaths (Neves, 1935). According to Abecasis (1955), in 1797 the number of deaths duplicated the births in Aveiro and the city started progressive decline.

Since the middle of the XVIIIth century, several attempts to open the inlet were performed unsuccessfully. In 1802 the engineers Reynado Oudinot and Luiz Carvalho were contracted to restore and fix the inlet, by cutting the sand spit and building a long and strong dike from Gafanha until the ocean, crossing the sand barrier (Neves, 1935; Abecasis, 1951; Cunha, 1959). In 1803, Luiz Carvalho assumes the exclusive direction of the project, which was affected by several difficulties until April 3rd 1808, when the new inlet was successfully opened (Neves, 1935; Abecasis, 1951; Cunha, 1959). Due to a big flood, the water level inside the lagoon raised about 2 meters above the sea level and, on the 3rd of April, 1808, at 7 p.m., Luiz Carvalho ordered the demolition of the temporary works built at the location chosen for the new inlet and opened the trail through which the accumulated water ran down to the sea (Neves, 1935; Abecasis, 1951; Cunha, 1959). Three days after, the new inlet was 4 to 6 m deep and 264 m wide and the drainage issues were solved (Neves, 1935; Cunha, 1959). According to Castanho et al. (1974), after the inlet fixation, an ebb delta bar arose in front of the inlet with depths between 2 and 3 m in the navigation channel.

In 1818, Luiz Carvalho started to build a new dike located 300 m north of the first dike. However, this dike was quickly destroyed due to its weak consistency. From 1823 to 1858 there were no new construction works in the inlet, and the interventions were restricted to the needed repairing of the dike that was many times damaged by the sea waves (Neves, 1935). In June 1858, Silvério da Silva assumes the position of engineering director of the port and in December 1859 proposed to rebuild and to extend seawards the south dike and build a new experimental jetty on the northern side of the inlet channel. A 295 m long northern jetty was constructed 300 m north of the southern jetty, increasing this distancen (between jetties) submersed bar towards the sea (see Figure 68; Neves, 1935; Abecasis, 1951; Cunha, 1959).

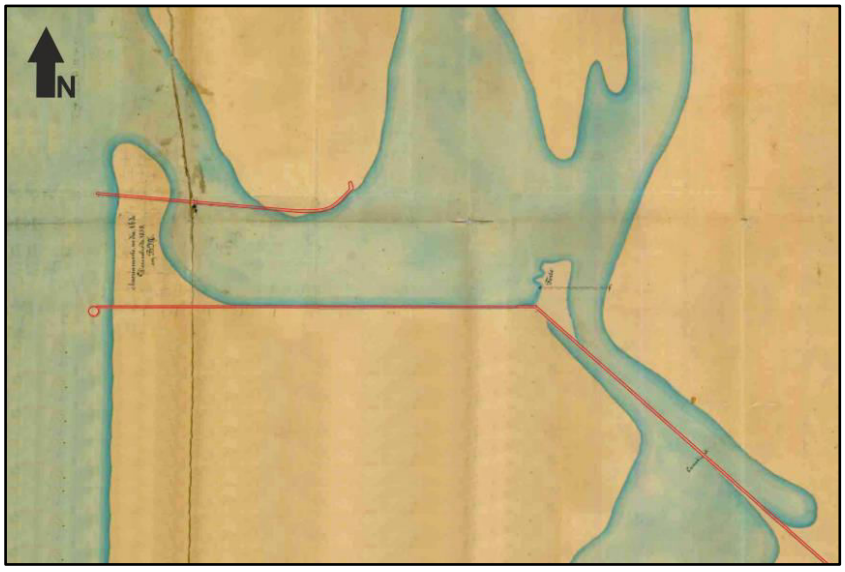

Figure 68. Work plan (in red) plant from 1858 to rebuild and to extend seawards the south dike and build a new jetty on the north side of the inlet channel (modified from "Projecto do Melhoramento da Barra D'Aveiro" *in* Martins, 2012).

After a very long dry season, the inlet presented in 1873/74 an anomalous configuration, with a 120 m wide sand spit parallel to the coastline advancing from the north to 300 m south of the south dike (see Figure 69). In order to face this issue, Silvério da Silva extended the south dike towards the recently formed sand barrier, which was opened by a big flood occurred in March 1874. Silvério da Silva was also responsible for the complete reintegration of the southern part of the lagoon in the whole system, by restoring the communication between the southern and the northern parts of the lagoon, and for the Vagueira inlet closure, opened in 1838 due to a flood (Abecasis, 1955; Alveirinho Dias et al., 1994).

Figure 69. Work plan plant from February 1874 showing the sand spit advancing from the north (modified from "Planta indicativa do Plano d' Obras para o melhoramento da Barra de Aveiro: Projecto de 26 de Fevereiro de 1874" *in* Amorim and Garcia, 2008).

In 1927 the engineering director of the port, João von Hafe, presented his project to improve the Aveiro inlet. His innovative project included (Abecassis, 1955):

- The construction of a triangular system of curvilinear dikes in the upstream section of the inlet channel to guide the currents from the northern and southern parts of the lagoon;
- A 300 m extension of the northern jetty seawards that would go out on the sea and convergent with the southern jetty;
- The deepening of the inlet channel at -3 m by dredging.

The von Hafe's project was accepted; however some modifications advised by a committee of British consulting engineers were introduced to his initial project, namely the reduction in 250 m of the length of the northern jetty, the widening of the inlet channel from 300 m to 350 m, the modification of the widths of the S. Jacinto and Mira channels respectively from 190 m and 110 m to 270 m and 80 m, and the dredging of the navigation channel to become 200 m wide, 500 m long and at 4 m deep (Abecasis, 1951). The works officially started in October 1932 and were concluded in 1936, with a jetty limiting the northern margin of the inlet channel and continuing northeastwards by an interior dike, a triangular system of dikes for currents convergence from the S. Jacinto and Mira channels, and a significant dredging in the inlet navigation channel (see Figure 70).

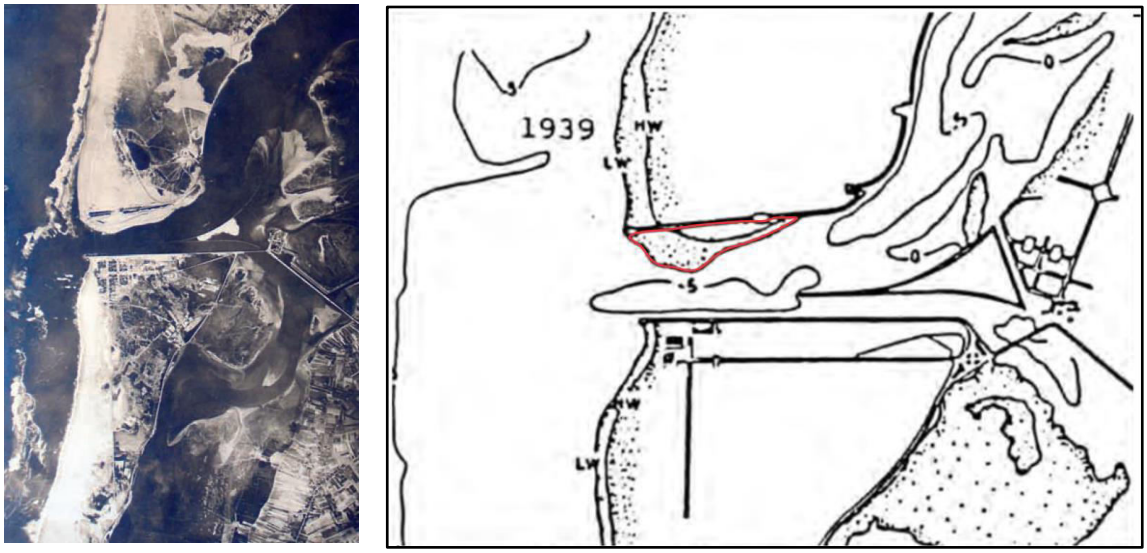

(a) **(b)**

Figure 70. (a) Aerial photograph from 1934 (Amorim and Garcia, 2008); **(b)** Aveiro inlet plant from 1939, showing the inner bank in red (from Castanho et al, 1981 in Alveirinho Dias et al., 1994).

After these works, the inlet navigation channel and subsequently the port access conditions were reasonably improved: the inlet channel was deeper and its orientation and configuration were better defined and more stable, the outer sand bar was repelled 300 m seawards, the navigational draft increased from 4 to 5 m in mean high-water, and the tidal range at the entrance of the lagoon increased from 2 to 2.7 m in spring tides, a favorable factor for the channel depth maintenance. However, some serious issues started to reveal, namely, the instability and the subdivision of the outer navigation channel, the strong transverse currents occurred in the channel under wave action, and the narrowing of the inlet channel due to the entrance and accumulation

along the northern jetty of littoral sands (Abecasis, 1951). Therefore, the new channel soon became inappropriate for the increasing navigation, and a new project had to be considered.

In 1937 a new project to improve the Aveiro entrance channel was proposed aiming to increase the inlet channel depth to 7.2 m in mean high-water and to obtain a straight entrance channel west-east directed free of cross wave currents. The works took place from 1949 to 1958 with the extension of the north jetty 690 m seawards, and the building of a new southern jetty 780 m long, rooted 400 m to the south of the old jetty built by Luiz Carvalho, and slightly convergent with the former (see Figure 71; Abecasis, 1955). Even before the conclusion of the works, the inlet navigation channel showed a great improvement, which started to be noticed mainly when the northern jetty reached the length sustained by von Hafe. In fact, the suppression of the narrow inlet, due to the inner bank formed close to the north jetty (see Figure 70b), and the deepening of the outer bar and the channel between the two jetties led to an increase of the tidal prism in the lagoon, together with an increase of the drag capacity of the ebb currents (Castanho et al., 1974; Vicente, 1990). These currents, more important than the flood currents, became capable of eroding the channels inside the lagoon, the channel between the two jetties and the outer bar, by carrying sediment out to the sea. The bar therefore moved seaward while the depth of the navigation channel increased (Castanho et al., 1974). However, the jetty extension intercepted the littoral sediment movement to the south leading to the progress of the beach on the northern side of the north jetty, whereas in the southern part of the south jetty the beach was decreasing, reaching at some points recesses of about 90 m in 5 years (Castanho et al., 1974; Alveirinho Dias, 1994). Once the north jetty became unable to retain the sediments coming from the littoral drift, the sand began to gather round the bar, in an ever increasing quantity. The complex action of the different shaping agents led to a state of equilibrium in which all the littoral drift sands passes naturally beyond the lagoon inlet, due mainly to the string ability of the ebb currents achieved by the increase of the tidal prism admitted by the lagoon (Castanho et al., 1974).

According to Castanho et al. (1974), the variations observed in the “Barra de Aveiro” and its adjacent area were, due to the variations in the littoral sediment movement, in the south direction. In the years in which the littoral drift exceeds the mean annual value of 1 000 000m^3 the bar is sanded up. In this case, the navigation passage is moved southwards. In the years in which littoral drift in the south direction is less than the annual mean value, the bar is eroded, the navigation channel is located to the right in the alignment of the inner channel, and the depths increase (Castanho et al., 1974).

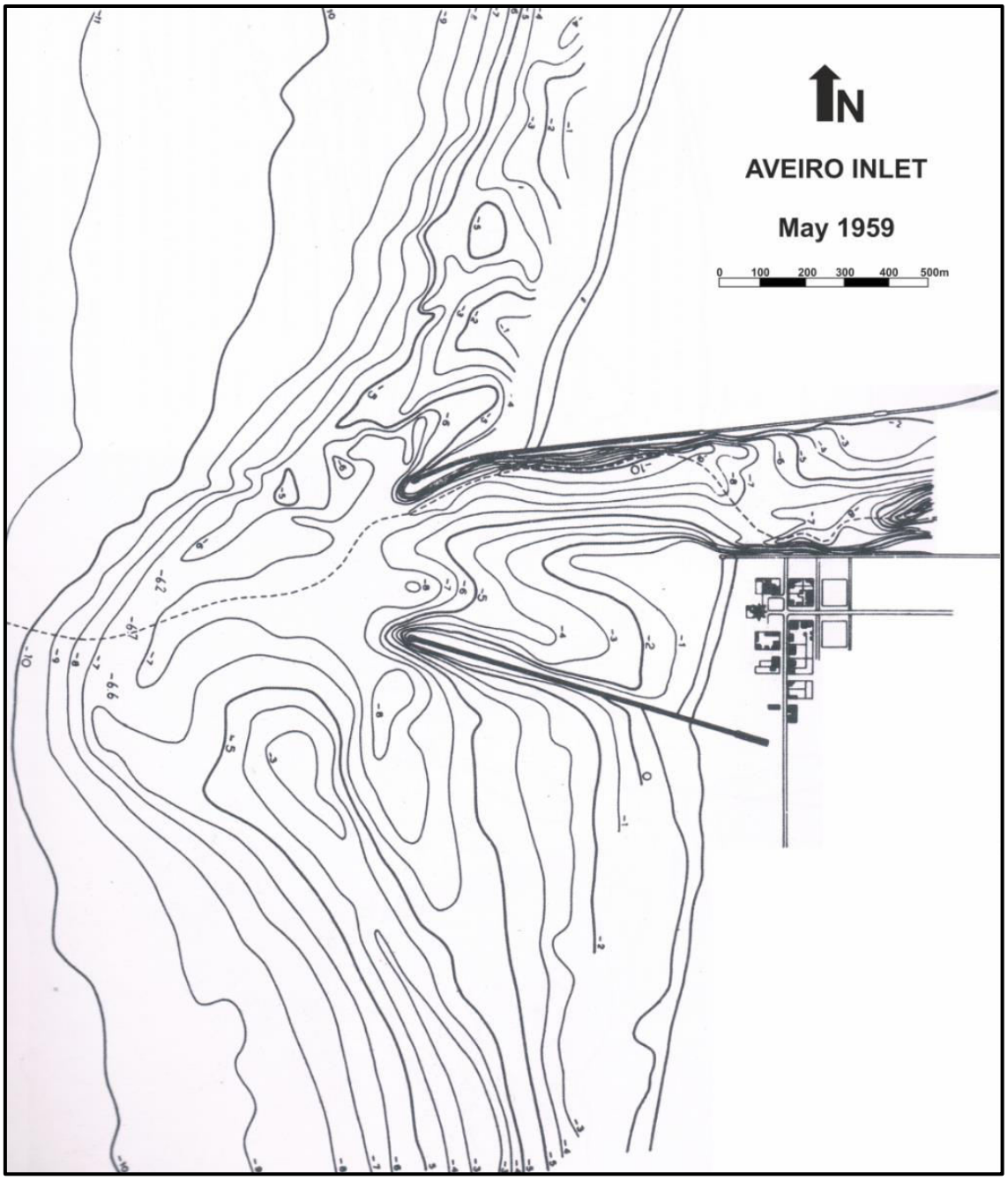

Figure 71. Aveiro inlet hydrographic plan from May 1959 (modified from Hydrographic plan of 1959, Port of Aveiro *in* Amorim, 2008). Bathymetric contours referred to the Hydrographic Zero datum (ZH).

Between 1983 and 1987 the northern jetty was extended 500 m seawards, which originated new re-adjustments of the sandbar. In fact, the north jetty increased its ability to retain sediments in the adjacent beach and oriented to southwest the ebb currents, resulting in a strong modification in the ebb and flood current patterns (Vicente, 1990).

In 2009/2010 a new project to improve the inlet configuration was approved to extend the north jetty 200 m with an orientation that should be coincident with the orientation of the final part of the jetty before the intervention and to define a new navigation channel -13.2 m (ZH) deep by dredging 1 300 000 m^3 of sand from the inlet navigation channel and almost 45 000 m^3 from the internal channel (Figure 72). These works, started in December 2011 and concluded in December 2013, allowed the entrance of larger ships (with drafts of 10.5 m and 200 m long), guaranteed the safety and the operationally of the harbor, and avoided the silting of the inlet area (APA, 2009; Rosa et al., 2012). Although they serve the main navigation purposes and, therefore, have significant impact in the local economy, according to Dias and Mariano (2011) the 200 m north jetty extension slightly changed the local hydrodynamic patterns, and that may induce changes in the overall lagoon circulation related with the tidal prism decrease for the main channels. Figure 74 and Table 11 summarize the most important engineering works that took place in the “Barra de Aveiro” and surrounding areas through time.

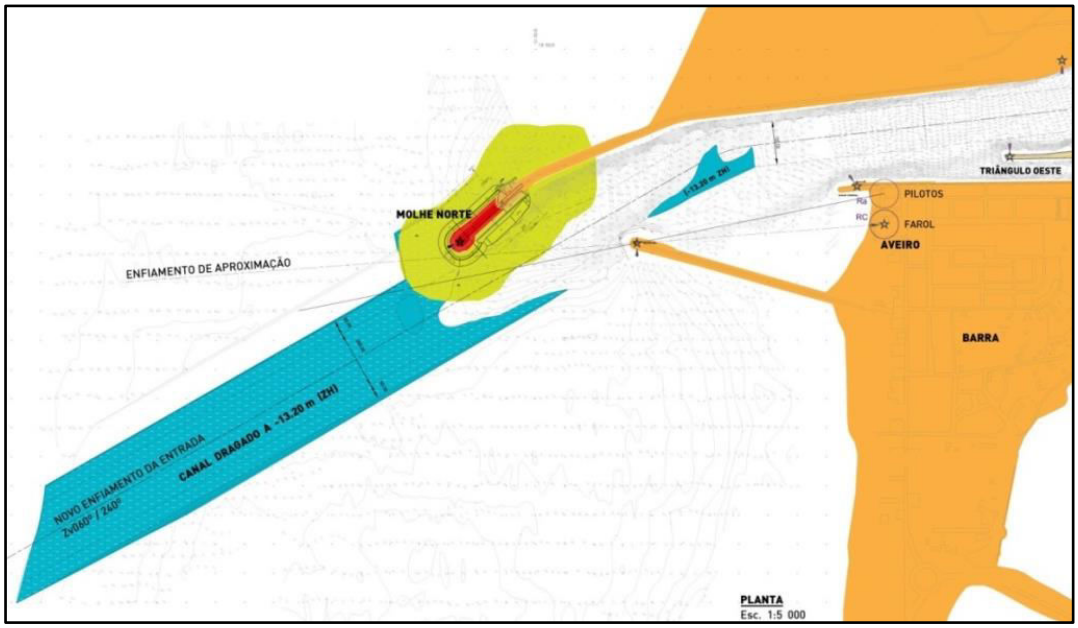

Figure 72. Work plan plant from December 2008 for the Aveiro inlet improvement. The blue polygons illustrate the dredging target areas and the red area shows the 200 m jetty prolongation (modified from APA, 2009).

Table 11. Most important engineering works carried out in the "Barra de Aveiro" and adjacent areas from 1808 until nowadays.

Date	North jetty	Central jetty	South jetty	Other
1808		Central jetty construction.		Inlet opening.
1818	Construction of a dike located 300 m north of the central dike. Quickly destroyed due to its weak consistency.			
1859	Construction of a 295 m long jetty 300 m north of the central jetty increasing this distance towards the sea.	Extend seawards.		
1863				Vagueira inlet closure.
1886				Restoring the communication between the southern and the northern parts of the lagoon – Espinheiro channel.
1874		Extended seawards (to open a long sand spit coming from north parallel to the coast, which was opened by a big flood, occurred in March 1874).		
1932-1936	Extended 50 m seawards.	Definitive consolidation.		Construction of a triangular system of dikes for currents convergence from the S. Jacinto and Mira channels. Deepen the inlet channel at -4 m by using dredging techniques.
1949-1958	Extended 690 m seawards.		Construction of the south jetty - 780 m long, rooted 400 m south of the central dike.	Navigation channel dredge at -7.2 m depth.
1983-1987	Extended 500 m seawards.			
2011-2013	Extended 200 m seawards.			Navigation channel dredge at -13.2 m depth.

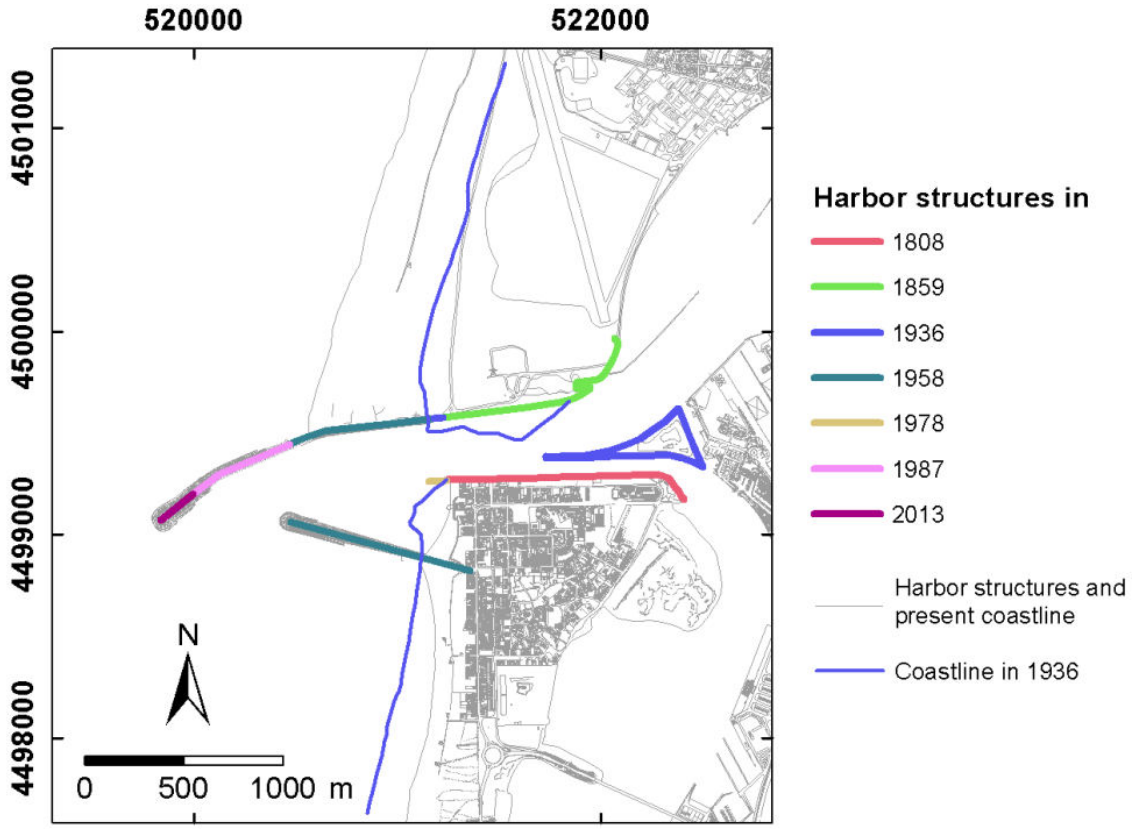

Figure 73. Most important engineering works carried out in the “Barra de Aveiro” and adjacent areas from 1808 until nowadays. Coordinate system in UTM Zone 29N, datum.

V.4. Data and methods

The datasets used for this work consisted of: (1) 8 old bathymetric maps from 1936 to 1985; (2) 5 recent bathymetric datasets acquired between 2010 and 2013; (3) sidescan sonar data collected in December 2011 and January 2012; and (4) 49 surface sediment grab samples collected in March 2012. The author participated in the planning and execution of the sidescan sonar and sediment sampling surveys that took place in 2011 and 2012. The methodology used for each dataset is described in detail below.

V.4.1. Bathymetric data

Old bathymetric maps 1936 - 1985

In order to assess the long term evolution of the “Barra de Aveiro” and the sandbank formation and evolution between 1936 and 1985, the following bathymetric

maps were used: August 1936, July and August 1950, January 1954, May and June 1965, March 1966, July and August 1976, July 1978, and May and June 1985. These old maps were scanned and inserted into a georeferenced GIS database (*ArcGIS*); the maps were georeferenced and the iso-bathymetric lines were vectorized. The data were interpolated with the *Natural Neighbors* (*NaN*) method (using a cell size of 10x10 m²) and the bathymetric surfaces were compared.

Recent bathymetric datasets 2010 - 2013

The more recent evolution of the area (2010-2013) was studied based on single-beam echosounder bathymetric surveys carried out by the Port of Aveiro Authority (APA, S.A.). For this study, 5 bathymetric datasets were used to characterize the sandbank evolution and adjacent area through time: November 2010, June 2011, February 2012, November 2012, and November 2013. The bathymetric datasets were inserted into a georeferenced GIS database (*ArcGIS*) and converted to UTM coordinates, datum WSG84. The data were interpolated with the *Natural Neighbors* (*NaN*) method, using a cell size of 10x10 m². The bathymetric surfaces obtained (see Figure 83 to Figure 87) were used for:

a) a general characterization of the study area;

b) the sandbank delimitation;

c) the estimation of the sediment budget between successive bathymetric surfaces, obtained by subtraction of those surfaces;

d) the sandbank volume estimation for each bathymetric dataset, based on the difference between the surface obtained with all the bathymetric data points (with sandbank) and a theoretical surface estimated based on the data, with the exclusion of the points in the bank area (without sandbank).

The estimations c) and d) were performed using the *ArcGIS* tools *minus* and *cut/fill* that allowed the subtraction of successive bathymetric surfaces, which is essential to estimate sedimentary balances and understand the morphologic evolution of the study area through time.

V.4.2. Sidescan sonar data

The sidescan sonar data used in this work were acquired in a 3 days survey, in which the author participated both in the planning and execution phases, carried out on the 21st and 22nd of December 2011 and on the 13th of January 2012, on board of

the vessel “Duas Águas” (Figure 74a) from the Port of Aveiro Authority (APA, S.A.) and using a combined sidescan sonar (100 kHz and 400 kHz) and sub-bottom profiler (0.5 to 12 kHz) *Edgetech 512i* system (Figure 74b) from the University of Aveiro. The positioning of the sidescan sonar data was performed with a differential GPS system “Leica GX 1230”, used in RTK mode.

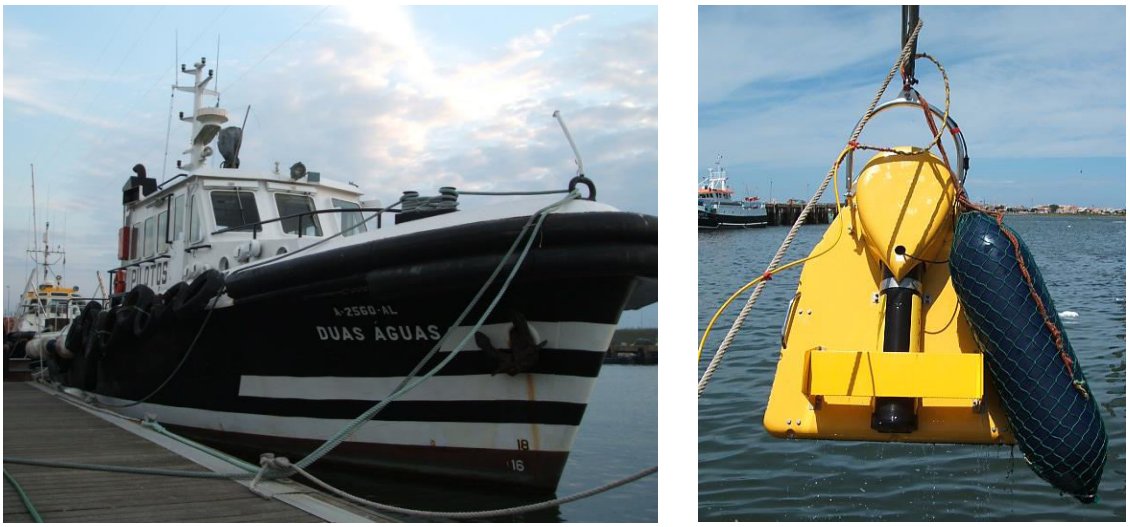

(a) **(b)**

Figure 74. (a) The vessel “Duas Águas” from the Port of Aveiro Authority (APA, S.A.) and **(b)** the combined sidescan sonar and sub-bottom profiler *Edgetech 512i* system from the University of Aveiro.

Thirty nine sidescan sonar lines (≈ 95 km) were acquired at a 100 m range, covering an area greater than 10 km^2 (see Figure 75), in double frequency: 100 kHz and 400 kHz. The higher frequency data (400 kHz) data were processed and the mosaic was built using the *SonarWeb* software from *Chesapeake Technology* (see detailed information about sidescan sonar systems and data processing in sections III.2 and III.2.3, respectively) through the application of the following main steps/corrections:

(1) removal of the water column;
(2) selection of the “Bronze” color scale as the sonar imagery color, with a contrast of 95.3%;
(3) computation of the corrected navigation by using the “course made good” method and smoothed with a downsample ping interval of 100;
(4) application of the appropriated fish to GPS antena offsets and layback corrections for all the lines;
(5) correction of the data for the slant range and beam angle effects;
(6) creation of a mosaic with a resolution of 12 cm and its export as a georeferenced image.

The mosaic was imported into a georeferenced GIS database (*ArcGIS*) and the final mosaic was built using the ArcGIS tools (Figure 96).

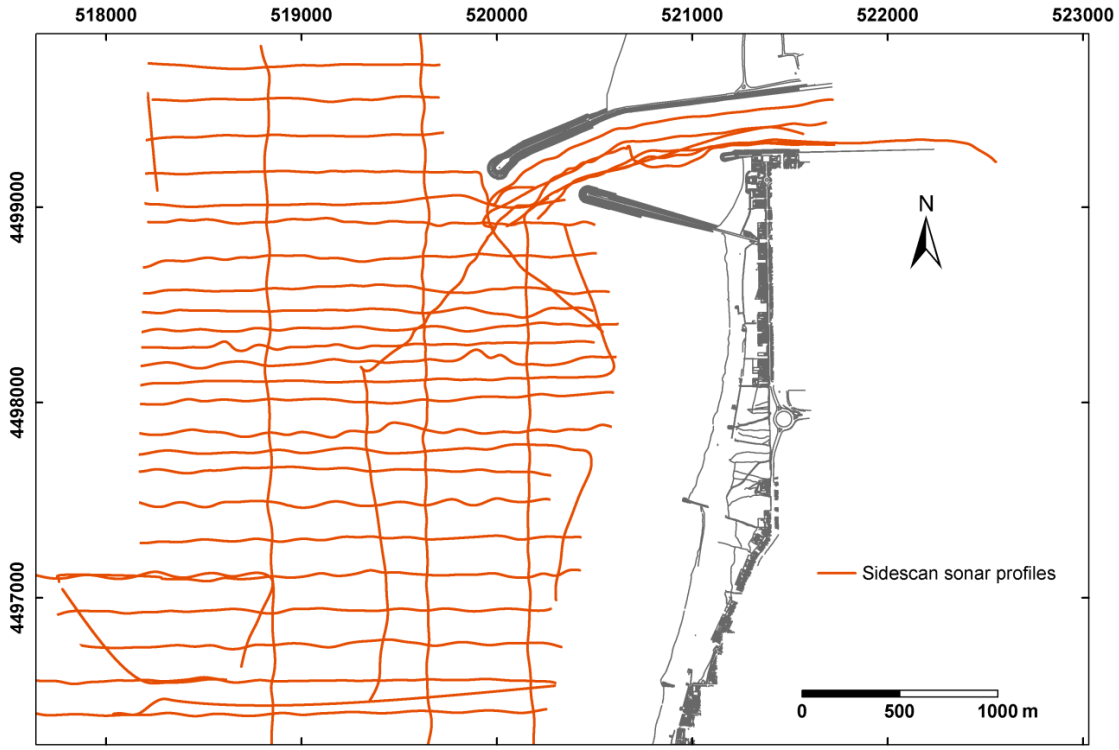

Figure 75. Sidescan sonar lines acquired on the scope of this work. Coordinate system in UTM Zone 29N, datum WGS84.

V.4.3. Sediments sampling and grain size analysis

The sediment samples used in this work were collected on 22 March 2012 on board of the vessel “Ria Azul” from the Port of Aveiro Authority (APA, S.A.) and using a sediment grab Petit Ponar (see Figure 76). The author also participated in the campaign.

A set of 49 surface sediment grab samples were collected for this work in the “Barra de Aveiro” and adjacent near shore shelf (see Figure 77). The precise positioning of each sampling station was performed with a differential GPS system “Leica GX 1230”, used in RTK mode. The grain size analysis was based on the European Standard EN 933-1:2000 (EN, 2000) and the workflow is schematized in Figure 78. Each sediment sample was dried at 40^{o}C and then homogenized and divided into 2 subsamples by quartering: one of the subsamples was preserved and stored in plastic bags properly labeled and the other was analyzed for granulometry. The fine fraction (<63 µm - silt and clay particles) was separated by wet sieving through a 63 µm screen

(see Figure 79a) and both fractions (<63 and >63 µm) were dried and weighed. The sedimentary fraction >63 µm was dry sieved (see Figure 79b) through a battery of sieves ½ phi spaced (from 31.5 mm or -5 ϕ to 63 µm or 4 ϕ).

(a) **(b)**

Figure 76. (a) Vessel “Ria Azul” from Port of Aveiro Authority (APA, S.A.) and **(b)** sediment grab Petit Ponar used for sediment sampling.

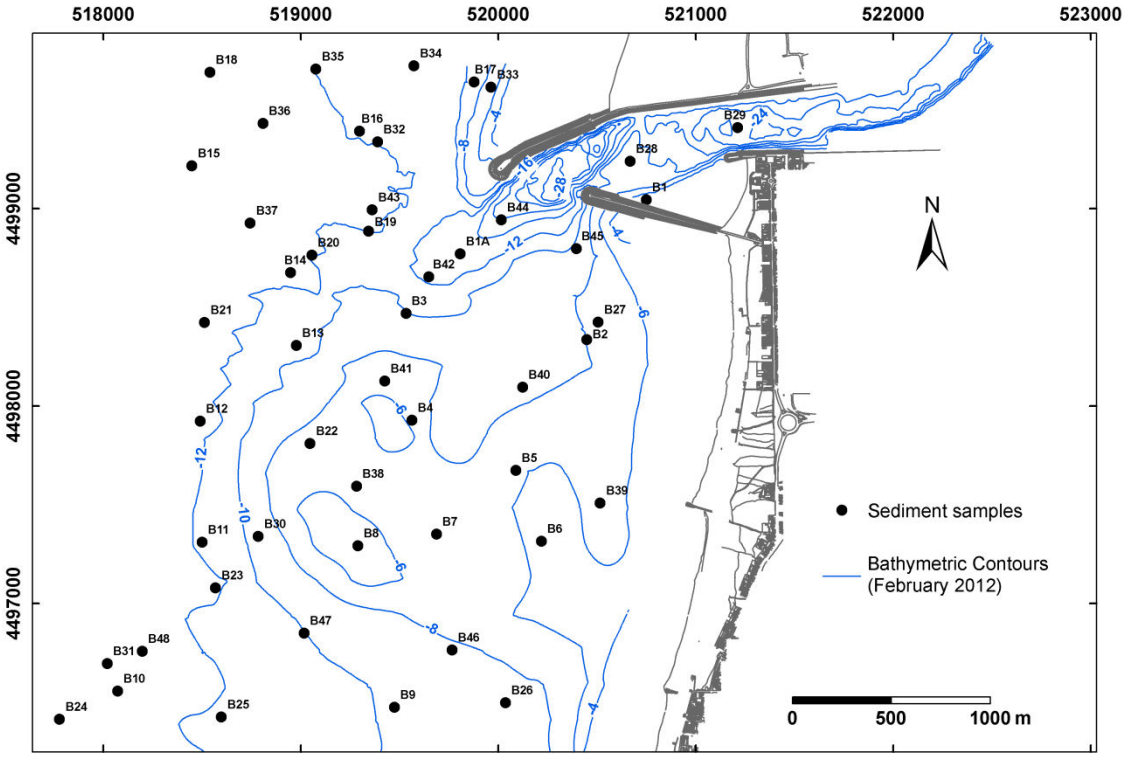

Figure 77. Sediment samples collected for this study in the “Barra de Aveiro” and adjacent near shore shelf on March 22nd 2012 using a “Petit Ponar” grab sampler. Coordinate system in UTM Zone 29N, datum WGS84 and bathymetric contours referred to the Hydrographic Zero datum (ZH).

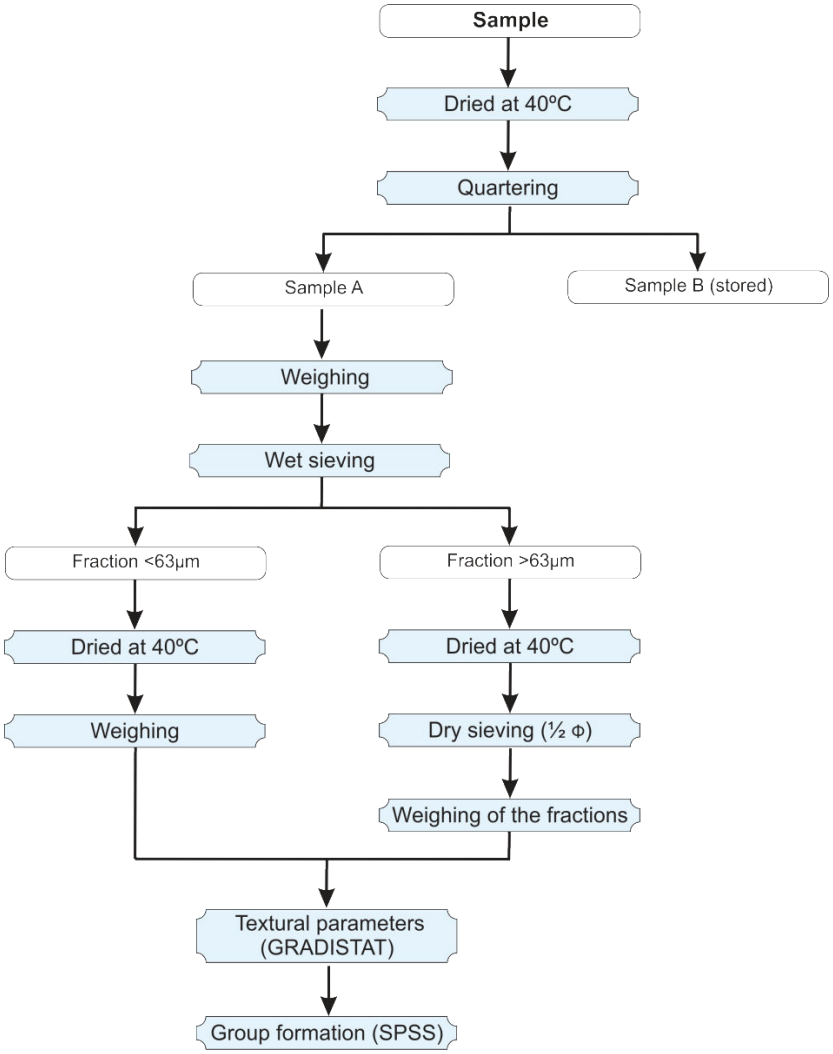

Figure 78. Workflow for grain size sediment analysis used in the work. The light blue boxes represent the techniques and methodologies and the rounded boxes represent the products.

(a) **(b)**

Figure 79. Grain size sediment analyses: **(a)** wet sieving through a 63 µm screen; **(b)** ½ phi spaced dry sieving.

The grain size distribution and statistics were calculated using the "GRADISTAT" program (version 8.0), a package for the analysis of unconsolidated sediments that runs within a Microsoft Excel spreadsheet (Blott and Pye, 2001). Using this software, the mean size, mode(s), sorting (standard deviation), skewness, and kurtosis textural parameters were estimated logarithmically (in phi units) using Folk and Ward graphical methods (Folk and Ward, 1957). The median grain size also known as D_{50} was also estimated using the same software (Blott and Pye, 2001; for more detailed information about the the grain size analysis please refer to section III.3). The mean size, sorting, skewness, and kurtosis textural parameters were subjected to a cluster analysis using the software SPSS Statistics (version 20), from IBM, in order to find the correlation between the sedimentary samples. The sedimentary data were then inserted into a georeferenced GIS database (*ArcGIS*).

V.5. Results and discussion

V.5.1. Sediment balance and sandbank evolution

Old bathymetric maps analysis (1936 – 1985)

Eight hydrographic surveys from 1936 to 1985 were compared (Figure 80 and Figure 81) in order to understand the evolution of the inlet area and the adjacent sandbank. In 1936 the inlet area was narrower than nowadays due to an inner sand accumulation close to the north jetty and the inlet navigation channel was about 4 m deep (Figure 80a). At that time, there was no external sandbank, although some bathymetric perturbations were already noticed due to the inlet influence.

The two next hydrographic surveys were acquired during the important engineering works carried out from 1949 to 1958 (Figure 74 and Table 11). In 1950 (Figure 80b) the north jetty was already 200 m longer than in 1936 and the S. Jacinto coastline followed its evolution, advancing about 200 m seawards in the jetty area. The internal sandbank (sand accumulation located south of the north jetty) migrated seawards and the internal navigation channel became deeper close to the central jetty, reaching a depth of 9 m. At this time it is noticed that the isobathymetric lines moved seawards in front of the inlet, indicating the sediment accumulation in front of the inlet. In 1954 (Figure 80c) the north jetty was 270 m longer than 4 years before and the south jetty was already 320 m long. The S. Jacinto coastline followed once again the north jetty growth and advanced 260 m seawards. The internal sandbank and the inlet channel were then dredged, leading to a general deepening of the navigation channel. In fact, in 1954 the deeper part of the navigation channel was localized close to the north jetty registering depths of 9 m. The isobathymetric lines moved seawards once again, presenting a "C" shape.

In 1965 (Figure 80d), i.e. 7 years after the terminus of the important works carried out from 1948 to 1958, the south jetty was already with its actual length and the north jetty was 220 m longer than in 1954. At this date a deepening of the navigation channel is noticed and the erosion of an area south of the southern jetty and south directed (probably due to the ebb currents) is observed, making the “C” shaped sand accumulation more evident. This ebb delta was probably originated by the littoral drift sediments coming from the north that were deviated seawards by the north jetty and the ebb currents.

In 1966 (Figure 81a) the ebb delta appears to be cut due probably to dredging operations to deepen the external navigation channel and the sandbank starts its individualization. The navigation channel is now in general deeper, reaching 12 m depth between the central and the north structures. In 1976 (Figure 81b) the ebb delta growths towards the south and the sandbank shows a slight migration seawards. The inlet channel is shallower between the two jetty heads changing from 9 m to 6 m deep. The deepest areas of the navigation channel are located between the central and the north structures and north of the south jetty, both areas at 12 m of depth. In 1978 (Figure 81c) the ebb delta is still migrating offshore and the sandbank is growing towards the bar. In 1985 (Figure 81d) the north jetty was in the middle of a 500 seaward extension works, and at the survey date, 200 m had already been extended. At that date the deepest part of the channel area was located between the two jetty heads reaching 18 m depth. The area close to the north jetty between this structure and the central dike is then also deep, registering almost 14 m water depth. At that date the bank was well individualized, although its morphology and location was very different from its shape and localization in 2012 (see dashed green area in Figure 81d). In fact, from 1985 to 2012 the sandbank lost its elongated form and migrated southwestwards, probably as a response to the changes in hydrodynamic conditions due mostly to the 500 m north jetty extension (1983-1987) and the maintenance dredging operations.

In summary, the analysis of the old bathymetric maps from the study area between 1936-1985 shows the existence of a ebb delta formed by the sediments coming from north by the littoral drift and allows an assessment of the influence of the engineering works on its formation and evolution. This bar was deflected seawards, forming a “C”-shaped sand accumulation, due probably to (1) the offshore directed construction of the jetties that created a jet stream southwest directed and (2) the ebb currents, approximately perpendicular to the littoral drift, that, according to Castanho et al. (1974), got stronger as a result of the deepening and widening of navigation channel during the works carried out in 1949-1958 that increased the tidal prism in the lagoon and the drag capacity of the ebb currents.

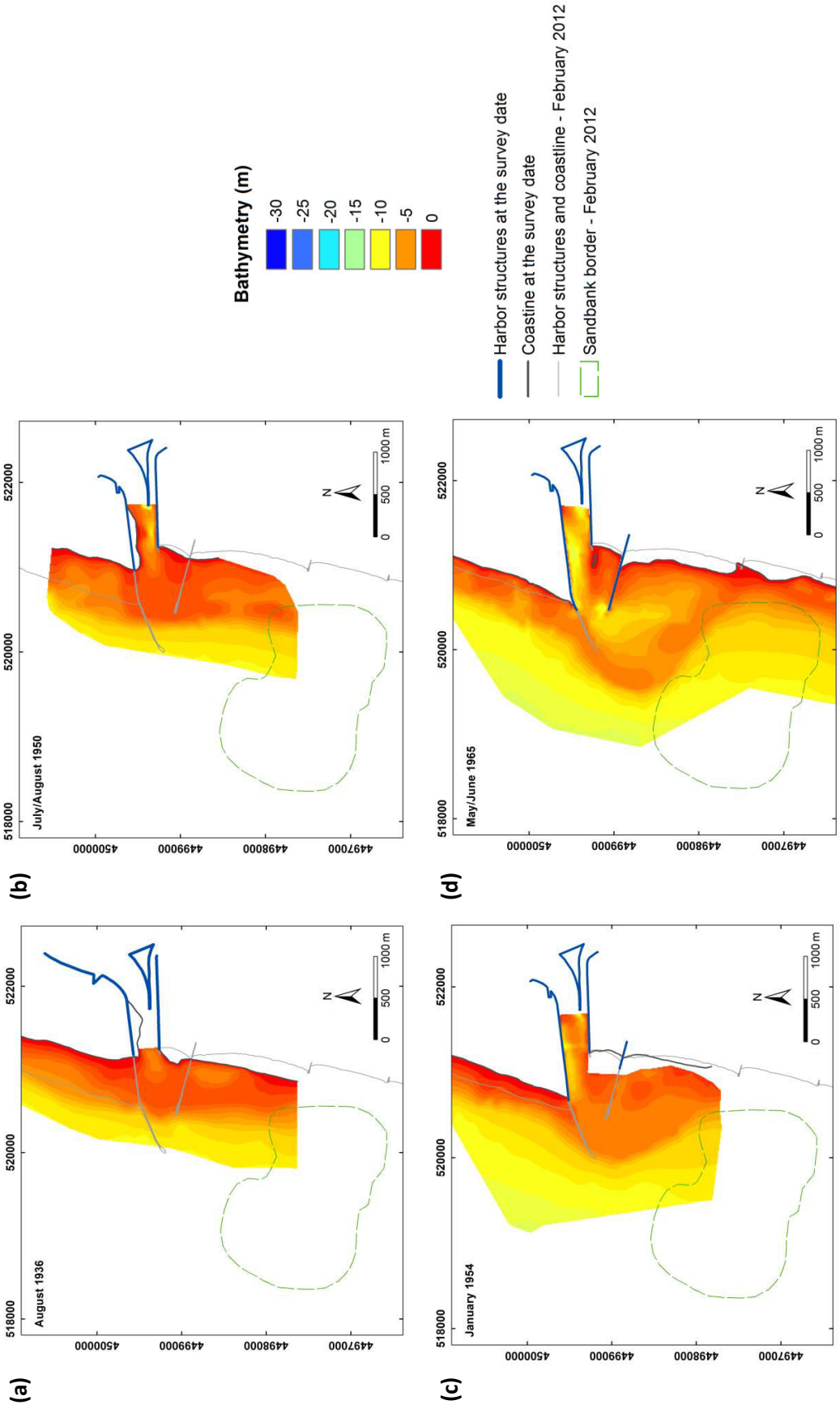

Figure 80. Bathymetry from **(a)** August 1936; **(b)** July/August 1950; **(c)** January 1954; and **(d)** May/June 1965. Coordinate system in UTM Zone 29N, datum WGS84 and bathymetry referred to the Hydrographic Zero datum (ZH).

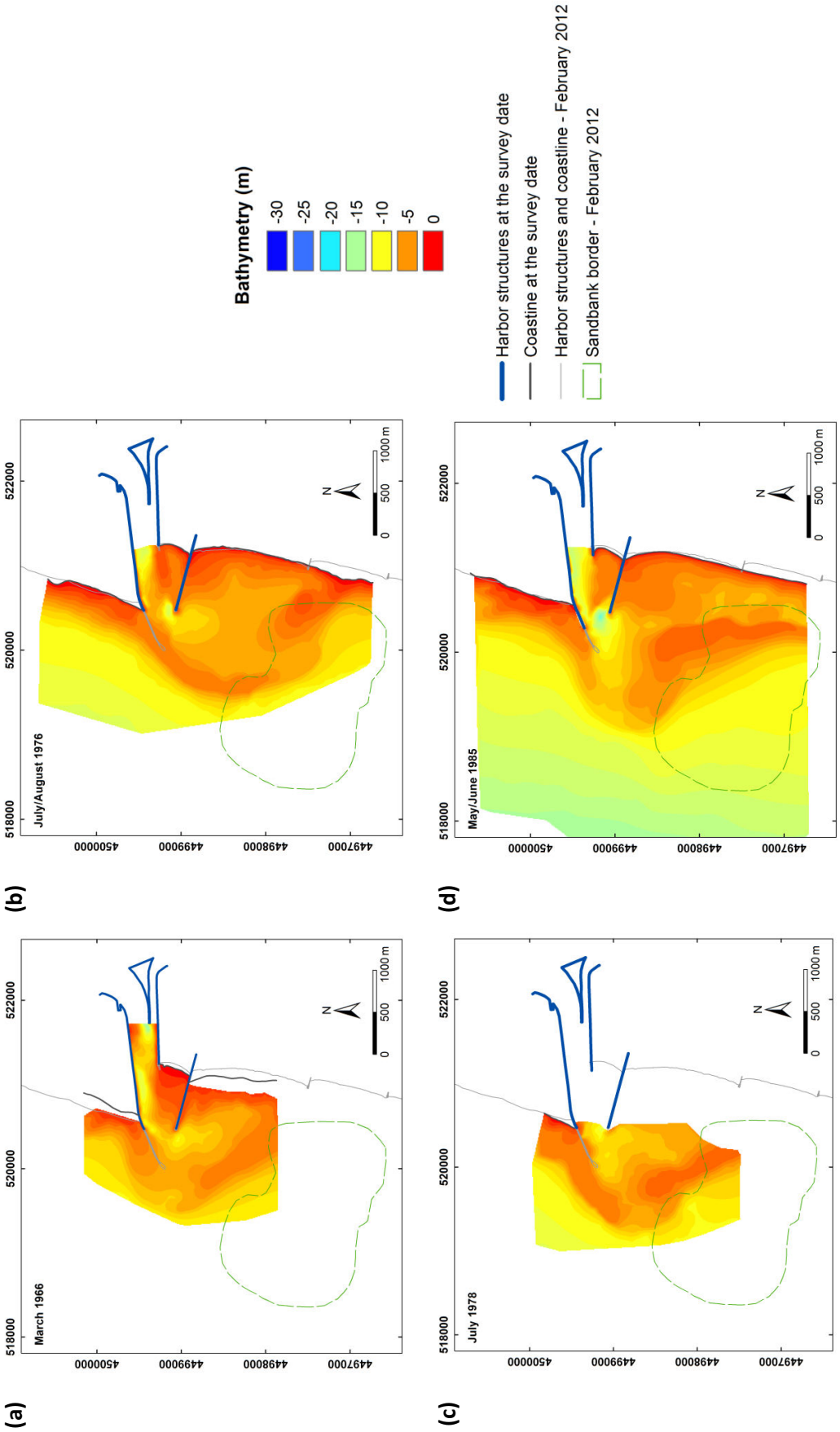

Figure 81. Bathymetry from **(a)** March 1966; **(b)** July/August 1976; **(c)** July 1978; and **(d)** May/June 1985. Coordinate system in UTM Zone 29N, datum WGS84 and bathymetry referred to the Hydrographic Zero datum (ZH).

The formation of the sandbank seems to be related to the remaining south part of the ebb delta that was individualized due to the dredging operations for maintenance of the navigation channel and the strong ebb currents that reduced the sediment accumulation trend in front of the inlet.

Regarding the coastline evolution and from the comparison between the old maps and the present coastline, it is possible to assess that the coast line shows an advance in the north part of the north jetty of about 450 m from 1936 until present, which represents a coastline advance rate of 5.8 m/year. However, it was from 1950 to 1954, during the seaward extension of 690 m of the north jetty (see Figure 73 and Table 9), that the coastline in S. Jacinto had its main advance towards the sea, approximately 300 m, which translates in a mean rate advance per year of 10 m. On the contrary, in the inlet southern beaches the coastline retreated, due to the north jetty ability to retain the sediments from the littoral drift and dredging activities. In the Barra beach the retreat observed from 1936 to 2014 ranged from 150 to 200 m, which represents an annual rate retreat of 1.9 to 2.6 m/year.

Recent bathymetric datasets analysis (2010 – 2013)

The bathymetric datasets used to characterize the more recent evolution of the sandbank and its adjacent area were interpolated with the Natural Neighbors (NaN) method and the obtained bathymetric surfaces are presented in Figure 83 to Figure 87. For each bathymetric surface the sandbank was identified and delimited based on a slope of 0.3º, chosen to be higher than the maximum natural slope in the study area. In order to better characterize the evolution of the study area, the bathymetric surfaces were used to estimate the sediment budget, i.e. the accumulated and eroded sediments, either due to dredging/dumping operations or to natural readjustments of the bottom surface between successive surveys (Figure 88 to Figure 91), which is essential to understand the sandbank morphology evolution through time. In the bathymetric maps (Figure 83 to Figure 87), the location of 3 profiles (A-A’, B-B’, and C-C’), used for comparison and shown in Figure 94, is also displayed.

For the analysis of the bathymetric data, it is important to take in consideration the recent engineering works that took place in the study area, with the purpose of distinguishing and separating the “natural” from the anthropogenic processes. Figure 73 and Table 9 summarize the most important engineering works that took place in the “Barra de Aveiro”, whereas Table 12 and Figure 82 report the most recent dredging operations and respective dredged sand deposits that occurred in this area from 2008 to the end of 2013. According to Table 12 and Figure 82, the dredged sediment from the navigation channel area were either deposited 6 miles offshore or, more recently, close to the beach in the Areas 1 and 2, located respectively between the south jetty and the first groin and between the third and fourth groins.

Table 12. Dredging operations (date, local and volume) and dumping areas. For the location of dredging and dumping areas see Figure 82.

Year	Dredging operations: Month/Time of the year	Dredging operations: Volume (m^3)	Dredging operations: Local	Local of deposit (see Figure 82)
Specific Dredging				
2008	Summer	412 454	North jetty (Area A), main navigation channel, and South Terminal	6 miles offshore
2009	Summer Winter	1 000 000 100 000	Inlet navigation channel (Area B) North jetty emergency dredging (Area C)	Area 1 Area 1
2010	Set. to Nov.	279 000	South jetty (Area D) and 8 more areas inside the lagoon	50 000m^3 in Area 1 229 000 m^3 6 miles offshore
2012	June	169 218	North jetty extension area (Area E)	169 218 m^3 in Area 1
2013	May June July October November	141 123 109 021 1 155 477 97 724 101 573	Inlet navigation channel (Area F)	1 274 135 m^3 in Area 1 330 783 m^3 in Area 2
Maintenance Dredging				
2003 to 2010	- February	-	Several maintenance dredging operations in Area G	-
2010 to 2011	February September	-	Several maintenance dredging operations in Area D	-

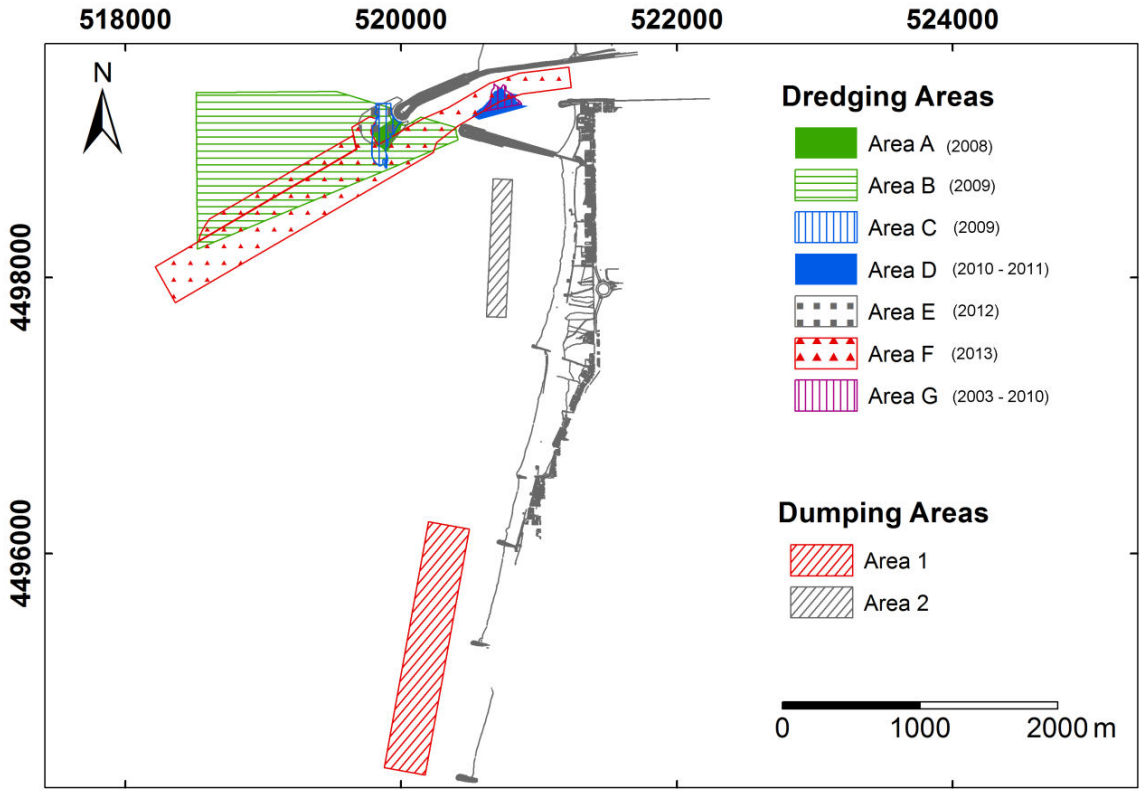

Figure 82. Dredging and sediment dumping areas indicated in Table 12. Coordinate system in UTM Zone 29N, datum WGS84.

In November 2010 (Figure 83) the sandbank was composed by two main elevations, one located closer to the shore, with a roughly N-S orientation, and the other located more offshore, oriented WNW-ESE. The most seaward elevation is shallower and presents a minimum depth of approximately 4.2 m (see Table 13). In average, the sandbank was 7.7 m deep with a mean slope of 0.46º, and a maximum slope of 1.54º. The inlet navigation channel has a maximum depth of 28.9 m between the two jetty heads.

In June 2011 (Figure 84) the sandbank morphology was slightly modified with the seaward elevation getting deeper (the minimum depth in the sandbank is now almost 5 m, see Table 13). The landward bank lost almost 90 cm of its maximum height and migrated towards the shore, which is visible in Figure 88 with the sediment accumulation trend in the east part of the bank and the removal tendency in the central. As a result, the distance between the two main elevations increased. A third smaller elevation, located in the northern area of the sandbank, starts to appear, very well marked in Figure 88 and coming from the north of the north jetty (littoral drift). In average, the sandbank was then 8 m deep and presented a mean slope of 0.35 º, with a maximum slope of 1.41º. Therefore, and in general, from November 2010 to June 2011, the sandbank got deeper and with a lower slope, covering a wider area (Figure 88 and Table 13). The inlet navigation channel is now deeper, with a maximum depth value of 29.0 m.

In February 2012 (Figure 85) the northern elevation increases its volume and significance, growing southward and becoming shallower by about 2 m (its shallowest depth changed from 6.7 m in June 2011 to 4.7 m in February 2012). The sediment accumulation in this part of the sandbank is very visible in Figure 89. The eastern elevation still migrates landward and gets shallower, with the shallowest point (4.5 m depth) of the sandbank at that time being located in this elevation. In average, the bank was at that time deeper, with a mean depth of 9.9 m, steeper, with a mean slope of 0.44º and a maximum slope of 1.8º, and covered a greater area than in June 2011 (Table 13). The inlet navigation channel became deeper between the two jetty heads, with a maximum depth on 29.8 m, although there is a significant accumulation of sediments north and south of the north jetty head (Figure 89).

In November 2012 (Figure 86) the northern elevation is still migrating southward, fact very clearly evident in Figure 90 with an accumulation of sediment indicating this movement to the south. At this time the highest point of this part of the bank is located at a depth of 4.65 m and getting closer to the main elevation located in the southern part of the bank, with a minimum depth of 4.6 m. The eastern elevation seems to continue its migration towards the coast, although this movement is now less significant, and it loses height (its shallowest location is now deeper, at 5.3 m water depth). In average, the sandbank was at that date 8.1 m deep and presented a mean slope of 0.44º, with a maximum slope of 1.91º. In general, from February to November

2012, the sandbank gets shallower, presents the same mean slope, although the maximum slope increased, and covers a larger area (Table 13). The maximum depth of the inlet navigation channel between the two jetty heads is now less deep, with a value of 29.5 m, although the there is a significant removal of sediments around the north jetty head (Figure 89) result of the dredging operation that took place in 2012 (Table 12).

In November 2013 (Figure 87) the sandbank presents a very different morphology, being composed by just one single elevation. The northern elevation, that was progradating southwards, appears to have joined the southern elevation, forming a single and higher structure. This fact is evidenced by the sediment accumulation in the central part of the bank as is show in Figure 91. The eastern part of the bank appears to be spread out, although it was possibly covered/masked by the dredging sediment that was dumped in 2013 very close to this area (see Table 12, Figure 82 and Figure 91). The sandbank now covers a smaller area, although it increased in height, with its mean depth changed to 7.9 m and its highest part located at 3.1 m depth; it is also steeper, with a mean slope of 0.48º and a maximum slope of 2.46º (Table 13). This decrease of the sandbank area is also due to the dredging operations to redefine the navigation channel that took place in 2013 (see Table 12 and Figure 82), which caused the removal of sediments located in the northwestern part of the bank (see Figure 91), leading to the reduction of the sandbank area and volume. Due to these several dredging operations, the navigation channel is now deeper as a whole, changing from a depth that ranged from 9 m to 14 m to depths almost always deeper than 13 m (see longitudinal profiles of the navigation channel from November 2010 to November 2013 in Figure 92). The maximum depth is still located between the two jetties heads and reaches now the maximum value of 30.2 m.

Table 13. Quantitative estimates of the sandbank extent, depth, and slope.

Date	*Perimeter (km)*	*Area (km^2)*	*Minimum depth (m)*	*Mean depth (m)*	*Depth Standard deviation (m)*	*Maximum slope (°)*	*Mean slope (°)*	*Slope Standard deviation (°)*
November 2010	6.2	2.76	4.1	7.6	1.73	1.54	0.46	0.26
June 2011	6.5	2.79	4.9	8.0	1.79	1.41	0.35	0.19
February 2012	7.0	3.04	4.5	9.9	2.00	1.83	0.44	0.23
November 2012	7.7	3.17	4.6	8.1	2.09	1.91	0.44	0.25
November 2013	5.8	2.19	3.1	7.9	2.09	2.46	0.48	0.28

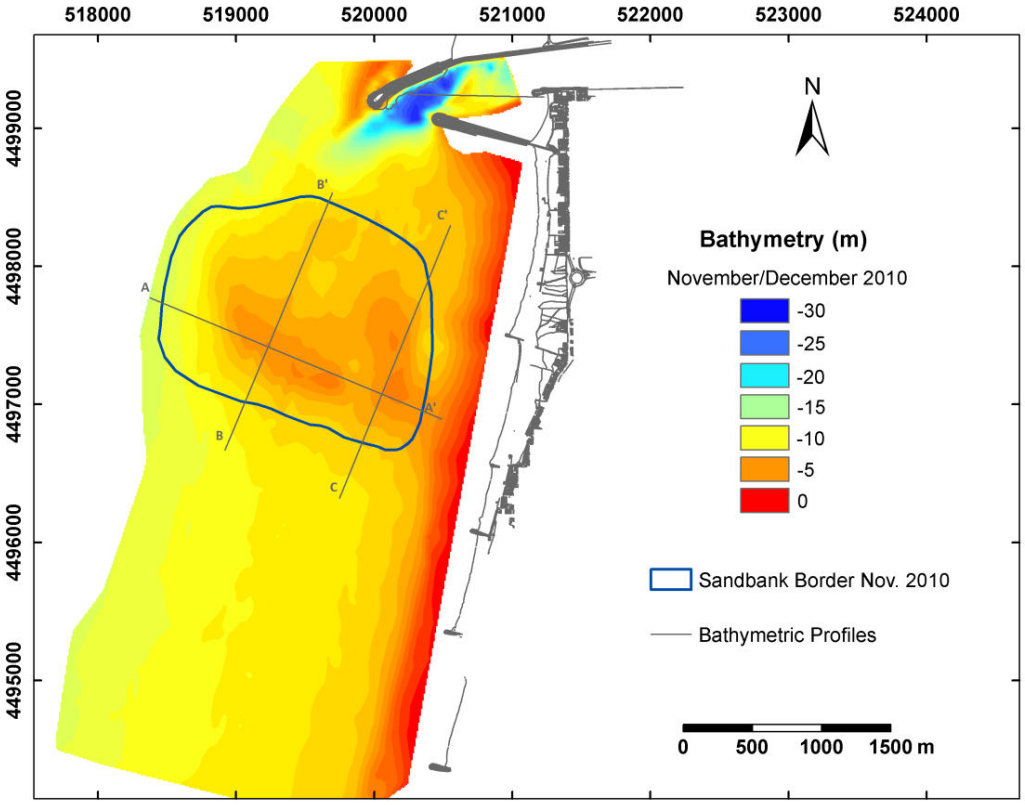

Figure 83. Bathymetry acquired in November 2010 (sandbank and adjacent areas) and in December 2010 (inlet area). Coordinate system in UTM Zone 29N, datum WGS84 and bathymetry referred to the Hydrographic Zero datum (ZH).

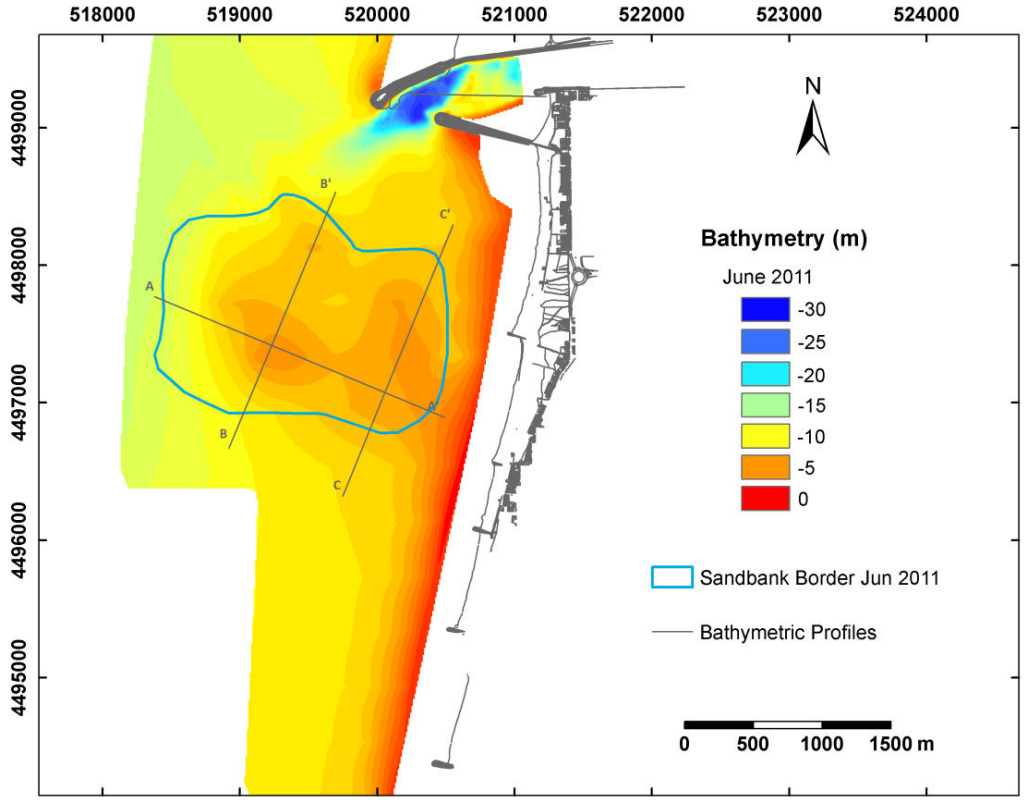

Figure 84. Bathymetry acquired in June 2011 used for this study. Coordinate system in UTM Zone 29N, datum WGS84 and bathymetry referred to the Hydrographic Zero datum (ZH).

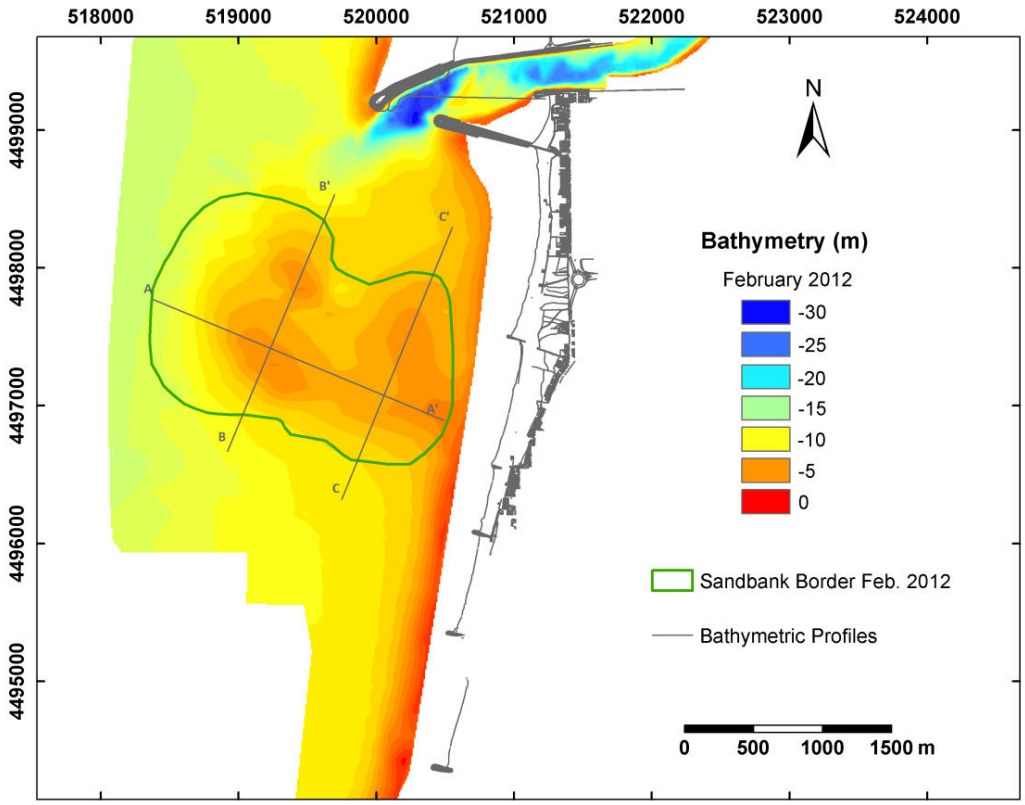

Figure 85. Bathymetry acquired in February 2012 used for this study. Coordinate system in UTM Zone 29N, datum WGS84 and bathymetry referred to the Hydrographic Zero datum (ZH).

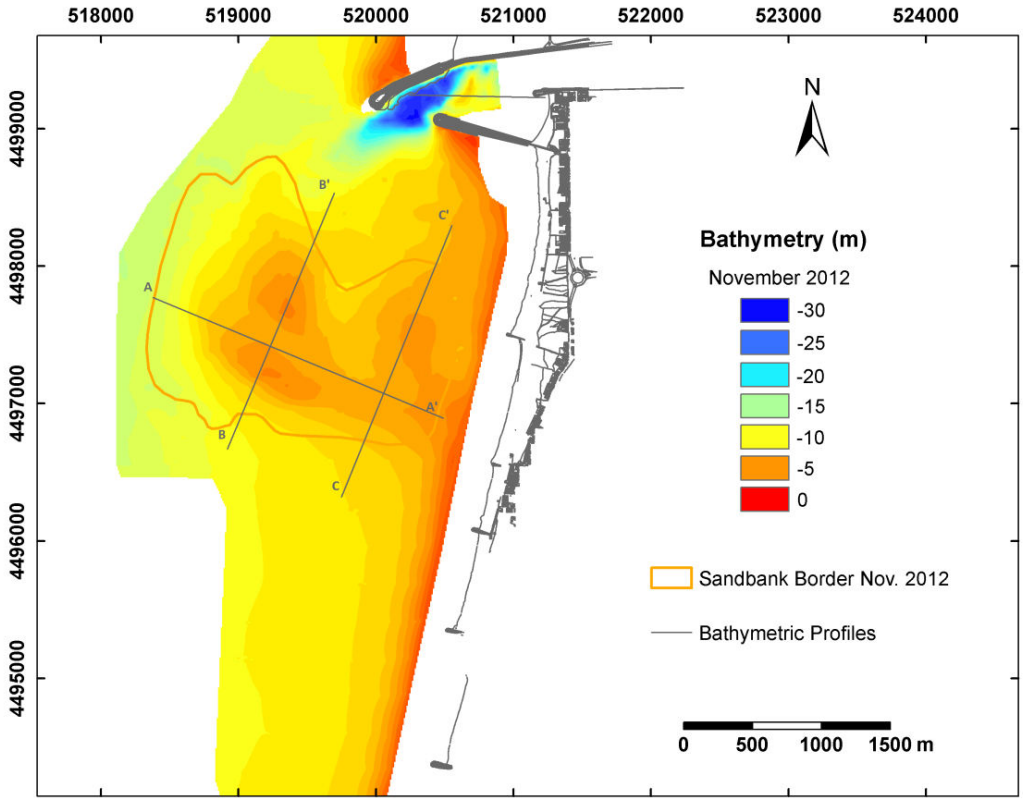

Figure 86. Bathymetry acquired in November 2012used for this study. Coordinate system in UTM Zone 29N, datum WGS84 and bathymetry referred to the Hydrographic Zero datum (ZH).

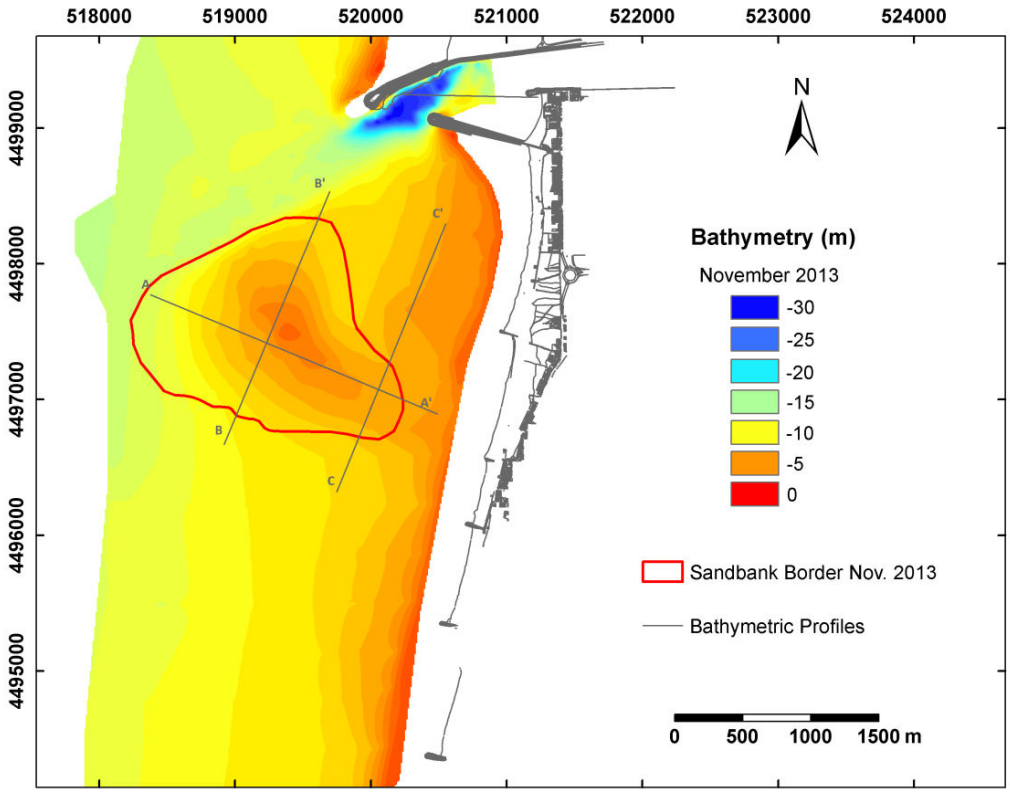

Figure 87. Bathymetric bottom surface acquired in November 2013 and used for this study. Coordinate system in UTM Zone 29N, datum WGS84 and bathymetry referred to the Hydrographic Zero datum (ZH).

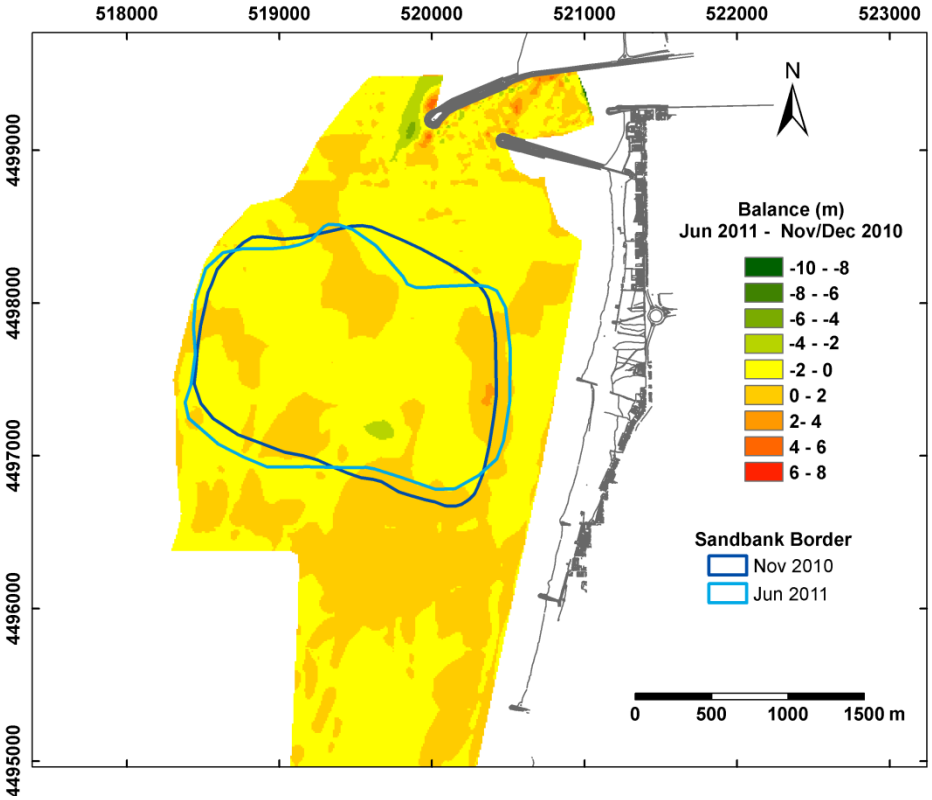

Figure 88. Sedimentary balance (m) occurred from November/December 2010 to June 2011. Positive values refer to sediment accumulation and negative to removal. Coordinate system in UTM Z29N, WGS84.

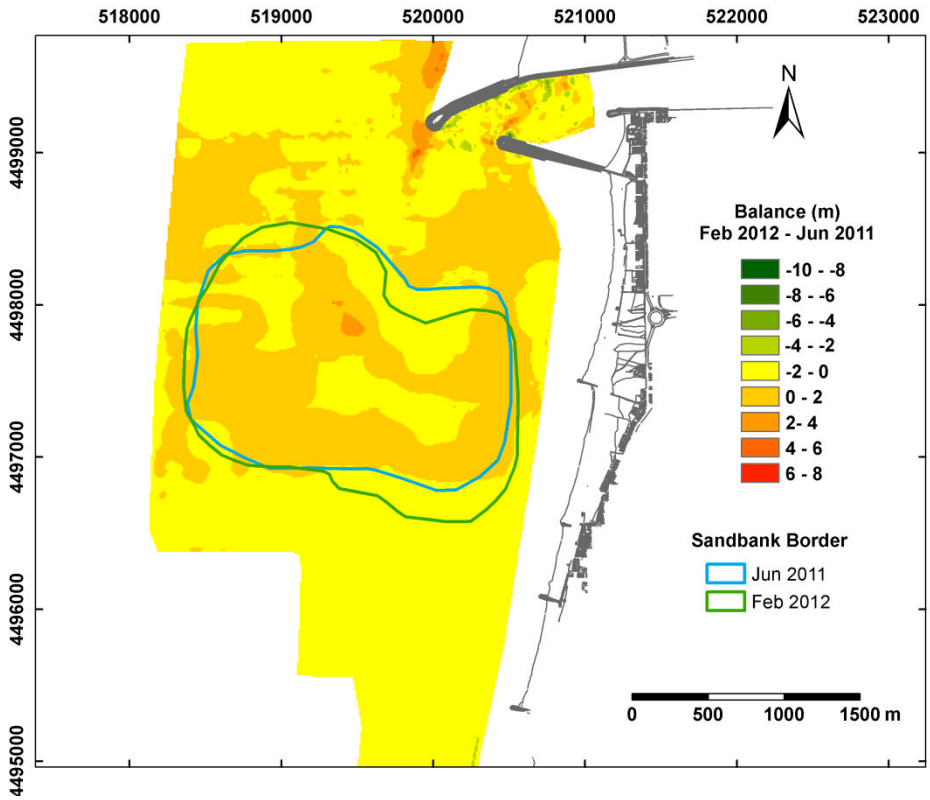

Figure 89. Sedimentary balance (m) occurred from June 2011 to February 2012. Positive values refer to sediment accumulation and negative to removal. Coordinate system in UTM Z29N, WGS84.

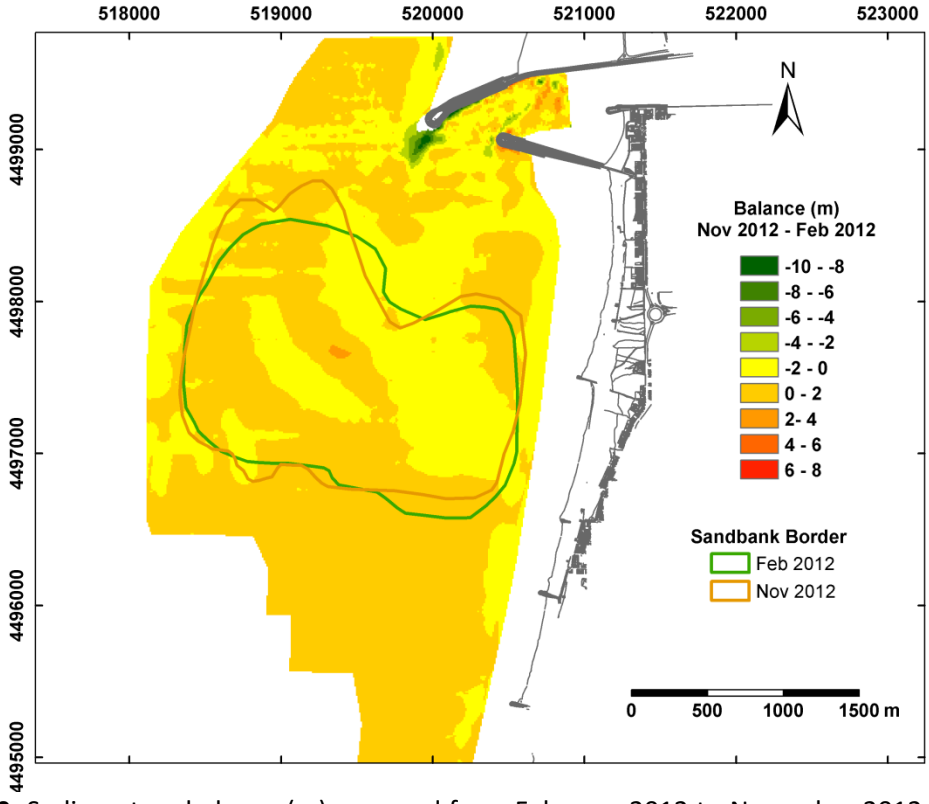

Figure 90. Sedimentary balance (m) occurred from February 2012 to November 2012. Positive values refer to sediment accumulation and negative to removal. Coordinate system in UTM Z29N, WGS84.

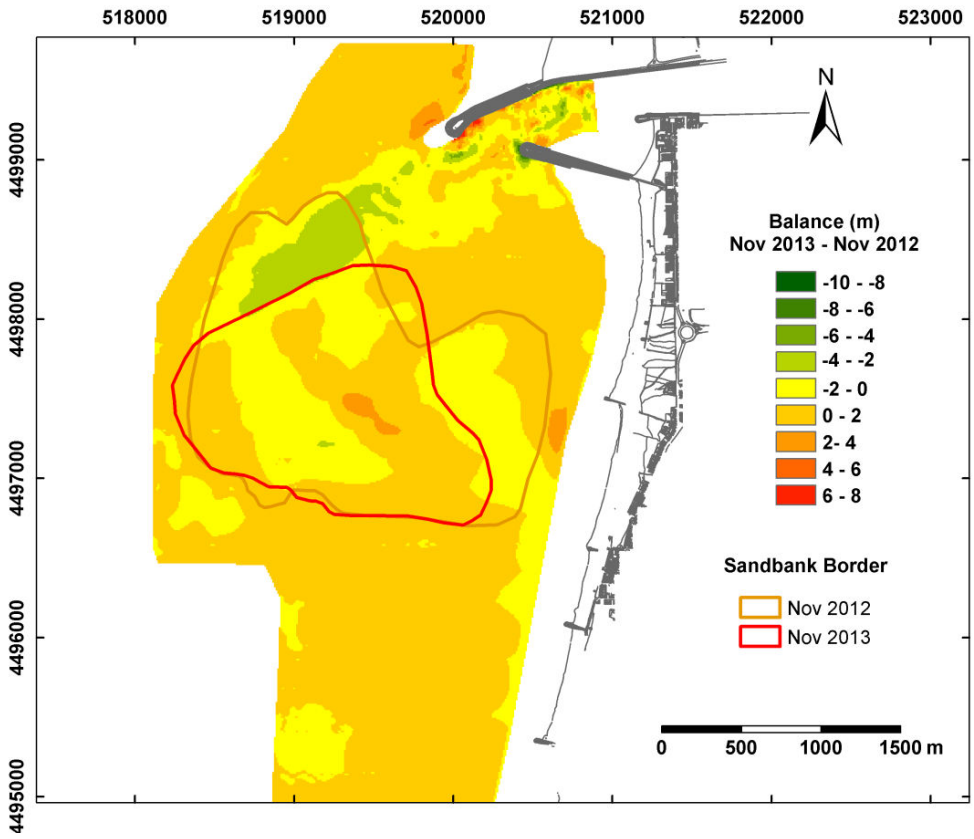

Figure 91. Sedimentary balance (m) occurred from November 2012 to November 2013. Positive values refer to sediment accumulation and negative to removal. Coordinate system in UTM Z29N, WGS84.

Figure 93 shows the sandbank edge evolution through time, delimited by a slope value of 0.3 degrees, higher than the maximum natural slope in the study area. The sandbank area and perimeter increased (24% and 15%, respectively) from November 2010 to November 2012, although from November 2012 to November 2013, a significant reduction in its area and perimeter (24% and 30%, respectively) was observed (see also Table 13). This results in a total reduction of the sandbank area and perimeter of 6% and 21%, respectively, for the 3 years in analysis.

In order to evaluate the migration of the sandbank, the center of mass (centroid) was estimated and is shown in Figure 93. The centroid moved 170 m northwestwards from November 2010 to June 2011, 76 m southwards until February 2012, 76 m northeastwards until November of the same year, and 254 m southwestwards until November 2013.

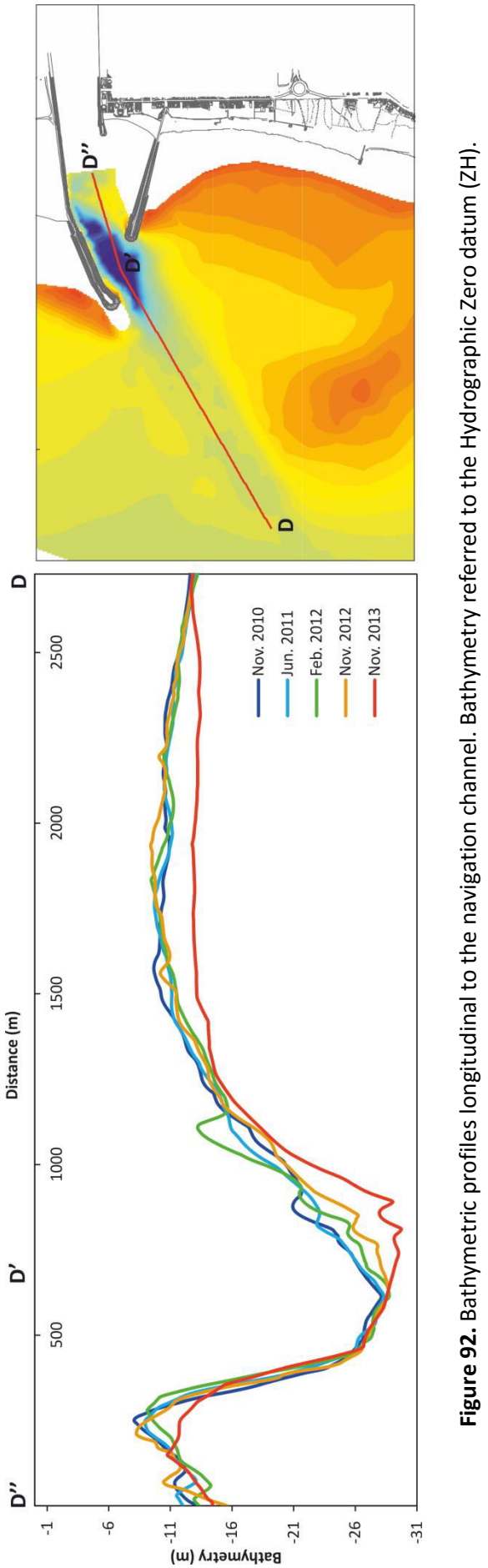

Figure 92. Bathymetric profiles longitudinal to the navigation channel. Bathymetry referred to the Hydrographic Zero datum (ZH).

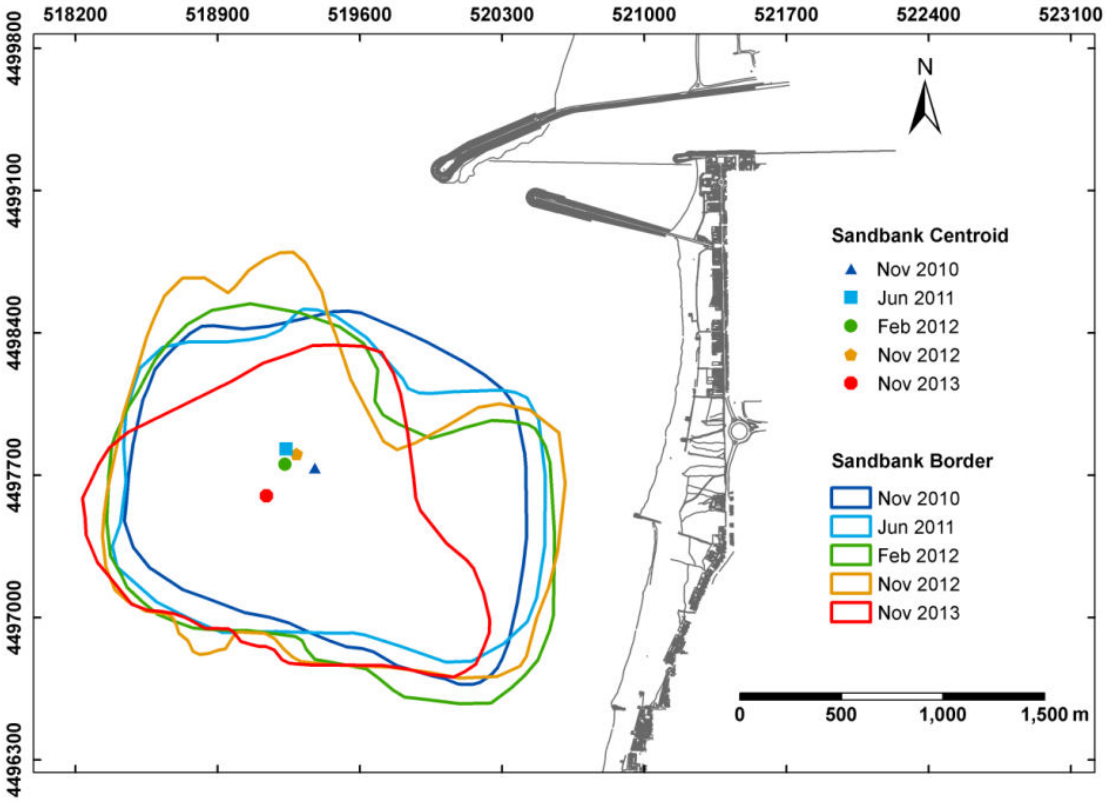

Figure 93. Sandbank edge and mass center evolution through time, between November 2010, June 2011, February 2012, November 2012, and November 2013. Coordinate system in UTM, Zone 29N, datum WGS84.

The center of mass analysis shows two main migration episodes: (1) about 150 m northwestwards from November 2010 to June 2011, associated to the formation of the northern elevation, that caused the movement of the center of mass towards this area; and (2) approximately 220 m southwestwards, from November 2012 to November 2013, probably associated to the southward migration of the northern elevation, but most possibly due to the dredging operations to deepen the navigation channel that took place in 2013, which originated the large reduction of the sandbank area and volume in its northwestern part, very well seen in the sandbank edge contour evolution from 2012 to 2013 (see the sediment removal in the navigation channel in Figure 91 and the edge evolution in Figure 93). The resultant migration of the centroid from 2010 to 2013 was approximately 276 m southwestwards.

The analysis of the bathymetric profiles along (Figure 94a) and across (Figure 94b and c) the sandbank (see also from Figure 83 to Figure 87 for the profile location) shows that the northern elevation, absent in November 2010, is already noticed in June 2011 and starts growing and migrating southwards until November 2013 (Figure 94b). The southwest elevation appears to have the same migration trend southwards, although with a less significant displacement and just until November 2012.

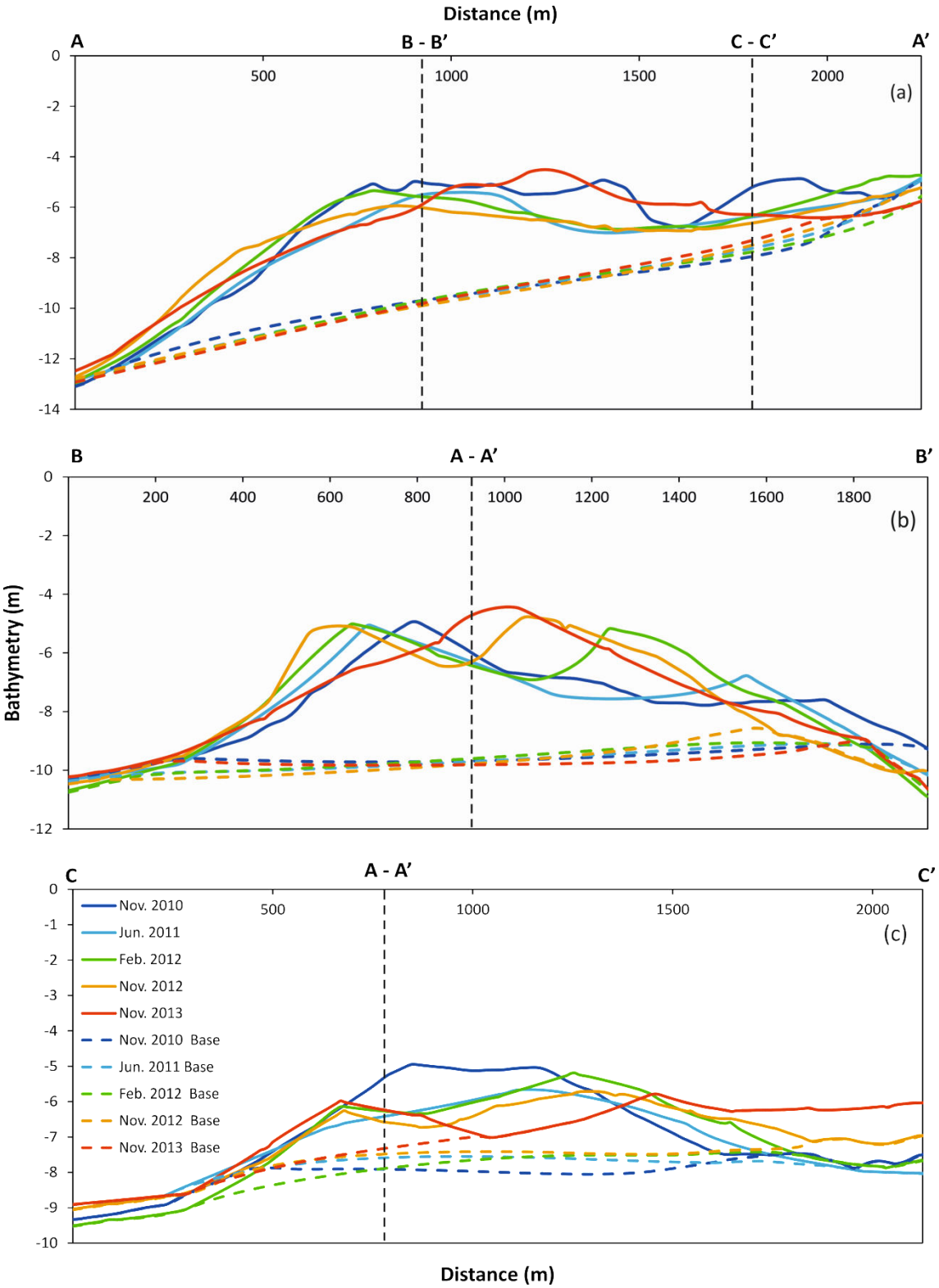

Figure 94. Bathymetric profiles in the sandbank-area. (a) Longitudinal profile along the main sandbank axis (A – A’ in Figure 83 to Figure 87); (b) Transversal profile to the main sandbank axis in the western part of the bank (B – B’ in Figure 83 to Figure 87); (c) Transversal profile to the main sandbank axis in the eastern part of the bank (C – C’ in Figure 83 to Figure 87). Bathymetry referred to the Hydrographic Zero datum (ZH).

In November 2013 the southwest elevation of the bank was either eroded and disseminated or migrated northwards and joined with the sediment coming from the northern elevation. The elevation located closer to the coast (Figure 94a and c) appears to have migrated northeastwards (also noticed in the bathymetric surface analysis) and to have lost its significance and topographic relevance, probably due to the sand deposit from the dredging operations occurred during 2013, which probably masked the importance of this elevation. In fact, from 2010 to 2013 the depth of this elevation decreased approximately 1.5 m, although the area located north showed an increase of almost 2 m of its bathymetric surface (see C' area in Figure 94c).

Additionally, a contour line that connects the higher (and therefore shallower) points of the bank was drawn and the result is presented in Figure 95 (in order to better visualize the morphological evolution, avoiding overlapping lines, just the years that present the most significant changes are shown in the figure). This analysis shows the seawards deflection through time of a ebb delta formed by the sediments coming from north by the littoral drift, forming a "C"-shaped sand accumulation. The more recent bathymetries show a clear interruption of this "C"-shaped sand accumulation in the inlet area and its deflection is seawards but also south directed, which could be the result of several factors: (1) dredging operations to deepen the navigation channel; (2) the southwestwards extension of the north jetty that created a jet stream also southwest directed; and (3) the stronger ebb currents, as a result of the deepening and widening of the navigation channel.

Another important information that may be derived from Figure 95 is the area where the sandbank crest connects with the shore south of the inlet. This location indicates the area where the littoral drift is restored and delimitates the influence of the inlet in the littoral drift. From this analysis (Figure 95) it is visible that the area where the littoral drift is restored is moving south through time. If in 1954 the inlet influence was mostly restricted to the inlet area, in 1966 its influence almost reached the first groin area (1200 m south of the south jetty head), and in 2013 the jetties influence achieved the second groin (2300 m south of the south jetty head).

As already mentioned above, the sandbank volume estimation for each bathymetric dataset was performed based on the difference between the bathymetric surface obtained using all the bathymetric data points (with sandbank) and a theoretical surface estimated based on the data with the exclusion of the points in the bank area (without sandbank; see the estimated surfaces in Figure 94 – dashed lines). According to this estimation (Table 14), the bank reduced its volume from November 2010 to June 2011, increased until November 2012, and decreased again until November 2013, reaching 4.3 million of m^3 of sediment at that date.

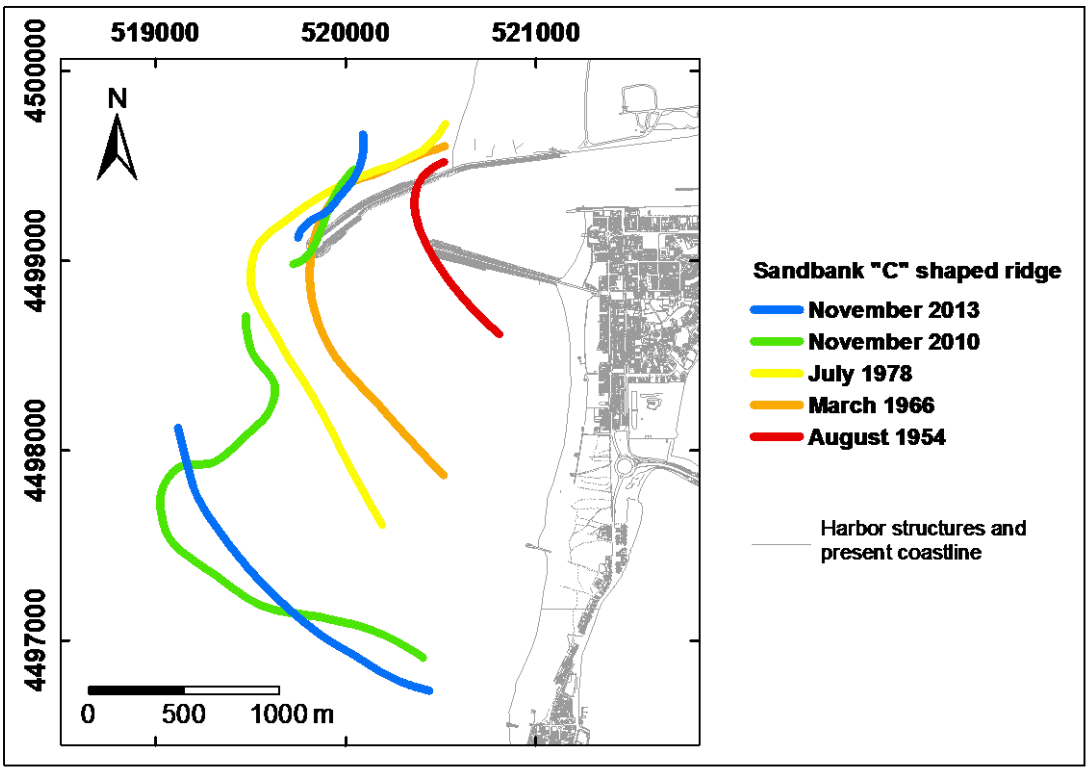

Figure 95. Sandbank “C” shaped crest evolution through time, between August 1954 and November 2013. Coordinate system in UTM, Zone 29N, datum WGS84.

The sedimentary balance was estimated based on 2 different methods: (1) the differences between the calculated sandbank volumes for each bathymetric episode (see Table 14) and (2) the differences between successive bathymetric surfaces in the sandbank area (see Table 15). The results obtained show the same trend and similar values, with the exception of the balance between June 2011 and February 2012, which show a difference of 8% in the sandbank volume.

Table 14. Sandbank volume estimation between November 2010 and November 2013.

	Volume (m^3)	*Area (km^2)*	*Balance (m^3)*
November 2010	4 740 000	2.7	
			-710 000
June 2011	4 030 000	2.8	
			+790 000
February 2012	4 820 000	3.0	
			+200 000
November 2012	5 020 000	3.1	
			-700 000
November 2013	4 320 000	2.2	

Table 15. Volumes of sediment accumulation and removal between successive bathymetric surveys in the sandbank area.

Period in consideration	*Sediment Accumulation (m^3)*	*Sediment Removal (m^3)*	*Balance (m^3)*	*Area (km^2)*	*Height (cm)*
Nov 2010 to June 2011	363 000	-1 051 000	-688 000	3.0	-23
June 2011 to Feb 2012	852 000	-361 000	491 000	3.2	15
Feb 2012 to Nov 2012	722 000	-521 000	201 000	3.4	6
Nov 2012 to Nov 2013	845 000	-1 611 000	-766 000	3.3	-23

In general, from 2010 to 2013, the sandbank is loosing sediment through time, probably by both natural and anthropogenic reasons, as described above: 420 000 m^3 using the method (1) and 660 000 m^3 using the methodology (2). From 2010 to 2013 the sandbank reduced approximately 9% of its initial volume.

V.5.2. Sidescan sonar data

In order to characterize the sedimentary dynamics and the nature of the seabottom of the sandbank, a sidescan survey, complemented with sediment sampling for sonar backscatter calibration was carried out. The sidescan sonar data acquired in the study area allowed the construction of the mosaic shown in Figure 96. This mosaic indicates the existence of three main areas with different average backscatter intensity: Area 1: high backscatter (brownish yellow color); Area 2: intermediate backscatter (brown color); and Area 3: low backscatter (dark brown color). Area 1 occurs mainly in the inlet area (between the two jetties), although it is also observed outside the inlet doing a semi-arc with its convexity directed offshore. Area 2 occurs in limited extents and it is generally associated to bathymetric depression zones; these areas are observed in the northwest and southwest of the semi-arc previously mentioned and in the southwestern part of the mosaic. Area 3 corresponds to the remaining regions of the mosaic, associated probably with finer sediment than the sediment present in areas 1 and 2. The north part of the mosaic (also included in Area 3) presents a very low backscatter and therefore very dark brown colors; which is probably associated to sediment even finer then the sediment that composes the remaining parts of Area 3.

Asymmetrical bedforms were identified in several areas of the mosaic (Figure 97) and give important indications about the predominant bottom currents and may help to constrain the estimates of the flow velocity of the study area. In fact, asymmetrical bedforms are generally produced by currents that are unidirectional or predominant in one direction (for more detailed information on bedforms see section III.2.4), presenting a steep lee side (downstream) and gentle rear side. Moreover, the

shape of the bedform may also give important indication of the flow velocity (see section III.2.4 and Figure 31).

Figure 96. Sidescan sonar mosaic produced for the study area, acquired in a 3 days survey (21 and 22 December 2011 and 13 January 2012). Coordinate system in UTM Zone 29N, datum WGS84. Part of the zoning in the figure is due to ArcGIS display of the mosaic at this scale.

The bedforms were described according to their wavelength and height, estimated using the principles mentioned in section III.2.4, mainly in Figure 29 and Equation (12); their symmetry, which may indicate the direction of the predominant current; and their shape and size, which indicates about the velocity flow of the area.

The sidescan sonar mosaic interpretation and in particular the bedform analysis indicates that between the two jetties the predominant currents are mainly parallel to the navigation channel in the WSW direction (Figure 97). In fact, asymmetrical bedforms with wavelengths that range from 5 to 16 m and heights that varies from 30 to 80 cm were identified. According to these measurements and the classification described in section II.2.4 these bedforms can be classified as megaripples. Note that the smaller bedforms are mainly located close to the edge of the navigation channel indicating weaker velocity flows. The greater megaripples are located closer to the

center of the navigation channel which indicates an increase of the velocity flows (see section III.2.4 where this correlation is explained).

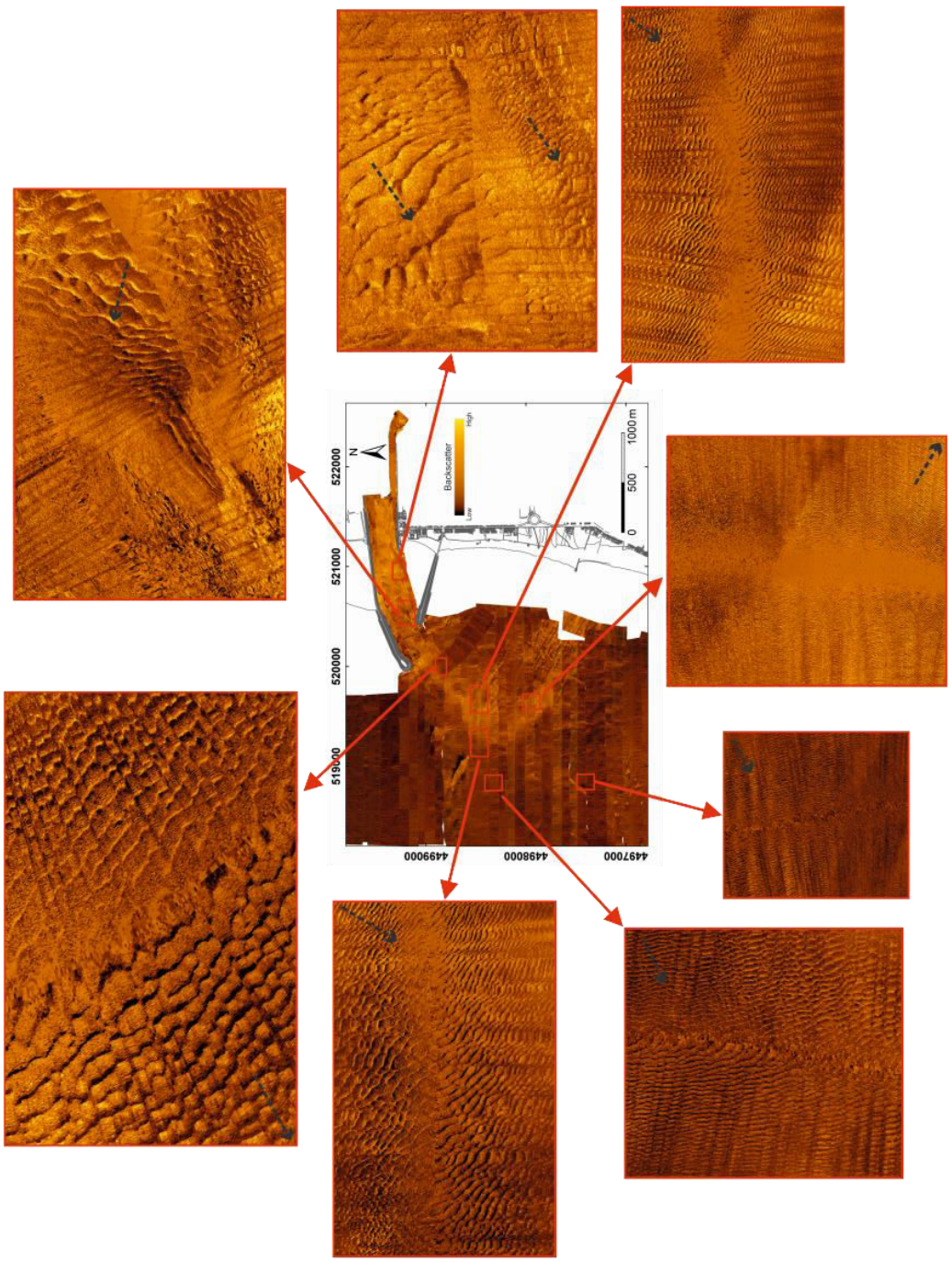

Figure 97. Bottom bedforms and probable predominant current (dashed arrow) identified in the sidescan sonar mosaic of the study area. Coordinate system in UTM Zone 29N, datum WGS84.

The area around the south jetty shows asymmetrical megaripples indicating a predominant bottom currents WNW directed and with wavelengths that range from 6 to 10 m and heights of ~50 cm. The greater bedforms are located closer to the center of the navigation channel, are very sinuous in shape, and sometimes it is possible to identify the presence of superposed ripples (Figure 97).

Outside the lagoon the megaripples get smaller with the distance from the inlet area ranging from 7 m wavelength and 80 cm high close to the inlet area (outside the jetties) to 1.5 m wavelength and 20 cm high farther from the inlet (Figure 97). This fact may indicate a decrease of the velocity flows with the distance to the inlet. In general the asymmetrical bedforms show predominant bottom currents that appear to be from WSW to SSW, with exception to the southeastern part of the previously mentioned semi-arc that presents megaripples southeast directed.

V.5.3. Grain size parameters characterization

The textural analysis of the sediment samples collected in the study area presents a grain median size (D_{50}) of 1.81 ϕ in average, corresponding to medium sand class, varying from -0.14 ϕ (very coarse sand) to 2.81 ϕ (fine sand; see Table 16). According to D_{50}, most of the samples (≈78%) are included into the fine (≈47%) and medium (≈31%) sand classes (see Table 17).

Table 16. General characterization of the gain size parameters.

	D_{50} (ϕ)	Mean size (ϕ)	Sorting(ϕ)	Skewness	Kurtosis
Average	1.81	1.78	0.62	-0.09	1.22
Minimum	-0.14	-0.16	0.16	-0.51	0.74
Maximum	2.81	2.82	1.68	0.37	2.35
Standard deviation	0.69	0.71	0.19	0.11	0.18

The grain mean size of 1.78 ϕ in average was estimated for the collected sediments samples, corresponding to medium sand class, varying from -0.16 ϕ (very coarse sand) to 2.82 ϕ (fine sand; see Table 16). According to mean size, most of the samples (≈80%) are included into the fine (≈47%) and medium (≈33%) sand classes (see Table 17). The average sorting value is 0.62 ϕ that corresponds to moderately well sorted sediment, varying from very well sorted (0.16 ϕ) to poorly sorted sediment (1.68 ϕ). Most of the samples (≈74%) are moderately well sorted (≈45%) to well sorted (≈29%) sediment. Almost 50% of the samples present a symmetric curve, with a skewness average value of -0.09 (symmetrical), a minimum value of -0.51 (very coarse skewed) and a maximum value of 0.37 (very fine skewed). The average value for the kurtosis is 1.22 (leptokurtic), with more than 59% of the samples (Table 17), showing a

leptokurtic curve. The minimum kurtosis value is 0.74 (platykurtic) and the maximum is 2.35 (very leptokurtic). The mean size is the textural parameter that presents a higher dispersion to the average, with the highest standard deviation (0.71 ϕ), and the skewness is the less dispersive textural parameter, with a standard variation of 0.11 ϕ.

Table 17. Textural parameters frequency and percentage for the sedimentary samples collected on the study area.

Class	Frequency	Percentage (%)
Median size (D_{50})		
Very coarse sand (-1 ϕ – 0 ϕ)	1	2.0
Coarse sand (0 ϕ – 1 ϕ)	10	20.4
Medium sand (1 ϕ – 2 ϕ)	15	30.6
Fine sand (2 ϕ – 3 ϕ)	23	46.9
Mean size		
Very coarse sand	1	2.0
Coarse sand	9	18.4
Medium sand	16	32.7
Fine sand	23	46.9
Sorting		
Very Well Sorted	2	4.1
Well Sorted	14	28.6
Moderately Well Sorted	22	44.9
Moderately Sorted	7	14.3
Poorly Sorted	4	8.2
Skewness		
Very Fine Skewed	1	2.0
Fine Skewed	3	6.1
Symmetrical	24	49.0
Coarse Skewed	16	32.7
Very Coarse Skewed	5	10.2
Kurtosis		
Platykurtic	3	6.1
Mesokurtic	13	26.5
Leptokurtic	29	59.2
Very Leptokurtic	4	8.2

All the study area is covered by sands that range from fine to very coarse sand (see Figure 98 and Figure 99). The coarse and very coarse sand samples were collected mainly in the inlet and in its proximal adjacent area (blue and green dots in Figure 98 and red and green dots in Figure 99). The medium sand samples (yellow dots in Figure 98 and pink dots in Figure 99) were found mainly in the sandbank area and surrounding the inlet area, and the fine sand (orange dots in Figure 98 and violet dots in Figure 99), that represents almost 50% of the sampling, appears to correspond to the near-shore shelf sediment without the inlet influence. These results are in agreement with the work published by Freitas et al. (2005) with the collection and grain size analysis of 19 superficial sediment samples in the bar channel of "Ria de Aveiro" and near-shore shelf. The spatial distribution of sediment by size (D_{50} and mean size) appears to indicate that the coarser sediment is present on the most energetic and hydrodynamic area (inlet area).

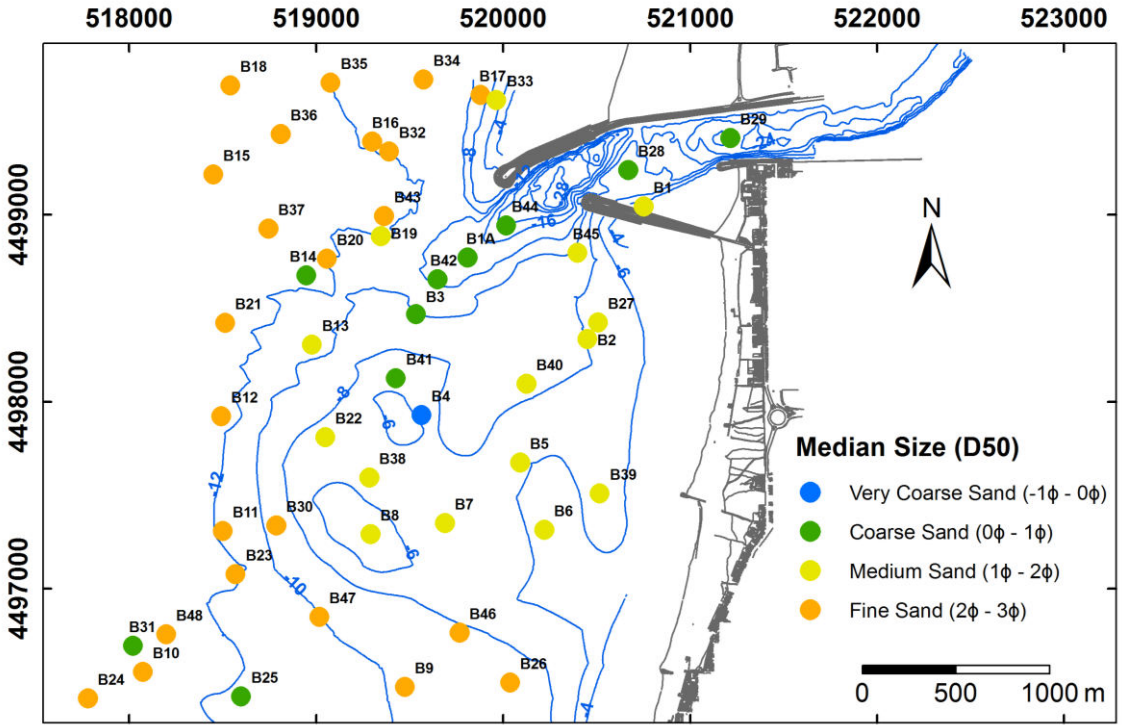

Figure 98. Sediment median size (D_{50}) estimated with the "GRADISTAT" program. The blue lines in the map correspond to the isobathymetric lines from February 2012 (2 m in the open sea and 4 m in the inlet area and inside the lagoon). Coordinate system in UTM Z29N, datum WGS84 and bathymetry referred to ZH.

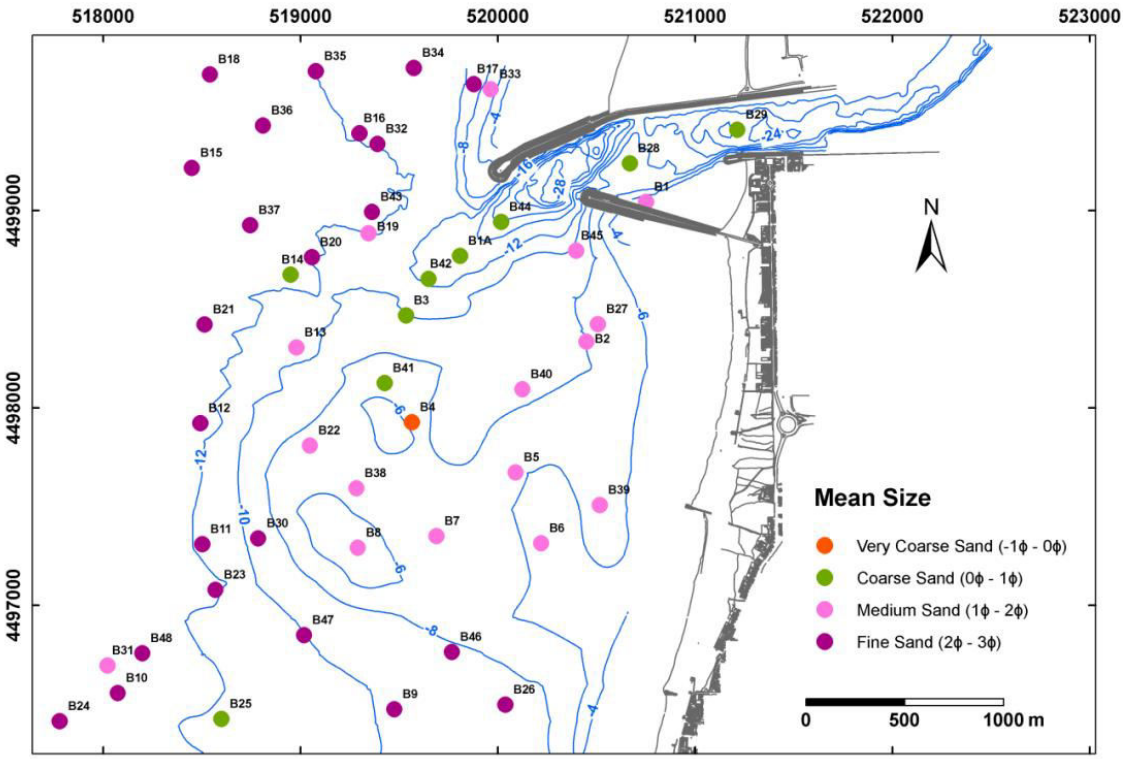

Figure 99. Sediment mean size based on Blott and Pye (2001) classification and estimated with the "GRADISTAT" program. The blue lines in the map correspond to the isobathymetric lines from February 2012 (2 m in the open sea and 4 m in the inlet area and inside the lagoon). Coordinate system in UTM Z29N, datum WGS84 and bathymetry referred to ZH.

The sedimentary samples together with the sidescan sonar data allowed mapping the bottom sediments in the “Barra de Aveiro” and near shore shelf area showed in Figure 100. For that, an interpretation of the sidescan sonar mosaic calibrated with the sedimentary samples was performed, based on the positive correlation between mean backscatter intensity and mean grain size supported by several authors (e.g. Davis et al., 1996; Blondel et al., 1998; Goff et al., 1999; Preston et al., 2004; Collier and Brown, 2005) that have demonstrated the dependence of the acoustic backscatter variations on the sediment grain-size distribution (remind section III.2.4). The 3 different backscatter areas identified in the previous section (V.5.2) were now correlated with the sediment grain-size: Areas 1 and 2 (higher backscatter) correspond to areas with coarse and medium sand samples were collected and Area 3 (low backscatter) exhibits fine sands (Figure 100).

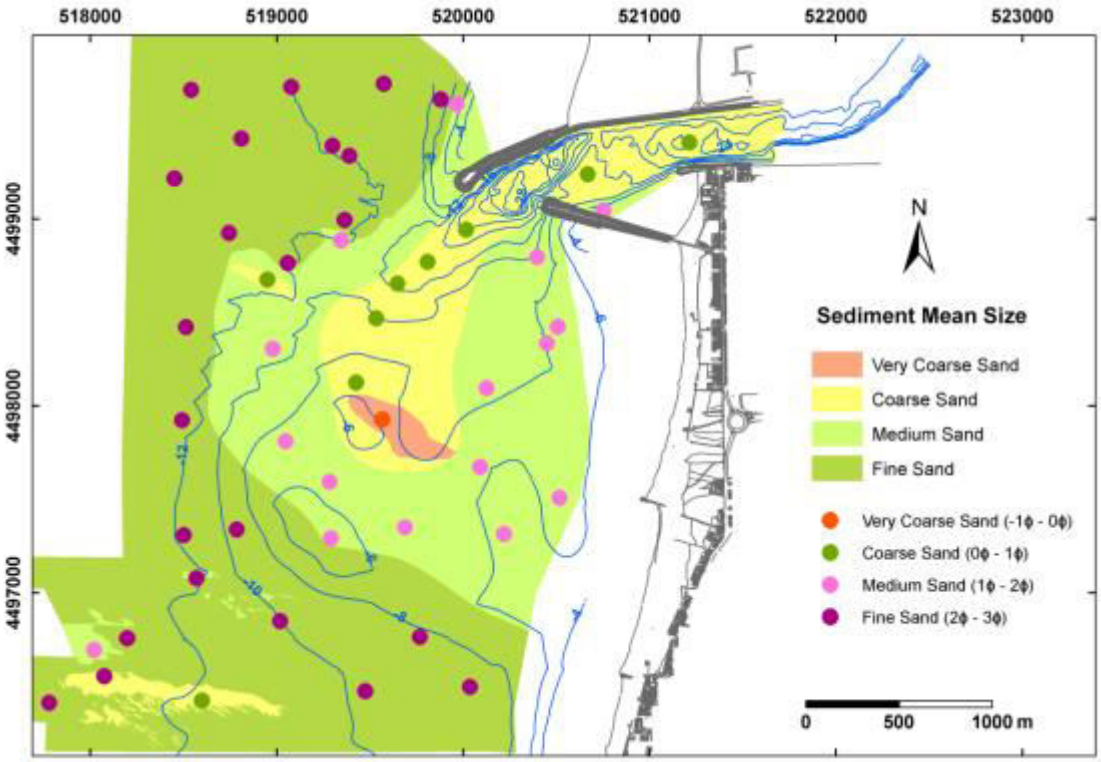

Figure 100. Sediment mean size map produced by integrating the information from the sedimentary samples with the sidescan sonar mosaic. The blue lines in the map correspond to the isobathymetric lines from February 2012 (2 m in the open sea and 4 m in the inlet area and inside the lagoon). Coordinate system in UTM Z29N, datum WGS84 and bathymetry referred to ZH.

The poorly and moderately sorted sediment samples, represented by the pink and purple dots, respectively, in Figure 101, are mainly located in the inlet and in the northeast part of the sandbank. This fact may be due to the high energetic conditions of the area and/or to a mixture of different sediment populations. The central and western part of the sandbank is mainly composed of well sorted and very well sorted

sediment, as shown by the light blue and green dots, respectively, in Figure 101, which may indicate that this area is in hydrodynamic balance. The north and the southeastern part of the study area present in general moderately well sorted sediment (dark blue dots in Figure 101), which represent almost 45% of the sampling.

The variations in both mean grain size and in sorting inside the sandbank area may be related with the different energetic conditions that act in the bank area, which appear to decrease from the inlet area to the south. In fact, from the inlet towards the sandbank, the sediments become finer and well sorted due to the decrease of the energetic conditions.

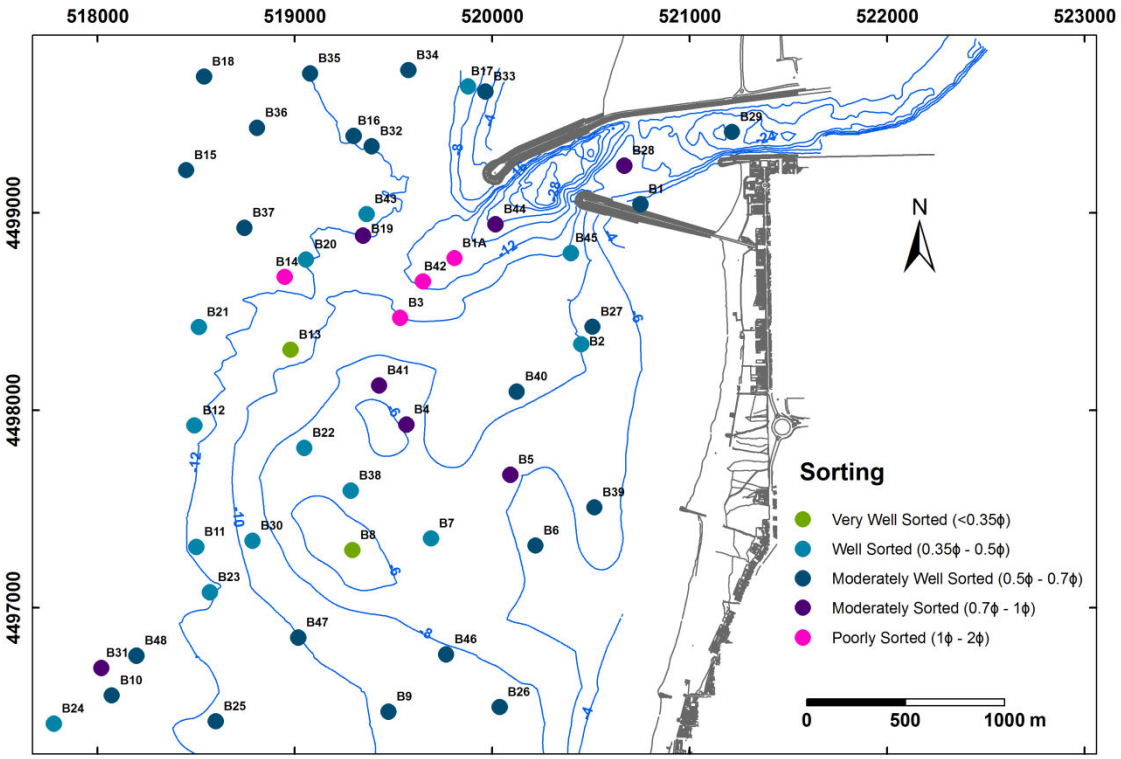

Figure 101. Sorting of the sediment distribution curve based on Folk and Ward (1957) and estimated with the GRADISTAT program. The blue lines in the map correspond to the isobathymetric lines from February 2012 (2 m in the open sea and 4 m in the inlet area and inside the lagoon). Coordinate system in UTM Z29N, datum WGS84 and bathymetry referred to ZH.

Regarding the skewness, almost half of the samples present a symmetrical distribution curve (ligth blue dots in Figure 102), being located predominantly in the sandbank area. Just 8% of the samples present a fine or very fine skewed distribution (dark blue and pink dots, respectively, in Figure 102) and these are located southwest of the sandank. The coarse and very coarse skewed sediments (green and light brown dots, respectively, in Figure 102) are found in the inlet area and out of the mouth, with

the coarse skewed sediment being also located in the surrounded areas of the sandbank. The areas where these sediments are located are probably associated to high and very high energetic conditions that promote the removal of part of the fine fraction and lead to a coarse or very coarse skewed sediment (see section III.3 and Figure 34).

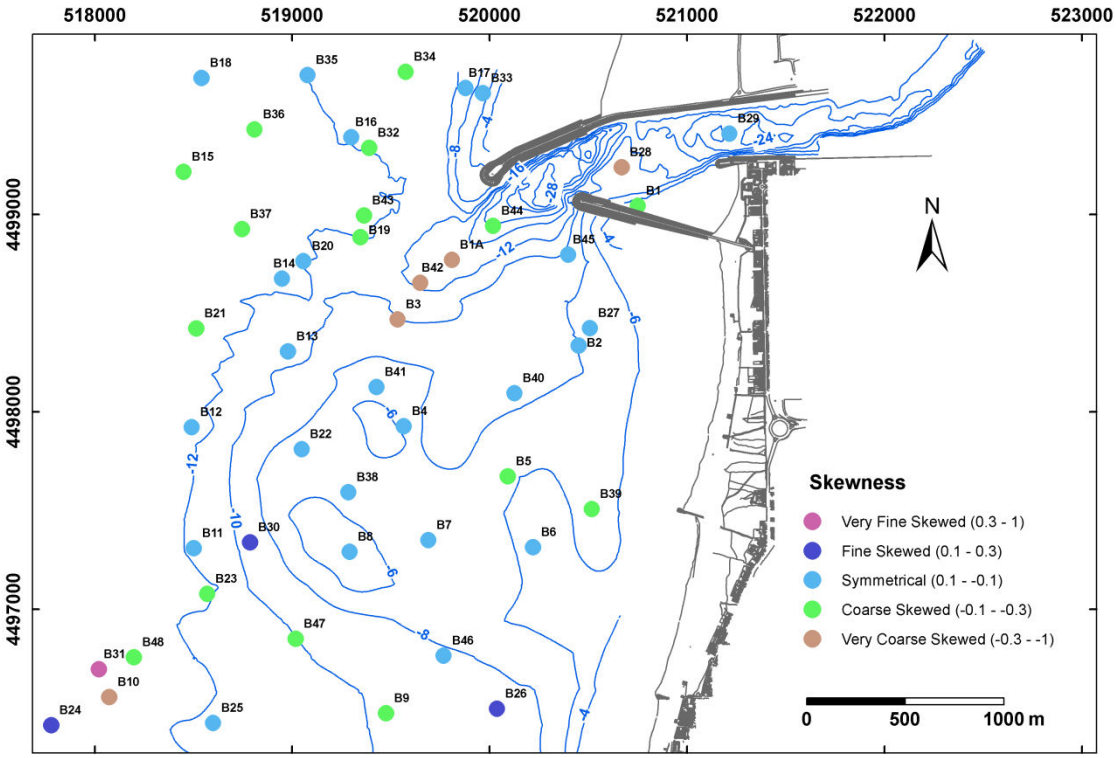

Figure 102. Skewness of the sediment distribution curve based on Folk and Ward (1957) and estimated with the GRADISTAT program. The blue lines in the map correspond to the isobathymetric lines from February 2012 (2 m in the open sea and 4 m in the inlet area and inside the lagoon). Coordinate system in UTM Z29N, datum WGS84 and bathymetry referred to ZH.

Almost 70% of the samples present a leptokurtic or very leptokurtic distribution curve (green and blue dots, respectively, in Figure 103), being located predominantly in the north, south and western parts of the study area, including the northwestern area of the sandbank, and in the lagoon inlet. In the outer part of the inlet and in the shallowest part of the sandbank 3 platykurtic samples were found (light brown dots in Figure 103). The sediments collected in the eastern part of the sandbank present a mesokurtic distribution, as well as to the northwest of the inlet (pink dots in Figure 103).

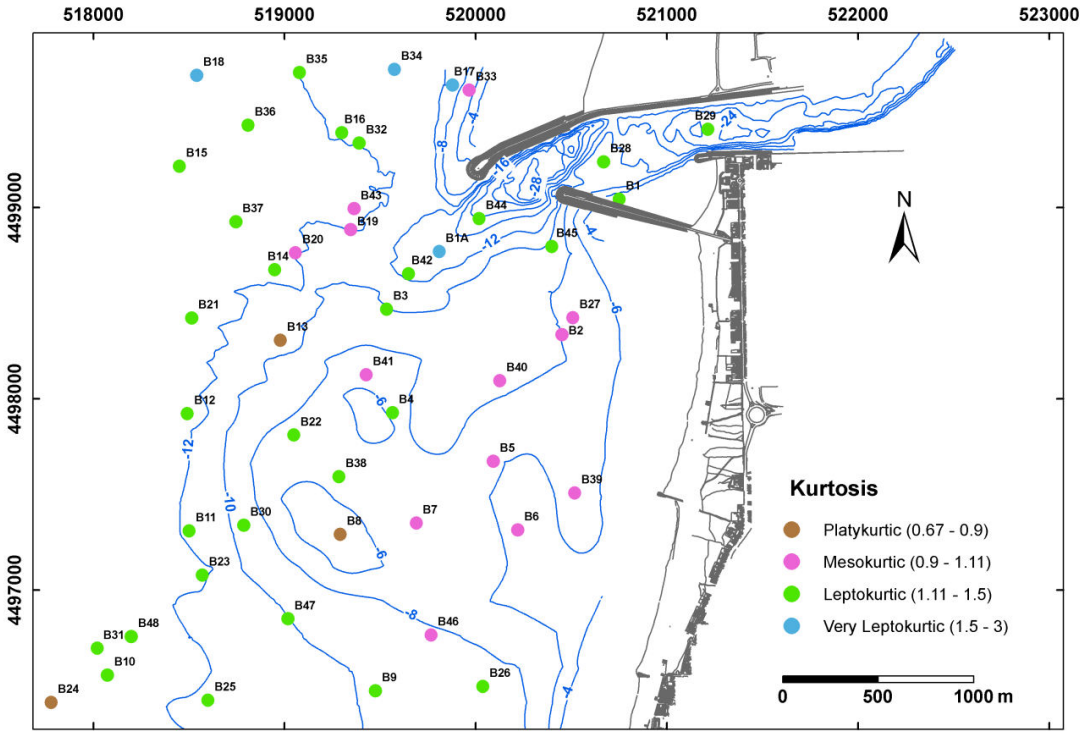

Figure 103. Kurtosis of the sediment distribution curve based on Folk and Ward (1957) and estimated with the GRADISTAT program. The blue lines in the map correspond to the isobathymetric lines from February 2012 (2 m in the open sea and 4 m in the inlet area and inside the lagoon). Coordinate system in UTM Z29N, datum WGS84 and bathymetry referred to ZH.

The four textural parameters mean size, sorting, skeweness, and kurtosis were correlated between each other (see Figure 104), being possible to recognize that the coarser sands are more poorly sorted (Figure 104a) and generally more coarsely skewed (Figure 104b). The better sorted samples are generally symmetric (Figure 104c) and platykurtic (Figure 104d), and the very coarse and coarse skewed are mesokurtic to leptokurtic (Figure 104e).

The analysis of the four textural parameters seems to show the inlet influence area on the sedimentary cover of the near shore shelf, which is evident on the NE/SW axis that connects the inlet and the sandbank.

In order to find the spatial correlation between the sedimentary samples, the four textural parameters were subjected to a cluster analysis using the software SPSS Statistics (version 20), from IBM. The clustering was performed using the mean size, sorting, skewness, and kurtosis as variables, the average linkage method (between groups), and the Euclidean distances. Based on the obtained dendogram and using a cutting distance of 10 (Figure 105), three groups of stations were established: groups 1, 2, and 3. More than 63% of the sedimentary samples belong to the group 1, almost 25% to the group 2, and only 12% are included into group 3. Based on the geographical location of the groups (Figure 106), it appears that group 1 is associated with the

superficial sediments of the inner near-shore shelf and the groups 2 and 3 are related to the lagoon inlet and its adjacent area of influence.

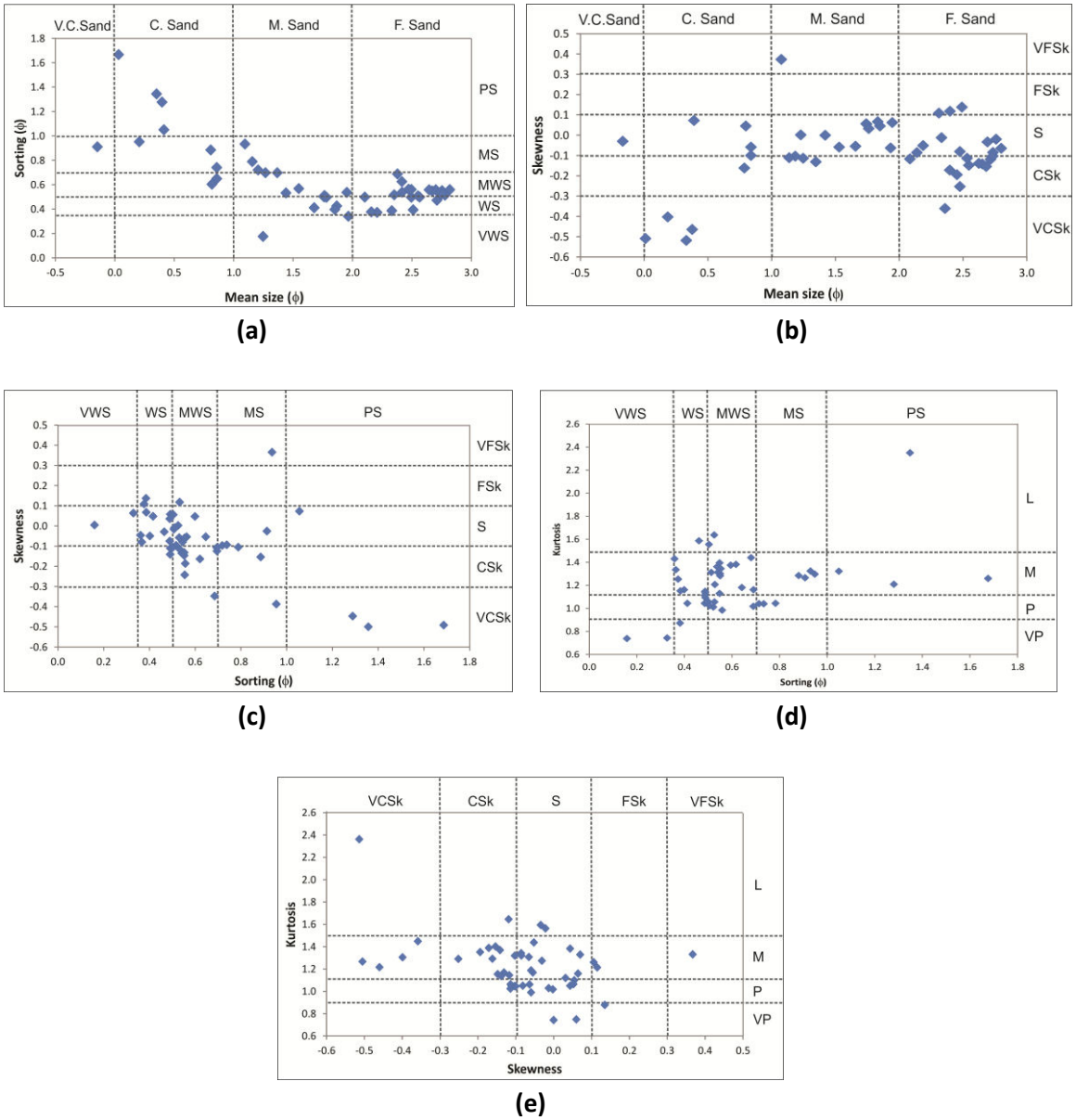

Figure 104. Correlation between the grain size parameters **(a)** mean size vs sorting; **(b)** mean size vs skewness; **(c)** sorting vs skewness; **(d)** sorting vs kurtosis; and **(e)** skweness vs kurtosis. V.C.Sand - Very coarse sand; C. Sand - Coarse sand; M. Sand - Medium sand; F. Sand - Fine sand; VWS - Very Well Sorted; WS - Well Sorted; MWS - Moderately Well Sorted; MS - Moderately Sorted; PS - Poorly Sorted; VFSk - Very Fine Skewed; FSk - Fine Skewed; S – Symmetrical; CSk - Coarse Skewed; VCSk - Very Coarse Skewed; P – Platykurtic; M – Mesokurtic; L – Leptokurtic; VL - Very Leptokurtic.

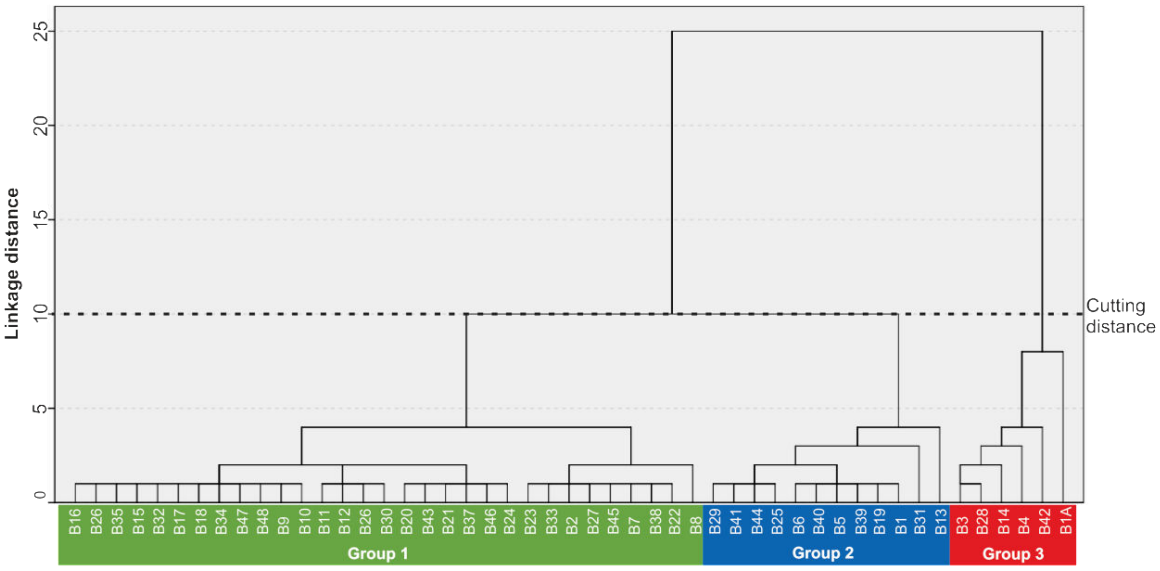

Figure 105. Tree diagram obtained in the cluster analysis using average linkage (between groups) and Euclidean distances. Three main groups may be individualized from the dendogram, with the cut off at 10.

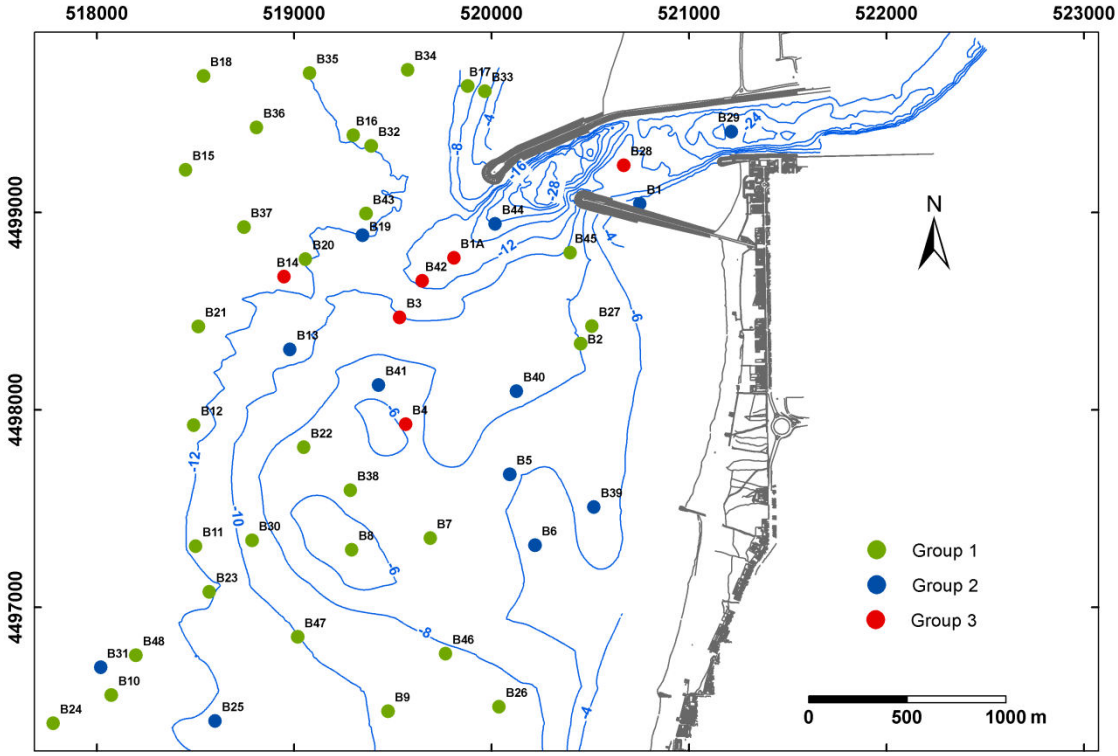

Figure 106. Location of the sediment samples classified as group 1 (green dots), group 2 (blue dots), and group 3 (red dots). The blue lines in the map correspond to the isobathymetric lines from February 2012 (2 m in the open sea and 4 m in the inlet area and inside the lagoon). Coordinate system in UTM Z29N, datum WGS84 and bathymetry referred to ZH.

Group 1 is exclusively composed by fine (more than 74%) and medium sand (almost 26%), with a mean size average of 2.34 ϕ, whereas group 2, with a mean size average of 1.13 ϕ, is mainly composed by medium sand (almost 67%) with approximately 33% of samples classified as coarse sand (see Table 18 and Table 19). Group 3 presents a mean size average of 0.2 ϕ and it is almost exclusively constituted by coarse sand, having only one sample belonging to the very coarse sand class. Group 1 is the one that presents a higher dispersion to the mean size average, with a standard deviation of 0.3 ϕ, whereas group 3 is the less dispersive, with a standard deviation of 0.18 ϕ. The average sorting value is 0.49 ϕ for group 1, 0.66 ϕ for group 2, and 1.2 ϕ for group 3, indicating that the sorting is, in general, getting poorer from group 1 to 3, and consequently from the inlet distal areas to the inlet proximal areas. Group 3 is the group that presents a higher dispersion to the sorting average, with a standard deviation of 0.23 ϕ, whereas group 1 is the less dispersive, with a standard deviation of 0.06 ϕ. Groups 1 and 2 are mainly characterized by symmetrical (about 50%) and coarse skewed (more than 35% for group 1 and more than 40% for group 2) sediment distributions, with skewness average values of -0.06 and 0.04 (symmetrical), respectively. Group 3 is exclusively composed by very coarse skewed (almost 67%) and symmetrical (more than 33%) samples, with an average for skewness of -0.31. Group 3 is the one that presents a higher dispersion to the skewness average, with a standard deviation of 0.22 ϕ, whereas groups 1 and 2 show a smaller standard deviation of 0.09 ϕ. Groups 1 and 3 present a predominance of sediments with a leptokurtic curve (more than 61% and more than 83%, respectively), whereas half of the group 2 presents mesokurtic curves.

Table 18. General characterization of the textural parameters by group.

	Mean size (ϕ)	Sorting(ϕ)	Skewness	Kurtosis
Group 1				
Average	2.34	0.49	-0.06	1.22
Minimum	1.67	0.33	-0.36	0.74
Maximum	2.82	0.68	0.14	1.64
Standard deviation	0.30	0.06	0.09	0.16
Group 2				
Average	1.13	0.66	-0.04	1.10
Minimum	0.80	0.16	-0.16	0.74
Maximum	1.54	0.93	0.37	1.37
Standard deviation	0.21	0.14	0.09	0.14
Group 3				
Average	0.20	1.20	-0.31	1.45
Minimum	-0.16	0.91	-0.51	1.21
Maximum	0.40	1.68	0.07	2.35
Standard deviation	0.18	0.23	0.22	0.30

Table 19. Textural parameters frequency and percentage for the sedimentary samples collected on the study area divided by groups. F represents the frequency and % the percentage.

	Group 1		Group 2		Group 3	
Class	**F**	**%**	**F**	**%**	**F**	**%**
Mean size						
Very coarse sand	0	0	0	0	1	16.7
Coarse sand	0	0	4	33.3	5	83.3
Medium sand	8	25.8	8	66.7	0	0
Fine sand	23	74.2	0	0	0	0
Sorting						
Very Well Sorted	1	3.2	1	8.3	0	0
Well Sorted	14	45.2	0	0	0	0
Moderately Well Sorted	16	51.6	6	50.0	0	0
Moderately Sorted	0	0	5	41.7	2	33.3
Poorly Sorted	0	0	0	0	4	66.7
Skewness						
Very Fine Skewed	0	0.0	1	8.3	0	0
Fine Skewed	3	9.7	0	0	0	0
Symmetrical	16	51.6	6	50.0	2	33.3
Coarse Skewed	11	35.5	5	41.7	0	0
Very Coarse Skewed	1	3.2	0	0.0	4	66.7
Kurtosis						
Platykurtic	2	6.5	1	8.3	0	0
Mesokurtic	7	22.6	6	50.0	0	0
Leptokurtic	19	61.3	5	41.7	5	83.3
Very Leptokurtic	3	9.7	0	0	1	16.7

The four textural parameters were then correlated and plotted by groups (see Figure 107), where it is possible to notice that the mean size is the most important parameter in the groups splitting. The samples belonging to group 3 (red symbols in Figure 107) are coarser, more poorly sorted, and generally more coarsely skewed. Group 1 (green symbols in Figure 107) is characterized by finer sediment, better sorted, and generally symmetric. Group 2 seems to present an intermediate behavior, although the correlation plots and also the cluster analysis show that this group looks closer to group 1. Figure 107c is a good example, showing groups 1 and 2 very well individualized; moreover this plot shows that the sediment frequency curves with the same skewness are generally worse calibrated in group 2 than in group 1.

The cluster analysis of the four textural parameters - mean size, sorting, skewness and kurtosis – allowed the spatial correlation between the sedimentary samples. The results showed that group 1 (finer sediments) is related to the superficial sediments of the inner near-shore shelf and the groups 2 and 3 (coarser sediments) are

related to the lagoon inlet and its adjacent area of influence, giving an indication about the main area of influence of the inlet in the nearshore and in particular in the sandbank.

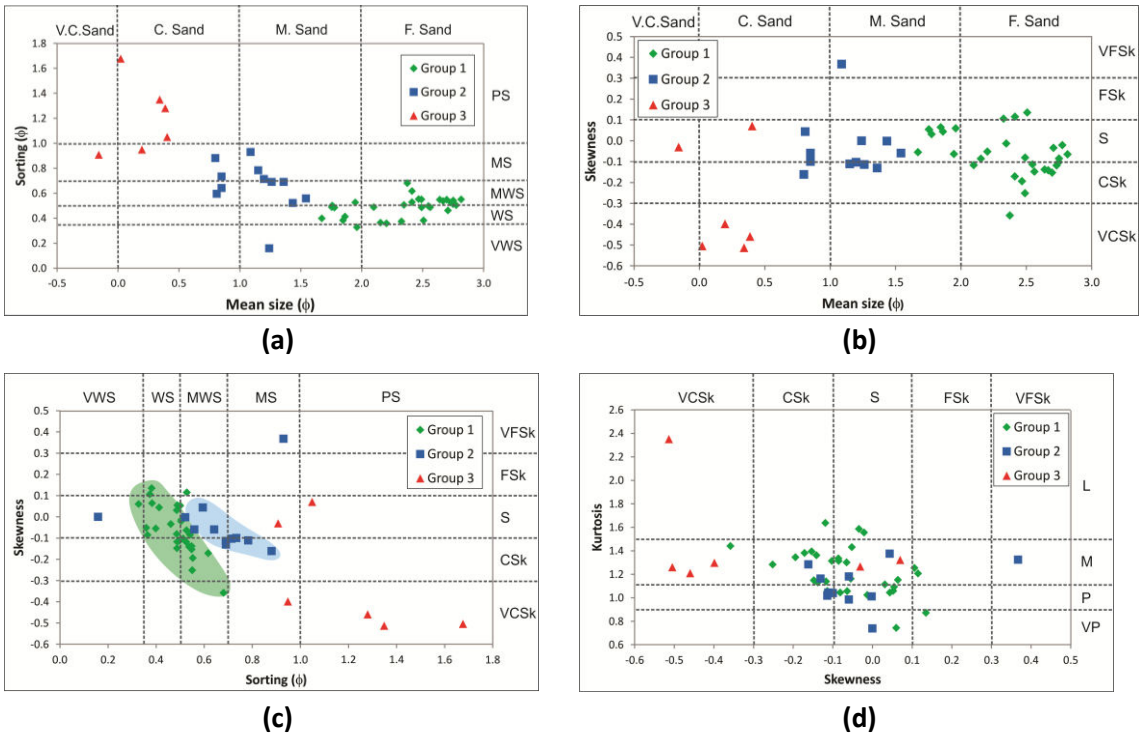

Figure 107. Correlation between the grain size parameters by group **(a)** mean size vs sorting; **(b)** mean size vs skewness; **(c)** sorting vs skewness; **(d)** skweness vs kurtosis. V.C.Sand - Very coarse sand; C. Sand - Coarse sand; M. Sand - Medium sand; F. Sand - Fine sand; VWS - Very Well Sorted; WS - Well Sorted; MWS - Moderately Well Sorted; MS - Moderately Sorted; PS - Poorly Sorted; VFSk - Very Fine Skewed; FSk - Fine Skewed; S – Symmetrical; CSk - Coarse Skewed; VCSk - Very Coarse Skewed; P – Platykurtic; M – Mesokurtic; L – Leptokurtic; VL - Very Leptokurtic.

V.5.4. Population analysis and conceptual model

Sediments that present very asymmetric curves and more than one mode may indicate a mixing of two or more populations or the removal of part of the sediment from a single population (remind section III.3). Figure 108 shows that the samples that present extreme values of skewness and/or more than one mode are mainly located in the inlet area. The distribution curves of all samples were examined (some examples are presented from Figure 109 to Figure 111) and the samples were macroscopically observed (direct observation, naked eye, to identify the presence of bioclasts and terrigenous, including micaceous minerals) with the purpose of identify the population and the presence of more than one population.

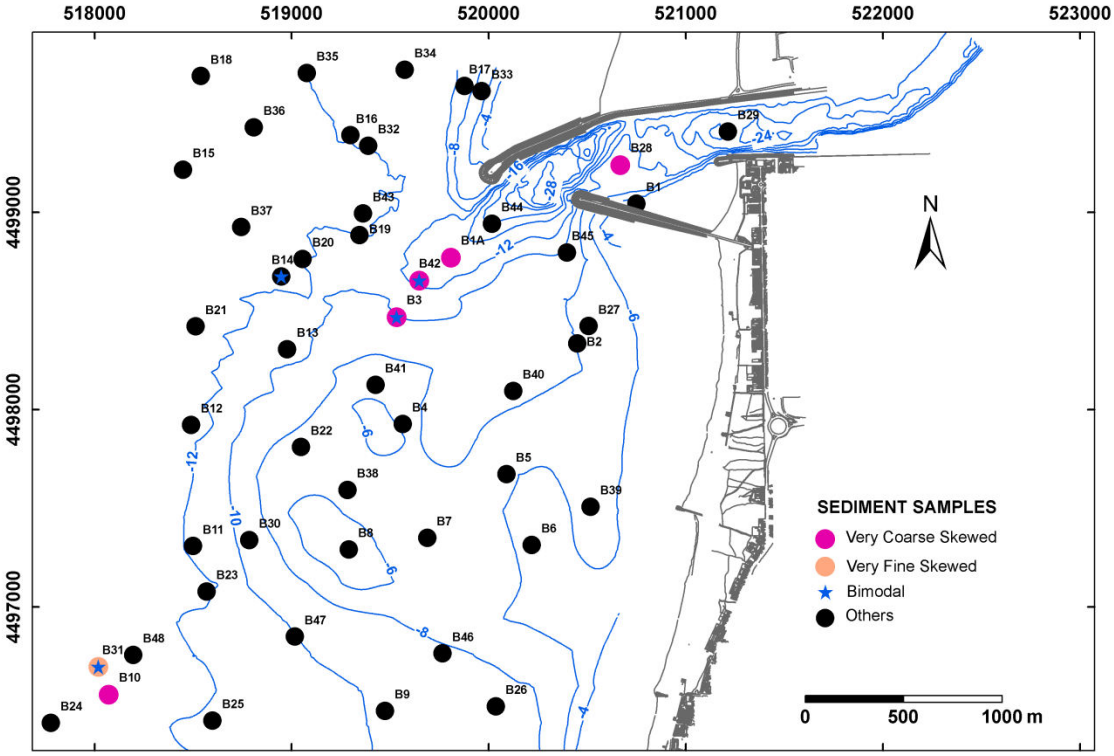

Figure 108. Location of the non-normal values of skewed (very coarse and very fine skewness) and the bimodal (blue star) sediment samples. The blue lines in the map correspond to the isobathymetric lines from February (2 m in the open sea area and by 4 m in the inlet area and inside the lagoon). Coordinate system in UTM Zone 29N, datum WGS84 and bathymetry referred to ZH.

Generally, the sediments collected in the study area are composed of silisticlastic sand with a minor biogenic component, present in part of the samples and essentially expressed on the coarse tails of the distribution curves (see for example Figure 110b). The population analysis led to the definition of five possible terrigenous populations and one biogenic:

- Population A – is the dominant sediment population in most part of the study area and is present in almost all the sediments except in the ones located in the inlet area and the northern and central part of the sandbank. It is a siliciclastic population with a modal value that ranges from 2 to 3 ϕ (see histogram of Figure 109a);

- Population B – very similar to population A, is the dominant population of the sediments located in the central and northeastern part of the sandbank and the southern area of the south jetty. This population is terrigenous and presents a mode that ranges from 1 to 2 ϕ (see histogram of Figure 110a);

- Population C – is the most significant population of the sediment samples collected in the inlet and in its prolongation until the northern part of the sandbank. It is a siliciclastic population that presents a mode that ranges from 0.5 to 1 ϕ (see histogram of a Figure 111);

- Population D – represents a secondary population that appears in several samples, with significance mainly on the samples located in the area dominated by population C. Population D corresponds to a coarse tail in the distribution curve (with a mode generally below to 0.5 ϕ) and presents a terrigenous origin (see histograms of Figure 110b and Figure 111b). Two samples (B5 and B39) located on the area dominated by population B also present this secondary population (see “Population B and D” area in Figure 112);

- Population E – represents another secondary population, also mainly expressed on the coarse tails of the distribution curves (see histograms of Figure 110c, Figure 110b, and Figure 111b), although of biogenic origin and less significant than population D. Population E is more representative in the samples located in the area dominated by population C, although it is also present in other samples, namely the samples dominated by population A;

- Population F – is the dominant population in two samples (see histogram of Figure 109b and c) and the secondary in sample B10. It corresponds to a terrigenous sand with modal values of 0.5 to 1 ϕ. This population does not fit in a possible conceptual model of the recent hydrodynamic conditions, and is probably related to the relic sediments that are present in the inner shelf.

The population analysis allowed mapping the major identified populations (Figure 112), as well as speculating that the siliciclastic component is probably influenced by two main hydrodynamic domains: wave regime which induces the littoral drift and the tidal currents. Based on this, the population A and B are probably originally from the same sediments, from the inner shelf and the littoral drift, although exposed to different energetic conditions, which allowed the slight shift observed on the granulometric curves.

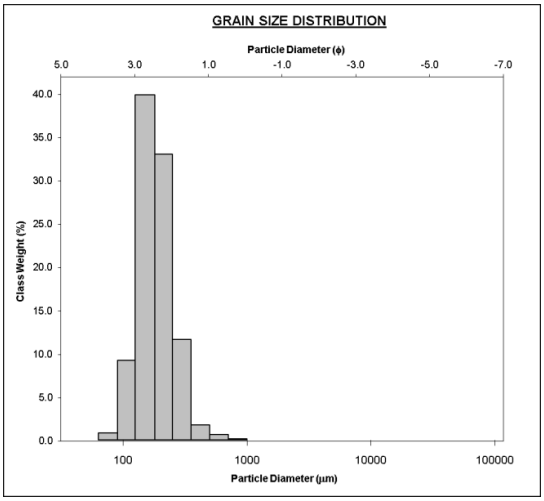

(a)

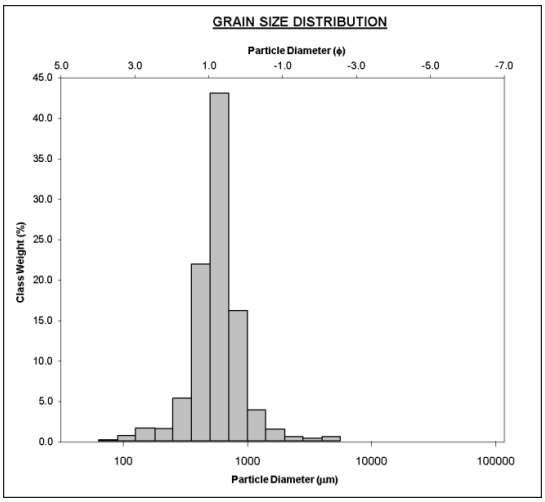

(b)

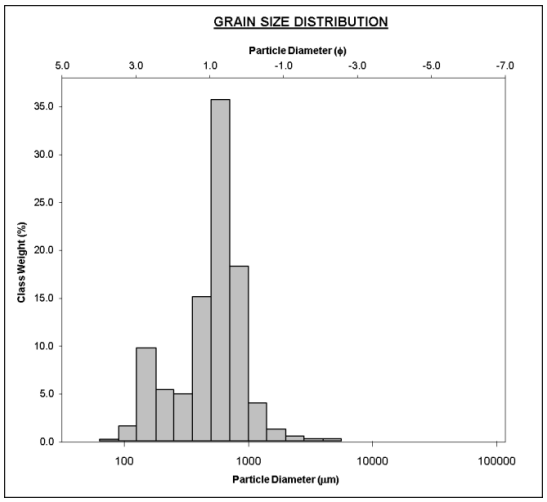

(c)

Figure 109. Granulometric histograms from **(a)** sample B20, showing the population A; **(b)** sample B25 showing the presence of the population F; and **(c)** sample B31, showing the mixture between the populations A and F, with a tail mainly represented by population E.

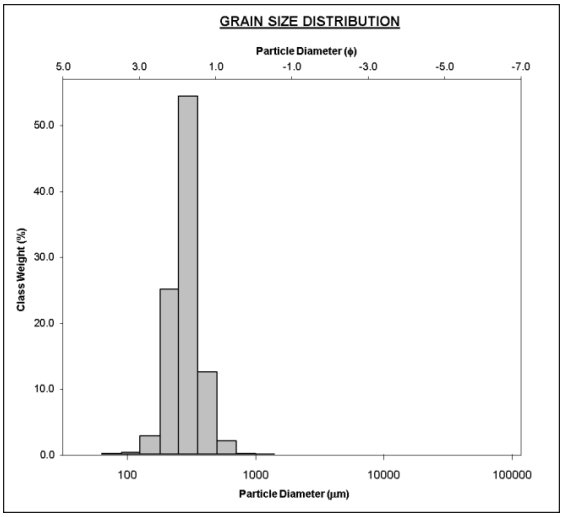

(a)

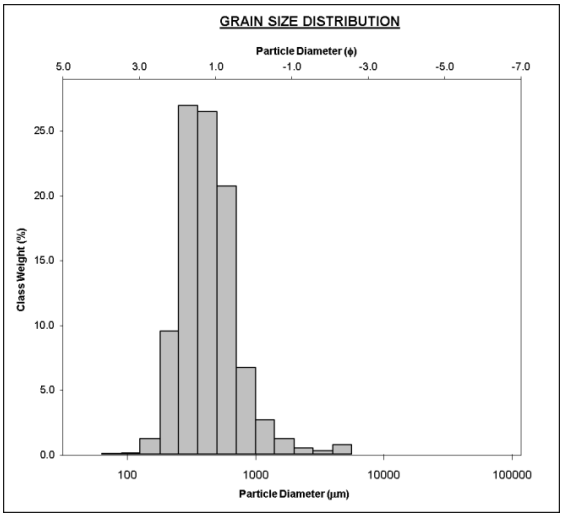

(b)

Figure 110. Granulometric histograms from **(a)** sample B38, showing population B, and **(b)** sample B39, showing the presence of the populations B, D and E.

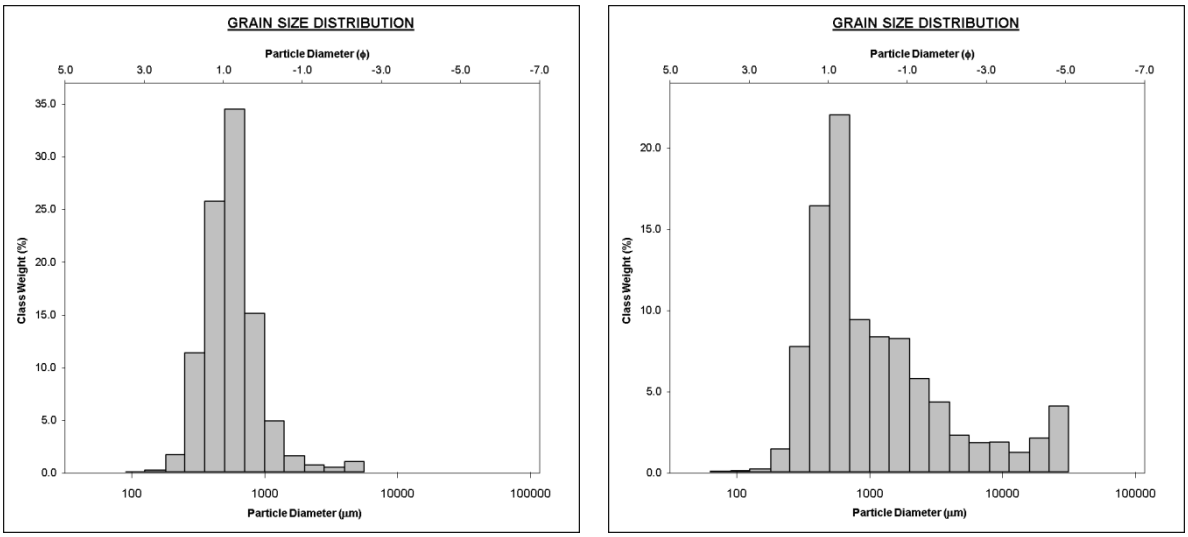

(a) **(b)**

Figure 111. Granulometric histograms from **(a)** sample B29, showing populations C and E, and **(b)** sample B42, showing the presence of the populations C, D and E.

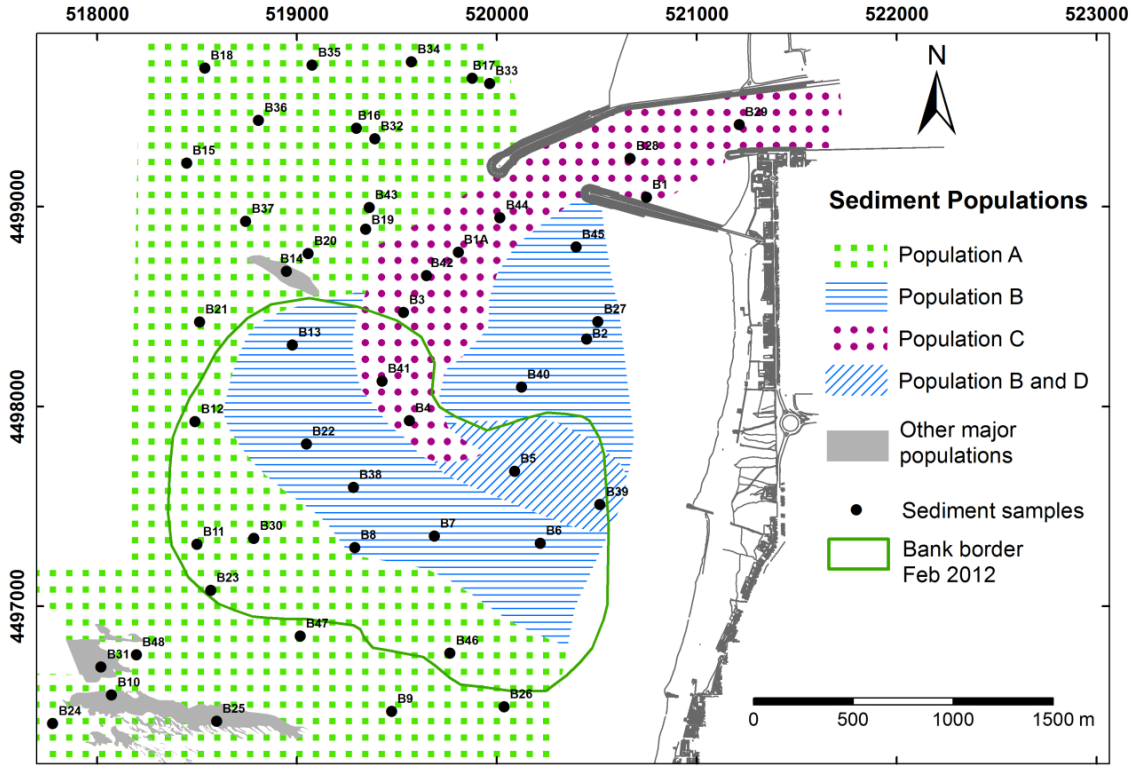

Figure 112. Most significant sediment populations identified on the samples collected in the study area. The delimitation of the dominant population areas was based on the sample analysis and on the sidescan sonar mosaic reflectivity patterns (see Figure 96). The green line in the map indicates the sandbank border in February 2012, which is the bathymetric survey acquired closest in time, to the sidescan sonar acquisition (December 2011 and January 2012) and collection of the sediment samples (March 2012). Coordinate system in UTM Zone 29N, datum WGS84.

In terms of populations, the inlet sedimentary influence extends to almost 2 km southwards, forming a semi-arc (see “Population C” in Figure 112) also noticed on the sidescan sonar mosaic shown in Figure 96. Moreover, two samples (B5 and B39) located on the area dominated by population B (“Population B and D” in Figure 112) also present population D as a secondary population, which may indicate the prolongation of the inlet influence, elongating southeastwards the lagoon influence semi-arc.

The sandbank presents the 3 main populations (see Figure 112). In the southern part of the bank the population A is dominant, reflecting low energetic conditions. The northern part of the bank presents sediments with a dominance of the population C, with the presence of the secondary populations D and E, which reveals the stronger energy conditions that act in this area. The central area of the sandbank is dominated by the population B, reflecting an intermediate condition in terms of energy between the northern and the southern part of the bank. These energy variations seem to be related to the distance from the inlet, tracing its influence in the sandbank and surrounding areas.

Based on all the data and the analyses carried out in the scope of this study made it possible to propose a map with a conceptual model of the different processes acting at present in the “Barra de Aveiro” and its adjacent areas, in particular the sandbank region, which was the main objective of this study (Figure 113).

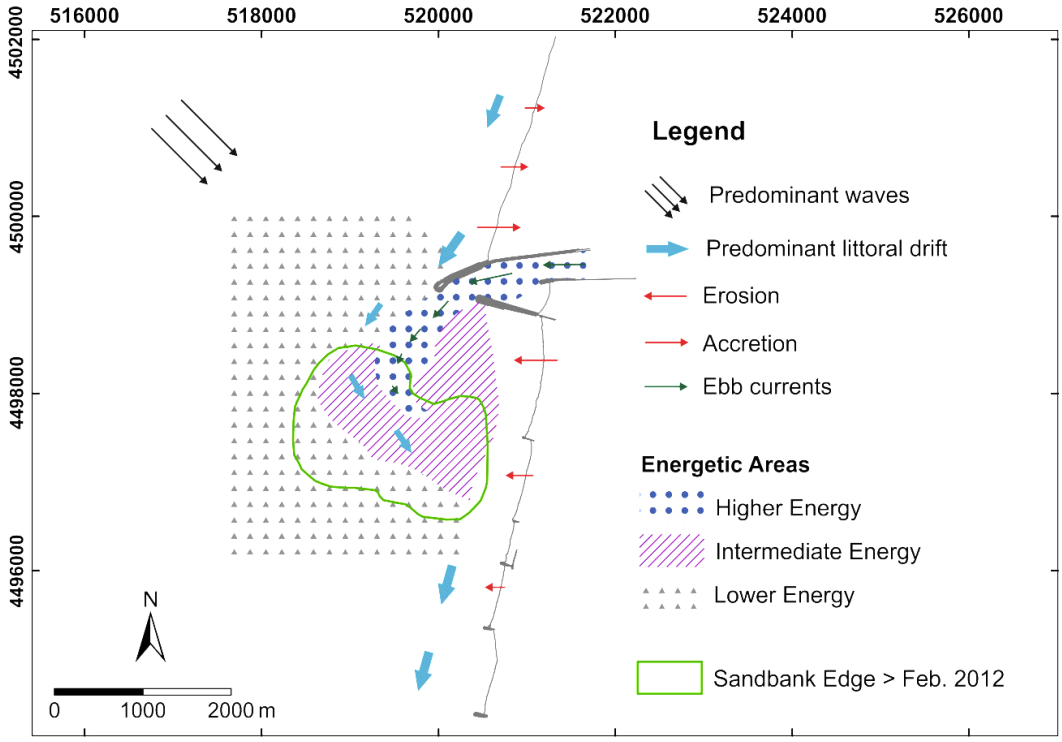

Figure 113. Map representing a conceptual model of the different acting processes present in the “Barra de Aveiro” and the near shore shelf sedimentary dynamics. Coordinate system in UTM Zone 29N, datum WGS84.

V.6. Conclusions

The evolution of the "Barra de Aveiro" and its adjacent area, constantly subjected to engineering works, were investigated based on bathymetric, geophysical and sedimentological data, with the aim to contribute to a better characterization and understanding of the inlet and sandbank evolution and to assess the interplay between natural processes and the impacts of engineering works on the morphodynamics of the area. The integration of all the results allowed to the following conclusions to be drawn for this area:

(1) Since the Xth century that the Aveiro sandy littoral has always shown a very high mutability through time, becoming more stable after the inlet artificial opening in 1808, which allowed the socio-economic development of the region. The sedimentary balance of the area is the result of the transported sediment load (both littoral drift and river discharge), the exposition of the coast to storms, storm surges, sea level rise, costal retreat, and the anthropogenic actions in the coast, such as hard structures construction and dredging operations. The littoral drift that transports the sediment coming from the north, mainly from the Douro hydrographic basin, was responsible for the existence of the ebb delta in front of the inlet, which was deflected seawards, forming a "C"-shaped sand accumulation, due probably to the offshore directed construction of the jetties that create a jet stream southwest directed and the ebb currents, approximately perpendicular to the littoral drift, that got stronger as a result of the tidal prism increase in the lagoon.

(2) The formation of the sandbank seems to be related to the remaining south part of the ebb delta that started its individualization in 1965/66 due to the strong ebb currents that reduced the sediment accumulation trend in front of the inlet and the frequent dredging operations of the navigation channel.

(3) The sandbank permanency and evolution are related to a complex interaction of factors, the most important being: (a) the littoral drift that seems to represent the main sedimentary source of the sandbank; (b) the southwest-directed jet stream related to the littoral drift interaction with the north jetty; (c) the ebb currents, whose direction is related to the north jetty length and orientation; (d) the energy decrease of the ebb currents with the distance to the inlet, revealed by the granulometric variation of the surface bank sediments, which allowed the sand accumulation in the bank area and/or the removal of the finer sediment in the most energetic parts of the bank (northeastern part); (e) the engineering works such as the

extension of the north jetty, that re-direct the ebb currents and the jet stream, and the dredging operations for navigation channel maintenance.

(4) The inlet area is responsible for the littoral drift deflection/interruption and its area of influence is increasing through time, mainly due to the dredging operations and the north jetty extension (Figure 95). According to the bathymetric data, the littoral drift is restored downdrift in the second groin area (2300 m south of the south jetty head). This is consistent with the calculated r value in section V.2 and also with the results obtained by Teixeira (1994) that indicate sand bypass.

(5) The coastline advance (in the north – S. Jacinto beach) and retreat (in south of the inlet – Barra beach) were estimated based on the coastline evolution from 1936 to 2014. An annual coastline advance rate of 5.8 m/year was estimated for the S. Jacinto beach; in the Barra beach, however, the estimated annual retreat ranges from 1.9 to 2.6 m/year.

(6) The sandbank area and perimeter increased (24% and 15%, respectively) from November 2010 to November 2012, although from November 2012 to November 2013, a significant reduction in its area and perimeter (24% and 30%, respectively) was noticed, probably due to the important engineering works that took place between December 2011 and December 2013, mainly the dredging of the navigation channel that occurred during 2013 and which removed the northwestern part of the sandbank.

(7) The sandbank centroid modifications through time lead to a two main sandbank migration episodes (Figure 93): (a) about 150 m northwestwards from November 2010 to June 2011, associated mainly to the bank expansion northwestwards during this period (related to the formation of the northern elevation, that shifted the center of mass northwestwards); (b) approximately 220 m southwestwards, from November 2012 to November 2013, probably related to the southward migration of the northern elevation and, most likely, the dredging operations that occurred in 2013 and which originated the reduction of the sandbank area and volume in its northwestern part.

(8) From November 2010 to November 2013, the estimated volume of the sandbank ranged from 4 to 5 million of m^3 of sediment. The most recent bathymetric data (November 2013) indicates that the sandbank is composed by approximately 4.3 million of m^3 of sediment (Table 14).

(9) The granulometry analysis integrated with the sidescan sonar allowed to map the bottom grain size distribution in the study area (Figure 100): the inlet and its external proximal adjacent area is composed by coarse and

very coarse sand, whereas the medium sand is mainly found in the central sandbank area and surrounding the inlet area (i.e. surrounding the coarser sediments), and the fine sand, that represents almost 50% of the sampling, appears to correspond to the near-shore shelf/littoral sediment without the inlet influence.

(10) The sediment size distribution are very closely related to the local energetic conditions (Komar, 1976; Friedman and Sanders, 1978); therefore, the study area is divided into 3 main zones according to the local hydrodynamic energy: the inlet area and the outer semi-arc of coarse and very coarse sand, which represent the most energetic area; an intermediate energy area that corresponds mainly to the central part of the sandbank; and the remaining area, composed by finer sediment, which corresponds to lower energetic conditions. Therefore, the sandbank is subjected to a higher energetic condition on its northeastern part, reducing the energy southwestwards.

(11) The inlet area has in general higher energetic conditions, and presents the highest energy mainly between the two jetty heads and between the central dike and the north jetty, which correspond to constrained areas due to the presence of the port structures. Therefore, these areas are nowadays “naturally" deep and are becoming deeper though the time. On the contrary, the area located between these deep areas (north of the south jetty) corresponds to an enlargement area and therefore the energy decreases leading to the “natural” sediment accumulation. In fact, this area is frequently dredged in order to maintain the safe navigation in the entrance channel.

(12) The semi-arc configuration corresponding to the most significant population of the sediment in the inlet and in its prolongation until the northern part of the sandbank (population C - coarser sediment, Figure 113) is probably associated to the higher hydrodynamic energetic conditions generated by the interaction of different factors: the ebb currents, the incoming waves and the littoral drift currents. This is in agreement with numerical simulations performed by Plecha et al. (2009) and Rosa et al. (2012).

Chapter VI. Conclusions and future work

The Portuguese coast has been suffering serious erosional problems in the recent past, evident from the extreme decrease of the beach width in most of the coastal areas. The construction of several hard structures, such as groins, in order to attenuate the coastal erosion, interrupts the littoral drift transport and induces significant erosional problems downdrift. The beach nourishment has been an option to the hard structure construction, since it protects the structures localized near to the coast and simultaneously restores and widens the beach recreational area. However, this soft structure stabilization implies the extraction and transportation of the sediment from one area to the affected area, which is a very expensive process. The offshore extraction of sediments from coastal areas has become a common practice in many countries and has shown several advantages compared with onshore exploitation, since extraction from rivers, estuaries and nearshore sand bars has proven to have significant negative environmental and social impacts. Nevertheless, offshore extraction creates offshore sandpits which take a significant time to recover and have negative impacts, not only in the hydro and morphodynamics of the area, but also in affecting the local ecosystems. Several previous studies, such as those described in Chapter IV.2, have concentrated on the impacts of these offshore sandpits on the coastline; in this work we concentrate on the evolution and recovery time of these exploration pits, combining observational and numerical modelling.

Another issue of great importance for coastal zones and in particular to port areas, inlets and estuaries, are offshore sandbanks, such as ebb tidal deltaic systems. It is important to understand how these evolve naturally through time, particularly in areas of high hydrodynamism, and to understand the impacts on their evolution of engineering works in their vicinity. Port inlets, such as the “Barra de Aveiro”, are subjected to several engineering for inlet stabilization and configuration and for the maintenance of the navigation channels, in order to guarantee the secure navigational access to the port area. The result is a configuration and morphology of the exterior sandbank that is a consequence of the interaction of both the frequent engineering construction works and its natural evolution.

As stated in Chapter I, the main objective of this work was the investigation of the morpho-sedimentary dynamics and evolution of the features described above in two geographically and hydrodynamically distinct areas. The first case study was the Vale do Lobo offshore area where sand exploitation took place in a narrow sandpit for artificial beach nourishment. The second case study was the Aveiro inlet and nearshore, where dredging operations have been taking place together with jetty reconfigurations, both of which have impact on the local hydromorphodynamics and the evolution of the exterior sandbank. These two areas were chosen because for both cases it was possible to obtain a good coverage of bathymetric and complementary data through a significant time span, to allow us to conduct a study well constrained by observations. The fact that these two areas are located in very different hydrodynamic

contexts makes them even more interesting and complementary. Considering that offshore sand and gravel exploitation in sandpits for artificial beach nourishment is nowadays a central issue (Santos et al., 2014) and that some of the innovative solutions for artificial beach nourishment, such as the "sand engine" involve the exploitation of offshore sand for the creation of artificial sandbanks, the two case studies investigated in this thesis are highly complementary for the assessment of the feasibility and impacts of such solutions.

The two main questions addressed in this thesis were:

1. What is the morphodynamic evolution through time of an offshore sandpit site after a localized dredging operation in an area with low hydrodynamism such as offshore Vale do Lobo?
2. How did the "Barra de Aveiro" and its adjacent near-shore shelf evolve through time in the past decades and how did the port engineering works affect its sedimentary dynamics and morphological evolution?

This final chapter presents a summary of the results obtained when trying to answer these questions and proposes recommendations for future work in the study of effect of the engineering work on the morpho-sedimentary dynamics and evolution of these study areas.

VI.1. Morphodynamic evolution of a sandpit after localized dredging in an area with low hydrodynamism

The Vale do Lobo beach nourishment undertaken in 1998/1999 represented one of the first offshore sand extraction in the Algarve, where a total of about 700 000 m^3 of sand were extracted approximately 3.5 km offshore Vale do Lobo, between the 15 and 20 m isobaths (referred to ZH), causing shallow dredging depressions across a wide area (Teixeira, 2011). In contrast, the sand extraction of approximately 340 000 m^3 of sediment performed in from March to May 2006 created an oval shaped borrow pit, elongated in the NW-SE direction, about 900 m long, 150 m wide and 5 m deep, located about 3.5 km offshore Vale do Lobo, between the 16 and 18 m isobaths (referred to ZH).

As shown in section IV.5.1, the excavation has been becoming smoother, less deep and elongated in the NW-SE direction. In fact, 2.5 years after dredging operation, an infill of the deepest area of the sandpit was observed, as well as some sediment accumulation mainly on the upper part of the NE flank, resulting on the migration to

the SW of the excavation rim. 4 years after the extraction, the results show that the trend remains almost the same, with an infill of the deepest area of the pit, which is almost 2 m less deep, and some sediment accumulation in the upper part of the flanks (mainly in the NE flank). This seaward prograding pattern of the sandpit, the S-SE directed wind induced mean currents (Rosa et al., 2011a), and the sediment fluxes pattern suggest that the main source of the sediment accumulated on the pit should be sand from the N-NW surrounding areas.

The modelling results, discussed in section IV.5.3 and IV.4.4, indicate that the mean flow velocity and the orbital velocity decrease inside the excavation area, which results in a decrease of the sediment transport capacity inside the excavation area and, as a consequence, the sandpit acts as a trap for the sediment, fostering sediment accumulation and the pit recovery through time. The numerical model results also suggest that the sandpit refilling process is essentially storm-dependent and, therefore, episodic rather than continuous in time. In fact, significant wave height greater than 2 m, combined with strong winds, generate currents and wave orbital velocities capable of high sediment mobilization.

The bathymetric analysis results showed that the sandpit has been recovering through time at a rate that ranges from 6.5 to 7.2 cm/year. The estimates for the sandpit recovery time based on a mean refilling rate points toward a value of approximately 22 years for near-full pit refill. However, due to the episodic and storm dependent refiling of the sandpit, the calculated estimations proposed in this work use the number of stormy days, rather than the total time, which we believe is a more robust method. The estimations from this work point to the need of 412 stormy days, which corresponds to 38 years for a near-complete sandpit recovery, considering the wave data set used by Almeida et al. (2011) as representative of the future wave climate.

The results and methodologies presented in this part of the work hopefully contribute to a better understanding of the processes involved in the evolution of the sandpit under study and allow a better assessment of its environmental impacts, namely by providing more reliable estimates of its recovery time. The approach used is of course applicable to other offshore excavation areas and the numerical modeling procedure provides a useful management tool to select the most appropriate offshore sand borrow or exploitation sites with minimal impacts as concerns recovery times and coastal sedimentary balance.

VI.2. Sedimentary dynamics and morphological evolution of the "Barra de Aveiro" and the adjacent near-shore shelf

As shown in sections V.3 and V.5.1, the "Barra de Aveiro" and its adjacent near-shore shelf area have been subjected to several engineering works through time, mainly since 1808 when the artificially open was definitely established, either both for the harbor and inlet configuration or and for navigation channels opening/maintenance. The present morphology, hydro and sedimentary dynamics, and configuration of the "Barra de Aveiro" and its adjacent area are the result of a progressive adjustment and long term evolution as a response to the new hydrodynamic conditions induced by the frequent engineering works and the "natural" evolution. The sedimentary balance of the area is the result of the transported sediment load, the exposition of the coast to the storms, the storm surges, the sea level rise, and the anthropogenic actions in the coast, such as hard structures construction or reconstruction and dredging operations.

The old bathymetric maps analysed in this work indicate that the littoral drift, mainly transporting the sediment coming from the north, was responsible for the existence of the ebb delta in front of the inlet. With the seaward extension of the jetties and the deepening of the inlet channel, several modifications in the dynamic of the inlet and adjacent area occurred: the creation of a jet stream directed southwest, an increment of the tidal prism in the lagoon, a strengthening of the ebb currents, and a slight rotation from west to southwestwards of the ebb currents, following the north jetty orientation. These dynamic changes were probably in the origin of the deflection seawards through time observed in the external bar, forming a "C"-shaped sand accumulation. Probably due to the strong ebb currents, that reduced the sediment accumulation trend in front of the inlet, and the frequent dredging operations at the entrance navigational channel, the external sandbank started its individualization around 1965/66 from the ebb delta formed mainly by sediments coming from north.

The recent monitoring of the sandbank showed that its area and perimeter was increasing through time. However, probably due to the important engineering works that took place between December 2011 and December 2013, mainly the dredging of the navigation channel occurred during 2013 that removed the northwestern part of the sandbank, a significant reduction in the sandbank area and perimeter was noticed. Concerning the sandbank volume, the recent bathymetric data, allowed the volume estimation of the sedimentary structure as ranging from 4 to 5 million of m^3 of sand.

The granulometry analysis carried out, together with the sidescan sonar, allowed mapping the bottom grain size distribution, intensely related with the local energetic conditions, in the study area. The main results were:

- the inlet and in its external proximal adjacent area is composed by coarse and very coarse sand, which indicates this area as the most energetic;
- the medium sand is mainly found in the central sandbank area and surrounding the inlet area (i.e. surrounding the coarser sediments), that corresponds to an intermediate area in terms of energetic conditions;
- the fine sand represents almost 50% of the sampling and appears to correspond to the near-shore shelf/littoral sediment without the inlet influence and reflects lower energetic conditions.

In summary, the results obtained in this thesis indicate that the morphodynamic and sedimentary evolution of the Aveiro inlet and its adjacent area are governed by a complex interaction of natural and antropogenic factors, of which the most important are:

(a) the wave regime predominantly from northwest;

(b) the littoral drift southwards is deviated seawards due to the presence of the inlet north jetty, creating a jet stream southwest directed. The littoral drift seems to represent the main sedimentary source of the sandbank as shown by the similarity of the superficial sediment type;

(c) the ebb currents, which direction is straightly related with the north jetty length and orientation. The ebb currents strength had increased in time due to the deepening of the inlet channel that lead to an increase of the tidal prims. The ebb currents energy is higher between jetties, having a maximum between the two jetty heads and between the central dike and the north jetty (confined areas), which leads to the “natural” deepening of these areas, and decreases its strength between these deeper areas (north of the south jetty) and when it founds the open sea. These areas correspond to the decrease of the constraint due to the existence of the port structures leading to the “natural” sediment accumulation. The reduction of the energetic conditions in the sandbank is noticed by the granulometric variation of the surface bank sediments, which allows the sand accumulation in the sandbank area and/or the removal of the finer sediment in the most energetic parts of the bank (northeastern part). According to the sedimentary and geophysical data, in the inlet area the ebb current is southwest directed and seems to be inflected to southeast doing a semi-arc due probably to the interaction with two main factors: the predominant waves coming from the northwest quadrant which induce the southward littoral drift currents, seawards deviated in the inlet area and redirected towards the coast south of the inlet (around the second groin); the bathymetric elevation that corresponds to the sandbank may act as an obstacle and contribute to this inflexion .

(d) the engineering works, such as the extension of the north jetty and the dredging operations for navigation channel maintenance, which induce the re-direction and the strengthening of the ebb currents and the jet stream.

In 2012 (more specifically from December 2011 to December 2012) an extension of 200 m of the north jetty was performed and the navigation channel was dredged at 13.2 m of depth. Therefore the study area is once again re-adjusting to the new hydrodynamic conditions. According to the most important factors that act in the study area, it is possible to hypothesize about the morphological response to the new conditions. The inlet channel has a tendency to deepen and the deepest area would be now closer to the new portion of the north jetty, which, according to Castanho et al. (1974) and Dias and Mariano (2011), would increase the tidal prism and probably the drag capacity of the Aveiro lagoon. The ebb currents shall probably be stronger and slightly inflected southwards and the sandbank should migrate southwards and probably also to the west. If no dredging operations were carried out in the inlet area, the result would be the sediment accumulation in the navigation channel and probably the sandbank would connect again to the submersed sand bar coming from the north forming again a “C” shaped sedimentary structure, although located further from the coast and dislocated southwards when compared with its position in the past.

VI.3. General conclusions

In general, the main objectives of this thesis were attained and the results obtained allow a better understanding about the morpho-sedimentary dynamics and the evolution of the two studied areas that were subjected to engineering works. When a new engineering intervention is performed, a progressive morphological and sedimentary adjustment occurs in order to respond to the new hydrodynamic conditions induced by these works. The full understanding of these morphological adjustments is very important to assess the hydrodynamic changes and the potential environmental impacts associated to these works. A deeper knowledge of these coastal systems and of the interaction between natural and antropogenic-related processes should hopefully lead to a better management of the coastal areas and the marine natural resources.

In order to fully assess the impacts on hydrodynamics and sedimentation caused by engineering works dredging operations, sand and gravel extraction and offshore constructions, an integrated approach combining bathymetric, geophysical, and sedimentary data, for morphodynamic and sedimentological studies, coupled with

numerical modeling, when possible, is essential. The use of sidescan sonar methods coupled with sediment sampling (ground truthing) and granulometry analysis for sidescan sonar data calibration and interpolation, allow obtaining a well constrained and realistic superficial sedimentological map of the seafloor. Such studies coupled to morphodynamic numerical models, when possible, are a very useful tool for further predictions of the morphological impacts of the engineering works in coastal areas, being of crucial importance for coastal areas and marine resources protection and management.

The evolution of sandpits have been previously studied by several authors such as Bender and Dean (2003), Hitchcock and Bell (2004), Roos (2004), Walstra et al. (2005), Diesing et al. (2006), Kubicki et al. (2007) among others (see section IV.2) and supported by European and national projects, such as SANPIT - Sand transport and morphology of offshore sand mining pits/areas and SANDEX - Sand extraction in the portuguese continental shelf: impacts and morphodynamic evolution. In this study we focused on the evolution of the Vale do Lobo sandpit that represents, to our knowledge, an innovative approach, being the first that combines observations with numerical modeling for a sandpit evolution study located in the Portuguese coast.

The study of the Aveiro inlet and its adjacent sandbank represents also, to our knowledge, the first integrated approach on the formation and evolution of this external sandbank, combining bathymetric, geophysical, and sedimentary data, for morphodynamic and sedimentological studies; it therefore complements the pioneering study of this area by Teixeira (1994). In this case, due to time limitations, it was not possible to carry out the numerical modelingfor this area and therefore this is one of the main objectives for future work. It is well known the importance of the sandbanks (see section V.2), that are of considerable economic importance. The banks located close to the shore may provide a source for sediment, interacting with that on the beaches, and helping to stabilize them (Dyer and Huntley, 1999). Furthermore, wave dissipation by and refraction around banks may also be crucial in maintaining the form of the coastline and protecting some stretches from erosion in storm events. In fact, the limited depth above sandbanks dissipates much energy from waves and storm surges, reducing erosion forces on the adjacent coast (Ferreira et al., 1994; Dyer and Huntley, 1999). Additionally, they may contain exploitable reserves of sand and gravel, corresponding to an important marine sediment source. Sandbanks are also key to navigation because they may constitute hazards to shipping (Dyer and Huntley, 1999).

Consequently, a better understanding of the processes of formation, growth and maintenance of the Aveiro sandbank and the research into their behavior and on erosion–transport–deposition processes are of great importance. Moreover, an understanding of the hydrodynamical context and the present day sediment transport regime will allow prediction of short-term change, which is highly relevant for

engineering and coastal management work of a social and economically important area such as the Aveiro Harbor entrance.

The study of seabed features such as the Aveiro sandbank and the contribution for the understanding of the response of the coast to these shoals can be valuable for implementing and improving innovative soft engineering solutions to combat coastal erosion such as the "sand engine" (Stive et al., 2013). This new coastal management solution has recently been implemented in the Netherlands (Figure 114), where the nourishment is implemented in the form of a large shoal connected to the beach, (Stive et al., 2013) rather than a beach nourishment as in the Vale do Lobo example.

Figure 114. Aerial photograph taken on September 2011 of the Sand Engine performed in the Dutch coast (Stive et al., 2013).

It is hoped that the results and methodologies presented in this work will contribute to a better understanding of the processes involved in the evolution of the two study areas and allow a better assessment of the environmental impacts of the engineering works and how these evolve through time. Furthermore, the results of this thesis should also hopefully contribute to a better constrained evaluation and implementation of innovative proposed solutions, such as the "sand engine" described above, as these likely involve offshore sand exploitation and require a good understanding of the sandpit and nearshore sandbank morphological evolution.

VI.4. Future work

The present work investigated the processes that act in coastal areas and how they "naturally" and progressively suffer adjustments in order to respond to changes of the hydrodynamic conditions induced by the engineering works to which they are frequently subjected. Given the complexity of the involved processes, future work should include:

- Further monitoring of the study areas for a longer time period to allow the follow-up of the morphological evolution of the study areas;
- Reducing the time span between surveys, in order to assess about seasonal changes in the study areas;
- Measurements of hydrodynamic parameters (such as currents with ADCPs) in order to better understand the hydrodynamics of the study areas and correlate it with the morphological adjustments;
- Bathymetric surveys that should be carried out using multibeam systems with motion sensors and accurate DGPS positioning to ensure very accurate estimates of the morphological volume variations;
- Morphodynamical numerical modelling of the "Barra de Aveiro" and adjacent area in order to better assess the future evolution of this area, in face of the most recent engineering works, mainly the sandbank evolution and navigation channel maintenance. The morphodynamical numerical modelling could also be used to access the sandbank evolution and sedimentation to different wave climates, as performed to Vale do Lobo sandpit;
- The application of other complementary geophysical methodology, such as high resolution reflection seismics (Chirp sonar/Sparker), mainly in the Aveiro area, to investigate the subsurface sedimentary structure of the sandbank, and therefore better understand its formation and evolution through a much longer time span.

References

Abecasis C., 1951. O regime das embocaduras lagunares e o problema do melhoramento da barra de Aveiro; Lisboa.

Abecasis C., 1955. The history of a tidal lagoon and its improvement (The case of Aveiro, Portugal). *Proceedings of Fifth Conference on Coastal Engineering*, 329-363.

Abrantes I. 1994. A cobertura sedimentar da plataforma e da vertente continental superior entre Espinho e Aveiro, Ms. Thesis, University of Aveiro, 178p.

Abrantes I. 2005. Os sedimentos superficiais da margem continental, sector Espinho – Cabo Mondego: a utilização das fracções finas como traçadores de dinâmica sedimentar actual. PhD thesis, University of Aveio, 239p.

Abrantes I., Rocha F., 2007. Sedimentary Dynamics of the Aveiro Shelf (Portugal). *Journal of Coastal Research*, (SI 50), 1005–1009. ISI>://000251837500013.

Abrantes I., Rocha F., Vidinha J., Alveirinho Dias J.M., 2005. Influence of Aveiro Lagoon heavy metal contents in the adjacent continental shelf (Portugal). *Ciencias Marinas*, 31(1B), 149–160.

Almeida L., Ferreira Ó., Voudouskas M., Dodet G., 2011. Historical Variation and trends in storminess along the Portuguese South Coast. *Natural Hazards and Earth System SciencesI,*11, 2407-2417.

Alveirinho Dias J.M., 1987. Dinâmica sedimentar e evolução recente da plataforma continental portuguesa setentrional. University of Lisbon, Ph.D. thesis, 500p.

Alveirinho Dias J.M., 1988. Aspectos geológicos do litoral algarvio (in Portuguese). *Geonovas*, 10, 113-128.

Alveirinho Dias J.M., Neal J., 1992. Sea Cliff Retreat in Southern Portugal: Profiles, Processes and Problems. *Journal of Coastal Research*, 8(3), 641-654.

Alveirinho Dias J.M., Monteiro J.H.; Gaspar L., 1980. Potencialidades em Cascalho da Plataforma Continental Portuguesa a Norte do Canhão Submarino da Nazaré. *Comunicações dos Serviços Geológicos de Portugal*, 66:227-240, Lisboa, Portugal. ISSN: 0037-2730.

Alveirinho Dias J.M., Ferreira Ó., Pereira M., 1994. Estudo Sintético de Diagnóstico da Geomorfologia e da Dinâmica Sedimentar dos Troços Costeiros entre Espinho e Nazaré. 1994. Available in: http://w3.ualg.pt/~jdias/JAD/eb_EspinhoNazare.html, last access: 8/4/2014.

Alveirinho Dias J.M., Boski T., Rodrigues A., Magalhães F., 2000. Coast line evolution in Portugal since the Last Glacial Maximum until present - a synthesis. *Marine Geology*, *170*(1-2), 177–186. doi:Doi: 10.1016/s0025-3227(00)00073-6.

Alves T., Gawthorpe R.L., Hunt D.W., Monteiro H., 2003. Cenozoic tectono-sedimentary evolution of the western Iberian margin. *Marine Geology*, 195(1-4), 75–108. doi:10.1016/S0025-3227(02)00683-7.

Amorim I., 2008. Porto de Aveiro: Entre a Terra e oMar. APA – Administração do Porto de Aveiro, 227p.

Amorim I., Garcia J., 2008. A Barra e os Portos da Ria de Aveiro 1808 – 1932, Arquivo da Administração do Porto de Aveiro, Catalogo da Exposição, Aveiro, 104p.

Andeweg B., 2002. Cenozoic tectonic evolution of the Iberian Peninsula, causes and effects of changing stress fields. PhD Thesis, VU University Amsterdam.

Andrade, C., 1990. O ambiente de barreira da ria Formosa. Doctoral Thesis. Algarve (Portugal), Universidade de Lisboa, 645p.

Andrade C., Freitas M.C., Cachado C., Cardoso A.C., Monteiro J.H., Brito P., Rebelo L., 2002. Coastal zones - Climate change in Portugal. Scenarios, impacts and adaptation measures. SIAM Project. Tech. rep., 173-219.

APA, 2009. Projecto de Reconfiguração da Barra do Porto de Aveiro – Projecto de Execução, Vol. 3. Memória Descritiva e Justificativa, Administração do Porto de Aveiro APA, Janeiro 2009, 106 p.

ARH, 2012a. Plano de Gestão das Bacias Hidrográficas que Integram a Região Hidrográfica das Ribeiras do Algarve (RH8), Volume I - Relatório, Parte 2 - Caracterização e Diagnóstico, Tomo I - Caracterização Territorial e Fisiográfica, Tomo IA - Peças Escritas. Administração da Região Hidrográfica do Algarve - Agência Portuguesa do Ambiente.

ARH, 2012b. Plano de Gestão das Bacias Hidrográficas dos rios Vouga , Mondego e Lis Integrados na Região Hidrográfica 4. Parte 2 - Caracterização e Diagnóstico. 1.3 – Geológica e Geomorfológica. Administração da Região Hidrográfica do Centro - Agência Portuguesa do Ambiente.

Bastos A.C., Paphitis D., Collins M.B., 2004. Short-term dynamics and maintenance processes of headland-associated sandbanks: Shambles Bank, English Channel, UK. *Estuarine, Coastal and Shelf Science*, *59*(1), 33–47.

Bastos M.R., 2009. On the track of salt : Adding value to the history of saltponds exploration in the coastal management scene of Aveiro lagoon. *Journal of Integrated Coastal Zone Management*, 9(3), 25–43.

Bender C. J., Dean R. G., 2003. Wave field modification by bathymetric anomalies and resulting shoreline changes: a review with recent results. *Coastal Engineering*, 49, 125–153.

Bertin X., Oliveira A., Fortunato A., 2009. Simulating morphodynamics with unstructured grids: Description and validation of a modeling system for coastal applications. *Ocean Modelling* 28(1–3), 75-87.

Bijker E.W., 1971. Longshore transport computations. Journal of Waterway, Ports, Harbor, *Coastal and Ocean Engineering*, 97 (4), 687-703.

Bird E., 2008. Coastal Geomorphology – An Introduction. 2nd Edition; Wiley, 411p.

Blondel P., 2009. The Handbook of Sidescan Sonar, Springer-Praxis, 316p.

Blondel P., 2008. A review of acoustic techniques for habitat mapping. *Hydroacoustics*.

Blondel P., Murton B.J. 1997. Handbook of seafloor sonar imagery. Chichester, Wiley. 314 p.

Blondel P., Parson L.M, Robigou V. 1998. TexAn: Textural Analysis of Sidescan Sonar Imagery and Generic Seafloor Characterisation. Proc. OCEANS'98, IEEE-OES, 419-423.

Blott S.J., Pye K., 2001. GRADISTAT: a grain size distribution and statistics package for the analysis of unconsolidated sediments. *Earth Surface Processes and Landforms*, *26*(11), 1237–1248. doi:10.1002/esp.261.

Booij N., Ris R.C., Holthuijsen L.H., 1999. A third-generation wave model for coastal regions 1. Model description and validation. *Journal of Geophysical Research* 104 (C4), 7667–7681.

Brissette M.B., Clarke J., 1999. Side Scan Versus Multibeam Echosounder Object Detection: A Comparative Analysis. *International Hydrographic Review*, 76(2), 21-34.

Brown C., Blondel P., 2009. Developments in the application of multibeam sonar backscatter for seafloor habitat mapping. *Applied Acoustics* 70, 1242-1247.

Bruun P., Gerritsen F., 1959. Natural bypassing of sand at coastal inlets. *Journal of Waterways and Harbors Division*, 85(4), 75-107.

Cáceres R.A., Zyserman J.A., Perillo G.M., 2016. Analysis of Sedimentation Problems at the Entrance to Mar del Plata Harbor. *Journal of Coastal Research*, 318, 301–314.

Cachão M., 1995. Utilização de nanofósseis calcários em biostratigrafia, paleoceanografia e paleoecologia. Aplicações ao Neogénico do Algarve (Portugal) e do Mediterrâneo Ocidental (ODP 653) e à problemática de Coccolithus pelagicus. Unpublished PhD Thesis, Fac. Ciências da Univ. de Lisboa, Lisboa, 450.

Cachão M., Boski T., Moura D., Dias R.P., Silva C.M., Santos A., Pimentel N., Cabral J., 1998. Proposta de articulação das unidades sedimentares neogénicas e quaternárias do Algarve (Portugal). Actas do V Congresso Nacional de Geologia, Comunicações do Instituto Geológico e Mineiro, Lisboa, 84, A169-A172.

Capitão R.P., Fortes C.J., Carvalho M.M., 1997. Análise da dinâmica costeira no troço Cabo Mondego - Estuário do Mondego. Erosões em Buarcos. Estudo de agitação marítima. Tech. Rep. 167/97 NPP, LNEC, Lisbon, Portugal, 28p.

Capus, C.G., Banks, A.C., Coiras E., Ruiz I.T., Smith C.J., Petillot Y.R., 2008. Data correction for visualisation and classification of sidescan SONAR imagery. IET Radar Sonar and Navigation 2(3): 155-169.

Carr E.E., Kraus N.C., 2001. Morphologic Asymmetries at Entrances to Tidal Inlets, US Army Corps of Engineers, 1–16.

Caston G.F., 1972. Linear sand banks in the southern North Sea. Sedimentology, 18, 63-78.

Caston G.F., 1981. Potential gain and loss of sand banks in the Southern Bight of the North Sea. *Marine Geology* 41, 239-250.

Castanho J.P., 1971. Características das ondas na rebentação – sua aplicação ao transporte sólido litoral. III Jornadas Luso-Brasileiras de Engenharia Civil.

Castanho J.P., Gomes N., Carvalho J., Vera-Cruz D., Araújo O., Teixeira A., Weinholtz M., 1974. Means of controling litoral drift to protect beaches, dunes, estuaries and harbour entrances. Establishment of artificial beaches. Memória 448 – Laboratório Nacional de Engenharia Civil, 26p.

Castanho J.P., Gomes N., Oliveira I.B.M., Simões J.P., 1981. Coastal Erosion by Harbour Works on the Portuguese Coast and Corrective Measures. 24th International Navigation Congress, P.I.A.N.C., Edinburgh.

Chang Y.C., Hsu S.K., Tsai C.H., 2010. Sidescan Sonar Image Processing: Correcting Brightness Variation and Patching Gaps. *Journal of Marine Science and Technology*, 18(6), 785–789.

Chavez P.S., Isbrecht J., Galanis P., Gabel G.L., Sides S.C., Soltesz D.L., Ross S.L., Velasco M.G. 2002. Processing, mosaicking and management of the Monterey Bay digital sidescan-sonar images. *Marine Geology*, 181, 305-315.

Chester D.K., 2012. Pleistocene and Holocene geomorphological development in the Algarve, southern Portugal. *Geomorphology*, 153-154, 17–28. doi:10.1016/ j.geomorph.2012.01.020.

Clifton H. E., Hunter R. E., Phillips R. L., 1971. Depositional structures and processes in the nonbarred high-energy nearshore. *Journal of Sedimentary Petrology*, 41, 651-670.

Cobra D.T., Oppenheim A.V., Jaffe J.S., 1992. Geometric Distortions in Side-Scan Sonar Images: a Procedure for their Estimation and Correction. *IEEE Journal of Oceanic Engineering*, 17, n.3, 252-268.

Coelho C.D., 2005. Riscos de Exposição de Frentes Urbanas para Diferentes Intervenções de Defesa Costeira. PhD Thesis, Aveiro, 404p.

Collier J.S., Brown C.J., 2005. Correlation of sidescan backscatter with grain size distribution of surficial seabed sediments. *Marine Geology*, 214, 431-449.

Combe A.J., 2002. Personal Communication, April, 2002. *In* Bender C.J., Dean R.G., 2003. Wave field modification by bathymetric anomalies and resulting shoreline changes: a review with recent results. *Coastal Engineering*, 49, 125–153.

Combe A.J., Soileau C.W., 1987. Behavior of man-made beach and dune: Grand Isle, Louisiana. Coastal Sediments ’87. ASCE, New York, 1232– 1242.

Cooper K., Boyd S., Eggleton J., Limpenny D., Rees H., Vanstaen K., 2007. Recovery of the Seabed Following Marine Aggregate Dredging on the Hastings Shingle Bank off the Southeast Coast of England. *Estuarine Coastal and Shelf Science*, vol. 75, 547-558.

Correia, F., Dias, J.A., Boski, T., Ferreira, Ó., 1996. The retreat of the Eastern Quarteira cliffed coast (Portugal) and its possible causes. In: Jones, P.S., Healy, M.G., Williams, A.T. (eds.). Studies in European Coastal Management. Cardigan, Samara Publishing Limited, 129-136.

Correia F., Ferreira Ó., Alveirinho Dias J.M., 1997. Contributo das arribas para o balanço sedimentar do sector costeiro Quarteira - Vale do Lobo (Algarve - Portugal). *Seminário sobre a zona Costeira do Algarve*, Faro, 31-39.

Costa M., Baptista R., Rusu L., 2003. Vinte anos de dados de agitação marítima na costa Portuguesa. *3as Jornadas Portuguesas de Engenharia Costeira e Portuária*. Aveiro, Portugal, 12-13 November, 12p.

Costa M., Silva R., Vitorino, J., 2001. Contribuição para o estudo do clima de agitação marítima na costa portuguesa. *Proceedings of 2as Jornadas Portuguesas de Engenharia Costeira e Portuária*, Permanent International Association for Navigation Congresses (PIANC), Sines, Portugal.

Cunha S.R., 1930. Relance da história económica de Aveiro: soluções para o seu problema marítimo a partir do século XVII. Conferência - Aveiro: Imprensa Universal, 14 de Junho de 1930, 62p.

Cunha S.R. 1959. O Porto de Aveiro. *Separata da Revista de Obras Públicas e Minas*. Edição Lusitânia, 2ª edição, 2-24.

Creel L., 2003. Ripple Effects: Population and Coastal Regions. Population Reference Bureau - Measure Communication: 1-8. (http://www.prb.org/pdf/RippleEffects_Eng.pdf).

Davis K.S., Slowey N.C., Stender I.H, Fiedler H., Bryant W.R., Fechner G., 1996. Acoustic backscatter and sediment textural properties of inner shelf sands, northeastern Gulf of Mexico. *Geo-Marine Letters*, 16, 273-278.

Davidson-Arnott R., 2010. Introduction to coastal processes and geomorphology. Cambridge University, 442p.

Dartnell P., Gardner J., 2004. Predicting Seafloor Facies from Multibeam Bathymetry and Backscatter Data Peter. *Photogrammetric Engineering and Remote Sensing*, 70(9), 1081-1091.

Dean R.G., Walton T.L., 1975. Sediment transport processes in the vicinity of inlets with special reference to sand trapping. *In*: Cronin L.E. (Ed.), Estuarine Research. Academic Press, New York, 129-149.

Demir H., Otay E.N., Work P.A., Borekci O.S., 2004. Impacts of dredging on shoreline change. *Journal of Waterway, Port, Coastal and Ocean Engineering*, 130(4), 170-178.

Devereux, C.M., 1983. Recent erosion and sedimentation in southern Portugal. Ph.D. Thesis, University College, University of London, UK.

Dias J.M., Lopes J.F., Dekeyser I., 1999. Hydrological characterization of Ria de Aveiro lagoon, Portugal, in early summer. *Oceanologica Acta* 22, 473–485.

Dias J.M., Lopes J.F., Dekeyser I., 2000. Tidal propagation in Ria deAveiro lagoon, Portugal. Physics and Chemistry of the Earth (B) 25, 369–374.

Dias J.M., 2001. Contribution to the study of the Ria de Aveiro hydrodynamics. Aveiro, Portugal: University of Aveiro, Ph.D. thesis, pp. 288.

Dias J.M., Lopes J.F., Dekeyser I., 2003. A numerical system to study the transport properties in the Ria de Aveiro lagoon. *Ocean Dynamics*, 53(3), 220–231. doi:10.1007/s10236-003-0048-5.

Dias J.M., Lopes J.F, 2006. Implementation and assessment of hydrodynamic, salt and heat transport models: The case of Ria de Aveiro Lagoon (Portugal). *Environmental Modelling & Software*, 21(1), 1–15. doi: DOI: 10.1016/j.envsoft. 2004.09.002.

Dias J.M., Mariano S.C., 2011. Numerical Modelling of Hydrodynamic Changes Induced by a Jetty Extension – the Case of Ria de Aveiro (Portugal). *Journal of Coastal Research*, (64), 1008–1012.

Dias J.M., Vaz L., Plecha S., 2011. Plano de Ordenamento da Orla Costeira, Caracterização Climática: Orla Costeira Ovar – Marinha Grande, Universidade de Aveiro, Portugal, 39 p.

Diesing M., Schwarzer K., Zeiler M., Klein H., 2006. Comparison of marine sediment extraction sites by means of shoreface zonation. *Journal of Coastal Research*, 783–788.

Dinis P.A., 2004. Evolução Pliocénica e Quaternária do Vale do Cértima, Ph.D. Thesis, University of Coimbra, 351p.

Dodet G., Bertin X., Taborda R., 2010. Wave climate variability in the North-East Atlantic Ocean over the last six decades. *Ocean Modelling*, 31(3-4), 120-131.

Dolbeth M., Ferreira Ó., Teixeira H., Marques J.C., Alveirinho Dias J.M., Pardal M., 2007. Beach morphodynamic impact in a macrobenthic community along a subtidal depth gradient. Marine Ecology Progress Series, 352, 113-124.

Duarte H., Pinheiro, L.M., Teixeira, F.C., Monteiro, J.H., 2007. High-resolution seismic imaging of gas accumulations and seepage in the sediments of the Ria de Aveiro barrier lagoon (Portugal). Geo-Marine Letters, 27(2-4), 115–126. doi:10.1007/ s00367-007-0069-z.

Duarte H., 2009. High-resolution seismic reflection investigation of gas accumulation and seepage in the tidal channels of the Ria of Aveiro barrier lagoon (Portugal). PhD thesis, University of Aveiro, 168p.

Dunbar C.O., Rodgers J., 1957. Principles of Stratigraphy. John Wiley and Sons, New York, 356 p.

Dyer K.R., Huntley D.A., 1999. The origin, classification and modelling of sand banks and ridges. *Continental Shelf Research*. Vol. 19, 1285-1330.

Elias E.P., Spek A.J., 2006. Long-term morphodynamic evolution of Texel Inlet and its ebb-tidal delta (The Netherlands), Marine Geology, 225, 5-21.

Elias E.P., Cleveringa J., Buijsman M.C., Roelvink J.A., Stive M.J., 2006. Field and model data analysis of sand transport patterns in Texel Tidal inlet (the Netherlands), Coastal Engineering, 53, 505-529.

Elias E.P., Hansen J.E., 2013. Understanding processes controlling sediment transports at the mouth of a highly energetic inlet system (San Francisco Bay, CA*). Marine Geology*, 345, 207–220.

Elliot T., 1978. Clastic shorelines. Chapter 7. *In* Reading H.G. (Eds), Sedimentary Environments and Facies. Elsevier, New York, 143-177.

EN, 2000. EN 933-1: 2000. Tests for geometrical properties of aggregates - Part 1: Determination of particle size distribution - Sieving method.

Faria J.M.R., Machado M.J., 1979. Contribuição para o estudo hidroclimatológico da bacia hidrográfica do Rio Vouga. *Rev. Inst. Nac. Meteor. Geof*. 2(1-2): 3-72.

Ferreira Ó., Alveirinho Dias J.M., 1992. Dune erosion and shoreline retreat between Aveiro and Cape Mondego (Portugal): prediction of future evolution. *Proceedings Intern. Coastal Congress*, 187–200.

Ferreira Ó., Alveirinho Dias J., Taborda R., 1994. Wave energy dissipation on a high energy barred nearshore - a natural and effective coastal protection. *Littoral 94*, Lisbon, Portugal, 369–379.

Figueiredo F.P., 2002. Gravimetria aplicada à organização geométrica da cobertura Meso-Cenozóica (Baixo Vouga). PhD thesis, Universidade de Coimbra, Portugal, 213 p.

Fitzgerald D.M., Kulp M., Penland S., Flocks J., Kindinger J., 2004. Morphologic and stratigraphic evolution of muddy ebb-tidal deltas along a subsiding coast: Barataria Bay, Mississippi River delta. Sedimentology, 51(6), 1157–1178.

Fiúza A.F., Macedo M.E., et al. 1982. Climatological space and time variation of the Portuguese coastal upwelling." *Oceanologica Acta* 5(1): 31-40.

Folk R.L., 1954. The distinction between grain size and mineral composition in sedimentary-rock nomenclature. *Journal of Geology*, 62, 344-359.

Folk R.L., Ward W.C., 1957. Brazos River bar: a study in the significance of grain size parameters. *Journal of Sedimentary Petrology*, 27, 3-26.

Fonseca J.C., Janica M.G.R., Proença M.C. 1988. Panorama no Distrito, *VII Jornadas da Saúde de Aveiro*, Administração Regional de Saúde, Gráfestal. 12.

Fonseca, L.E., 1996. Correções Radiométricas dos Dados Sonográficos da Bacia de Campos. *VIII Simpósio Brasileiro de Sensoriamento Remoto*, Salvador, BA, 899-904.

Fortunato A.B., Oliveira A., 2004. A modeling system for tidally driven long-term morphodynamics, *Journal of Hydraulic Research*, 42(4), 426-434.

Fortunato A.B., Oliveira A., 2007. Improving the Stability of a morphodynamic modeling system, *Journal of Coastal Research*, SI 50, 486-490.

Fortunato A.B., Pinto L., Oliveira A., Ferreira J.S., 2002. Tidally generated shelf waves off the Western Iberian Coast. *Continental Shelf Research* 22 (14), 1935–1950.

Friedman G.M., 1979. Differences in size distributions of populations of particles among sands of various origins. *Sedimentology* 26, 3-32.

Friedman G.M., Johnson K.G., 1982. Exercises in Sedimentology. Wiley: New York.

Friedman G.M., Sanders J.E., 1978. Principles of Sedimentology. Wiley: New York.

Freitas R., Sampaio L., Rodrigues A.M., Quintino V., 2005. Sea-bottom classification across a shallow-water bar channel and near-shore shelf, using single-beam acoustics. *Estuarine, Coastal and Shelf Science*, *65*(4), 625–632. doi:DOI: 10.1016/j.ecss.2005.07.011.

García-Gil S., Durán R., Vilas F., 2000. Side scan sonar image and geologic interpretation of the Ría de Pontevedra seafloor (Galicia, NW Spain). *Scientia Marina*, 64(4), 393-402.

Garcia Mondejar J., 1988. Plate reconstruction of the Bay of Biscay. *Geology*, 24, 635-638.

Garel E., Sousa C., Ferreira Ó., Morales J.A., 2014. Decadal morphological response of an ebb-tidal delta and down-drift beach to artificial breaching and inlet stabilisation. *Geomorphology*, 216, 13–25.

Garel E., Sousa C., Ferreira Ó, 2015. Sand bypass and updrift beach evolution after jetty construction at an ebb-tidal delta. Estuarine, *Coastal and Shelf Science*, 167, 4–13.

Girão A.A., 1951. Evolução morfológica da região do Baixo Vouga. *Boletim do Centro de Estudos Geográficos de Coimbra*, 2/3, 75-85.

Gomes F.V., Pinto F.T., 2007. Case Study: Vale do Lobo (Portugal). *EUROSION*. Hydraulic and Water Resources Institute – IHRH, 18pp. http://copranet. projects.eucc-d.de/files/000149_EUROSION_Vale_do_ Lobo.pdf (last update 04/01/2007).

Goff, J., A., Olson, H.C., Duncan, C.S., 2000. Correlation of side-scan backscatter intensity with grain-size distribution of shelf sediments, New Jersey margin. *Geo-Marine Letters*, 20, 43-49.

Gonçalves D.S., Pinheiro L.M., Silva P.A., Rosa J., Rebêlo L., Bertin X., Teixeira S.B., Esteves R., 2014. Morphodynamic evolution of a sand extraction excavation offshore Vale do Lobo, Algarve, Portugal. *Coastal Engineering*, 88, 75–87.

Granja H.M., Ribeiro I. C., Carvalho G.S., Matias M.S., 1999. Some neotectonic indicators in quarternary formations of the northwest coastal zone of Portugal. *Physics and Chemistry of the Earth*, Part A: Solid Earth and Geodesy 24(4): 323-336.

Hayes M.O., 1975. Morphology of sand accumulations in estuaries. *In*: Cronin L.E. (Ed.), *Estuarine Research*, vol. 2. Academic Press, New York, 3-22.

Harms J.C., Southard J.B., Spearing D.R., Walker R.G., 1975. Depositional environments as interpreted from primary sedimentar structures and stratification sequences. Society of economic paleontologists and mineralogists Short Course 2, 161 p.

Harris P.T., 1988. Large-scale bedforms as indicators of mutually evasive sand transport and the sequential infilling of wide-mouthed estuaries. *Sedimentary Geology* 57, 273-298.

Henriques V., Mendes B., Pinheiro L.M., Gonçalves D.S., Long D., 2012. MeshAtlantic - Recommended Operational Guidelines (ROG) for Sidescan Sonars. Version 3.0, 26p. (http://www.meshatlantic.eu/ assets/files/ROGS/MeshA ROG Sidescan Sonar.pdf).

Hesp P.A., Hilton M.J., 1996. Nearshore-surfzone system limits and the impact of sand extraction, J. Coast. Res. 12(3): 726–747. *In* Roos C.P., 2004. Seabed pattern dynamics and offshore sand extraction. PhD Thesis. University of Twente, 166p.

Hitchcock D., Bell S., 2004. Physical Impacts of Marine Aggregate Dredging on Seabed Resources in Coastal Deposits. *Journal of Coastal Research*, vol. 20, No. 1, 101-114.

Hoogewoning S.E., 2000. PUTMOR-field measurements. A six month measuring campaign at a lowered dumping pit near Hoek van Holland, Work document RIKZ/OS-2000.132x, RIKZ, Den Haag, The Netherlands. *In* Roos C.P., 2004. Seabed pattern dynamics and offshore sand extraction. PhD Thesis. University of Twente, 166p.

Hoogewoning S.E., Boers M., 2001. Fysische effecten van zeezandwinning, Report RIKZ-2001.050, RIKZ, Den Haag, The Netherlands. *In* Roos C.P., 2004. Seabed pattern dynamics and offshore sand extraction. PhD Thesis. University of Twente, 166p.

Huvenne V.A., Blondel P., Henriet J.P., 2002. Textural analysis of sidescan sonar imagery from two mound provinces in the Porcupine Seabight. *Marine Geology* 189, 323–341.

IH, 1985. Carta dos Sedimentos Superficiais do Cabo de S. Vicente ao Rio Guadiana, Instituto Hidrográfico, Escala 1:150000, 1ª Edição.

IH, 1994. Final report of sub-project "Wind wave climatology of the portuguese coast". Instituto Hidrográfico de Portugal. 6/94-A, 78p.

IHO, 2005. Manual on Hydrography, International Hydrographic Organization - Publication M-13, 1st Edition, 482p.

Inman DL. 1952. Measures for describing the size distribution of sediments. Journal of Sedimentary Petrology 22: 125–145.

Inman D.L., 1957. Wave-generated ripples in nearshore sands. Beach Erosion Board, Technical Memorandum 100.

Jones J., 1999. Marine Geophysics, Willey, 466p.

Kenny A.J., Todd B.J., Cooke R., 2001. Procedural Guideline No. 1-4: The application of sidescan sonar for seabed habitat mapping. *In* Davies, J., Baxter, J., Bradley M., *et al.* (Eds), Natura 2000 Marine Monitoring Handbook. Joint Nature Conservation Committee, Peterborough, UK, 199-210.

Kenyon N.H., Cooper B., 2005. Sand banks, sand transport and offshore wind farms. Technical Report, 106p.

Kojima H., Ijima T., Nakamuta T., 1987. Impact of offshore dredging on beaches along the Genkai Sea, Japan, Coastal Engineering '86, ASCE, Taipeh, Taiwan, pp. 1281–

1295. *In* Roos C.P., 2004. Seabed pattern dynamics and offshore sand extraction. PhD Thesis. University of Twente, 166p.

Komar, P.D. 1976. Beach processes and sedimentation. Prentice-Hall, Englewood Cliffs, N.J., 417p.

Kubicki A., Manso F., Diesing M., 2007. Morphological Evolution of Gravel and Sand Extration Pits, Tromper Wiek, Baltic Sea. *Estuarine Coastal and Shelf Science*, vol. 71, 647-656.

Kruger J.C., Healy T.R., 2006. Mapping the morphology of a dredged ebb tidal delta, Tauranga Harbour, New Zealand. *Journal of Coastal Research*, 22(3), 720–727.

Krumbein W.C., 1934. Size frequency distributions of sediments. *Journal of Sedimentary Petrology*, 4, 65–77.

Krumbein W.C., 1938. Size frequency distribution of sediments and the normal phi curve. *Journal of Sedimentary Petrology* 8: 84–90.

Krumbein W.C., Pettijohn F.J., 1938. Manual of Sedimentary Petrography. Appleton-Century-Crofts: New York.

Kullberg J.C., Pais J., Manuppella G., 1992. Aspectos gerais da tectónica alpina no Algarve. *Ciências da Terra*, Lisboa, 11, 293-302.

Kullberg J.C., Rocha R.B., Soares A.F., Rey J., Terrinha P., Azerêdo A.C., Callapez P., Duarte L.V., Kullberg M.C., Mrtins L., Miranda R., Alves C., Mata J. Madeira J., Mateus O., Moreira M., Nogueira C.R., 2013. A Bacia Lusitaniana: Estratigrafia, Paleografia e Tectónica, 195- 347. *In* Dias R., Araújo A., Terrinha P., Kullberg J.C., 2013. Geologia de Portugal, Vol. II – Geologia Meso-cenozóica de Portugal, 798 p.

Lafferty B., Quinn R., Breen C., 2006. A side-scan sonar and high-resolution Chirp sub-bottom profile study of the natural and anthropogenic sedimentary record of Lower Lough Erne, northwestern Ireland. *Journal of Archaeological Science*, 33(6), 756–766.

Le Bas T., Huvenne V., 2009. Acquisition and processing of backscatter data for habitat mapping – Comparison of multibeam and sidescan systems. *Applied Acoustics* 70, 1248-1257.

Li F., Roncevich L., Bicknell C., lowry R., Ilich K., 2009. Storm waves and their temporal and directional distribution, Perth, 1994-2008. *Coastal Conference 2009* – 5th Western Australian State.

Lopes J.F., Dias J.M., 2007. Residual circulation and sediment distribution in the Ria de Aveiro lagoon, Portugal. *Journal of Marine Systems*, 68(3-4), 507–528. doi:DOI: 10.1016/j.jmarsys.2007.02.005.

Lopes J.F., Dias J.M., Dekeyser I., 2006. Numerical modelling of cohesive sediments transport in the Ria de Aveiro lagoon, Portugal. *Journal of Hydrology*, 319(1-4), 176–198. doi:DOI: 10.1016/j.jhydrol.2005.07.019.

Lopes V., Silva P.A., Bertin X., Fortunato A., Oliveira A., 2009. Impact of a Dredged Sandpit on Tidal and Wave Hydrodynamics. *Journal of Coastal Research*, SI56, 529-533.

Louisiana Oil Spill Coordinator's Office (LOSCO), 1999. Color Infrared Orthophoto, Date of Source Image Aerial Photography, 24-Jan-1998. *In* Bender C. J., Dean R. G., 2003. Wave field modification by bathymetric anomalies and resulting shoreline changes: a review with recent results. *Coastal Engineering*, 49, 125–153.

Lurton X. (2002): An introduction to underwater acoustics - Principles and applications. Springer, London, 347p.

Lurton X., DeRuiter S., 2011. Sound Radiation of Seafloor-Mapping Echosounders in the Water Column, in Relation to the Risks Posed to Marine Mammals. International Hydrographic Review – Bureau, Monaco, 7-17.

Magalhães F, 1999. Os Sedimentos da Plataforma Continental Portuguesa: Contrastes Espaciais, Perspectiva Temporal, Potencialidades Económicas. Tese de Doutoramento, Universidade de Lisboa, Lisboa, 289 p.

Magalhães, F. 2003. Aggregate Deposits in the Portuguese Continental Shelf. *Thalassas*, 19(2), 23-31.

Magalhães F., Ângelo C., Taborda R., 2004. Towards the Adoption of Adequate Coastal Protection Strategies in Portugal. *Thalassas*, 20(2), 23-29.

MAGIS (n.d.). www.sandandgravel.com/extraction. *In* Roos C.P., 2004. Seabed pattern dynamics and offshore sand extraction. PhD Thesis. University of Twente, 166p.

Manso M.D., Dias J.M., Macedo F., 1996. Aplicación de un modelo de cadenas de Markov de primero y Segundo orden, *Avances en Geofísica y Geodesia*, 1(1), 151-157.

Manuppella G., 1992. Carta Geológica da Região do Algarve, escala 1/100 000, Notícia Explicativa. Serv. Geol. Port., Lisboa, 15.

Manuppella G., Rodrigues A., Bartolomeu A., Leal S.G., Ramalho M.M., Rocha R., Marques B., Telles Antunes M., Pais J., Rey J., 1985. Carta Geológica de Portugal, Folha 53-A, Faro (escala 1: 50 000). Serviços Geológicos de Portugal – Direcção Geral de Geologia e Minas; 52p.

Manuppella G., Ramalho M.M., Telles Antunes M., Pais J., 1987. Notícia Explicativa da Folha 53-A, Faro (escala 1: 50 000). Serviços Geológicos de Portugal – Direcção Geral de Geologia e Minas.

Marques F.M., 1997. Sea cliff evolution: the importance of quantitative studies for hazard and risk assessment, and for planning of coastal areas. Colectânea de Ideias Sobre a Zona Costeira de Portugal EUROCOAST, Portugal 67–86.

Martins C., 2012. A Barra da Laguna de Aveiro no Século XIX: Impactos da Ação Antrópica na Dinâmica Lagunar. Universidade do Porto, 165p.

Martins V., Rodrigues S., Grangeia C., Bernardes C., Silva P., Dias J.M., Rocha F., 2007. Sediments erosion/deposition in the Ria de Aveiro inlet. Book of Abstracts ISMS07, *International Symposium in Marine Sciences*, Valência, Spain, 28–31 March, p 142.

Martins V., Grangeia C., Abrantes I., Jesus C., Dias J.M., Silva P.A., Rocha F., 2011. Sediments flux through the Aveiro harbour jetties : Patterns of accretion and erosion. *Journal of Coastal Research*, (64), 1784–1787.

Martins V., Abrantes I., Grangeia C., Martins P., Nagai R., Sousa S.H.M., Rocha F., 2012. Records of sedimentary dynamics in the continental shelf and upper slope between Aveiro–Espinho (N Portugal). *Journal of Marine Systems*, 96–97(0), 48–60. doi:10.1016/j.jmarsys.2012.02.001.

Matos M.L., 1990. Um estudo do balanço de sal num estuário de costa plana. *Rec. Hídricos* 10: 13-21.

Mazel C., 1985. Side Scan Sonar training manual. New York, Klein Associates. Inc. Undersea Search and Survey. 144p.

McCammon RB. 1962. Efficiencies of percentile measures for describing the mean size and sorting of sedimentary particles. *Journal of Geology* 70: 453–465.

McLaren P., Bowles D., 1985. The effects of sediment transport on grain size distributions. *Journal of Sedimentary Petrology*, Vol. 55, n. 4, 457-470.

McManus J. 1988. Grain size determination and interpretation. *In* Techniques in Sedimentology, Tucker M (ed.). Blackwell: Oxford; 63–85.

McMullen K.Y., Poppe L.J., Denny J.F., Haupt T.A., Crocker J.M., 2008. Sidescan-Sonar Imagery and Surficial Geologic Interpretations of the Sea Floor in Central Rhode Rhode Island Sound. U.S. Geologiacal Survey (USGS), 26p.

Miall A.D., Principles of Sedimentary Basin Analysis. Springer-Verlag, 2nd Edition. 668p.

Middleton GV. 1976. Hydraulic interpretation of sand size distributions. *Journal of Geology* 84: 405–426.

Miller M.C., Komar P.D., 1980. A field investigation of the relationship between oscillation ripple spacing and the near-bottom water orbital motion. *Journal of Sedimentary Petrology*, 50, 183-191.

Mogridge G.R., Kamphuis J.W., 1972. Experiments on bedform generation by wave action. *Proceedings 13th Conference on Coastal Engineering*, ASCE, 1123-1142.

Moita I., 1986. Notícia explicativa da carta dos sedimentos superficiais da plataforma. Folha SED 7 e 8. Cabo de São Vicente ao Rio Guadiana. Instituto Hidrográfico de Portugal, 17p.

Moura D., Boski T, 1999. Unidades litostratigráficas do Pliocénico e Plistocénico no Algarve. Comunicações do Instituto Geológico e Mineiro, 86, 85-106.

MOP, 1951. Regime das embocaduras lagunares e o problema do melhoramento da Barra de Aveiro. Ministério das Obras Públicas : Direcção-Geral dos Serviços Hidráulicos, Lisboa, 150 p.

Moreira H.M., Queiroga H., Machado M.M., Cunha, M.R., 1993. Environmental gradientes in a southern estuarine system: Ria de Aveiro, Portugal, implication for soft bottom macrofauna colonization. *Netherlands Journal of Aquatic Ecology* 27, 465-482.

Neto A.A., 2001. Uso da Sísmica de Reflexão de Alta Resolução e da Sonografia na Exploração Mineral Submarina. *Brazilian Journal of Geophysics*, 18, 16.

Neves F., 1935. Breve História da Barra de Aveiro. Arquivo distrital de Aveiro, vol. I, 219-238.

Nickless E.P., 1973. The sand and gravel resources of the country around Hethersett. In: Assessment of British Sand and Gravel Resources no. 5. Inst. Geol. Sciences 73 (4): 100 p.

Nishimura C.E., 1997. Fundamentals of Acoustic Backscatter Imagery. Washington DC: Naval Research Laboratory, 67p.

O'Donoghue T., Clubb G.S., 2001. Sand ripples generated by regular oscillatory flow. *Coastal Engineering*, 44, 101-115.

Off T., 1963. Rhythmic linear sand bodies caused by tidal current. *Bulletin of the American Association of Petroleum Geologists*, 47(2), 324-341.

Oliveira, J.T., 1990. Part IV. South-Portuguese Zone: stratigraphy and synsedimentary tectonism. In: Dallmeyer, R.D., Martinez Garcia, E. (Eds.), Pre-Mesozoic Geology of Iberia. Springer-Verlag. 416 pp.

Oliveira J., Pereira E., Ramalho M., Antunes M., Monteiro J. (Coord.). 1992. Carta Geológica de Portugal. Escala 1/500000; Serv. Geol. Portugal.

Osborne P.D., Vincent C.E., 1993. Dynamics of large and small scale bedforms on a macrotidal shoreface under shoaling and breaking waves. *Marine Geology*, 115, 207-226.

Otto GH. 1939. A modified logarithmic probability graph for the interpretation of mechanical analyses of sediments. *Journal of Sedimentary Petrology* 9: 62–75.

Pacheco A., Carrasco A.R., Vila-Concejo A., Ferreira O., Alveirinho Dias J.M. 2007. A coastal management program for channels located in backbarrier systems. *Ocean & Coastal Management* 50 (1-2), 119-143.

Pais J., Legoinha P., Elderfield H., Sousa L., Estevens M., 2000. The Neogene of Algarve (Portugal). Ciências da Terra, 14, 277-288.

Pais J., Cunha P.P., Pereira D., Legoinha P., Dias R., Moura D., Brum da Silveira A., Kullberg J.C., González-Delgado J.A., 2012. The Paleogene and Neogene of Western Iberia (Portugal): A Cenozoic Record in the European Atlantic Domain. Springer, Berlin.

Palain, C., 1976. Une série détritique terrigène. Les Grés de Silves. Trias et Lias inférieur du Portugal. Memória N°25 (Nova Série) dos Serviços Geológicos de Portugal. 411 pp.

Pattiaratchi C., Collins M., 1987. Mechanisms for linear sand- bank formation and maintenance in relation to dynamical oceanographic observations, *Progress in Oceanography* 19, 117–176.

Peliz Á., Rosa T.L., Miguel A., Santos P., Pissarra J.L., 2002. Fronts, jets, and counter-flows in the Western Iberian upwelling system. *J. Mar. Syst*. 35, 61–77. doi:10.1016/S0924- 7963(02)00076-3.

Pessanha L.E., Pires H.O., 1981. Elementos sobre o clima de agitação marítima na costa sul do Algarve. Instituto Nacional de Meteorologia e Geofísica, Lisbon, Portugal, 66p.

Pianca C., Holman R., Siegle E., 2014. Mobility of meso-scale morphology on a microtidal ebb delta measured using remote sensing. *Marine Geology*, 357, 334–343.

Pinheiro L.M., Teixeira F.C., Gonçalves D.S., Pereira L.A., Ribeiro T. 2011. "Métodos geofísicos para a prospecção de agregados na plataforma continental e operações de dragagem em áreas portuárias". *In* Dragagens - Fundamentos, Técnicas e Impactos. Coelho C., Silva P., Pinheiro L.M., Gonçalves D.S. (Eds). 121-152.

Pires H.N., 1985. Alguns aspectos do clima de agitação marítima de interesse para a navegação na costa de Portugal. *O Clima de Portugal*, 37, 34 p.

Pires, H.O., 1998. Project INDIA, Preliminary report on Wave Climate at Faro. Lisbon, Instituto de Meteorologia, 36pp.

Plecha S., 2011. Contribution to the Study of the Ria de Aveiro Inlet Morphodynamics. PhD Thesis, University of Aveiro, 140p.

Plecha S., Silva P.A., Oliveira A., Dias J.M., 2009. Sediment Transport Modelling and Morphological Trends at a Tidal Inlet. *In* A. J. Manning (Ed.), Sediment Transport in Aquatic Environments, 163-186.

Plecha S., Silva P.A., Vaz N., Bertin X., Oliveira A., Fortunato A.B., Dias J.M., 2010. Sensitivity analysis of a morphodynamic modelling system applied to a coastal lagoon inlet. *Ocean Dynamics*, *60*(2), 275–284. doi:10.1007/s10236-010-0267-5.

Powell M.A., Thieke R.J., Mehta A.J., 2006. Morphodynamic relationships for ebb and flood delta volumes at Florida's tidal entrances. *Ocean Dynamics*, 56(3-4), 295–307.

Quaresma V.S., Dias G.T., Neto J.B., 2000. Caracterização da ocorrência de padrões de sonar de varredura lateral e sísmica de alta frequência (3.5 e 7.0 kHz) na porção sul sul da Baía de Guanabara. *Brazilian Journal of Geophysics*, 18(2):201-214.

Quinn R., Dean M., Lawrence M., Liscoe S., Boland D., 2005. Backscatter responses and resolution considerations in archaeological side-scan sonar surveys: a control experiment. *Journal of Archaeological Science*, 32, 1252-1264.

Ramos M., Silva P.A., Sancho F., 2005. Morphological modelling using a 2DH model. In: Van Rijn L., Soulsby R., Hoekstra P. and Davies A.G. (eds.). SANDPIT – Sand

Transport and Morphology of Offshore *Sand Mining Pits*. Aqua Publications, The Netherlands, ISBN 90-800356-7-X, AT 1-10.

Rebelo J.E., 1992. The ichthyofauna and abiotic hydrological environment of the Ria de Aveiro, Portugal, *Estuaries and Coasts* 15(3): 401-413.

Rey J., 1983. Le Crétacé de l'Algarve: Essai de synthèse. Com. Serv. Geol. Portugal, Serviços Geológicos de Portugal, Lisboa, vol. t.69, f.1.

Ribeiro C., Terrinha P., 2007. Formation, deformation and chertification of systematic clastic dykes in a differentially lithified carbonate multilayer. SW Iberia, Algarve Basin, Lower Jurassic. Sedimentary Geology, 196, 201-215.

Ridderinkhof W., Hoekstra P., van der Vegt M., de Swart H.E., 2016. Cyclic behavior of sandy shoals on the ebb-tidal deltas of the Wadden Sea. *Continental Shelf Research*, 115, 14–26.

Riddy P., Masson D.G., 1996. The Sea Floor - Exploring a Hidden World. *In* Summerhayes, C.P., Thorpe, S.A. (Eds.) Oceanography: an Illustrated Guide. London, UK: Manson Publishing.

Ris R.C., L.H. Holthuijsen, Booij N., 1999. A third-generation wave model for coastal regions 2. Verification. *Journal of Geophysical Research*. 104 (C4): 7667-7681.

Robinson A.H., 1975. Cyclic Changes in Shoreline Development at the Entrance to Teignmouth Harbour, Devon, England. John Wiley & Sons, London, UK, pp. 181–200.

Roos C.P., 2004. Seabed pattern dynamics and offshore sand extraction. PhD Thesis. University of Twente, 166p.

Roos C.P., Hulscher S.H., de Vriend H.J., 2008. Modelling the Morphodynamic Impact of Offshore Sandpit Geometries. *Coastal Engineering*, vol. 55, 704-715.

Rocha F.T., 1993. Argilas Aplicadas a Estudos Litoestratigráficos e Paleoambientais na Bacia Sedimentar de Aveiro. PhD thesis, Universidade de Aveiro, Portugal, 399 p.

Rocha F., Gomes C., 1995. Palaeoenvironment of the Aveiro region of Portugal during the Cretaceous, based on clay mineralogy. *Cretaceous Research*, 16, 187-194.

Rocha F.; Bernardes C., Delgado H., 2000. Caracterização textural e mineralógica dos sedimentos da laguna de Aveiro, Portugal. *3º Simp. Margem Contin. Atlant. Ibérica* , Univ. Algarve, Faro, 17-18p.

Roque C., Hernández-Molina F. J., Lobo F., Somoza L., Díaz-del-Río V., Vázquez J. T., Dias J., 2010. Geomorphology of the Eastern Algarve proximal continental margin

(South Portugal, SW Iberia Peninsula): sedimentary dynamics and its relationship with the last asymmetrical eustatic cycle. *Ciências da Terra*, 17, 7-28.

Rosa F., Rufino M.M., Ferreira Ó., Matias A., Brito A.C., Gaspar M.B., 2013. The influence of coastal processes on inner shelf sediment distribution: The Eastern Algarve Shelf (Southern Portugal). *Geologica Acta*, 11(1), 59–73. doi:10.1344/ 105.000001755.

Rosa T.L., Barata A., Cabaço J. G., Teles M., 2012. Interventions to Dredge the Aveiro Bar (Portugal) and Improve Protection of the Coastal Area to the South. *Journal of Integrated Coastal Zone Management*, 12(1), 57–75. doi:10.5894/rgci286.

Rosa J., Gonçalves D.S., Silva P.A., Pinheiro L.M., Rebêlo L., Fortunato A., Bertin X., 2011a. Estudo da Evolução de uma Área de Extracção de Sedimentos ao largo de Vale do Lobo (Algarve Portugal) - Comparação entre Dados Numéricos e Dados Batimétricos Adquiridos. *Revista de Gestão Integrada / Journal of Integrated Coastal Zone Management*, 369-377.

Rosa J., Silva P.A., Bertin X., Fortunato A.B., 2011b. Waves, wind and tidal forcing on a sandpit morphodynamics. *Journal of Coastal Research*, SI64, 1170-1174.

(Rosa and Silva, personal communication, 2012)

Saha S., Moorthi S., Pan H., Wu X., Wang J., Nadiga S., Tripp P., Kistler R., Wollen J., Behringer D., Liu H., Stokes D., Grumbine R., Gayno G., Wang J., Hou Y., Chuang H., Juang H., Sela J., Iredell M., Treadon R., Kleist D., VanDelst P., Keyser D., Derber J., Ek M., Meng J., Wei H., Yang R., Lord, S., van den Dool H., Kumar A., Wang W., Long C., Chelliah M., Xue Y., Huang B., Schemm J., Ebisuzaki W., Lin, R., Xie P., Chen M., Zhou S., Higgins W., Zou C., Liu Q., Chen Y., Han Y., Cucurull L., Reynolds R., Rutledge G., Goldberg M. 2010. The NCEP climate forecast system reanalysis. *Bulletin of the American Meteorological Society* 91, 1015–1057.

Santos F.D., Lopes A.M., Moniz G., Ramos L., Taborda R., 2014. Gestão da zona costeira - o desafio da mudança. Retrieved from http://www.apambiente.pt /_zdata/DESTAQUES/2015/GTL_Relatorio Final_20150416.pdf (last version Novembro de 2015)

SeaBeam Instruments, 2000. Multibeam Sonar Theory of Operation, L-3 Communications SeaBeam Instruments, 107 p. http://www.ldeo.columbia .edu/res/pi/MB-System/sonarfunction/ SeaBeamMultibeamTheoryOperation.pdf

Seippel R., 1983. “Transducers, Sensors and Detectors”, Prentice-Hall.

Sherman D.J., Greenwood B., 1984. Boundary roughness and bedforms in the surf zone. *In* Greenwood B., Davis R.A. Jr. (Eds.), Hydrodynamics and Sedimentation in Wave-dominated Coastal Environments. Developments in Sedimentology 39, Elsevier, Amsterdam, 199-218.

Silva P.A., Ramos M., Almeida M., Dubert J., 2006. Water exchange mechanisms between Ria de Aveiro and the Atlantic Ocean. *Journal of Coastal Research* SI39, 1622-1626.

Silva P.A., 2011. Impactos da Exploração de Inertes na Plataforma Continental. *In* Dragagens - Fundamentos, Técnicas e Impactos. Coelho C., Silva P., Pinheiro L.M., Gonçalves D.S. (Eds), 279p.

Soulsby R., 1997. Dynamics of marine sands, a manual for practical applications. Thomas Telford, ISBN 0-7277-2584X, HR. Wallingford, England.

Spencer D., 1963. The interpretation of grain size distribution curves of clastic sediments. Journal of Sedimentary Petrology, 33, 180-190.

Stewart R. 2009. Our Ocean Planet, Oceanography in the 21st Century – An Online Textbook (http://oceanworld.tamu.edu/resources/oceanography-book/coastalzone.htm).

Stive M.J., De Schipper M., Luijendijk A., Ranasinghe R., van Thiel de Vries J., Aarninkhof S., Marx S., 2013. The Sand Engine: A Solution for Vulnerable Deltas in the 21st Century? *Coastal Dynamics*, 1537–1546.

Svašek J.N., 1965. Gedrag van een proefsleuf in de bodem van de Noordzee te Scheveningen, Report K-272, Rijkswaterstaat - Deltadienst, waterloop- kundige afdeling. *In* Roos C.P., 2004. Seabed pattern dynamics and offshore sand extraction. PhD Thesis. University of Twente, 166p.

Svašek J.N., 2001a. PUTMOR - field measurements at a temporary sand pit, part 1: processing and validation, Report 01037/1177, Svašek b.v. *In* Roos C.P., 2004. Seabed pattern dynamics and offshore sand extraction. PhD Thesis. University of Twente, 166p.

Svašek J.N., 2001b. PUTMOR - field measurements at a temporary sand pit, part 2: data analysis, Report 01244/1177, Svašek b.v. *In* Roos C.P., 2004. Seabed pattern dynamics and offshore sand extraction. PhD Thesis. University of Twente, 166p.

Svašek J.N., 2001c. PUTMOR - field measurements at a temporary sand pit, part 3: final report, Report 01453/1177, Svašek b.v. *In* Roos C.P., 2004. Seabed pattern dynamics and offshore sand extraction. PhD Thesis. University of Twente, 166p.

Swales A., Oldman J.W., Smith K., 2006. Bedform geometry on a barred sandy shore, *Marine Geology*, 226, 243-259.

Swift D.J., 1975. Tidal sand ridges and shoal-retreat massifs. Marine Geology 18, 105–134.

Swift D.J., Phillips S., Thorne J.A., 1991. Sedimentation on continental margins IV: Lithofacies and depositional systems. *In*: Swift D.J., Tillman R.W., Oertel G.F., Thorne J.A. (Eds.), Shelf Sands and Sandstone Bodies: Geometry, Facies and Sequence Stratigraphy, International Association of Sedimentologists Special Publication, 14, 89-152.

Taborda R. 1999. Modelação da dinâmica sedimentar na plataforma continental portuguesa. PhD Thesis, Univ. of Lisbon, 366p. (not published).

Teixeira C., Zbyszewski G., 1976. Carta Geológica de Portugal 1:50 000 - Notícia Explicativa da folha 16-A – Aveiro; Serviços Geológicos de Portugal.

Teixeira S.B., 1994. Dinâmica Morfosedimentar da Ria de Aveiro (Portugal). University of Lisbon, Ph.D. Thesis, 396p.

Teixeira S.B., 2006. Slope mass movements on rocky sea-cliffs: A power-law distributed natural hazard on the Barlavento Coast, Algarve, Portugal. Continental Shelf Research, 26, 1077-1091.

Teixeira S.B., 2011. Alimentação Artificial de Praias com Dragados no Algarve. In: Coelho C., Silva P.A., Pinheiro L.M. and Gonçalves D.S. (eds), Dragagens - Fundamentos, Técnicas e Impactos. Universidade de Aveiro, Lusoimpress, 221-240.

Teixeira S.B., Rosa M., 2009. Alimentação artificial da praia do troço costeiro Forte-Novo-Garrão (Loulé). Projecto de Execução. Administração da Região Hidrográfica do Algarve, Faro. 31p.

Terrinha P., 1998. Structural Geology and Tectonic Evolution of the Algarve Basin, South Portugal. PhD dissertation. Imperial College, London, 430 p.

Terrinha P., Coward M.P., Ribeiro A., 1990. Salt tectonics in the Algarve Basin: the Loulé diapir. *Comunicações dos Serviços Geológicos de Portugal* t.76, 33–40.

Trask P.D., 1932. Origin and Environment of Source Sediments of Petroleum. Gulf Publishing Company: Houston.

Turker M., 1982. The Field Description of Sedimentary Rocks. Geological Society of London Handbook Series.Open University, 112p.

Vanney J.R., Mougenot D., 1981. La plate-forme continentale du Portugal et les provinces adjacentes: analyse géomorphologique. *Mem. Serv. Geol. Port*. 28 145 p.

Vicente C.M., Uva L.P., 1984. Sedimentation in dredged channels and basins, prediction of shoaling rates. *In* Edge B.L. (Ed.), Coastal Engineering 1984 — Conference: Proceedings of the International Conference on Coastal Engineering. World Scientific, ASCE - American Society of Civil Engineers, New York, NY, U.S.A.. ISBN: 9780872624382, 1863–1878.

Walstra D., Chesher T., Davies A., Ribberink J., Sergent P., Silva P.A., Vittori G., Walther R., van Rijn L.C., 2005. Intercomparison of the state of the morphological models. In van Rijn, L., Soulsby, R., Hoekstra, P., Davies, A.G. (Eds.) SANDPIT – Sand Transport and Morphology of Offshore Sand Mining Pits. Aqua Publications, The Netherlands, ISBN 90-800356-7-X, AY 1-23.

Wang Y.H., Tang L.Q., Wang C.H., Liu C.J., Dong Z., 2014. Combined effects of channel dredging, land reclamation and long-range jetties upon the long-term evolution of channel-shoal system in Qinzhou bay, SW China. *Ocean Engineering*, 91, 340–349.

Tolman H.L., 2009. User Manual and System Documentation of WAVEWATCH III Version 3.14. Tech. Note 276, NOAA/NWS/NCEP/MMAB, 220 pp.

Uda T., Takahashi A., Fujii M., 1995. Bar topography changes associated with a dredged hole off the Nivodo River mouth, Coast. Eng. Jap. 38(1): 63– 89. *In* Roos C.P., 2004. Seabed pattern dynamics and offshore sand extraction. PhD Thesis. University of Twente, 166p.

Udden J.A., 1914. Mechanical composition of clastic sediments. Bulletin of the Geological Society of America, 25, 655-744.

Urick R.J., 1983. Principles of Underwater Sound. 3rd edition: McGraw Hill, 423p.

USGS, 2014. WHSC Sidescan Sonar systems. U.S. Geological Survey. http://woodshole.er.usgs.gov/operations/sfmapping/sonar.htm.

van Dalfsen J.A., Essink K., 1997. Risk analysis of coastal nourishment techniques (RIACON), Report RIKZ-97.022, National Institute for Coastal and Marine Management, Den Haag, The Netherlands. *In* Roos C.P., 2004. Seabed pattern dynamics and offshore sand extraction. PhD Thesis. University of Twente, 166p.

Van Dalfsen J.A., 1998. Long-term effects of subaqueous sand extraction north of the island of Terschelling, Report RIKZ-98.034, National Institute for Coastal and Marine Management, Den Haag, The Netherlands. *In* Roos C.P., 2004. Seabed

pattern dynamics and offshore sand extraction. PhD Thesis. University of Twente, 166p.

van de Graaff J., van Overeem J., 1979. Evaluation of sediment transport formulae in coastal engineering practice. *Coastal Engineering* 3:1–32

van der Werf J., Ebbe J., Ribberink J.S., O'Donoghue T., Doucette J.S., 2006. Modelling and measurement of sand transport processes over full-scale ripples in oscillatory flow. *Coastal Engineering*, 53, 657-673.

van Rijn L., Walstra, D.J., 2002. *Morphology of Pits, Channels and Trenches. Part I: Literature Review and Study Approach*. Report Z3223, WL Delft Hydraulics.

van Rijn L., Soulsby R., Hoekstra P., Davies A.G., 2005. SANDPIT, Sand Transport and Morphology of Offshore Mining Pits. Aqua Publications, The Netherlands, 156p.

Vanney J.R., Mougenot D., 1981. La plate-forme continentale du Portugal et les provinces adjacentes: analyse géomorphologique. *Mem. Serv. Geol. Port*. 28, 145 p.

Vaz L., 2012. Hydrodynamic study of the wave effect in the Aveiro inlet. University of Aveiro, 64p.

Vaz N., Dias J.M., 2008. Hydrographic characterization of an estuarine tidal channel. *Journal of Marine Systems*, 70(1-2), 168–181. doi: DOI: 10.1016/j.jmarsys.2007.05.002.

Vicente C.M., 1990. Evolução costeira devida a obras portuárias: casos da praia da Figueira da Foz e da embocadura da Ria de Aveiro. Actas do 1º Simpósio sobre a Protecção e Revalorização da Faixa Costeira do Minho ao Liz, Porto, 164-177.

Vicente C., Clímaco M., 1986. Analysis of the evolution of Figueira da Foz beach. Report 106/86 –NET, LNEC, Lisboa, 51p.

Visher GS., 1969. Grain size distributions and depositional processes. *Journal of Sedimentary Petrology* 39: 1074–1106.

Wentworth C.K., 1922. A scale of grade and class terms for clastic sediments. Journal of Geology, 30, 377-392.

White J., Jegat V., Lancker V., Deleu S., Vanstaen K., 2007. Multibeam Echo Sounders *In* Review of Standards and Protocols for Seabed Habitat Mapping. Coggan R., Populus J., White J., Sheehan K., Fitzpatrick F., Piel S. (eds.), MESH, 210 pp.

Wilson R.L., 1988. Mesozoic Development of the Lusitanian Basin, Portugal. *Rev. Soc. Geol. Espanha*, *I* (3-4), 394–407.

Wilson R.C., Hiscott R.N., Willis M.G., Gradstein F.M., 1989. The Lusitanian basin of west-central Portugal: Mesozoic and Tertiary tectonic, stratigraphy and subsidence history. *AAPG Memoir*, 46, 341-361.

Xu W., 1998. Signal Direction-of-Arrival and Amplitude Estimation for Multiple-Row Bathymetric Sidescan Sonars. Master Massachusetts Institute of Technology and Woods Hole Oceanographic Institution, 88p.

Zhang K.Q., Douglas B.C., Leatherman S.P., 2000. Twentieth-century storm activity along the US east coast. *Journal of Climate* 13 (10), 1748-1761.

Zhang Y., Baptista A.M., Myers E.P., 2004. A cross-scale model for 3D baroclinic circulation in estuary-plume-shelf systems: I. Formulation and skill assessment. *Continental Shelf Research* 110 (10), 1431-1456.

Appendix I. Paper published

Coastal Engineering 88 (2014) 75–87

Contents lists available at ScienceDirect

Coastal Engineering

journal homepage: www.elsevier.com/locate/coastaleng

Morphodynamic evolution of a sand extraction excavation offshore Vale do Lobo, Algarve, Portugal

D.S. Gonçalves [a,b,*], L.M. Pinheiro [a,b], P.A. Silva [a,c], J. Rosa [a,c], L. Rebêlo [d], X. Bertin [e], S. Braz Teixeira [f], R. Esteves [g]

[a] CESAM, University of Aveiro, Campus de Santiago, 3810-193 Aveiro, Portugal
[b] Geosciences Department, University of Aveiro, Campus de Santiago, 3810-193 Aveiro, Portugal
[c] Physics Department, University of Aveiro, Campus de Santiago, 3810-193 Aveiro, Portugal
[d] Geology, Hydrogeology and Coastal Geology Unit, National Laboratory of Energy and Geology — LNEG, I.P., P.O. Box 7586, 2611-901 Amadora, Portugal
[e] UMR 7266 LIENSs, CNRS-La Rochelle University, France
[f] Portuguese Environment Agency/ARH Algarve, Rua do Alportel, n° 10, 2°, 8000-293 Faro, Portugal
[g] Hydrographic Institute, Division of Oceanography, Rua das Trinas, 49, 1249-093 Lisboa, Portugal

ARTICLE INFO

Article history:
Received 30 October 2013
Received in revised form 31 January 2014
Accepted 5 February 2014
Available online xxxx

Keywords:
Offshore sand extraction
Morphodynamics
Sandpit evolution
Recovery rate
Storm events

ABSTRACT

Offshore sand and gravel extraction for aggregates and beach nourishment is an important economic activity and has been a common practice in various countries worldwide for many years. The evolution of a sandpit, in particular its migration and rate of replenishment, depends strongly on the type of sediments involved, and on the physical and hydrodynamic characteristics of the surrounding area. In order to fully assess the associated impacts on local ecosystems and on the neighboring coastline morphology it is essential to make accurate predictions of the excavation recovery times. For this purpose it is fundamental to investigate areas where there is an adequate observational control of the evolution of the sandpit, prior and after the excavation, to properly calibrate existing numerical models with observations and fully evaluate their prediction adequacy. The present work investigates the evolution of an offshore sandpit located off Vale do Lobo, Algarve, Portugal, within a time span of four years (2006–2010), based on 4 bathymetric surveys, prior to and after the dredging operations, complemented with the analysis of wave data and numerical modeling simulations. The bathymetric data were used to evaluate the morpho-sedimentary evolution and to calculate the sediment volume changes. The results show an infill of approximately 17% of the initial exploration pit in the first 4 years, with an overall smoothing of the initial excavation bottom topography. Observations combined with modeling results demonstrate that the pit evolution depends mainly on storm events, since it is essentially during these periods that there is a significant sediment movement at the site water depth. Based on (1) the predicted number of stormy days for the forthcoming years, assuming that (2) the yearly average of such events in the past 57 years is representative, and considering (3) a decrease of the sandpit recovery rate in time, predicted by models and observations, it was possible to estimate that the Vale do Lobo sandpit recovery period is of ca. 38 years for its full, or near full, replenishment.

1. Introduction

The offshore extraction of sediments from coastal areas has been a common practice in many countries for many years, and it has become, in some places, the main source of aggregates for beach nourishment and for construction (Cooper et al., 2007; Kubicki et al., 2007). It has been shown to have several advantages compared with onshore exploitation, since extraction from rivers, estuaries and nearshore sand bars has proven in the past few years to have significant negative environmental and social impacts. Nevertheless, offshore sand extraction can also have negative impacts in the marine environment, not only in the morphodynamics of the region, but also in the local ecosystems, and this is often not restricted to the excavation area (Kubicki et al., 2007; van Rijn and Walstra, 2002; van Rijn et al., 2005).

The morphology and morphodynamics of the seabed are strongly affected by the creation of the local depression due to the excavation. The induced bottom morphology changes will in general influence the local flow and the wave field and consequently the sand transport rates (van Rijn and Walstra, 2002). Locally, the sediments from the surrounding areas tend to move inside the depression. Changes in the wave field, through refraction and, less significantly, also through diffraction, can modify the longshore sediment transport patterns and affect the shoreline morphology (Demir et al., 2004). Over longer time scales, the sandpit area can migrate towards the shore and may act as a sink for the sediments from the nearshore system (van Rijn and Walstra, 2002). The severity and persistence of such impacts depend, among others factors, on the hydrodynamic conditions, the nature of the substrate, the

* Corresponding author at: CESAM, University of Aveiro, Campus de Santiago, 3810-193 Aveiro, Portugal.
E-mail address: danielamsg@ua.pt (D.S. Gonçalves).

http://dx.doi.org/10.1016/j.coastaleng.2014.02.001
0378-3839/

sandpit geometry and its distance to the shore, and the time-scale of the seabed perturbation (Cooper et al., 2007; Roos et al., 2008). In order to minimize these effects and nearshore coastal erosion, the mining areas need to be located offshore of the closure depth.

This work investigates the morpho-sedimentary evolution of an excavation area, located offshore Vale do Lobo in the Algarve, south of Portugal (Fig. 1), resulting from the sand exploitation for the nourishment of the Vale do Lobo beach (Gonçalves, 2009). The study is based on 4 bathymetric surveys, prior to and after the dredging operations and within a time span of four years (2006–2010), complemented with the analysis of wave data and numerical morphodynamic modeling simulations. The main aims of this paper are to understand the physical mechanisms responsible for the sandpit evolution and to estimate the sandpit recovery time from the observed and predicted filling rate.

2. Study area

The Vale do Lobo area is located in Loulé, on the southern Portuguese coast (Fig. 1). This coastal area is characterized by the existence of a medium height (10 to 15 m) active cliff and a narrow beach. The almost vertical cliff, that extends from Quarteira, in the west, to the Vale do Garrão area, in the east, is shaped in poorly consolidated red sandstones from the Plio-Pleistocene (Manupella, 1992). The cliffs in the Quarteira–Vale do Garrão coast are intercalated by sandy barriers that enclose the river mouths of the area (Teixeira, 2011).

The main sediment circulation cell offshore Vale do Lobo (Fig. 1) extends from Albufeira to Faro. The longshore transport is dominant and mainly wave induced, with a negligible aeolian transport. The cliffs are the main source of sand that feeds the longshore drift (Dias and Neal, 1992), with a small fluvial direct contribution (Rosa et al., 2013). The annual net transport rate is about 110 000 m^3/yr directed eastwards (Teixeira, 2011).

The study area is mainly constituted by lithoclastic coarse sand (CS-1 in Fig. 1). Nearer the shore, the sediments consist in general of lithoclastic medium sand (grain size between 0.25 and 0.5 mm and identified as MS-1 in Fig. 1); further offshore lithoclastic gravelly sand (grain size higher than 2 mm; gS-1 in Fig. 1) predominates (IH, 1985). The lithoclastic coarse sand identified in the excavation area (black box in Fig. 1) presents a dominant grain size between 0.5 and 2 mm, with a fraction of sediments with a grain size higher than 2 mm that is lower than 15%, and it is essentially quartzitic with a low percentage (<10%) of carbonates (Teixeira, 2011). Based on side scan sonar data and in situ observations through scuba diving, Teixeira (2011) mapped the rocky outcrops offshore Vale do Lobo shown in Fig. 1 (R — gray polygons).

This coastal area has suffered serious erosion problems in the recent past. The construction of several groins in the Vilamoura area in the 70s (west of Quarteira; Fig. 1), to attenuate the coastal erosion, has interrupted the downdrift littoral transport and induced significant erosional problems eastwards, increasing the natural coastline retreat trend for that costal sector. According to Marques (1997), the coastline mean retreat rate for the Vale do Lobo area has evolved from ~0.55 m/yr, in the 1974 to 1980 period, to ~1 m/yr between 1983 and 1992.

In order to mitigate the intense coastal erosion felt in this zone, an artificial beach nourishment was carried out. The Vale do Lobo beach nourishment undertaken between October 1998 and January 1999 was the first case of an offshore sand extraction in the Algarve, and a total of approximately 700 000 m^3 of sand were extracted (Teixeira,

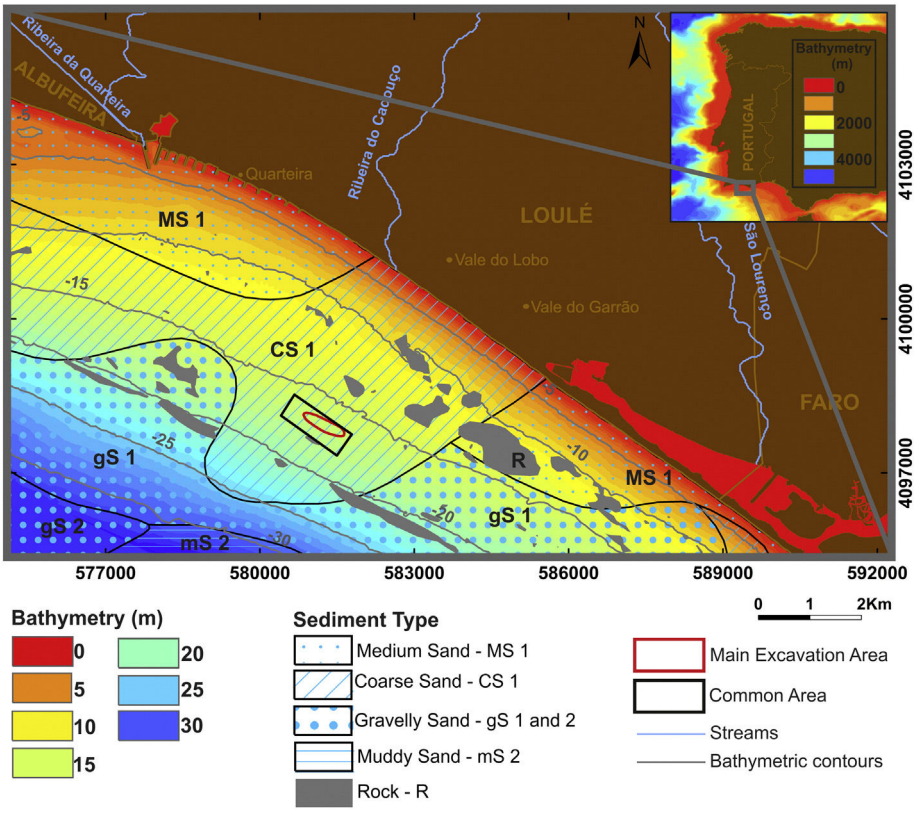

Fig. 1. Bathymetry and superficial sediments in the study area offshore Vale do Lobo, Algarve, Portugal. The red ellipse shows the location of the main excavation area and the black polygon indicates the area common to all available bathymetric surveys. The bathymetry shown is from the Portuguese Hydrographic Institute (2001 survey, courtesy of the Administration of the Hydrographic Region of the Algarve — ARH Algarve). The inset in upper right corner shows the location of the study area in mainland Portugal; bathymetry from the GEBCO 2008 (2 miles spacing) digital bathymetric grid. On top of the bathymetry are represented the superficial sediments in the study area, based on the Hydrographic Institute Map of Superficial Sediments (IH, 1985), side scan sonar data, in situ observations and manual sampling (60 cm deep) through scuba diving (Teixeira, 2011). The numbers 1 and 2 after the sediment type indicate if it corresponds to a lithoclastic or lithobioclastic sediment, respectively. Coordinate system in UTM Zone 29N, datum WGS84 and bathymetry referred to the Hydrographic Zero datum (ZH). (For interpretation of the references to color in this figure legend, the reader is referred to the web version of this article.)

2011). The dredging area was located approximately 3.5 km offshore Vale do Lobo, between the −15 and −20 m isobaths (referred to the Hydrographic Zero datum — ZH[1]) and, according to the information provided by Regional Hydrographic Administration for the Algarve Region — ARH Algarve, the dredging method employed in this extraction caused shallow dredging depressions across a wide area.

In 2006, between March and May, a second artificial beach nourishment was performed, this time from a more localized offshore sandpit excavation. Approximately 370000 m^3 of sediments were dredged from the internal continental shelf off Vale do Lobo (Teixeira, 2011), creating a local depression on the seabed. The borrow pit was located about 3.5 km offshore Vale do Lobo, between the 16 and 18 m isobaths (referred to ZH), with the main axis oriented NW–SE, approximately parallel to the shoreline with the longest side aligned by the bathymetric contours, as represented in Figs. 1 and 2b. The pit generated by the dredging was small and deep, approximately 900 m long, 150 m wide and 5 m deep. This study is focused on the analysis of the evolution of the second excavation, for which an adequate dataset of repetitive bathymetric surveys covering the same area is available, prior to, and after the excavation. These datasets allow us to monitor in detail the sandpit evolution through time. The fact that this is a localized pit, instead of a widely distributed dredged area, like in the first excavation in 1998, also makes the study of the sand pit evolution better constrained.

The Vale do Lobo area has a mesotidal and semi-diurnal tidal regime. The mean tidal range is 2 m and the spring-tide range is 3 m. The wave climate is characterized by prevailing smooth and moderate sea states, with approximately 90% of the significant wave heights (H_s) lower than 2 m, and 5 to 10% of the wave heights reaching a 2.5 m to 3.5 m range (Almeida et al., 2011). The storm occurrences from the SW quadrant are dominant (70% of storm occurrences), occur mainly during the winter and are responsible for the highest waves (the typical H_s during storms, is about 4 m, but it can reach 7 m). SE storms occur when the Mediterranean easterly winds are strong (30% of storm occurrences), mainly between October and May, with typical H_s lower than 4 m and maximum values under 6 m (Almeida et al., 2011). A numerical study of the hydrodynamics in the area of the sandpit corresponding to the second dredging was made by Lopes et al. (2009) and Rosa et al. (2011a,b). According to Lopes et al. (2009), the tide is well polarized, mainly aligned along the N–S direction, and the maximum tidal currents can reach 0.15 m/s in the Vale do Lobo area. In the vicinity of the excavation the velocity of the tidal current is lower than 0.05 m/s, even in spring tides. The mean currents in the area are strongly correlated with the wind field: for calm wind conditions, the velocity intensity is insignificant; however during the storms from the SW quadrant, the wind induces strong currents (~0.2 m/s) southeastwards. The near-bed wave orbital velocities at the sand pit location are generally low (<0.1 m/s), excluding during the storm events when they reach maximum values of 0.5 m/s. The influence area of the sandpit was accessed with the numerical model SWAN by propagating representative waves of the mean and extreme wave climate: the modifications in the wave field were not perceptible behind the 4 m bathymetric contour.

3. Data and methods

The datasets used for this work consisted of: (1) 4 bathymetric dataset surveys acquired prior to and after the 2nd excavation, occurred in 2006 and (2) wave data from the Faro directional wave buoy, for the period 2006–2010. The methodology used for each dataset is described in detail below.

[1] The Hydrographic Zero (ZH) is the vertical reference for water level measurements and corresponds to the level of the lowest astronomical tide.

3.1. Bathymetric data

The sandpit area of the 2nd sand extraction, carried out in May 2006, was monitored with bathymetric surveys prior to (March 2006) and after the excavation (May 2006, November 2008 and May 2010). The bathymetric data used for this work were acquired with single beam echo sounders, with the exception of the data from May 2010, which was acquired with a multibeam system. The 4 bathymetric datasets were inserted into a georeferenced GIS database (*ArcGIS*) and converted to UTM coordinates, datum WSG84. The data were filtered with a low-pass Gaussian filter to reduce the noise, and interpolated with the Natural Neighbors (NaN) method (cell size 5 × 5 m^2). The bathymetric surfaces obtained (Fig. 2) were used to calculate the sediment budget in the excavation pit and surrounding area (the accumulated and eroded sediments, either due to the extraction or to natural readjustments of the bottom surface between successive surveys). For that purpose, the *ArcGIS* tools *minus* and *cut/fill* were used. These tools allow the subtraction of successive bathymetric surfaces, which is essential to understand the sandpit morphology evolution through time, in particular its migration and replenishment.

In order to obtain a first estimate of the recovery time for the excavation area and test if a variable refilling rate, exponentially decreasing in time, is applicable to the study area, Eq. (1), which assumes a continuous sediment mobilization in time, was used. In this equation, the remaining excavation volume, V, after a period of time, t, is determined based on the initial excavation volume, V_0, and the recovery characteristic time-scale, τ (time after which the excavation volume is 37% of the initial volume; Vicente and Uva, 1984; Ramos et al., 2005).

$$V = V_0 e^{-t/\tau} \Leftrightarrow \tau = \frac{t}{\ln\left(\frac{V_0}{V}\right)}. \quad (1)$$

3.2. Wave Data

In order to characterize the wave climate in the study area during the period analyzed, the measured three-hourly values of significant wave height (H_s), mean period (T), and mean wave direction (θ) datasets from Faro directional wave buoy (operated by the Portuguese Hydrographic Institute — IH) were used, from 2006 to 2010. This is a *Datawell-Waverider* buoy located offshore Faro (36°54′17″ N, 7°53′54″W), at approximately 93 m water depth (ZH). However, a set of gaps was identified in the data. The missing data for a time span of 6 h or less were filled in by direct interpolation (weighted mean); for longer gaps (more than 6 h) the data were filled in using data from the numerical model WaveWatchIII (Tolman, 2009) forced by wind fields originating from the Climate Forecast System Reanalysis (CFSR, Saha et al., 2010) with spatial and temporal resolutions of 0.3° and 3 h, respectively.

The numerical modeling of waves in the southern coast of Portugal is very challenging due to the superimposition of two wave regimes. The former corresponds to a long-period swells generated in the North Atlantic Ocean and coming from the WSW to WNW while the latter corresponds to wind seas coming from the SE and locally called “Levante” wind. This bi-modal wave regime causes the wave direction and peak period to jump regularly from one mode to another and this phenomenon is difficult to capture with a numerical model. A first grid of the numerical model WaveWatchIII (Tolman, 2009) is implemented in the North Atlantic Ocean with a 0.5° resolution, following the configuration described in Dodet et al. (2010). A second grid is nested in the Gulf of Cadiz and the SW Portuguese Coast (6–10°W; 31–39°N) with a 0.05° resolution.

WaveWatchIII results were evaluated against wave measurements at the Faro wave buoy (Fig. 3). This comparison shows firstly that significant wave heights H_s are well reproduced, with a root mean square

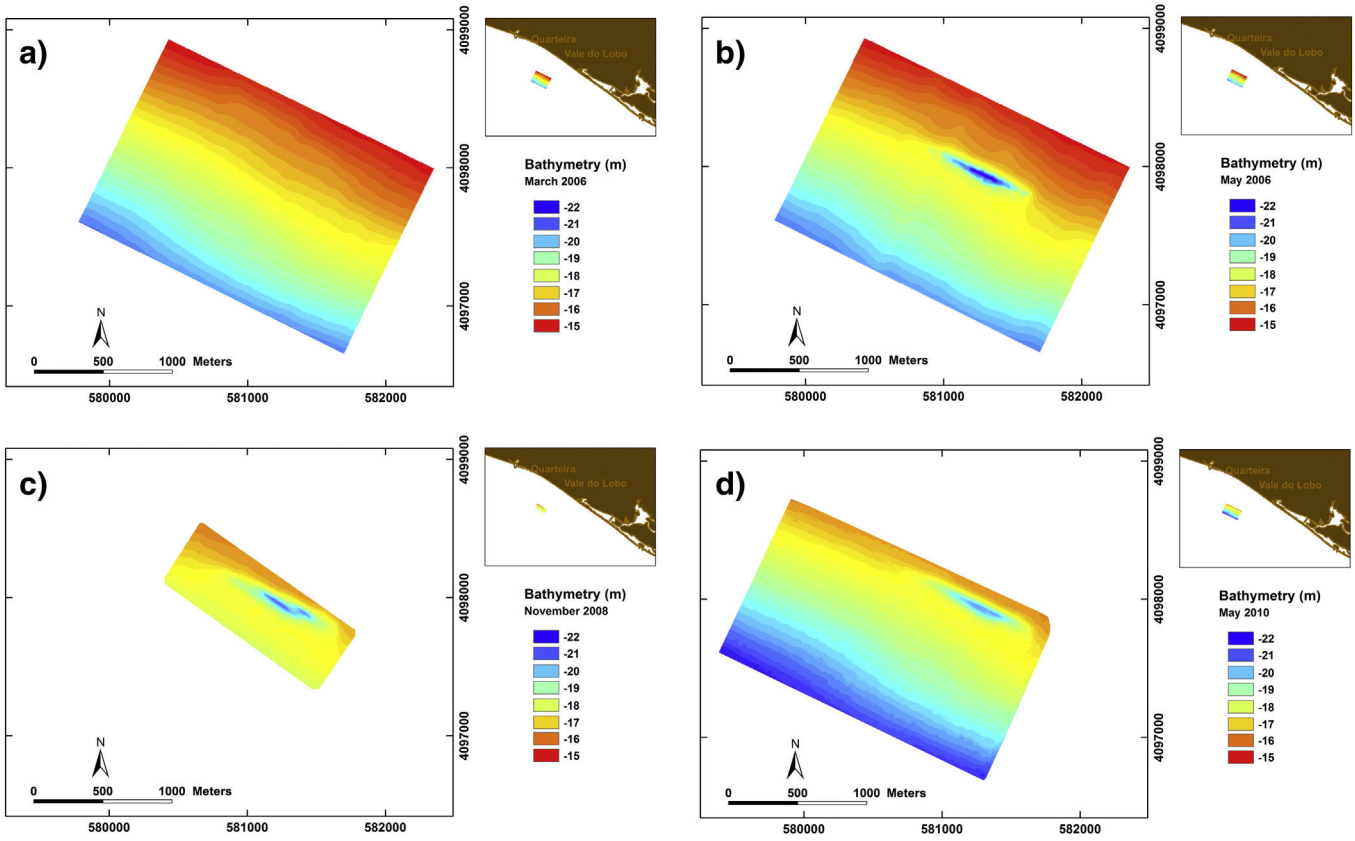

Fig. 2. Bathymetric bottom surfaces used for this study: (a) March 2006; (b) May 2006; (c) November 2008; and (d) May 2010. Coordinate system in UTM Zone 29N, datum WGS84 and bathymetry referred to the Hydrographic Zero datum (ZH).

discrepancy (RMSD) of 0.26 m, which results in a 25% discrepancy once normalized by the data. Moreover, the bias in H_s is −0.1 m, which is in accordance with the results of Dodet et al. (2010) that found a negative bias between 0.10 and 0.30 m considering 6 buoys located in the west and north coast of the Iberian Peninsula. However, there is a discrepancy observed for significant wave heights lower than 1 m. Since this problem essentially concerns small waves (Fig. 3c and d), the bias and the RMSD normalized by the observed data (NRMS) were recalculated for H_s larger than 1.0 m. This new comparison yields a bias of 0.02 m and a NRMSD of 20%. Wave direction (Fig. 3a and b) and peak periods have a RMSD of 48° and 2.3 s respectively. These weaker scores result mainly from the regular jumps between the two modes described above, which are not all captured by the model. As described above, this problem essentially concerns small waves (Fig. 3c and d), then the recalculated RMSD for H_s larger than 1.0 m yields a RMSD of 30° and 1.3 s for wave direction and peak period, respectively. According to these errors, it can be argued that the model accuracy is sufficient to produce a continuous time series of wave parameters over 2006–2010 in order to fill the gaps of the Faro buoy measurements for storm event identification purposes. The result was a complete and unique three-hourly interval dataset covering the whole period from January 2006 to December 2010.

The 2006–2010 wave dataset was analyzed for two periods of time: May 2006 to November 2008 and December 2008 to May 2010; for both these periods, the duration and frequency of storms were calculated. In order to classify a data sequence as a storm, the following criteria need to be satisfied (Li et al., 2009; Zhang et al., 2000):

1) The event should consist of at least one sample above the peak threshold value (H_{peak} = mean + 2 standard deviation);
2) The storm continues while the significant wave height remains above the duration threshold value (H_{dur} = mean + standard deviation);
3) Two consecutive storms are distinguished if the storm interval is not shorter than 3 h and if the interval between storm peak and storm peak is not less than 30 h.

According to Pessanha and Pires (1981), in the Portuguese south coast a storm is defined as an event with a H_s offshore higher than 3 m. According to Almeida et al. (2011), this corresponds to the mean H_s plus two times the standard deviation (H_{peak}). Therefore, since the average of the significant wave height is close to 1 m (Costa et al., 2001), the H_{peak} used in this work is 3 m and the H_{dur} considered is equal to 2 m. After the classification of a data sequence as a storm, individual storm characteristics were assessed through the calculation of the H_s minimum, maximum, median and mean, storm duration and wave mean direction of the individual storm event. The number of stormy days and the number of storms for the two periods were identified. According to Almeida et al. (2011), to properly characterize the variability of storm occurrence in the study area, a high percentile of H_s 99.8 is required to assess extreme wave height variability of occurrence of storms. Therefore, the H_s 99.8 was also estimated for the two intervals of time.

3.3. Morphodynamic modeling system

In order to better understand the morphodynamic evolution of the study area in the periods between the 4 bathymetric surveys, and to determine for which periods there was a more significant sediment movement, a numerical modeling system was used. The numerical simulations of the sediment dynamics and morphological evolution of the sandpit were performed with the morphodynamic modeling system MORSYS2D (Bertin et al., 2009; Fortunato and Oliveira, 2004, 2007). This modeling system integrates the circulation model ELCIRC (Zhang et al., 2004), the wave propagation model SWAN (Booij et al., 1999)

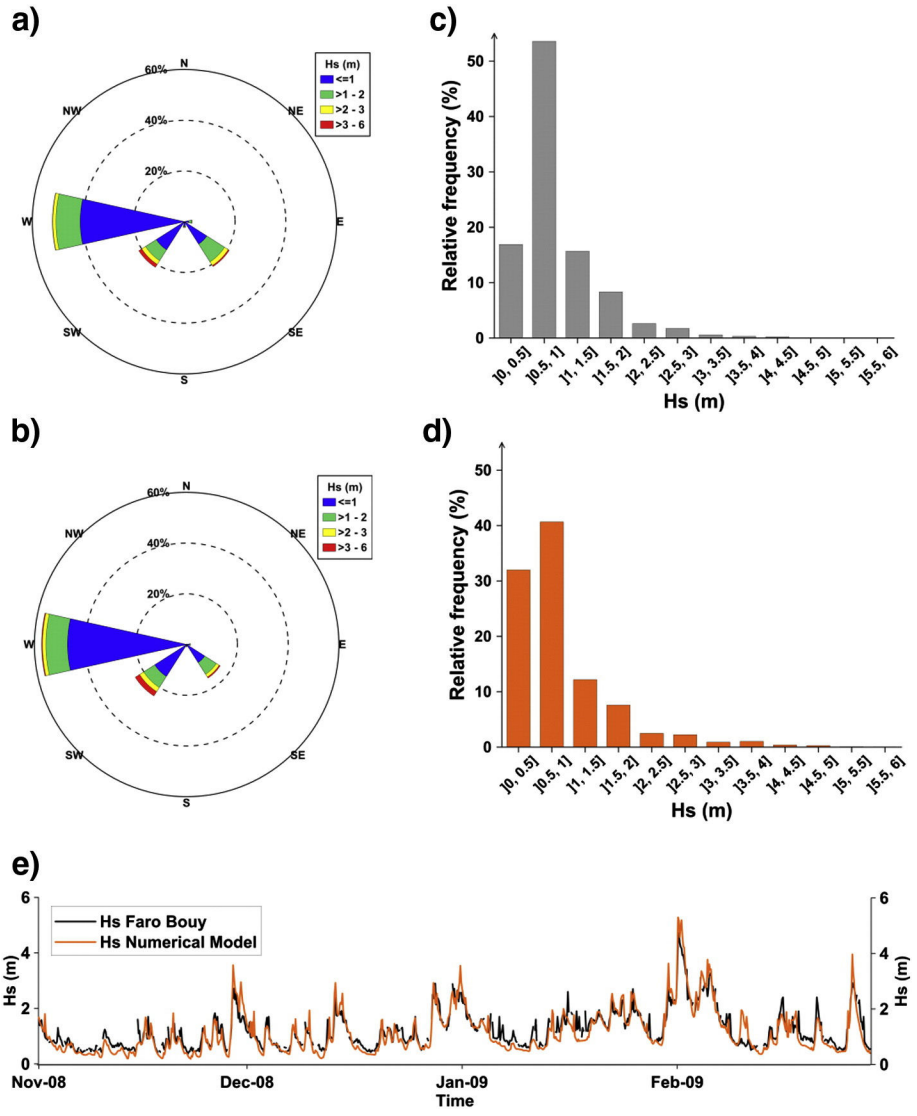

Fig. 3. Comparison between wave measurements at the Faro wave buoy and WaveWatchIII modeling results: wave rose diagram for the wave direction and the significant wave height considering the whole dataset (2006–2010) based on (a) Faro buoy measurements and (b) WaveWatchIII modeling results; H_s relative histogram based on (c) Faro buoy measurements and (d) WaveWatchIII modeling results; and (e) measured H_s (black line) plotted over numerical modeling results (orange line) for a period of 4 months (November 2008–March 2009). (For interpretation of the references to color in this figure legend, the reader is referred to the web version of this article.)

and the sediment transport and bottom evolution model SAND2D (Bertin et al., 2009; Fortunato and Oliveira, 2004, 2007), in order to simulate the non-cohesive sediment dynamics in estuaries, tidal inlets and coastal areas, driven by tides, wind, river flows and waves. SWAN or Simulating Waves Nearshore is a numerical wave model that, based on a Eulerian formulation, computes random and short-crested waves in coastal regions, by describing the evolution of the two-dimensional wave energy spectrum in arbitrary conditions of wind, currents, and bathymetry (Booij et al., 1999; Ris et al., 1999). In MORSYS2D, SWAN is used in a stationary mode to simulate wave propagation and deformation from the open sea up to coastal zones (Bertin et al., 2009). The hydrodynamic model ELCIRC is an open-source three-dimensional baroclinic model that calculates tidal elevations and currents and wind-induced mean currents by solving the shallow water equations using a semi-implicit Eulerian–Lagrangian finite volume and finite difference method (Zhang et al., 2004). Within MORSYS2D a single vertical layer is used. SAND2D (Bertin et al., 2009; Fortunato and Oliveira, 2004, 2007) computes the sand fluxes in combined current and wave flows, from three well known semi-empirical formulations (Bijker, 1971; Ackers and White (1973), see also van de Graaff and van Overeem, 1979; and Soulsby van Rijn, see Soulsby, 1997), and computes the sea bottom changes through the numerical resolution of the Exner equation that describes the conservation of mass of the sediment.

For the present work, the numerical model configuration includes the most representative forcing, such as tides, wind, and waves, provided by regional models. The ELCIRC model was forced by a regional model of tides (Fortunato et al., 2002) and the SWAN spectral wave model was forced offshore by a regional application of the WAVEWATCH III (WW3) model (Dodet et al., 2010). Concerning wind, WW3 was fed by data obtained from the National Centers for Environmental Prediction (NCEP) and a uniform computational domain was assumed. The wave model WW3 was validated through the comparison of the model data with the Faro buoy data (see Section 3.2). For the ELCIRC model, an unstructured triangular grid with 6710 nodes was used, where the element size ranges from 1500 m offshore to 5 m at the sandpit area. SWAN was run with 3 nested grids: a larger one with a spacing of 1000 m and an area of 65 × 110 km; an intermediate grid with a spacing of 100 m and an area of 20 × 42km; and a high resolution grid centered in the sandpit with a spacing of 20 m and an area of 6 × 10km. The net sediment transport rates were computed considering a constant median sediment size

(d50) of 0.77 mm, based on granulometry analysis conducted by Teixeira (2011). Previous applications of the MORSYS2D have shown a dependence of the morphodynamic numerical solutions on the sediment transport formulation considered. The results of Bertin et al. (2009) to a dissipative beach and of Plecha (2011) to a tidal dominated inlet have shown a better performance of Ackers and White formulation than the Bijker and Soulsby-van Rijn formulations, which estimated larger transport rates. However, in the present work, the sediment fluxes are computed in non-breaking wave conditions with rather small mean currents and Ackers and White formulation did not provide an accurate morphodynamic evolution of the sandpit. Instead, as shown in Rosa et al. (2011a), Bijker formula provided the best results when compared with the bathymetric observations for a constant bottom roughness, Ks equal to 0.1 m.

The MORSYS2D numerical model simulations were used in this work to assess the morphological changes in the sandpit during two different time intervals with very contrasting weather and wave conditions:

- From March 28th to April 29th 2008 (henceforth referred to as April 2008), when two important storm events took place;
- From April 30th to May 31st 2008 (henceforth referred to as May 2008), a period without storm events.

In order to estimate the sandpit morphological variations during these two time intervals, the bathymetric datasets generated by the numerical model, concerning the dates previously described (March 28th, April 29th, and May 31st, 2008), were inserted into a georeferenced GIS database (*ArcGIS*), converted to UTM coordinates, datum WSG84, and interpolated using the Natural Neighbors (NaN) method (cell size 5 × 5m). The obtained bathymetric surfaces were used to assess the sandpit evolution between March 28th and May 31st 2008, using the *ArcGIS* tools *Minus* and *Cut/Fill*.

4. Results and discussion

4.1. Sediment balance, sandpit evolution and recovery time

The volumes of sediment accumulation and removal for the area common to all the available bathymetric surveys (ca. 615 000 m^2; black polygon in Fig. 1), which covers essentially only the main pit area and its immediate vicinity, were computed (Table 1). This was carried out through the subtraction of the successive bathymetric surfaces described in Section 3.1. Considering this common area, the extracted sand volume for the 2006 surveys gave a net value of 285 000 m^3, which corresponds to ca. 77% of the value reported by the contractor of 370 000 m^3 (Teixeira, 2011). However, for this comparison, the full excavation area should be used. As can be observed in Fig. 2, the 2006 surveys, just prior to and just after the excavation, cover a greater area, which corresponds to the full area of excavation; the subsequent surveys cover smaller areas in the vicinity of the main pit area. Calculating the extracted sand volume for the 2006 surveys for the full excavation area, a net value of 340 000 m^3 was obtained, which corresponds to ca. 91% of the value reported by the contractor of 370 000 m^3 (Teixeira, 2011). Between May 2006 and November 2008 there were no sand extractions. The observations show for this period an accumulation of about 58 000 m^3 and a sediment removal of approximately 20 000 m^3, resulting in a net positive sedimentary balance of about 38 000 m^3. A similar trend was observed for the period between November 2008 and May 2010, with an accumulation of about 40 000 m^3 and a sediment removal of about 8000 m^3, resulting in a positive sedimentary balance near to 32 000 m^3 (Table 1). Therefore, assuming that there are no significant errors in the bathymetric datasets, it is possible to estimate a net accumulation rate of about 2.85 cm/yr for the study area, during the 4 year period between May 2006 and May 2010. The sand removed during the dredging process in March 2006 left an oval shape depression on the seabed, referred to above as the main pit area, elongated in the NW–SE direction (Figs. 4 and 5).

A smoothing of the topography roughness is evident. In general, the sandpit topography in 2010 became smoother and less deep (about 2 m) than the original topography of May 2006. The analysis of the bathymetric profiles along the pit axis (Fig. 4) shows that 2.5 years after the excavation (in November 2008), the pit was filled in its deepest and central parts and that its slopes were accumulating sediment mainly on the upper part of the NE flank (red and yellow curves in Fig. 4). 4 years after the extraction (May 2010 — green curve in Fig. 4), an infill of the deepest area of the pit is clearly visible; the flanks are still accumulating sediment, once again, mainly the NE flank (the onshore flank).

Fig. 5 shows the pit edge evolution in time; in this work, a slope value of 0.5°, higher than the maximum natural slope in the study area, was used to delimit the pit edge. During the four years after the dredging, the NE flank showed a displacement of about 15 m in average towards SW, with a maximum displacement of about 20 m. However, there was an increase in the pit's maximum length along the main axis, due to sediment loss (see also Fig. 4a), and the excavation became more elongated in the NW–SE direction (Fig. 5). The shrinking observed mainly in the NE flank, due to sediment accumulation, is causing the migration of this flank southwestwards (see also the transverse profiles in Fig. 4). This migration is also evident from the analysis of the sandpit centroid (see Fig. 5), which moved about 7.8 m to the SW. The same trend is shown by the longitudinal axis of the sandpit, which moved southwestwards about 8.7 m (Fig. 5). The perimeter of the excavation rim grew around 25%, from about 2000 m in May 2006 to more than 2500 m four years later (Table 2). The same trend was observed for the area of the pit at the surface, which increased about 10% during the same four years, from around 162 500 m^2 in 2006 to 178 000 m^2 in 2010. These results suggest that the sandpit is becoming shallower and smoother but slightly wider. The sandpit mean slope decreased 18% from May 2006 to November 2008, and 14% from November 2008 to May 2010. The slope variability also decreased during the 4 study-years. The maximum slope of the pit flanks in all bathymetric surveys was observed on the NE flank and showed a decrease of about 45% from May 2006 to November 2008. However, from 2008 to May 2010, the maximum slope decreased only 7% (Table 2), which suggests that the side walls suffered more significant adjustments in the firsts 2.5 years following the excavation, while from November 2008 to May 2010, because the sandpit reached a more stable condition, the adjustments were less significant.

An estimation of the recovery time for the sandpit between 2006 and 2010 was obtained from Eq. (1) based on the bathymetric data that encompasses just the main excavation area (red ellipse in Fig. 1); this gave an estimated value of 22 years. Since this corresponds only to a 63% infill, the full recovery time will necessarily be longer.

The sandpit refilling rate for the periods between May 2006 and November 2008, and from November 2008 to May 2010 were also

Table 1
Volumes of sediment accumulation and removal between successive bathymetric surveys in the main pit area, calculated using *ArcGIS*. The first dataset corresponds to a time span of about 2 months, whereas the others correspond to periods of about 2.5 and 1.5 years, respectively.

Period in consideration	March to May 2006	May 2006 to November 2008	November 2009 to May 2010
Sediment accumulation	0	58 000	40 000
Sediment removal	285 000	20 000	8000
Balance	−285 000	+38 000	+32 000

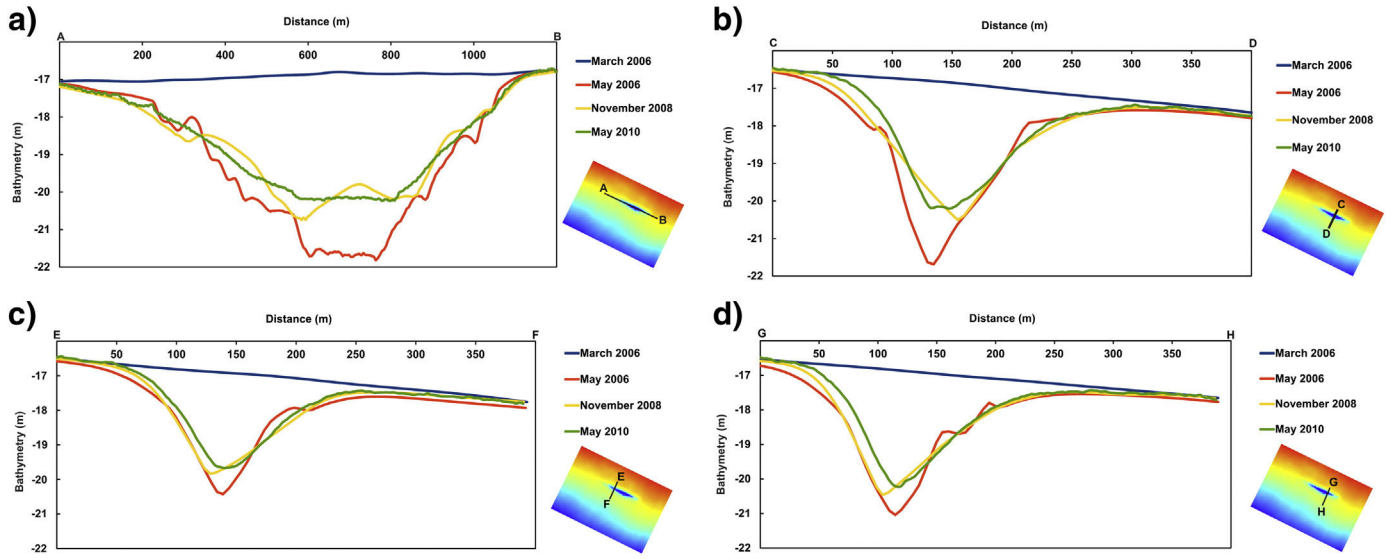

Fig. 4. Bathymetric profiles in the pit-area. (a) Longitudinal profile along the main pit axis; (b) transversal profile to the main pit axis in the central part of the pit; (c) transversal profile to the main pit axis in the NW part of the pit; (d) transversal profile to the main pit axis in the SE part of the pit. Bathymetry referred to the Hydrographic Zero datum (ZH). (For interpretation of the references to color in this figure, the reader is referred to the web version of this article.)

estimated based on the observed bathymetric data. In November 2008, 2.5 years after the extraction, about 22 000 m^3 of sediment were accumulated in the sandpit, resulting in a refilling rate of about 6.5 cm/yr for this period. However, between November 2008 and May 2010, almost 17 000 m^3 of sediment was accumulated in the excavation area, corresponding to a recovery rate of about 7.2 cm/yr. According to these results, the refilling rate in our case study, contrary to what is expected from Eq. (1) and other authors (Kubicki et al., 2007), is increasing in time. An explanation for this fact is proposed in the following sections.

4.2. Ocean wave climate between 2006 and 2010

From 2006 to 2010 the Faro buoy wave data show that the wave climate of the study area was mainly dominated by smooth to moderate sea states. The significant wave height average for this 5-year period was almost 1 m and the corresponding mean period (T) was 4.8 s. The wave histogram for these 5 years (Fig. 3c) further shows that almost 70% of the significant wave height was lower than 1 m and more than 95.5% was smaller than 2.5 m. The wave rose diagram (Fig. 3a) for the 5-year measurements shows that about 73% of the incident waves were from W–WSW and about 20% from the SE quadrant. Based on the criteria previously presented for storm classification (see Section 3.2), the storm events that occurred in the study area from May 2006 to May 2010 were identified and are described in Table 3 (May 2006–November 2008) and in Table 4 (December 2008–May 2010). For each individual storm event the average, minimum, and maximum significant heights (H_s), were estimated, as well as the mean period, the mean direction and the storm duration. According to Tables 3 and 4, the storm events only occurred from October to April. Furthermore, during these 4 years in study (May 2006 to May 2010), the winter stormy days (from December 21st to March 21st) represent more than 70% of the total stormy days, and February was the month with the higher number of stormy days, almost 35% of the total.

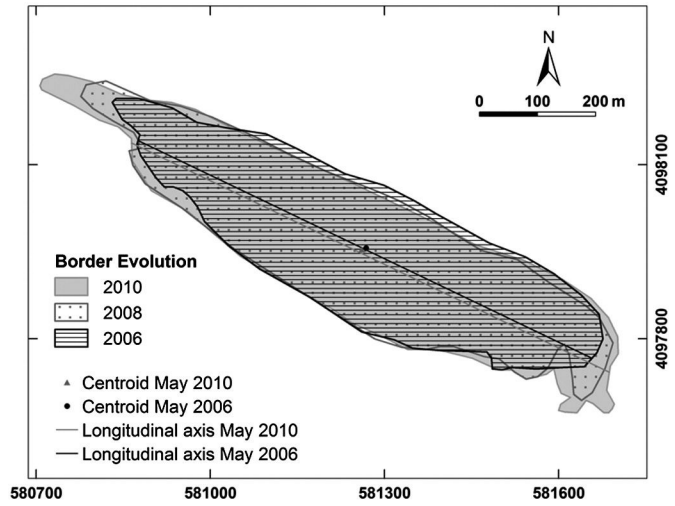

Fig. 5. Pit-area rim evolution through the time: May 2006, November 2008 and May 2010. Coordinate system in UTM Zone 29N, datum WGS84.

In order to better visualize the information presented in Tables 3 and 4, for each study period (May 2006 to November 2008 and December 2008 to May 2010) the significant wave height frequency histograms (Fig. 6c and d) and a wave rose diagram for the mean wave direction and the significant wave height (Fig. 6a and b) are shown. From May 2006 to November 2008, during the identified storm events more than 71% of the significant wave heights were higher than 2.5 m and about 40% were higher than 3 m. For the storm events identified from December 2008 to May 2010, more than 71% of the significant waves were higher than 2.5 m and 40.5% higher than 3 m. For the first period and according to Table 3, the storm events occurred mainly during the winter and February was the month with more stormy days (almost 37% of the total stormy days). The longest storm that occurred during this period took place in February 2008 with 5.6 stormy days; however, the highest H_s maximum (5.35 m) and H_s mean (3.84 m) were observed in the storm that took place in April 2008. For the second study period (December 2008 to May 2010; see Table 4), the storm events occurred almost all during the winter and February was again the month with more storms and more stormy days, corresponding to more than 47% of the total stormy days in this period. December had also a significant number of stormy days (almost 30%). Within this period, the storm with the highest significant wave height occurred in January 2010, with 5.15 m of H_s maximum and a H_s mean of 3.24 m. However, and once again, this storm was not the longest storm, which took place in December 2009, with almost 6.3 stormy days. From May 2006 to November 2008, the wave rose diagram (Fig. 6a) shows that, during

Table 2
Quantitative estimates of the pit extent and maximum slope of the flanks.

Date	Pit perimeter (m)	Pit area (m^2)	Maximum slope (°)	Mean slope (°)	Standard deviation (°)
May 2006	2000	162 500	7.6	1.7	1.4
November 2008	2350	165 500	4.2	1.4	0.9
May 2010	2530	178 000	3.7	1.2	0.8

the storm events, the SE–ESE incident waves had a significant contribution (almost 40%), when compared with the period from December 2008 to May 2010 (Fig. 6b), where the SE–ESE component was significantly smaller (about 10%). In both periods the incident waves from WSW–SW are the most representative during the storm occurrences, and correspond to almost 55% in the first study period and 85% in the second.

From May 2006 to November 2008 (Table 5) thirteen storms were identified, in a total of 30.6 stormy days. Concerning these storm events, the average significant wave height was 2.9 m and the H_s for 99.8 percentile was estimated at 5.2 m. The average of the wave period was 6.3 s. For the other study period between December 2008 and May 2010 (Table 5), seventeen identified storms had a total duration of 41.4 days, with an average significant wave height of 3.0 m, a $H_{s99.8}$ of 5.3 m, and a mean wave period of 7.1 s. Therefore, the period from December 2008 to May 2010 (Table 5), although shorter, presented a larger number of storm events and stormy days than the precedent study period (2006–2008). Moreover, the H_s for the 99.8 percentile, which according to Almeida et al. (2011) properly characterizes the variability of storm occurrence in the study area, is higher in the second study period than in the first 2.5 years after the sand extraction.

4.3. Influence of storm events on sediment mobilization

Rosa et al. (2011a,b) computed the total (wave and mean current) sediment fluxes at the sandpit site for the month of April 2008 from two well-known formulations — Bijker (Bijker, 1971) and Soulsby-van Rijn (Soulsby, 1997), and showed that the sediment fluxes are different from zero when the significant wave height exceeds 2 m (Fig. 7). Only in this case, the near bed wave orbital velocity exceeds the critical value and is capable of mobilizing the bottom sediments promoting, in conjunction with the wind induced mean current, significant changes in the sandpit morphology.

In order to further verify the effect of the significant wave height in the sandpit morphological variations, two different time intervals with very unlike weather and wave conditions were selected: March 28th to April 29th and April 30th to May 31st, 2008 (see Section 3.3.). As shown in Fig. 7a, on April 2008 two very important storm events occurred, identified as S12 and S13 in Table 3. The first storm (S12) was felt during almost 4 days (90 h), with the predominant incident waves from SW–WSW, a significant wave height mean of 3.84 m, and a maximum significant wave height of 5.35 m felt on April 10th. The second storm (S13) had a maximum significant wave height of 3.15 m on April 19th, was felt during almost 3 days (69 h), the incident waves come from WSW–SW, and had a mean significant wave height of 2.58 m. In contrast, throughout May 2008 the significant wave height was always lower than 1.54 m with an average value of 0.78 m for the whole period, which corresponds to a low energy sea state.

The comparison between two output models interpolated bathymetries (Fig. 8a), before (March 28th) and after (April 29th) the two important storm events, shows areas with a significant accretion, mainly in the deepest part and in the north flank of the sandpit, or erosion, in the south flank. A similar analysis carried out for May 2008 (Fig. 8b) shows that almost no bathymetric changes occurred during this time period in the sandpit. Modeling results for the time period between 2006 and 2008 that illustrate this point are depicted in the auxiliary animated figure included in the online version of this paper.

The volume calculations confirm that an important quantity of sediment was mobilized during April 2008 within the excavation and surrounding areas, recovering the sandpit in about 14% of its initial excavation volume; in contrast, a similar estimation for May 2008, shows that the sandpit evolution in this month is almost null (about 0.3% of the initial excavation volume). These results therefore corroborate the idea that high significant wave height, such as those observed during a storm, play a very important role in the sandpit morphological evolution and recovery. Furthermore, the numerical results suggest that sedimentation inside the sandpit is episodic rather than continuous in time. This fact, plus the increasing number of stormy days observed during the period between December 2008 and May 2010, can explain why, against theoretical expectations (e.g. Kubicki et al., 2007), the sandpit filling rate estimated from the bathymetric data increased from 6.4 cm/yr, in the first period between May 2006 and November 2008, to 7.2 cm/yr, in the second period between December 2008 and May 2010.

Based on the previous results, we can estimate that on average, the sandpit recovers 0.24% for every stormy day. Therefore, for a complete sandpit replenishment, about 350 stormy days are required. Almeida et al. (2011) combined measured and modeled wave data, creating a single dataset covering the period of January 1952 to December 2009. According to these data, an average of 11 stormy days per year was estimated. Considering this average number of stormy days per year representative of the future wave climate and the 350 stormy days required for a full sandpit recovery, then 32 years are needed for the complete sandpit replenishment. However, a decrease in the refilling

Table 3
Identified storm events from May 2006 to November 2008.

Storm event	Date (at H_s max)	Mean H_s (m)	H_s min (m)	H_s max (m)	Mean T (s)	Mean direction	Duration (d hh)
S1	18 Oct 2006	2.49	2.02	3.30	6.16	WSW	1 03
S2	26 Oct 2006	2.93	2.01	4.03	6.66	WSW	1 03
S3	24 Nov 2006	3.27	2.25	4.19	6.77	WSW	2 12
S4	16 Feb 2007	2.36	2.04	3.12	5.91	SW	1 15
S5	20 Nov 2007	2.54	2.05	3.22	6.16	SW	1 09
S6	19 Dec 2007	3.45	2.20	5.26	6.05	SSE	3 09
S7	03 Jan 2008	2.67	2.02	4.41	7.12	WSW	2 06
S8	13 Feb 2008	2.87	2.02	3.71	5.77	SE	5 15
S9	17 Feb 2008	2.95	2.04	4.31	5.76	SE	2 06
S10	23 Feb 2008	3.04	2.19	4.13	5.76	SE	2 00
S11	05 Mar 2008	2.52	2.01	3.05	5.91	E	0 12
S12	10 April 2008	3.84	2.20	5.35	8.67	SW	3 18
S13	19 April 2008	2.58	2.01	3.15	5.62	WSW	2 21

Table 4
Identified storm events from December 2008 to May 2010.

Storm event	Date (at H_s max)	Mean H_s (m)	H_s min (m)	H_s max (m)	Mean T (s)	Mean direction	Duration (d hh)
S14	01 Feb 2009	2.91	2.02	4.70	6.69	SW	3 15
S15	05 Feb 2009	2.63	2.02	3.20	6.40	WSW	3 00
S16	17 Mar 2009	3.01	2.16	3.82	5.94	SE	2 12
S17	19 Dec 2009	3.17	2.21	4.06	6.86	SW	1 06
S18	23 Dec 2009	3.56	2.12	4.98	7.65	SW	6 06
S19	31 Dec 2009	3.47	2.06	5.00	7.40	WSW	4 12
S20	04 Jan 2010	3.24	2.10	5.15	8.86	WSW	2 12
S21	11 Jan 2010	2.97	2.16	3.82	7.90	WSW	1 03
S22	12 Jan 2010	2.65	2.08	3.24	5.74	SW	0 12
S23	14 Jan 2010	2.70	2.12	3.70	8.07	WSW	1 06
S24	28 Jan 2010	2.77	2.03	3.19	5.32	ESE	0 06
S25	16 Feb 2010	3.22	2.10	4.26	6.74	SW	3 03
S26	21 Feb 2010	3.01	2.05	3.97	6.58	SW	3 21
S27	27 Feb 2010	3.04	2.10	4.63	8.84	WSW	2 03
S28	03 Mar 2010	3.29	2.05	4.80	8.47	SW	2 09
S29	09 Mar 2010	2.64	2.10	3.12	7.69	WSW	0 12
S30	16 April 2010	2.67	2.24	3.75	6.00	S	2 15

rate in time, as stated in Eq. (1), is probably a more suitable model, if t now represents the number of stormy days. According to this for a near-full (63%) sandpit recovery, about 412 stormy days are needed, what corresponds, considering the same average of 11 stormy days/yr (Almeida et al., 2011) used previously, to 38 years.

4.4. Physical processes controlling the sandpit evolution

To better understand the sandpit evolution, a study of the sediment dynamics was made based on the computed sediment fluxes with the Bijker formulation and encompassing the S12 storm. Fig. 9 shows the

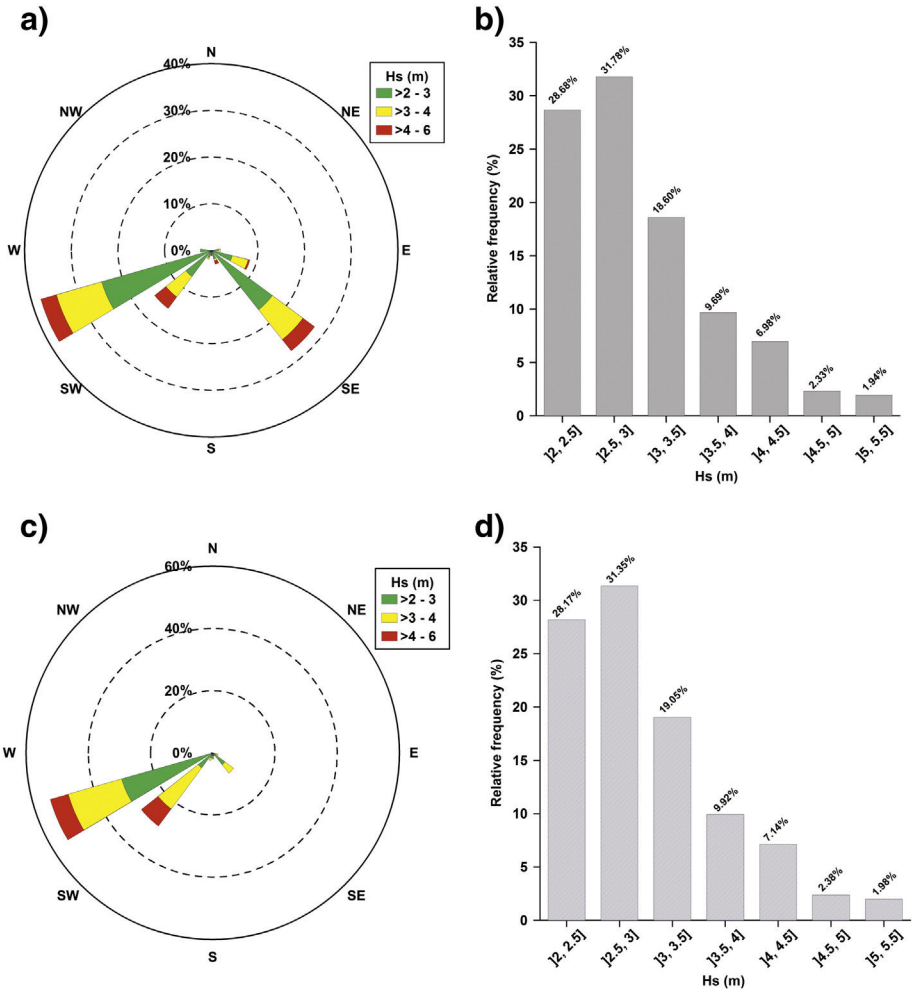

Fig. 6. Significant wave height and wave direction: wave rose diagram for the wave direction and the significant wave height for the identified storm events (a) from May 2006 to November 2008 and (b) from December 2008 to May 2010; and H_s relative histogram for the identified storm events (c) from May 2006 to November 2008 and (d) from December 2008 to May 2010.

Table 5
Comparison between the two intervals of time, from May 2006 to November 2008 and from December 2008 to May 2010, showing the number of storms, total duration of the storm event (days), H_s (mean, maximum, minimum and $H_{s99.8}$), mean period, mean direction and the sedimentation rate previously estimated from the bathymetric data.

Interval of time	Time (yr)	Number of storms	Stormy days/yr	H_s mean (m)	H_s max (m)	H_s min (m)	$H_{s99.8}$	mean T (s)	Sed. rate (cm/yr)
May 2006 to Nov. 2008	2.5	13	12.3	3.0	5.35	2.0	5.3	6.4	6.5
Dec. 2008 to May 2010	1.5	17	27.6	3.1	5.15	2.0	5.0	7.2	7.2

magnitude and direction of the mean sediment fluxes between the 9th and the 14th of April, 2008 in the vicinity of the sandpit. The magnitude of the sediment fluxes is well related with the water depth showing higher values in the shallower zones (see Figs. 1 and 2, for the bathymetric contours). Inside the pit the magnitude of the flux has a minimum, explaining a decrease in the sediment transport capacity and pit infill over time. This arises from a decrease of the magnitude of the orbital velocity and mean current inside the sandpit. Lopes et al. (2009) have run SWAN for an extreme wave condition ($H_s = 6$ m; WSW and $T = 16$ s), which is similar to the maximum wave height registered during the period in analysis, and showed that the amplitude of the wave orbital velocity inside the sandpit decreases 15%. Moreover, a considerable attenuation of the orbital velocity was also observed on the lee side of the sandpit arising from energy dispersion, which can justify the lower values of sediment transport at the east–north end of the excavation.

Concerning the sediment flux direction, they follow the pattern of the mean wind induced currents (see Rosa et al., 2011a): the fluxes are mainly oriented from the NW to SE, along the sandpit longitudinal axis, responding to the southwesterly strong winds, and inflect at the NE sandpit flank to the south direction. The sediment fluxes field in Fig. 9 is representative of the conditions that the sandpit is subject

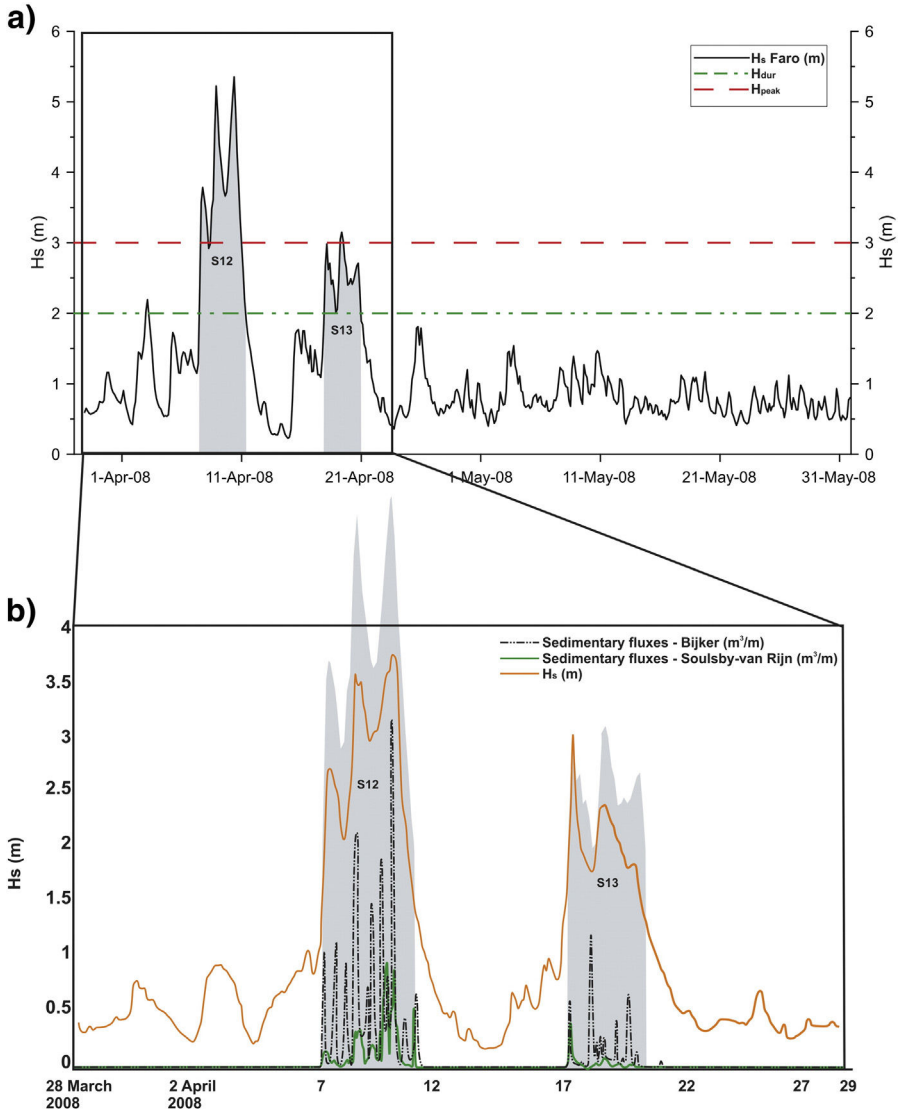

Fig. 7. (a) Measured significant wave height (black line) between March 28th and May 31th 2008. The dashed red and green lines represent, respectively, the H_{peak} and the $H_{duration}$ used to identify the storm events. (b) Computed significant wave height — m (orange line) and sedimentary fluxes for Bijker — m^3/m (black dot line) and Soulsby-van Rijn — m^3/m (green line) formulations for a point inside the sandpit, in the period between March 28th and April 29th 2008. The gray shadows in both graphics represent the storms S12 and S13 based on measured significant wave height. (For interpretation of the references to color in this figure legend, the reader is referred to the web version of this article.)
Adapted from Rosa et al. (2011b).

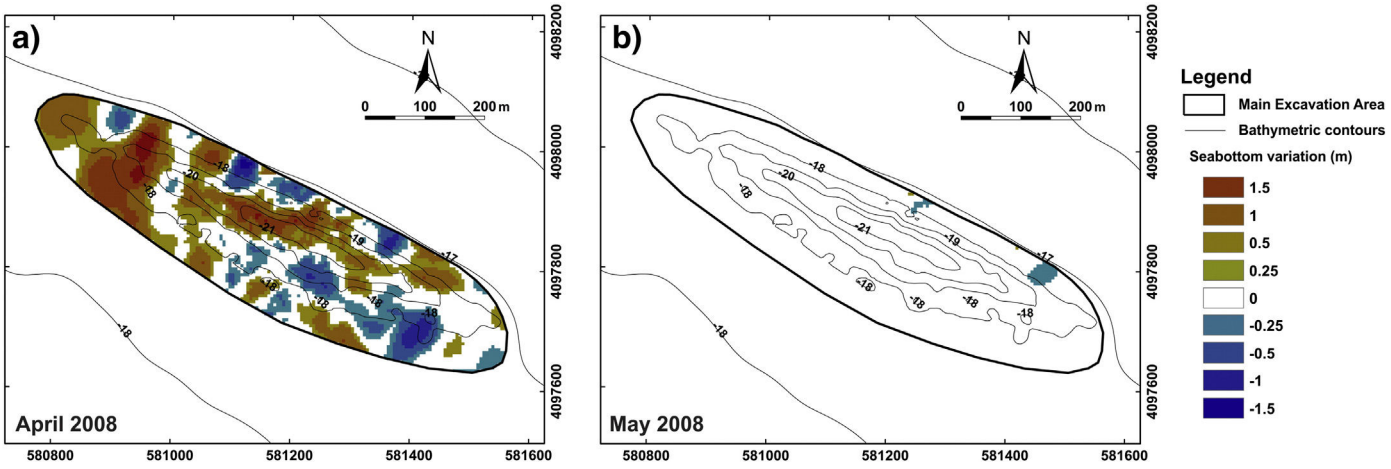

Fig. 8. Computed sea bottom variation, in meters, between (a) March 28th and April 29th, and (b) April 29th and May 31st. The cold colors represent sediment removal and the warm colors indicate sediment accumulation. Bathymetric contours are referent to May 2006 survey. Coordinate system in UTM Zone 29N, datum WGS84. (For interpretation of the references to color in this figure legend, the reader is referred to the web version of this article.)

when it is morphodynamically active. Although we employed a fully coupled 2DH modeling system, the water depth where the sandpit lies implies that wave-induced currents are negligible and thereby, wave effects are mostly restricted to sediment stirring. For significant wave heights higher than 2 m, the wave direction is mainly from WSW–SW (55–85%, as depicted in Fig. 6) and in 65% of the cases the wind direction is from SW (Rosa and Silva, personal communication, 2012). Therefore, the patterns of the evolution of the sandpit behavior suggested in Fig. 9, namely the pit infill and its migration, can be extrapolated for the overall period in the study.

5. Conclusions

The evolution of a sandpit offshore Vale do Lobo, Portugal, resulting from the sand extraction performed in 2006 for beach nourishment purposes was investigated based on four bathymetric datasets (one before, March 2006, and three after the sand extraction, May 2006, November 2008, and May 2010), wave data from 2006 to 2010, and numerical modeling. The integration of the observations and modeling results led to the following conclusions:

(1) The sand extraction carried out between March and May 2006 of about −340 000 m^3 produced a small, deep, and oval shaped borrow pit, elongated in the NW–SE direction, about 900 m long, 150 m wide and 5 m deep.
(2) The sandpit represents a depression on the seafloor and therefore acts as a trap for the sediment, fostering sediment accumulation and the pit recovery. In fact, the mean flow velocity and the orbital velocity decrease inside the pit, which results in a decrease of the sediment transport capacity inside the excavation area and, as a consequence, the pit tends to be filled through time.
(3) 2.5 years after dredging (in November 2008), an infill of the deepest area of the sandpit was observed, as well as some sediment accumulation mainly on the upper part of the NE flank, resulting on the migration to the SW of the excavation rim. A

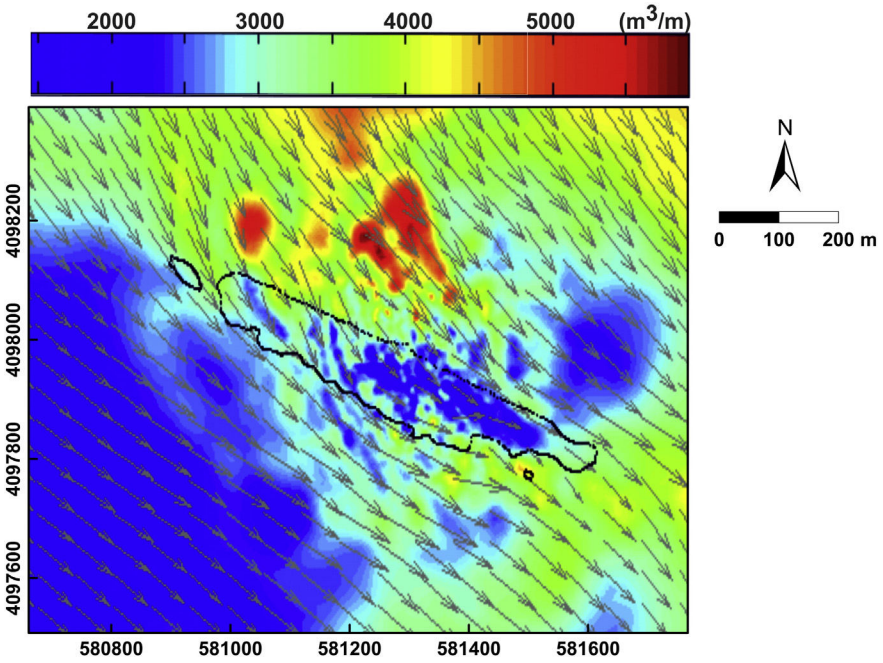

Fig. 9. Magnitude and direction of the sedimentary fluxes (m^3/m) for Bijker formulations inside and in the vicinity of the sandpit. MORSYS2D results between 9th and 14 of April 2008. Coordinate system in UTM Zone 29N, datum WGS84.

reduction in 45% of the maximum slope of the flanks, as well as a reduction of almost 18% of the mean slope, was observed during this period.

(4) 4 years after the extraction (May 2010), the trend remains almost the same, with an infill of the deepest area of the pit, which is almost 2 m less deep, and some sediment accumulation in the upper part of the flanks (mainly in the NE flank). The topography of the excavation area became smoother, with the surface roughness decreasing through the time. Overall, the sandpit bathymetry in May 2010 became smoother and less deep than the original pit shape four years earlier.

(5) Until the last survey (May 2010), the pit recovered almost 17% at a recovery rate estimated at 6.5 cm/yr until November 2008, and 7.2 cm/yr since then, until May 2010. The increasing refilling rate can be explained by the storm occurrences during these two periods. The period from December 2008 to May 2010, although shorter, presented a larger number of stormy days and a higher $H_{s99.8}$ than in the first 2.5 years after the extraction.

(6) The numerical model results suggest that the sandpit refilling process is essentially storm dependent and, therefore, episodic rather than continuous in time. In fact, significant wave height greater than 2 m, combined with strong winds, generate currents and wave orbital velocities capable of high sediment mobilization.

(7) The perimeter and the area of the pit are growing through the time. However, this growth is mostly in the NW–SE direction, resulting in an elongation of the sandpit.

(8) The NE flank of the sandpit is migrating southwestwards, what results in a migration in the same direction of the sandpit centroid and the sandpit longitudinal axis.

(9) The seaward prograding pattern of the sand deposition on the onshore flank (NE), the S–SE directed wind induced mean currents (Rosa et al., 2011a), and the sediment flux pattern suggests that the main source of the sediment accumulated on the pit should be sand from the N–NW surrounding areas, meaning that the pit worked as a drain of these sediments.

(10) The estimates for the sandpit recovery time based on a mean refilling rate points towards a value of approximately 22 years for near-full pit refill. However, the calculated estimations using the number of stormy days, rather than the total time, point to the need of 412 stormy days, which corresponds to 38 years for a near-complete sandpit recovery, considering the wave dataset used by Almeida et al. (2011) as representative of the future wave climate.

The results and methodology presented in this work contribute to a better understanding of the processes involved in the evolution of the sandpit under study and allow a better assessment of its environmental impacts, namely by providing more reliable estimates of its recovery time. Further monitoring of the study area for a longer time period, including in situ observations of the hydrodynamic parameters and additional multibeam bathymetric surveys, will allow the follow-up of the morphological evolution of the sandpit and a better constraining of the model parameters. The approach used is applicable to other offshore excavation areas and the numerical modeling procedure provides a useful management tool to select the most appropriate offshore sand borrow or exploitation sites with minimal impacts as concerns recovery times and coastal sedimentary balance.

Acknowledgments

This work was made under the scope of the SANDEX project PTDC/ECM/70428/2006 (SAND Extraction in the Portuguese continental shelf: impacts and morphodynamic evolution), and the PhD grant SFRH/BD/65770/2009, both financed by FCT.

Many thanks to Dr. Pedro Terrinha, from *UGM LNEG*, and all the scientific crew of the cruise carried out in November 2008 (ERSTA-SANDEX Cruise) which allowed the acquisition of important data for this work. Dr. André Fortunato and Dr. Anabela Oliveira from LNEC kindly provided the MORSYS2D code.

Appendix A. Supplementary data

Supplementary data to this article can be found online at http://dx.doi.org/10.1016/j.coastaleng.2014.02.001.

References

Ackers, P., White, W.R., 1973. Sediment transport: a new approach and analysis. J. Hydraul. Div. 99, 2041–2060.
Almeida, L., Ferreira, Ó., Voudouskas, M., Dodet, G., 2011. Historical variation and trends in storminess along the Portuguese South Coast. Nat. Hazards Earth Syst. Sci. I 11, 2407–2417.
Bertin, X., Oliveira, A., Fortunato, A., 2009. Simulating morphodynamics with unstructured grids: description and validation of a modeling system for coastal applications. Ocean Model. 28 (1–3), 75–87.
Bijker, E.W., 1971. Longshore transport computations. J. Waterw. Port Coast. Ocean Eng. 97 (4), 687–703.
Booij, N., Ris, R.C., Holthuijsen, L.H., 1999. A third-generation wave model for coastal regions, part i: model description and validation. J. Geophys. Res. 104 (C4), 7649–7666.
Cooper, K., Boyd, S., Eggleton, J., Limpenny, D., Rees, H., Vanstaen, K., 2007. Recovery of the seabed following marine aggregate dredging on the Hastings shingle bank off the southeast coast of England. Estuar. Coast. Shelf Sci. 75, 547–558.
Costa, M., Silva, R., Vitorino, J., 2001. Contribuição para o estudo do clima de agitação marítima na costa Portuguesa. 2as Jornadas Portuguesas de Engenharia Costeira e Portuária (in Portuguese).
Demir, H., Otay, E.N., Work, P.A., Borekci, O.S., 2004. Impacts of dredging on shoreline change. J. Waterw. Port Coast. Ocean Eng. 130 (4), 170–178.
Dias, J.A., Neal, J., 1992. Sea cliff retreat in southern Portugal: profiles, processes and problems. J. Coast. Res. 8 (3), 641–654.
Dodet, G., Bertin, X., Taborda, R., 2010. Wave climate variability in the north-east Atlantic Ocean over the last six decades. Ocean Model. 31 (3–4), 120–131.
Fortunato, A.B., Oliveira, A., 2004. A modeling system for tidally driven long-term morphodynamics. J. Hydraul. Res. 42 (4), 426–434.
Fortunato, A.B., Oliveira, A., 2007. Improving the stability of a morphodynamic modeling system. J. Coast. Res. SI 50, 486–490.
Fortunato, A.B., Pinto, L., Oliveira, A., Ferreira, J.S., 2002. Tidally generated shelf waves off the western Iberian coast. Cont. Shelf Res. 22 (14), 1935–1950.
Gonçalves, D.S., 2009. Estudo da Evolução de uma Área de Extracção de Areias na Margem Algarvia. Master Thesis Geosciences Department, University of Aveiro (148 pp.).
IH, 1985. Carta dos Sedimentos Superficiais do Cabo de S. Vicente ao Rio Guadiana, Instituto Hidrográfico, Escala 1:150 000, 1ª Edição.
Kubicki, A., Manso, F., Diesing, M., 2007. Morphological evolution of gravel and sand extraction pits, Tromper Wiek, Baltic Sea. Estuar. Coast. Shelf Sci. 71, 647–656.
Li, F., Roncevich, L., Bicknell, C., lowry, R., Ilich, K., 2009. Storm waves and their temporal and directional distribution, Perth, 1994–2008. Coastal Conference 2009 — 5th Western Australian State.
Lopes, V., Silva, P.A., Bertin, X., Fortunato, A., Oliveira, A., 2009. Impact of a dredged sandpit on tidal and wave hydrodynamics. J. Coast. Res. SI56, 529–533.
Manupella G., 1992. Carta Geológica da Região do Algarve, Escala 1:100 000 e Notícia Explicativa. Serviços Geológicos de Portugal, Lisboa.
Marques, F.M., 1997. Sea cliff evolution: the importance of quantitative studies for hazard and risk assessment, and for planning of coastal areas. Colectânea de Ideias Sobre a Zona Costeira de PortugalEUROCOAST, Portugal 67–86.
Pessanha, L.E., Pires, H.O., 1981. Elementos Sobre o Clima de Agitação Marítima na Costa Sul do Algarve. Instituto Nacional de Meteorologia e Geofísica, Lisbon, Portugal (66 pp.).
Plecha, S., 2011. Contribution to the Study of the Ria de Aveiro Inlet Morphodynamics. PhD Thesis University of Aveiro, Aveiro (163 pp.).
Ramos, M., Silva, P.A., Sancho, F., 2005. Morphological modelling using a 2DH model. In: Van Rijn, L., Soulsby, R., Hoekstra, P., Davies, A.G. (Eds.), SANDPIT — Sand Transport and Morphology of Offshore Sand Mining Pits. Aqua Publications, The Netherlands. ISBN: 90-800356-7-X (AT 1–10).
Ris, R.C., Holthuijsen, L.H., Booij, N., 1999. A third-generation wave model for coastal regions, part II: verification. J. Geophys. Res. 104 (C4), 7667–7681.
Roos, C.P., Hulscher, S.H., de Vriend, H.J., 2008. Modelling the morphodynamic impact of offshore sandpit geometries. Coast. Eng. 55, 704–715.
Rosa, J., Gonçalves, D.S., Silva, P.A., Pinheiro, L.M., Rebêlo, L., Fortunato, A., Bertin, X., 2011a. Estudo da evolução de uma área de extracção de sedimentos ao largo de Vale do Lobo (Algarve Portugal) — comparação entre dados numéricos e dados batimétricos adquiridos. Revista de Gestão Integrada/J. Integr. Coast. Zone Manag. 369–377.
Rosa, J., Silva, P.A., Bertin, X., Fortunato, A.B., 2011b. Waves, wind and tidal forcing on a sandpit morphodynamics. J. Coast. Res. SI64, 1170–1174.
Rosa, F., Rufino, M.M., Ferreira, Ó., Matias, A., Brito, A.C., Gaspar, M.B., 2013. The influence of coastal processes on inner shelf sediment distribution: the Eastern Algarve Shelf (southern Portugal). Geol. Acta 11, 59–73.
Saha, S., Moorthi, S., Pan, H., Wu, X., Wang, J., Nadiga, S., Tripp, P., Kistler, R., Wollen, J., Behringer, D., Liu, H., Stokes, D., Grumbine, R., Gayno, G., Wang, J., Hou, Y., Chuang, H., Juang, H., Sela, J., Iredell, M., Treadon, R., Kleist, D., VanDelst, P., Keyser, D., Derber, J., Ek, M., Meng, J., Wei, H., Yang, R., Lord, S., van den Dool, H., Kumar, A.,

Wang, W., Long, C., Chelliah, M., Xue, Y., Huang, B., Schemm, J., Ebisuzaki, W., Lin, R., Xie, P., Chen, M., Zhou, S., Higgins, W., Zou, C., Liu, Q., Chen, Y., Han, Y., Cucurull, L., Reynolds, R., Rutledge, G., Goldberg, M., 2010. The NCEP climate forecast system reanalysis. Bull. Am. Meteorol. Soc. 91, 1015–1057.

Soulsby, R., 1997. Dynamics of Marine Sands, A Manual for Practical Applications. Thomas Telford, HR. Wallingford, England0-7277-2584X.

Teixeira, S.B., 2011. Alimentação artificial de praias com Dragados no Algarve. In: Coelho, C., Silva, P.A., Pinheiro, L.M., Gonçalves, D.S. (Eds.), Dragagens — Fundamentos. Técnicas e Impactos. Universidade de Aveiro, Lusoimpress, pp. 221–240.

Tolman, H.L., 2009. User manual and system documentation of WAVEWATCH III version 3.14. Tech. Note 276, NOAA/NWS/NCEP/MMAB (220 pp.).

van de Graaff, J., van Overeem, J., 1979. Evaluation of sediment transport formulae in coastal engineering practice. Coast. Eng. 3, 1–32.

van Rijn, L., Walstra, D.J., 2002. Morphology of pits, channels and trenches. Part I: literature review and study approach. Report Z3223. WL Delft Hydraulics.

van Rijn, L., Soulsby, R., Hoekstra, P., Davies, A.G., 2005. SANDPIT, Sand Transport and Morphology of Offshore Mining Pits. Aqua Publications, The Netherlands (156 pp.).

Vicente, C.M., Uva, L.P., 1984. Sedimentation in dredged channels and basins, prediction of shoaling rates. In: Edge, B.L. (Ed.), Coastal Engineering 1984 — Conference: Proceedings of the International Conference on Coastal Engineering. World Scientific, ASCE — American Society of Civil Engineers, New York, NY, U.S.A. ISBN: 9780872624382, pp. 1863–1878.

Zhang, K.Q., Douglas, B.C., Leatherman, S.P., 2000. Twentieth-century storm activity along the US east coast. J. Clim. 13 (10), 1748–1761.

Zhang, Y., Baptista, A.M., Myers, E.P., 2004. A cross-scale model for 3D baroclinic circulation in estuary–plume–shelf systems: I. Formulation and skill assessment. Cont. Shelf Res. 110 (10), 1431–1456.